FRACTURE DEVELOPMENT AROUND MOSHANENG AND KANYE, SOUTHEAST BOTSWANA

by

MOTSOPTSE PHILLIP MODISI, B.Sc.(Hons), M.S.

A Thesis

Submitted to the School of Graduate Studies

in Partial Fulfilment of the Requirements

for the Degree

Doctor of Philosophy

McMaster University

FRACTURE DEVELOPMENT, SOUTHEAST BOTSWANA

DOCTOR OF PHILOSOPHY (1994) McMASTER UNIVERSITY

(Geology) Hamilton, Ontario

TITLE: Fracture development around Moshaneng and Kanye, southeast Botswana

AUTHOR: Motsoptse Phillip Modisi,

B.Sc.(Hons) (University of Ibadan)

M.S. (South Dakota School of Mines and Technology)

SUPERVISOR: Dr.P.M.Clifford

NUMBER OF PAGES: x, 335

ABSTRACT

SE Botswana, located in the NW part of the Kaapvaal Craton is a long lived tectonically stable environment dominated by brittle deformation for more than 2.6 Ga.

Relative chronologies in the development of fractures are rationalized according to major unconformities that developed during the Proterozoic in areas around Moshaneng and Kanye in SE Botswana. Periods of brittle deformation are divided into pre-Transvaal Supergroup, post-Transvaal Supergroup/ pre-Waterberg Group and post-Waterberg Group times. Pre-Transvaal lineaments trend ENE and NE and were probably formed as fractures in a rifting environment. Dikes are intruded along some of these lineaments. Post-Transvaal/ pre-Waterberg fractures consist of strike-slip faults that form a conjugate system of two major sets trending NE and NW. These fractures probably formed as a result of E-W compression. The displacement along the NE trending faults depicts reactivation along pre-existing fractures. Regional patterns of fault termination are discernable. Epidermal folds and thrusts were produced in the Transvaal Supergroup rocks. Rotational bulk strain is locally significant. Post-Waterberg deformation was dominated by dip-slip faults, vertical displacements and drape folds.

An orthogonal system of bedding-normal joints predominates in the layered

rocks. Inversion of the relative magnitudes of σ_2 and σ_3 probably accounts for a two phase tensile failure of layered rocks during the formation of the joint system. A diagonal system of bedding normal joints is superimposed on the orthogonal system possibly because of pre-existing folds that perturb the remote stress field. Joint spacings have a negatively skewed normal frequency distribution. Systematic joints show that spacing of set1 <set2 <set3 <set4.

Relics of joint patterns in chert breccia provide insight about post-Transvaal/ pre-Waterberg karstification residuum. The joint pattern accounts for the initial process of fragmentation that resulted in the formation of chert breccia.

On the subcontinental scale, high strain tectonic belts provide a chronology of large scale stress fields that could explain the intracratonic brittle deformations.

ACKNOWLEDGEMENTS

I express a special thanks to my supervisor, Dr. P.M. Clifford for giving me the opportunity to undertake this thesis work, and for coming through whenever it really counted. I thank members of my supervisory committee, Dr. D.C. Ford, who was there from beginning to end; Dr. C. Hale, Dr. B.J. Burley and Dr. W.A. Morris, who served and assisted at various times of my study.

The photographic work of Mr. J. Worwood and thin section preparation of Mr. L. Zwicker are acknowledged. Inumerable exchanges of ideas with graduate student colleagues at McMaster added value to and aided towards the completion of this thesis.

Aspects of the field work were discussed with Dr. V.B. Sibiya and Dr. A.R. Tombale whose familiarity and insight about the study area proved invaluable. I thank the Director of the Geological Survey of Botswana and his staff for the use of unpublished material and technical assistance during field research. The enthusiastic help I obtained from my then student field assitants, Mr. T. Mathake and Mr. A.M. Masokwane, is acknowledged.

It is difficult to imagine the successful completion of this work without the support I enjoyed from members of my family and from some very caring friends.

TABLE OF CONTENTS

PART 1

CHAPTER 1. REGIONAL GEOLOGICAL SETTING OF SE BOTSWANA

1.1 Introduction

The SE part of Botswana is located in the NW corner of the Archaean Kaapvaal Craton of southern Africa, a tectonic unit that had started to stabilize some 3.0 billion years ago (see figure 1.1). The time boundary separating Archaean-type tectonometamorphic basement from Proterozoic-type volcano-sedimentary platform deposits in southern Africa is diachronous (Tankard et al, 1982). Radiogenic isotope ages marking the attainment of stability are usually obtained from the latest Archaean acid plutons. Older ages of more than 3.0 Ga are characteristic of the SE part of the Kaapvaal Craton in the Republic of South Africa and the Kingdom of Swaziland (Windley, 1984; Hunter and Pretorius, 1981). The northern and eastern areas have younger ages, some as young as 2.6 Ga (Anhaeusser and Wilson, 1981).

1.2 Geology of the Kaapvaal Craton

The Archaean basement of the Kaapvaal Craton consists mainly of high grade meta-

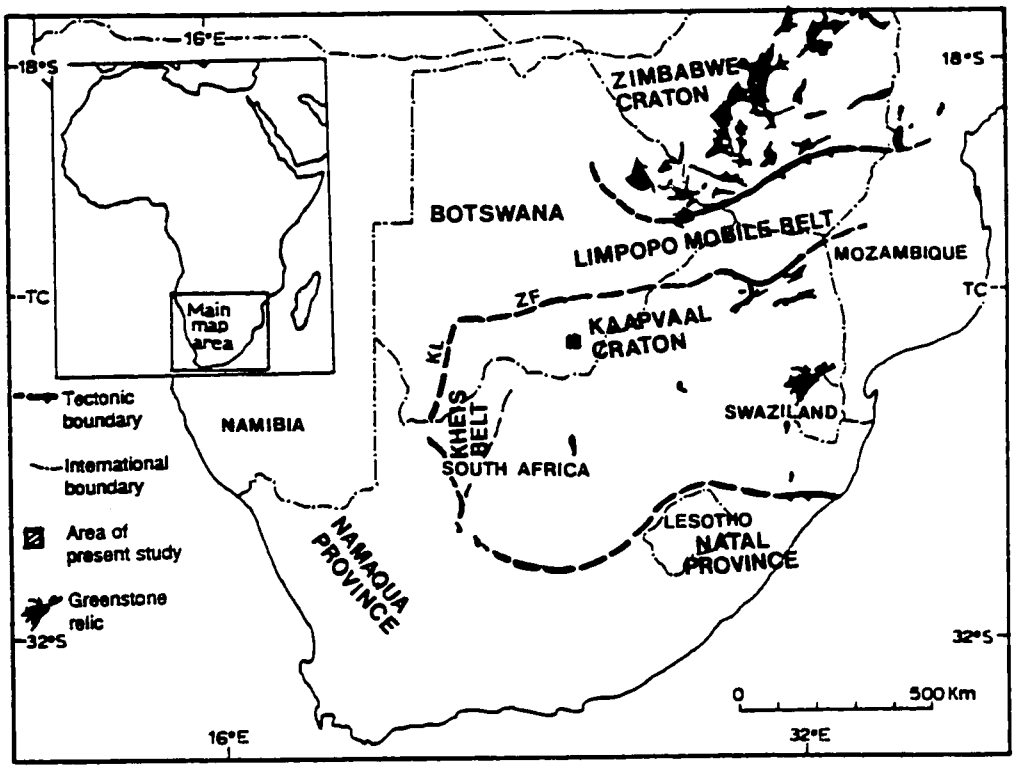

Figure 1.1: Geological map of southern Africa showing extent of the Kaapvaal Craton. The cratonic metamorphic basement includes volcanosedimentary greenstone belts shown in black. The lower grade Kaapvaal Craton is separated from the high grade Limpopo Mobile Belt by an ortho-amphibolite isograd in the east. In the west the boundary runs approximately parallel to the Zoetfontein Fault(**ZF**). **KL**= Kalahari Line, **TC**=Tropic of capricorn. (Map compiled from Tankard et al, 1982, Hunter and Pretorius, 1981).

igneous and meta-sedimentary rocks. Greenstone relics occur as elongated belts of deformed volcanic and sedimentary sequences. Deformed and undeformed granitoid plutons complete the menu of rock units comprising the Archaean basement (Anhaeusser and Wilson, 1981). Extensive exposures of the basement are restricted to the eastern and northern portions of the craton with some inliers in the central and western portions.

Overlying the basement are late Archaean to mid-Proterozoic platform cover-type volcanosedimentary sequences that have undergone relatively little metamorphism and ductile deformation. The earliest of the platform deposits is the Pongola Supergroup, deposited between 3.09 and 2.87 Ga in the SE part of the craton (Tankard et al, 1982; Button et al, 1981). The depositional axes of the Proterozoic sedimentary basins have a general ENE-WSW trend. Following the deposition of the Pongola Supergroup, the Witwatersrand, Ventersdorp and Transvaal Supergroups and the Waterberg Group represent, in order of decreasing age, volcanosedimentary deposits of a northwestward migrating depo-axis (see figure 1.2). The migration of the axis was complementary to that of the locus of granitoid emplacement in the same direction (Hunter, 1974b).

The Witwatersrand and Ventersdorp Supergroups are famous for their extensive fossil placer gold deposits in the Republic of South Africa. The Bushveld Igneous Complex is a major post-Transvaal igneous intrusion that was emplaced at about 1.95 Ga, preceding the deposition of the Waterberg arenaceous continental red beds. The Waterberg Group represents the last sedimentary package of Precambrian age to be

Figure 1.2: Generalized geological maps showing the progressive development of cratonic basins from the Archaean to the early Proterozoic in southern Africa. Crustal stabilization resulted in increased areal extent of each successive stratigraphic sequence. The progressive increase with time in the sedimentary/volcanic ratio is indicated. The age and thickness of each succession are also indicated. (Compiled from Windley, 1984 and Tankard et al, 1982)

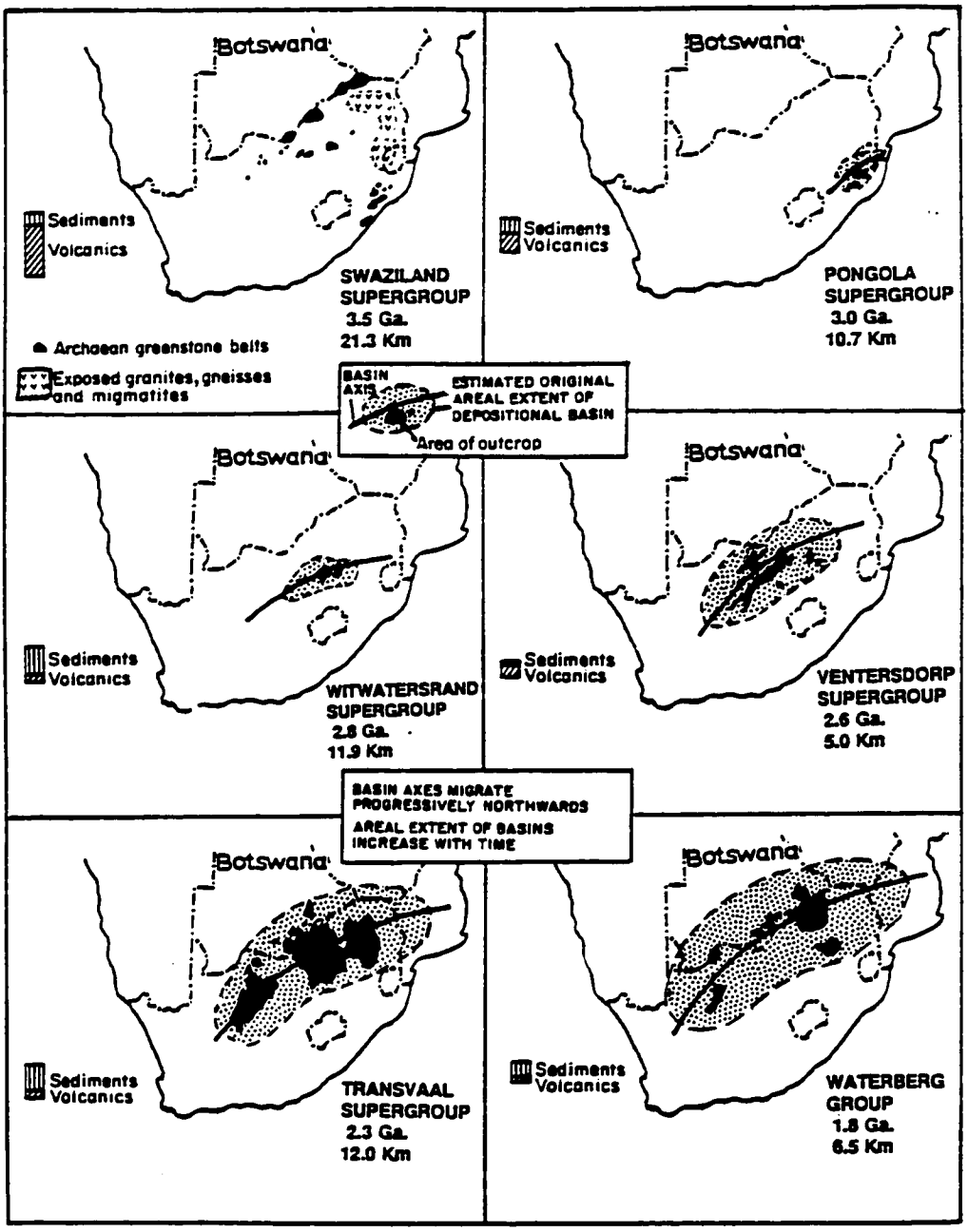
Botswana
Sediments
Volcanics
SWAZILAND SUPERGROUP
3.5 Ga.
21.3 Km
Archaean greenstone belts
Exposed granites, gneisses and migmatites
PONGOLA SUPERGROUP
3.0 Ga.
10.7 Km
BASIN AXIS
ESTIMATED ORIGINAL AREAL EXTENT OF DEPOSITIONAL BASIN
Area of outcrop
WITWATERSRAND SUPERGROUP
2.8 Ga.
11.9 Km
VENTERSDORP SUPERGROUP
2.6 Ga.
5.0 Km
BASIN AXES MIGRATE PROGRESSIVELY NORTHWARDS
AREAL EXTENT OF BASINS INCREASE WITH TIME
TRANSVAAL SUPERGROUP
2.3 Ga.
12.0 Km
WATERBERG GROUP
1.8 Ga.
6.5 Km

deposited on the Kaapvaal Craton. The depositional age of the Waterberg has been estimated at about 1.80 Ga (Tankard et al, 1982). SE Botswana does not host significant Phanerozoic deposits. A summary of the main sub-divisions of the Precambrian of southeast Botswana is given in table 1.1. The earlier platform deposits, namely, the Pongola and Witwatersrand Supergroups are confined to the Republic of South Africa and have not been recognized in Botswana. A geological map of SE Botswana is shown in figure 1.3.

1.3 Archaean basement

The exposed Archaean basement of SE Botswana is dominated by the Gaborone Granite Complex that extends 140 km in an E-W direction and 100 km in a N-S direction (Aldiss et al, 1989). Poorly exposed granitic and mafic gneisses, amphibolites and metasediments have been mapped to the south and northeast of the Gaborone Granite (Aldiss, 1985; Jones, 1973). The Complex consists of a spatial association of volcanic and granitic rocks of varying textures (Key, 1983; Key and Wright, 1982). The Kanye Volcanic Group is a massive, homogeneous very fine crystalline rock that coarsens towards the boundary with the granitic rocks. Rare occurrences of flow banding are present (Chaoka, 1988; Key and Wright, 1982). The Kanye Volcanic Formation surrounds the granitic rocks of the Gaborone Granite in a zone ranging between 2 and 20 km wide. Isotopic dating indicates a maximum age of over 3.0 billion years for the Kanye Volcanic Formation, obtained by the Rb-Sr whole rock

PLATFORM DEPOSITS	
POST-WATERBERG INTRUSIONS	Granite, syenite, dolerite
WATERBERG GROUP (c.1800 Ma.)	Continental red beds
POST-TRANSVAAL SUPERGROUP (c.1950 Ma.)	Mafic and ultramafic intrusive rocks
TRANSVAAL SUPERGROUP (c.2300 Ma.)	Shallow marine sediments, andesite
VENTERSDORP SUPERGROUP (c.2600 Ma.)	Mainly siliceous pyroclastic rocks with subsidiary water-lain sediments.
BASEMENT	
GABORONE GRANITE COMPLEX (c.2800 Ma.)	Granite
KANYE VOLCANIC FORMATION (c.3000 Ma.)	Felsite, granophyre
METAMORPHIC COMPLEX (Pre-Gaborone Granite Complex Age)	Siliceous gneisses, amphibolite and metasediments, gabbro.

Table 1.1: Sub-divisions of the Precambrian of SE Botswana (After Crockett, 1971b)

LITHOLOGY	UNIT	AGE
Undifferentiated dolerite		(Proterozoic to Mesozoic)
Arenaceous and argillaceous rocks, coal, tillite	Karoo Supergroup	Palaeozoic to Mesozoic
Syenite, granite, diorite		Mid to Late Proterozoic
Red to varicoloured arenaceous and argillaceous rocks	Waterberg Group	Mid-Proterozoic
Arenaceous and argillaceous rocks	Transvaal Supergroup	Early-Proterozoic
Quartzite, shale, dolomite, chert, banded iron formation		
Felsic porphyry, pyroclastics, conglomerate, and argillaceous rocks	Lobatse Volcanic Group	Late-Archaean to Early-Proterozoic
Granitoid rocks:(Gaborone Granite = GG, Mmathethe Granite=MG)	Basement	Archaean
Felsite, feldspar porphyry, granophyre		
M (Modipe) Gabbro		
Undifferentiated gneissic rocks, amphibolites, banded iron formation(l)		
Geological boundary		
Fault		

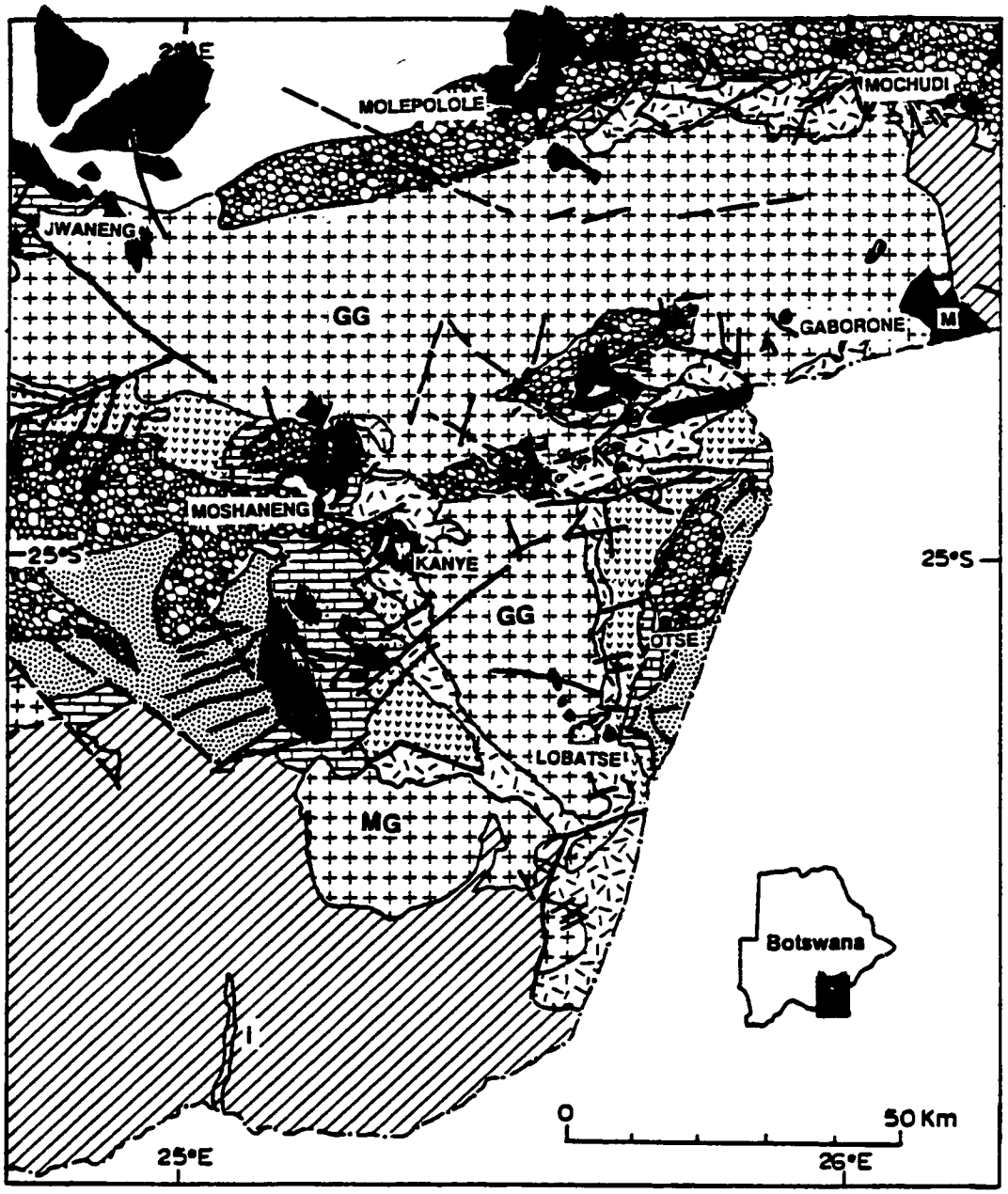

Figure 1.3: Geological map of southeast Botswana (Redrawn from Mortimer, 1984).

method (Crockett, 1969; Harding and Snelling, 1972; Key, 1977). The margin of the granite complex consists of porphyritic granophyre and microgranite (Ntlhantle Microgranite). Whole rock, major, trace and rare-earth element abundances show that rocks of the Kanye Volcanic Formation are virtually identical to the porphyritic granophyres of the Ntlhantlhe Microgranite (Chaoka, 1988). Textures then coarsen to a medium grained equigranular, flesh-coloured, alaskitic granite (Kgale Granite). The core of the complex is heterogeneous in texture, distinguished particularly by the dominant presence of a coarse textured rapakivi granite (Thamaga Granite). Locally the rapakivi granite is associated with anorthositic gabbro in the central part of the complex. Zircons separated from granite have yielded an age of 2,830 ± 10 Ma by the U-Pb dating method (Sibiya, 1988). The granite complex has intruded into the Modipe Gabbro in parts of its NE margin. The latter has yielded mineral ages ranging from 1,934 ± 30 to 3,130 ± 100 Ma by the K-Ar dating method (McElhinney, 1966). Three K-Ar ages from plagioclase concentrates had values between 1,900 and 2,000 Ma and six pyroxene concentrates varied between 2,600 and 3,130 Ma. The younger plagioclase concentrate age has been interpreted to represent mild metamorphism due to the emplacement of the Bushveld Igneous Complex of age 1,950 Ma, exposed further east in the Republic of South Africa (McElhinney, 1966). Rb-Sr whole rock determinations for three Gaborone Granite samples gave an isochron that showed an age of 2,340 ± 180 Ma. Whole-rock Rb-Sr radiogenic dating of the gabbro yielded a 2,630 ± 470 Ma age (McElhinney, 1966; Key, 1977). These ages are consistent with the relationship of the Gaborone Granite intruding into the Modipe Gabbro. However,

these ages are inconsistent with the U-Pb absolute age reported above for the central Gaborone Granite Complex. The U-Pb age demonstrates that the Gaborone Granite is probably of an earlier Archaean age. A Precambrian calendar, calibrated by isotopic age determinations for the different rock units of SE Botswana is shown in figure 1.4.

1.4 Lobatse Volcanic Group

The Pongola and Witwatersrand Supergroups have not been recognized in Botswana, their depositional basins having been confined further to the southeast in the Kaapvaal Craton. The oldest volcanosedimentary rocks deposited on the stabilized craton in Botswana belong to the Lobatse Volcanic Group. These rocks have been correlated with the Ventersdorp Supergroup on lithostratigraphic and geochronological bases. Radiogenic isotope dating utilizing Rb/Sr and U/Pb on rocks from the Lobatse Volcanic Group yields ages ranging from 2,208 to 2,695 Ma (Van Niekerk, 1968; Van Niekerk and Burger, 1968). Ages from these rocks seem to cluster around two periods; 2,200 Ma and 2,500-2,700 Ma. It has been suggested that the younger age reflects a thermal resetting. However, it has also been suggested that the zircons from which the older U/Pb ages are obtained are xenocrysts inherited from older crustal material (Tankard et al, 1982). This would mean that the younger dates represent the emplacement age of the Lobatse Volcanic Group.

The Lobatse Volcanic Group has been divided into a lower mainly volcanic unit (Nnywane Formation) and an upper sedimentary unit (Mogobane Formation) (Key,

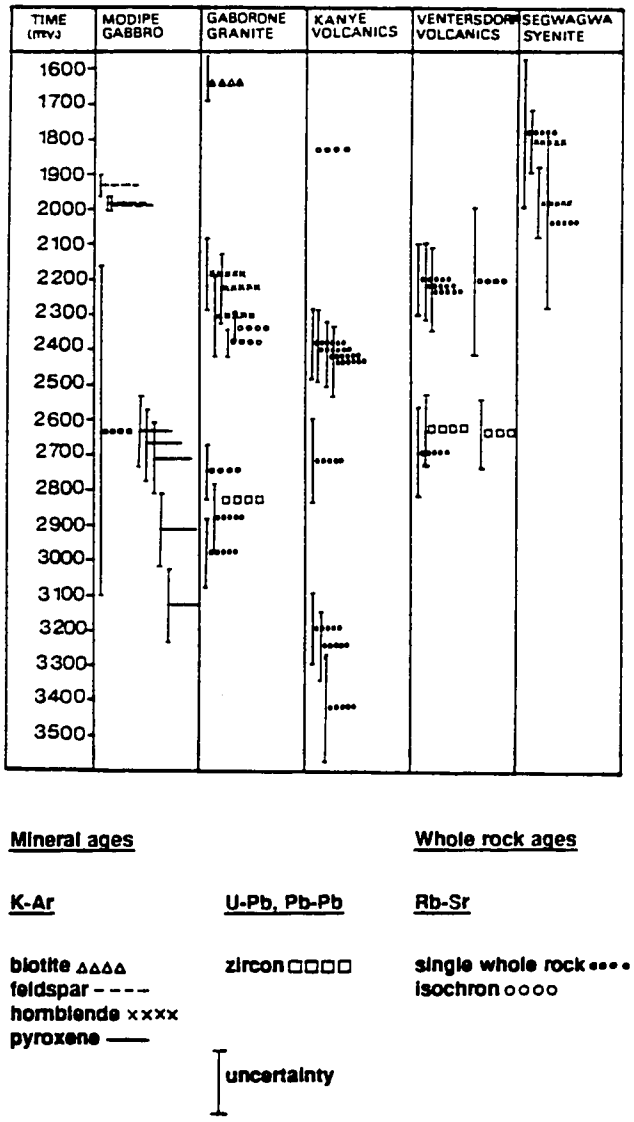

Figure 1.4: Summary of geochronological data from rocks of SE Botswana. The diagram is compiled from data given in Key (1977) and Sibiya (1988).

1983). The Nnywane Formation consists of up to 1,200 metres of rhyolites, tuffs, agglomerates and interbedded shales, siltstones and conglomerates. The formation includes a quartz-feldspar porphyry called the Plantation Porphyry, which has intruded into the other volcanic and sedimentary units. The overlying Mogobane Formation attains a maximum thickness of 1,500 metres, and consists mainly of black to grey shales with a local basal conglomerate and some intercalations of greywacke and conglomerate. Locally a 20 metre thick andesitic lava occurs at the top of the Lobatse Volcanic Group (Crockett, 1971a).

1.5 Transvaal Supergroup

The Transvaal Supergroup was deposited in the Bushveld Basin, centred in the northern part of the Republic of South Africa. The Supergroup largely consists of sedimentary rocks with subordinate volcanic horizons. The early deposits consist of proto-basinal terrestrial and shallow marine Wolksberg and Buffalo Springs Groups. This early phase has been documented along the northern margin of the Bushveld Basin outside Botswana (Tankard et al, 1982, Button, 1973a). Southeast Botswana accommodates the western margin of the basin (see figure 1.3 and figure 2.1).

Equivalent in age and deposited under similar conditions are sediments and volcanics of the Griqualand West Supergroup. These rocks occur in the North Cape Basin, mainly in the Republic of South Africa. The northern margin of this occupies southern Botswana (Crockett, 1972b; Button et al, 1981; Gould and Rathbone, 1985).

The South African Committee for Stratigraphy (SACS, 1980) refers to these deposits as the Transvaal and Griqualand West *Sequences*. The latter terminology has not received universal acceptance, with many workers preferring *Supergroup* to *Sequence* (Tankard et al, 1982; Key, 1983; Button et al, 1981).

The epeiric sea that was prevalent for much of the deposition of the Transvaal and Griqualand West covered a vast continuous area of 500,000 km^2 (Tankard et al, 1982). There is a school of thought however, that contends that the Transvaal sediments were deposited in a series of distinct smaller basins or "chain of great lakes," rather than a continuous epeiric sea (Crockett, 1972c, Crockett and Key, 1988). Transvaal rocks around Moshaneng and Kanye that are discussed in later chapters belong to the "Kanye Basin" (Crockett, 1972c).

The stratigraphic descriptions of these early Proterozoic sediments in the study area have, either explicitly or implicitly, been correlated with those of the Bushveld Basin rather than those of the North Cape Basin in previous studies (Cullen, 1955; Crockett, 1971c, 1972b, 1972c; Gould and Rathbone, 1985; Aldiss et al, 1989). In keeping with this tradition, the stratigraphic nomenclature used in the Bushveld Basin will be adhered to in this thesis. It is not the objective of the thesis to formalize the stratigraphy in the region; such work being outside the scope of the present study.

The period of Transvaal sedimentation is constrained by the minimum age of emplacement of the volcanic rocks of the Ventersdorp Supergroup below and the maximum age of intrusion of the Bushveld Igneous Complex. Sedimentation and volcanism of the Supergroup are estimated to have started at about 2.3 Ga and ceased

at 2.1 Ga (Button et al, 1981). Although the maximum thickness of the Transvaal at its depo-centre is about 12,000 metres, only some 6,000 metres is preserved in Botswana (Crockett, 1972c; Key, 1983). The Transvaal overlies the Ventersdorp with an angular unconformity but in many areas, the Transvaal onlaps directly onto the granitic and volcanic basement. A three part sub-division of the Transvaal is recognized all over the Bushveld basin, namely, the basal Black Reef Quartzite Formation, an overlying Chuniespoort Group with the Pretoria Group at the top. A summary of the stratigraphy of the Transvaal Supergroup exposed in southeast Botswana is given in table 1.2.

1.5.1 Black Reef Quartzite Formation

The basal unit of the Transvaal Supergroup is the Black Reef Quartzite Formation (BRQ), which has a locally developed basal conglomerate. The discontinuous pockets of conglomerate were deposited at cliff edges along the margins of the depositional basin (Aldiss et al, 1989, p.155). The tectonic environment was probably that of a rift basin that commenced in Pre-Transvaal times during Ventersdorp deposition. A maximum thickness of the Black Reef of 50 metres is preserved in eastern Botswana at the western margin of the Bushveld Basin (Key, 1983). The basal conglomerate consists of elongated clasts derived from the underlying Lobatse Volcanic Group. The main section of the formation consists of a gritty arenaceous sandstone with coarse, blue, quartz clasts that are typical of the quartz crystals of the underlying medium grained Kgale Granite. The Black Reef Quartzite

GROUP (Tankard et al, 1982; SACS, 1980)	 (Aldiss et al, 1989)	**FORMATION/ SUB-GROUP** (Tankard et al, 1982; SACS, 1980)	 (Aldiss et al,1989; Crockett, 1972c)	**LITHOLOGY**
PRETORIA		Several formations of clastic sediments and minor volcanics	Several formations based on Bushveld lithostratigraphy	Three cycles of arenaceous and argillaceous rocks, chert horizons and andesite.
CHUNIESPOORT		PENGE IRON FORMATION		iron formation
	TAUPONE DOLOMITE	MALMANI DOLOMITE SUB-GROUP	KGWAKGWE CHERT BRECCIA FORMATION	chert breccia
			RAMONNEDI FORMATION	dolomite, chert
		BLACK REEF QUARTZITE	BLACK REEF QUARTZITE	quartzite, shale, conglomerate

Table 1.2: Sub-divisions of the Transvaal Supergroup. Correlation of the stratigraphy recognized in the Kanye Basin of Botswana (Aldiss et al, 1989; Crockett, 1972c) and in the Bushveld Basin of South Africa (SACS, 1980; Tankard et al, 1982).

grades upwards into siltstones and shales. The sediments are typically plane bedded but also display graded bedding. Facies in the Black Reef largely represent deposition under fluvial and shallow marine conditions (Tankard et al, 1982; Button et al, 1981).

1.5.2 Chuniespoort Group

The BRQ is overlain by a succession of alternating dolomite and chert beds capped by banded iron formation. The distribution of these lower Transvaal rocks in SE Botswana is shown in figure 1.3. In the present study area (figure 6.5), the dolomite and chert constitute the Ramonnedi Formation of the Taupone Dolomite Group (Aldiss et al, 1989). The carbonate-chert sequence is correlated with the Malmani Sub-group and the banded iron formation with the Penge Formation, together forming the Chuniespoort Group in South Africa (SACS, 1980; Tankard et al, 1982). An aggregate maximum thickness of 1,776 metres is preserved in eastern Botswana (Key, 1983). In parts of eastern Botswana, the banded iron formation has not been fully developed and a ferruginous shale forms the top part of the Chuniespoort Group instead. Intraformational disconformities are marked by chert breccia consisting of angular chert fragments overlain by thin shales and occasional sandstone beds (Button, 1973). The carbonates and chert display stromatolite structures. The chert is usually more resistant to weathering, forming ridges with intervening depressions of dolomite. Karst features are developed in this sequence; their morphology is controlled by fracture patterns (Bons and Van Loon, 1985).

1.5.3 Pretoria Group

The boundary between the dolomite-chert sequence and the overlying Pretoria Group is marked by a distinct chert breccia marker horizon which is recognized throughout southern Africa (SACS, 1980; Key, 1983). This forms the basal unit of the Pretoria Group and is called the Bevet's Conglomerate Member. The Pretoria Group above this member consists of three main cycles of quartzite to shale with an aggregated maximum thickness of 4,900 metres in eastern Botswana (Key, 1983). The quartzitic formations normally form prominent ridges separated by plains and valleys underlain by finer grained lithologies. An amygdaloidal andesitic lava horizon with a maximum thickness of 800 metres occurs near the top of the Pretoria Group. The distribution of upper Transvaal clastic sediments correlated with the Pretoria Group (Crockett, 1971c) is shown in figure 1.3. They occupy the SW portion of the present study area (figure 6.5).

1.6 Waterberg Group

The Waterberg Group overlies all earlier rocks with a distinct unconformity. Horizontal beds form flat-topped hills, although locally tilted beds occur, mainly due to monoclinal folding. Sediments of equivalent age occur all over southern Africa and mark a period of terrestrial red-bed deposition in the early to mid-Proterozoic (Tankard, 1982). A U-Pb age from contemporaneous lava flows in South Africa

indicate that these red beds were deposited at about 1800 Ma.(Oosthuysen and Burger, 1964; Hunter, 1974, quoted in Tankard et al, 1982).

The Waterberg in eastern Botswana consists of purple to pink cross-bedded sandstones with interbedded pebble conglomerates. The composition of the conglomerate clasts is mainly vein quartz (Crockett and Jones, 1975). Locally, the presence of chert, banded iron formation and porphyritic felsite clasts indicates derivation from the underlying Ventersdorp and Transvaal sediments. Polymictic matrix-supported deposits are locally developed, some of which contain boulder size clasts of dolomite, chert and shale (Key, 1983). The arenaceous sediments grade upward into shales and siltstones with desiccation cracks and mud rip-ups. The environment of deposition is envisaged to be that of braided streams that flowed through alluvial plains. Some sections of the Waterberg have been ascribed to deposition in shallow marine environments. The depositional basins were formed by fault-bounded grabens with an overall rectilinear geometry (Crockett and Jones, 1975; Tankard et al, 1982).

1.7 Structural patterns of southern Africa

The structural framework of Africa has been summarised with the aid of extensive references to geochronological and structural data. Throughout the Precambrian, the continent underwent a process of successive cratonizations that increased the areal extent of the stable platform (Clifford, 1970). Southern Africa

forms a significant portion and perhaps a classical example of this structural development.

In a regional study where geological maps were integrated with gravity and aeromagnetic data, Pretorius (1979) provided the regional structural pattern of southern Africa. The structural pattern of the subcontinent is perceived as a superimposition of higher order harmonics on regional first order harmonics. These wave forms are recognized on vertical cross-sectional profiles of regional flexures. In this work, the geometric pattern of continental scale flexures formed the main part of the investigation with virtually no consideration for fractures. These large-scale flexures are equated with first order harmonics. A pattern of concentric and radial folds centred on the Zimbabwe Craton was defined as shown in figure 1.5 (Pretorius, 1979). The pattern started its development in the Archaean, with a concentric development of greenstone belts around the central part of the craton. Presently, this centre is marked by a depression in which an outlier of Phanerozoic Karoo deposits called the Featherstone Outlier is preserved. Proterozoic formations are preserved where concentric and radial downwarps intersect. Carboniferous Karoo deposits are preserved in arcuate depressions that wrap around the Zimbabwe Craton and elongate troughs that are radial from the craton. This pattern was initiated during the Archaean and has progressively developed through the Proterozoic to at least the Mesozoic. Proterozoic overthrust belts of different ages are centripetally arranged around the Zimbabwe Craton. The movements on these thrusts show that they converged towards, and overrode the Zimbabwe Craton (Pretorius, 1985). This model implies that southern

Figure 1.5: Concentric and radial pattern of tectonic domains within the Southern Africa Craton, showing the distribution of the shield and the circumscribing alternation of first-order anteclises and syneclises. Dividing lines between domains are radial upwarps (After Pretorius, 1979).

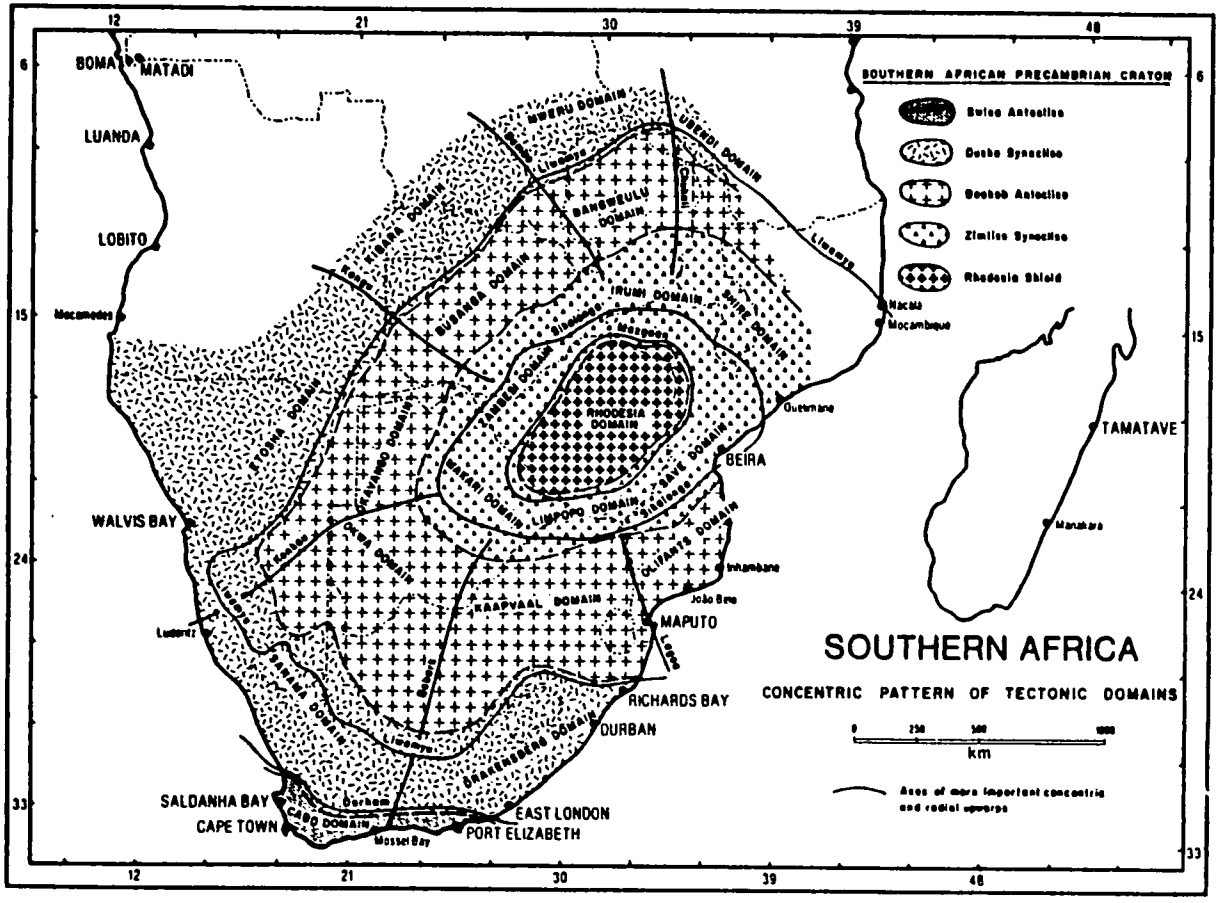
SOUTHERN AFRICA
CONCENTRIC PATTERN OF TECTONIC DOMAINS
SOUTHERN AFRICAN PRECAMBRIAN CRATON
Swiss Antecline
Swiss Syncline
Swiss Antecline
Zimlim Syncline
Rhodesia Shield
km
BOMA
MATADI
LUANDA
LOBITO
WALVIS BAY
SALDANHA BAY
CAPE TOWN
PORT ELIZABETH
EAST LONDON
DURBAN
RICHARDS BAY
MAPUTO
BEIRA
TAMATAVE
RHODESIA DOMAIN
KAAPVAAL DOMAIN
IRUMIDE DOMAIN
ZAMBESE DOMAIN
LIMPOPO DOMAIN
NAMAQUA DOMAIN
CAPE DOMAIN
12
21
30
39
48
6
15
24
33

Africa has been a united and coherent crustal block since the late Archaean to present times. This perception is consistent with the view that from early to middle Proterozoic times, Precambrian shields show little or no detectable motion between constituent cratons as demonstrated by palaeomagnetic results (Piper, 1987). The subcontinental structural pattern described above is in contrast to the perception that Africa evolved from the cratonization of fragmentary Archaean cratonic nuclei, each with independently developed structures. In this latter model, the nuclei are separated by tectonically younger mobile belts (Clifford, 1970). A driving mechanism for these tectonic developments has not been provided.

1.8 Structural patterns of the Kaapvaal Craton

On a regional scale, deformation within the supracrustals of the Kaapvaal craton is predominantly of a brittle nature. Greenschist facies is about the maximum metamorphic grade reached with little or no penetrative tectonic fabric in the platform cover rocks. The present regional structural pattern is characterised by broad basins and domes with which brittle fractures are associated (Button et al, 1981). These structures are caused mainly by regional crustal warping and differential movement of rigid crustal blocks. Syn-depositional faulting has given rise to coarse-clastic horizons at many levels in the stratigraphy of the platform supracrastal deposits.

It has been suggested that regional interference folding provides an explanation for the checkerboard pattern of domes and basins in the Kaapvaal Craton (Hunter,

1974b; Hunter and Pretorius, 1981; Dietvorst et al, 1991; Dietvorst, 1991). This pattern is illustrated in figure 1.6. Regional fold axes in the northwestern portion of the Kaapvaal Craton have an ENE to NE F_1 trend and a NNW to NW F_2 trend. The axes of these regional folds are parallel with the dominant fracture lineaments. It has been noted that the location of various post-Transvaal mafic complexes are located at the intersection of major synformal axes (Hunter, 1974b). Regions of intense folding and metamorphism are locally significant (Button et al, 1981). In southeast Botswana steeply dipping beds occur due to drape-folding over vertically displaced basement blocks. Complicated fault patterns occur in blocks that have been moved by gravity sliding along low angle faults (Crockett,1969, 1971b).

Figure 1.6: Checkerboard pattern of synclines and anticlines caused by interference of two fold episodes in the NW part of the Kaapvaal Craton. The F_1 axes are oriented ENE and the F_2 axes are oriented NNW. **B**=Botswana, **SA**=South Africa (Redrawn from Dietvorst et al, 1991).

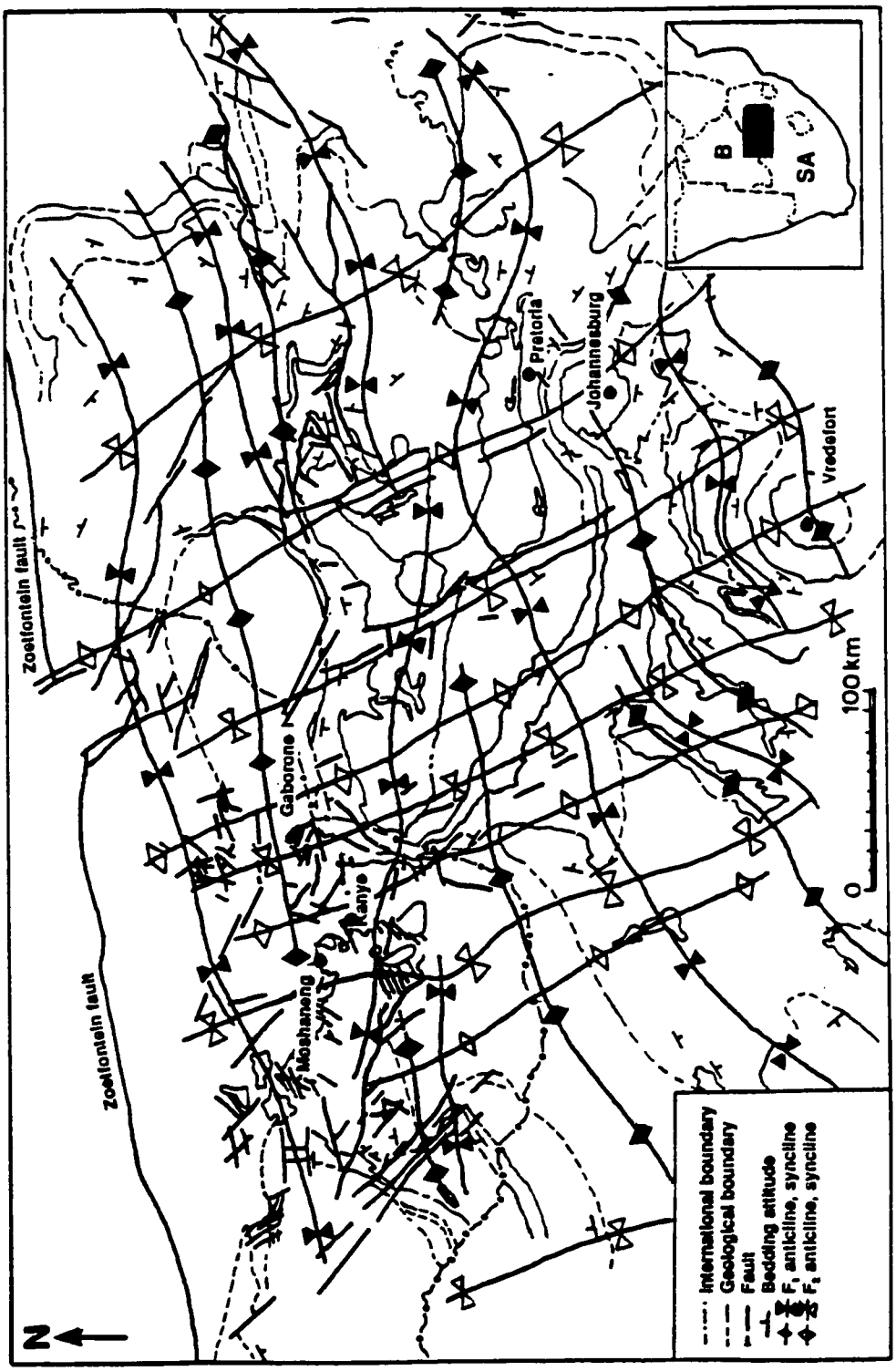
N
Zoetfontein fault
Zoetfontein fault
Gaborone
Moshaneng
Kanye
Pretoria
Johannesburg
Vredefort
B
SA
0
100 km
International boundary
Geological boundary
Fault
Bedding attitude
F1 anticline, syncline
F2 anticline, syncline

CHAPTER 2. PREVIOUS WORK AND SCOPE OF PRESENT STUDY

2.1 Previous work on regional structural analysis in SE Botswana

Crockett (1969, 1971b) has suggested that post-Transvaal tectonogenetic evolution of the Proterozoic formations of SE Botswana was characterized by the existence of mobile basin zones and relatively more stable platform zones (figure 2.1). In the basin zones, complicated structural patterns of faults and open folds were caused by gravity sliding of large masses of Pretoria Group rocks moving down slopes linking a platform zone with a subsiding basin zone. This model was apparently inspired by the Hubbert and Rubey (1959) hypothesis about the role of high fluid pressure in gravity sliding of crustal blocks. Argillaceous rocks constitute about 70% of the Pretoria Group. Freshly deposited, uncompacted, clayey sediments were subjected to great pressures with continued sedimentation and burial. The fluid pressure increased and reduced the frictional resistance along potential planes of shear fracture failure. Crockett (1969) further proposed that post-Waterberg deformation occurred by differential vertical movement along regional lineaments across which monoclines formed in the Waterberg rocks. Crush zones formed in the pre-Waterberg crystalline basement. Emplacement of igneous intrusions was localized along the lineaments, causing considerable dislocation of the surrounding country rocks. This

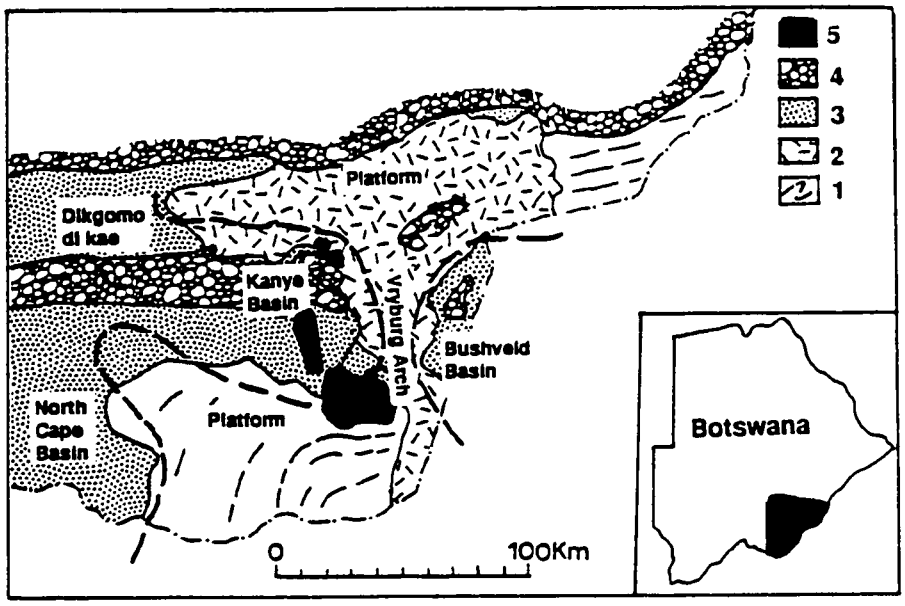

Figure 2.1: A simplified geological map of SE Botswana. The heavy line indicates the boundary between basins and platforms. Ornaments are 1) Archaean metamorphic complex 2) Kanye Volcanic Group and Gaborone Granite Complex 3) Ventersdorp and Transvaal Supergroups 4) Waterberg Group 5) Post-Waterberg syenite and granite (Redrawn from Crockett, 1971b).

dislocation mechanism gave rise to thrust faults in the Moshaneng area as shown in figure 2.2.

Dietvorst (1988), in a study that purported to be a variation from Crockett's model suggested that at least one episode of post-Transvaal Supergroup folding preceded faulting, giving rise to the complicated structural pattern in the Bushveld Basin in SE Botswana. The faults were interpreted to form boundaries between domainal blocks that had been tilted and rotated "along slightly to steeply inclined dip-slip faults". The "dip-slip displacement" on some of these faults is reported to be up to six kilometres. Dietvorst (1988) further concluded that joints have trends that are parallel to the fold axes of open folds in the Transvaal Supergroup rocks. The relative rotations of the fold axes, however, cannot be accounted for by dip-slip faulting alone. A significant component of strike slip is also required if the folds preserved within the fault-bounded domains are relics of pre-faulting folds.

A checkerboard pattern of domes and basins (see figure 1.6) has been described for the Kaapvaal Craton (Dietvorst, 1991). According to this author, the formation of these patterns was initiated when E-W trending synforms were generated in the Archaean basement. The synforms then became depositional basins in the early Proterozoic. Folding with E-W trending axes (F_1) continued during the emplacement of the Bushveld Complex. NNW fold axes (F_2) were generated post-Bushveld time, giving rise to the present interference pattern. These folds were interpreted to demonstrate continuous crustal shortening from Arhcaean times to the Mesozoic, with an interruption in the middle Proterozoic during the deposition of the Waterberg

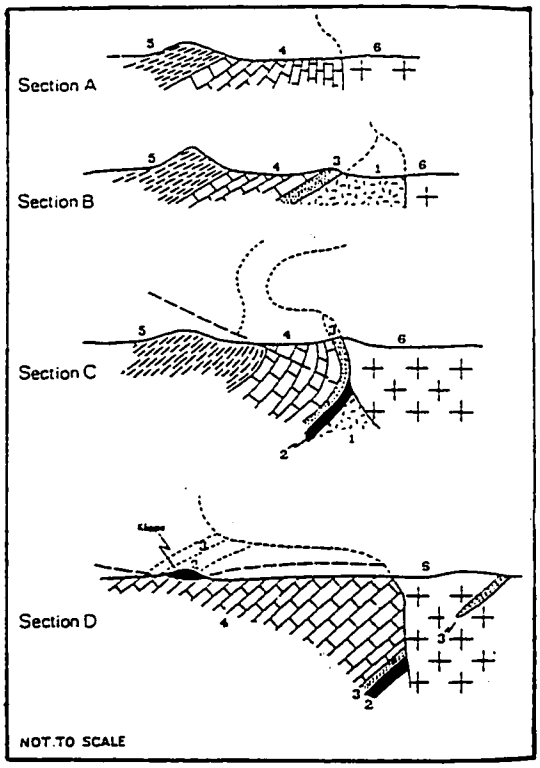

Figure 2.2: Cross-sections of the NE contact between granite and Transvaal Supergroup sediments near Moshaneng according to mapping by R.N.Crockett. Ornaments are 1) Kanye Volcanic Group 2) Ventersdorp Supergroup 3) Black Reef Quartzite Formation 4) Dolomite (Chuniespoort Group) 5) Waterberg Group 6) Post-Waterberg Moshaneng Granite. Thrust displacement indicated in section D was interpreted as having been caused by the emplacement of the Moshaneng Granite, which was then thought to be post-Waterberg. Current mapping shows that the granite is in fact part of the Gaborone Granite Complex that forms a basement to the supracrustals. (Cross-sections after Crockett, 1971b).

Group. It has been suggested that the tectonic basins coincide with groundwater basins, irrespective of lithology (Dietvorst et al, 1991). These basins occur where regional synformal axes intersect. Lock and Carney (1991) have suggested that a North-South fold trend in an area to the west of the present area of study is a result of a "ripple effect" of the Kheis deformation.

A study was conducted near Lobatse, SE Botswana, in which data were obtained from exposures and from aerial photographs (van Haren and Spaans (1988). The results were used to corroborate evidence from hydrogeological studies on the direction of groundwater flow. It was concluded in that study, that groundwater flow directions are controlled by the orientation of fractures in a small hydrogeological basin at Pitsanyane, a few kilometres to the north of Lobatse (see figure 1.3 for the location of Lobatse). Similar conclusions had been reached by Bons and van Loon (1985), who studied the same area. The groundwater basin consists of a karst aquifer in the Transvaal Supergroup rocks. Four sets of joints in that basin have a consistent relationship with fold axes and bedding plane attitudes.

A network of tension fractures and conjugate shear fractures is reported by BRGM (1985) south of Kanye, in the present area of study (see figure 6.5 for the geographic co-ordinates of the present study area). This area is underlain by rocks that are correlated with the Transvaal Supergroup and constitutes a symmetrical complement to eastern exposures around Lobatse, across a basement divide known as the Vryburg Arch or Bobark upwarp (see figure 2.1) (Key and Wright, 1982; Pretorius, 1979). Principal stress directions were worked out from the geometry and

relative orientations of fractures. In particular the orientation of tension gashes in the vicinity of the Taupone Fault provided the main argument for a chronology of stress systems. Three episodes of compression were inferred from patterns formed by quartz-filled tension gashes, conjugate joint sets, faults and associated orientations of the principal stresses. An early E-W compression was followed by an ENE-WSW compression which in turn was followed by a N-S compression. In this study, no consideration was given to the influence of folds in the development of fractures.

The presence of a major ENE trending dike swarm in SE Botswana has been suggested (Aldiss, 1985, 1986; Aldiss et al, 1989). The swarm was interpreted from photolineaments with very little exposure on the ground. Ground magnetic traverses showed that the lineaments are not associated with magnetic anomalies (Aldiss and Bantshang, 1984, quoted in Aldiss, 1986). The precise age of the dike swarm is not known but may be taken to be pre-Transvaal from photogeological evidence.

2.2 Structural problems in SE Botswana

Some specific structural problems in SE Botswana that need to be addressed are outlined below: 1.) The ubiquitous fractures revealed by regional reconnaissance geological mapping display patterns which have not been completely explained in terms of a genetic model or mechanism. 2.) The sequence of regional events that has led to the present structural pattern, especially the fracture pattern, has not been closely examined. 3.) Joints, which are the most common of geological structures in

the study area are the most enigmatic. There has hitherto been very little work produced to explain the origins of these structures.

2.3 Aim of study

The classical geometrical patterns of fractures formed in strike-slip fault zones are derived from deformations that have occurred in recent geological time and from laboratory models (Cloos, 1955; Tchalenko and Ambraseys, 1970; Naylor et al, 1986). Strike-slip faults identified in SE Botswana were formed during the Proterozoic and may have been subjected to reactivations or modifications. The applicability of the classical models of fracture patterns to ancient fault systems is tested in the present study.

Some previous studies of the regional geological structure incorporating SE Botswana have tended to emphasize on the development of flexures and folds (Pretorius, 1979; Dietvorst, 1988; Dietvorst, 1991; Dietvorst et al, 1991). Other studies have emphasized fractures (Crockett, 1969; 1972c; BRGM, 1985, 1986 and 1988; Van Haren and Spaans, 1988). The present study aims to bring some focus on the role of fractures in development of structures in a selected portion of SE Botswana (see figure 6.5), and their implication for the regional tectonics.

In this study, the spatial, as well as the temporal development of fractures are examined. Crockett (1969, 1971c) has suggested a plausible model of gravity sliding along low angle faults to explain structures displayed in the western margin of the

Bushveld Basin. This model has been extended to the Kanye Basin (see figure 2.1) across the Vryburg Arch or Bobark upwarp Axis, where rocks of the Transvaal Supergroup have been folded and faulted. The occurrence of thrust faults at Moshaneng (Crockett, 1971b, 1972a) has been attributed to dislocation of the country rock by igneous emplacement of the Moshaneng syenite and granite (see figure 2.2). Aldiss et al (1989) in a reconnaissance remapping of the area around Kanye have shown that the distribution of the Moshaneng granite established by Crockett (1972a) was incorrect. The model of dislocation by igneous intrusion to explain the thrust faults has therefore become untenable and requires re-examination. A new interpretation for the occurrence of thrust or reverse faults at Moshaneng is required, and this thesis will attempt to provide such an interpretation.

Detailed mapping in the Moshaneng area, undertaken at the beginning of this study (figure 4.2), has demonstrated peculiar structural characteristics involving apparent collapse in a localized graben structure at Tletletsi, thrust faulting and horizontal displacements. It is proposed that these structures, taken together, were developed as a result of dominantly strike-slip movement which has hitherto not been considered a significant influence on the pattern of fractures displayed in this region. It is suggested that oblique displacement along a bending strike slip fault resulted in the formation of transtensional and transpressive features as described in the literature (Harland, 1971; Sanderson and Manchini, 1984; Sylvester, 1988; Park, 1989).

A profusion of igneous activity may possibly be linked to local extensional regimes that prevailed during fault movement. It is therefore possible that the fractures

tapped magma chambers where the upward migration of the magma was facilitated by extensional stress regimes. Apparent collapse structures that are spatially associated with syenite and dolerite intrusions occur at the Masoke ring structure and the Segwagwa complex to the south of Moshaneng (see figure 6.5 for the location of these structures). The mechanism by which these structures formed needs to be established.

An important aspect of structural problems in southeast Botswana is to recognize fractures that were formed as a result of tensile stress as opposed to those formed by shearing. This distinction is particularly relevant to assessing ground water flow directions because these are controlled primarily by extension fractures rather than shear fractures (Viak, 1984; Ericsson and Ronge, 1986). In order to separate fractures according to shear and extension types, it is apparent that a genetic model should be established. Limited work has so far been carried out in parts of this region (BRGM, 1985, 1986 and 1988).

The distribution of fracture densities according to fracture orientation is a pertinent matter for investigation. Statistical treatment of joint spacing data will establish whether there is a systematic distribution of joint spacing in layered rocks that is similar to that which has been determined in homogeneous granitic intrusions (Segall and Pollard, 1983).

The Moshaneng area was chosen because it appeared to have some useful characteristics for the understanding of fracture development in SE Botswana. These include the presence of fairly good exposure, some with well developed joint systems; unconformities separating the major Proterozoic deposits; examples of both strike-slip

and dip-slip faults.

Some synformal folds are described as depositional basins by Dietvorst (1991). It is likely that these "folds" could have been initiated as grabens during the early phases of sediment accumulation. A hypothesis is put forward that proposes that some Proterozoic depositional basins in SE Botswana were initiated as grabens controlled by vertical differential block movement. These basins were extended laterally with continued sediment accumulation and downwarp, such that the original proto-basins coalesced to form a larger regional basin. This hypothesis is particularly applicable to basins of Transvaal Supergroup sediments. Folds were formed later in post-Transvaal times.

2.4 Techniques of investigation and arrangement of thesis

A literature review of structural models and mechanisms that are to be tested in SE Botswana is provided in chapter 3. The primary method of investigation is by field studies of rock exposures in selected areas. The locations of these are given on figure 4.1. Structural details of faults and joints are recorded at the rock exposures. Descriptions of the results are presented in chapters 4, 7, 8 and 9. An important method of study consists of the interpretation of remote sensing media in the form of aerial photographs and satellite imagery. The results for this aspect of the investigation are presented in chapter 6. The interpretation of reconnaissance aeromagnetic contour maps provides additional information on fault displacements. Ground magnetic and

palaeomagnetic techniques are tested. Results on magnetic techniques are presented in chapter 5. Chapter 10 is a synthesis of results of present work and previous regional structural studies. Chapter 11 summarizes the conclusions.

It should be understood that the study area was chosen primarily to provide an understanding of the mechanisms of fracture formation in SE Botswana; and not as a text book example of ideal structures. The exposure rate in the region is relatively good for a regional study, but does not provide complete and continuous exposure of faults and joints, particularly in certain rock types such as granite and argillaceous rocks. The results and interpretations presented here however, show that such inconveniences should not necessarily preclude studies of geological structures in this or other similar terrain, for purposes of contributing towards their general understanding.

2.5 Attitude data conventions

In this study, azimuth values are given as east of north on a 360° compass. One value gives the azimuth of a line. Two values separated by a slash give the attitude of a plane or an inclined line. In the case of a plane, the first value provides the strike, and the second value provides the dip. The dip is on the right hand side of the strike azimuth according to the right hand rule. In the case of an inclined line, the first value gives the azimuth of the plunge and the second value gives the amount of plunge. Azimuth, strike, dip and plunge are defined by Ragan (1985).

CHAPTER 3: FRACTURE PATTERNS: A REVIEW

" The importance of fractures can hardly be exaggerated. Most likely, man could not live if rocks were not fractured.."

Ernst Cloos, 1955

3.1 Introduction

Regional fracture systems are present in all types of geological terranes of any age. Patterns have been recognized at scales ranging from a single outcrop to areas covering thousands of square kilometres (Hancock, 1985; Babcock, 1973). Fractures represent brittle deformation that is usually confined to the upper few kilometres of the earth's crust.

This chapter provides a review of fracture patterns to set the stage for the analysis of fractures occurring in an interior stable Precambrian craton of the continental crust. In this tectonic environment, influences of convergent plate margin tectonics are not readily apparent. Deformation is dominated by extensional and transcurrent displacements. The most recent faults are mainly steeply-dipping. The dominant mode of deformation consists of brittle rupture and the relative displacement of rigid blocks.

In a discussion of fracture patterns in the cratonic environment, it is useful to describe patterns formed by joints separately from patterns formed by faults. The two

types of fractures are commonly associated in many aspects, including spatial, temporal and genetic relationships. Many regions, however have been extensively jointed without any significant development of faults. Fractures may also be associated with other structural elements such as folds and shear zones. Some fractures may form due to igneous intrusion. Other fractures form due to upwarp and rifting (Segall, 1984).

3.2 Some basic definitions and comments

3.2.1 Joints

A joint is a fracture along which no appreciable displacement has occurred. This definition is implicitly scale dependent. The "appreciable displacement" is recognized according to the scale of observation (Price and Cosgrove, 1990). Genetically, a joint is an extension fracture formed by mode I stress loading (Atkinson, 1987). Such a fracture remains a joint provided that there is no subsequent tangential slippage along it. The bulk extensional strain imparted to a body of rock due to the formation of joints is small, usually much less than 1%. Segall and Pollard (1983) were able to measure strain in the order of 1×10^{-4} to 5×10^{-4} caused by a single set of joints in the Mount Givens granodiorite in the Sierra Nevada, California, U.S.A. On a regional scale, the strain shown by barren joints is virtually immeasurable. The strain on a given volume of rock is appreciable when the fractures are filled with material such

that veins or dikes are formed.

3.2.2 Faults

Faults are fractures across which there has been significant tangential displacement. A fault may have formed by mode II or III displacement (Atkinson, 1987). A fault may also form by slippage along a pre-existing fracture. In describing faults and fault patterns, scale is an important factor. A single regional fault is usually composed of a number of smaller faults whose cumulative displacement accounts for the total displacement of the larger regional fault. The single individual fault may actually consist of a crush zone or fault gouge with its own internal fracture pattern (Rutter et al, 1986).

Bulk strain can be considerable on a selected portion of a rock body due to slippage on a set or system of faults. Reference to bulk strain was made as early as when the empirical principles of fracturing were invoked (Anderson, 1905, 1951). Alternate slippage on sets of conjugate faults for instance, can change the dimensions of a given body of rock or portion of the earth's crust. The notion of using bulk strain on faulted rock was used to characterize fracture development over a monoclinal fold on the Wingate sandstone in the Colorado National Monument (Jamison, 1989). A cross-section of a monocline was found to contain a myriad of faults (Jamison and Stearns, 1982). Conjugate sets of faults, where total slippage on both sets is about equal, give rise to irrotational bulk finite strain. Rotational bulk finite strain is

developed when slippage occurs along one set of faults or when slippage on one of the conjugate sets is greater than on the other set. A similar concept is discussed by Ramsay and Huber (1987, p.612) in rock that has been deformed by two sets of shear zones (see figure 3.1). In sheared rock, the relationship of the movement sense and the angle between the conjugate shears is reversed in contrast to what obtains in faulted rock (Ramsay and Graham, 1970). It is proposed that the estimation of bulk finite strain can be performed in a manner similar to that used by Jamison (1989) in map view, where there is a set or system of strike slip faults. Tectonic escape in plate tectonics can be regarded as a phenomenon of continental scale, horizontal view, plane bulk strain. Bulk strain resulting from rotational and irrotational finite strain has also been demonstrated in laboratory models (Cloos, 1955).

Individual faults are, however, planes of discontinuity which do not provide a useful measure of the bulk strain in the rock. Where conjugate sets of faults can be proven, the principal maximum stress direction can be inferred using the bisector of the acute dihedral angle between the conjugate fault sets. The stress directions can also be determined from fault and slip attitudes (Hobbs et al, 1976, p.331).

3.3 Joint patterns

Joint patterns can occur exclusively without associated faults; but they may be associated with other structures such as faults and/or folds (Maier and Mäkel, 1982). Joint systems commonly encountered in flat-lying sedimentary rocks are illustrated in

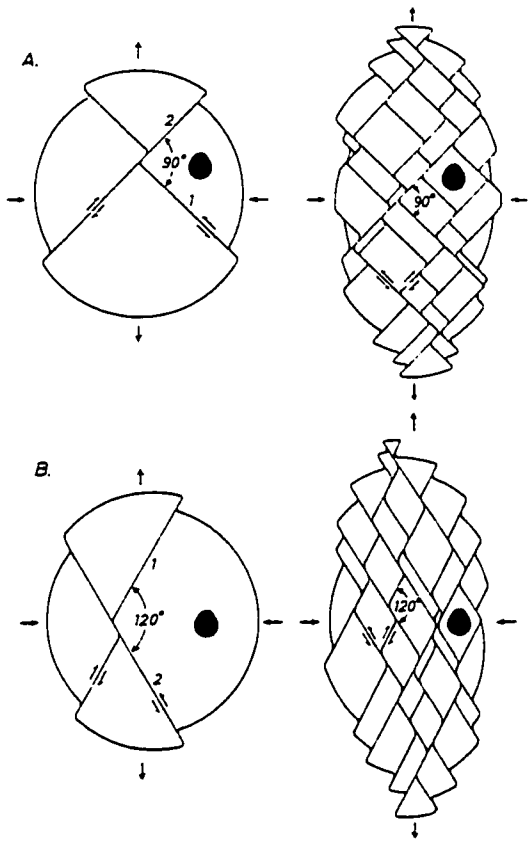

Figure 3.1: Models illustrating how conjugate shear zones can develop large bulk strains. In A and B, the initial and final angles between the shear zones remain unaltered, a feature which goes together with zero strain in the inter-shear zone lozenges. This situation can also be valid for blocks that are bound by brittle shear fractures. The compression and extension arrows, shear sense, shape of bulk ellipsoid and flexure of drag folds in B would be reversed in the case of brittle fractures.(adapted from Ramsay and Huber, 1987).

figure 3.2.

The architecture of joint systems has been described by Hancock (1985) using letters of the alphabet. Patterns formed by systematic joints can be divided into three main groups, namely: 1) single set system, 2) two orthogonal sets system and 3) two diagonal sets system.

3.3.1 Single set system

The I-shaped pattern is the simplest, usually consisting of a single set of parallel vertical joints. This pattern has been recognized in otherwise undeformed, quasi-homogeneous granitic rocks such as those studied by Segall and Pollard (1983) in the central Sierra Nevada; it is also developed in layered sequences (Hancock and Engelder, 1989).

3.3.2 Orthogonal two sets system

The H and T patterns are characteristic of an orthogonal joint system. Flat lying platform cover sediments commonly exhibit this type of pattern where the joints are perpendicular to bedding. The pattern can also occur in folded rocks. The orthogonal joint system has been described as a fundamental joint system consisting of a set of systematic joints and a set of non-systematic joints (Nickelsen and Hough, 1967). Other workers regard the two sets as systematic (Hancock and Engelder, 1989).

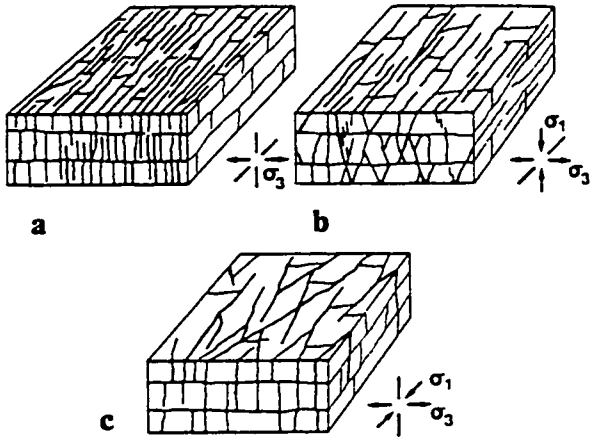

Figure 3.2: Characteristic neotectonic joint systems. (a) Single set of systematic vertical extension joints linked by nonsystematic cross-joints. Vertical extension joints can also be a feature of non-layered rock bodies, e.g. undeformed granite. (b) A spectrum of systematic joints comprising vertical extension joints and steep conjugate fractures enclosing a range of dihedral angles of less than 45°. Two steep fracture directions are expressed by arrays of en echelon vertical joints. Nonsystematic joints link systematic joints. (c) A spectrum of systematic joints comprising vertical extension fractures and vertical conjugate fractures enclosing a range of dihedral angles of less than 45°. Nonsystematic joints link systematic joints. The directions of the maximum and minimum principal effective stresses are shown. (After Hancock and Engelder, 1989).

Complex joint patterns on the Appalachian plateau of Pennsylvania arise from the overprinting of two or more fundamental systems (Nickelsen and Hough, 1967). This assertion is repeated by Babcock (1973), on a regional study of joints in southern Alberta. It is possible that the orthogonal system is formed when $\sigma_2 = \sigma_3$, a case where extension is laterally radial during uplift and exhumation of previously deeply buried rocks. Other possibilities are examined later in chapter 7 of this thesis.

3.3.3 Diagonal two sets system

Conjugate joint sets form V, Y, and X-shaped patterns. These patterns can form in horizontal and folded sediments. Diagonal or conjugate fracture systems are often regarded as a product of rocks meeting the Mohr-Coulomb failure criterion (Hancock, 1985). This implies that such "joints" are really shear fractures. However, in some publications, such fractures are discussed as if they were joints (Parker, 1942; Ramsay and Huber, 1987, p.655). Sometimes a terminology of "shear joint" is introduced (Price, 1966, p.116; Hancock, 1985, p.448). Although strictly speaking, such terminology is ambiguous, the close inter-relationship of shear and extension fractures should be taken in context.

3.3.4 Non-systematic joints and superimposed systems

Other patterns include the K-shaped pattern, related to joints formed under

hydrostatic conditions. Cooling joints in volcanic rocks may also occur in this form. The A-shaped pattern is formed when two or more of the basic systems described above are superimposed.

Non-systematic joints form a more complicated pattern. Many of them occur as cross-joints, merely connecting existing joints (figure 3.2). These fractures are developed after the main phase of joint development. Others may occur as a result of multiple deformations. Pinnate joints and tension gashes are fracture patterns that are associated with shearing (Ramsay and Huber, 1983, Hancock, 1985).

3.3.5 Regional joint patterns and their causes

Regional joint patterns have been mapped on stable platform regions of North America (Engelder and Geiser, 1980; Engelder, 1982). Similar structures have been studied in England, Europe and the Arabian platform (Hancock, 1985; Hancock and Engelder, 1989). Some of these structures have been attributed to neotectonic deformation related to current regional or local stress fields (Zoback, 1992). Engelder (1982) has suggested that joints in the mid-continent were formed as a result of the contemporary stress field within the lithosphere. Uplift and erosion accounts for some of these stress fields in the upper 0.5 Km of the earth's crust. The joints so formed have been termed unloading joints (Engelder, 1985). According to Jackson and McKenzie(1983), the formation of open fractures is probably limited to no more than 500m depth. In the presence of fluid pressure, joints may persist to depths of several

kilometres (Suppe, 1985). Engelder (1985, figure 12) has found that the trend of vertical joints changes with depth in his studies on the Appalachian Plateau. It was inferred that deep joints are tectonic and shallow joints are unloading structures. It can therefore be appreciated that a fracture pattern observed on the surface may not persist with depth.

3.3.6 Regional patterns and the stress field

The σ_1 direction is inferred as the bisector of the acute dihedral angle of diagonal (conjugate) sets of fractures. In this case, the fractures are of the shear type. However, where only one set of joints occurs, the σ_3 direction is taken as acting perpendicular to that set. The one set is regarded as extensional. An orthogonal system is interpreted as a product of extension. Price and Cosgrove (1990) assert that an elliptical basin undergoing subsidence, and then uplift will develop an orthogonal system of fractures. This notion stems from the parallel uplift model that explains the development of horizontal strain and the formation of vertical fractures (Price, 1966).

3.3.7 Joint patterns in folded strata

Joints which occur in folded rocks usually display a geometry that incorporates the Navier-Coulomb failure criterion (see figure 3.3). In this classical pattern, the joints are perpendicular to the folded layers. Whereas the diagonal joint

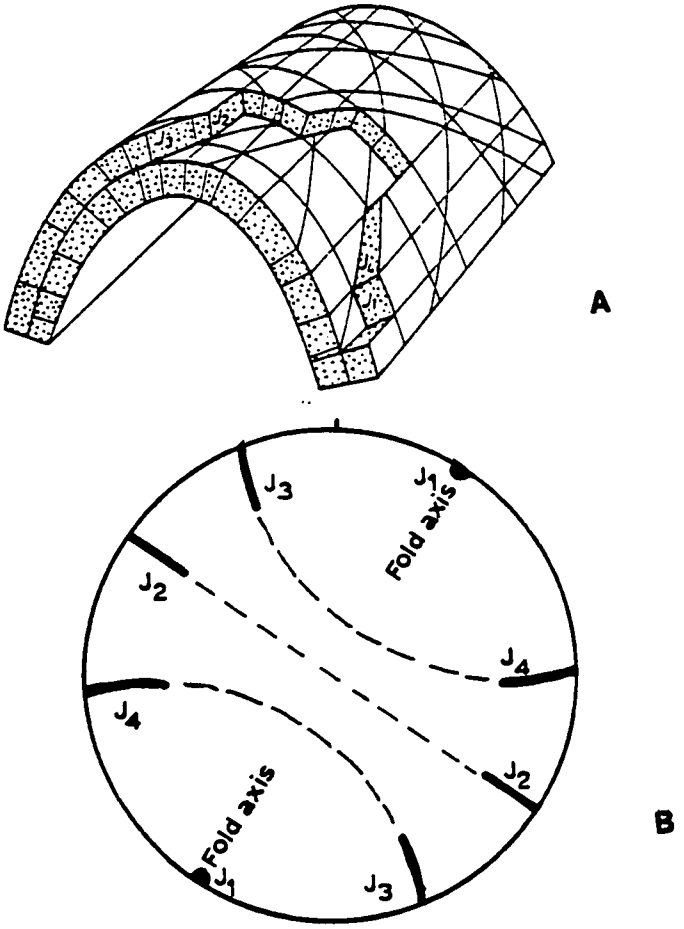

Figure 3.3: A The *classical* view of the relationships of joints to fold geometry. Joint surfaces stippled, bedding planes unstippled. J_1=cross joint, J_2=longitudinal joints, J_3 and J_4= diagonal joints(After Ramsay and Huber, 1987).

B Idealized schematic stereographic projection of poles to joints in folded strata. The joint sets are the same as those in A. The small circle tracing J_3 need not be the same as that tracing J_4 in all cases.

sets J_3 and J_4 were initiated under the Navier-Coulomb failure criterion, they have subsequently been folded with the layers as the sets J_1 and J_2 are developed. As folding progresses, the set J_2 becomes more closely spaced, eventually defining fracture cleavage. The above is only one of the proposed mecahanisms and sequence of fracture formation that may be tested by experimental models. The pattern of joints on folded beds was studied by Maier and Mäkel (1982) on tightly folded rocks of the Ardennes of Belgium. A relationship similar to the pattern displayed in figure 3.3 was revealed, where four sets of joints are developed. These sets are recognized when the folded beds are unfolded and rotated to horizontal. While the beds are still folded, a pattern of small circles is formed in a pole to planes stereographic projection as shown in figure 3.3B.

The overprinting of one of the simple joint system by another can sometimes be attributed to the influence of other geological structures such as folds. In the Appalachian Plateau, the trend of joint sets varies according to changes in the regional trend of the fold axes (Engelder and Geiser, 1980). A similar conclusion had been reached by Babcock (1973) in a study of regional joints in southern Alberta.

3.4 Fault patterns

3.4.1 Andersonian model

Characteristic patterns for each of the special types of faults are reviewed in this

and the following sections. The fault types are strike-slip, normal and reverse faults. The latter two types fall into the dip-slip group of faults. A general model for these faults is the Andersonian model for pure shear shown in figures 3.4(a) and figure 3.6A. In this model, plane strain is assumed and a two dimensional system of conjugate sets of faults is predicted (Anderson, 1905, 1951). The acute angle between these conjugate sets is bisected by the axis of maximum compressive stress or shortening axis. It has been argued that one of the principal directions of stress will normally be parallel to the vertical direction, i.e. the direction of gravity (Anderson, 1951, p.13). The other two directions are therefore usually horizontal. These assumptions imply that the three types of faults introduced above are the typical variations that occur within the earth's crust. Deviations from the above conditions are however, fairly common. These deviations result in the formation of oblique slip faults and aspects of transpression and transtension fracture systems. Fracture systems will be described with the various groups of faults mentioned above in mind.

Sufficient differences in the magnitude of the principal stresses leads to fracturing or rupture as the cohesive strength of the rock is overcome. The angular relationships between the fault sets and the principal stress axes as shown in figure 3.6A are predicted by the Navier-Coulomb criterion for brittle fracture (Price, 1966).

3.4.2 Poly-axial fault model

A model for deformation occurring entirely by slip along fractures in a

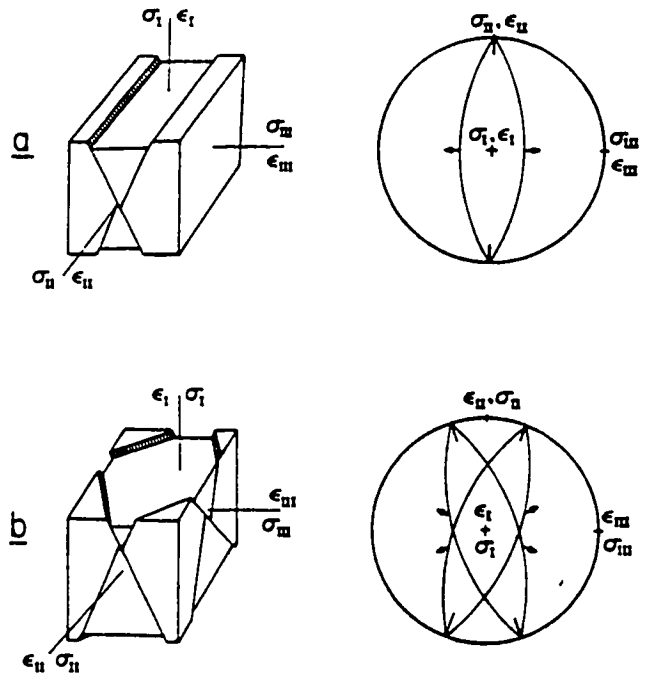

Figure 3.4: (a) Conjugate set of normal faults, and the associated principal stress and strain axes according to Anderson (1951).

(b) Four sets of normal faults that can accommodate three-dimensional strain, and the orientations of the principal stress and strain axes. Arrows indicate slip directions in both diagrams.

(After Reches, 1983)

polyaxial environment has been theoretically derived (Reches, 1978 and 1983). In this model, the three principal stress directions are of unequal magnitude. The model is supported by both experimental work and field occurrences (Reches and Dietrich, 1983, Aydin and Reches, 1982). The resulting pattern consists of four sets of non-parallel faults in orthorhombic symmetry that breaks the crust into rhombohedral blocks (figure 3.4b). This model provides a more general geometrical configuration of a fault system in contrast to the Andersonian model shown in figure 3.4a, which is based on plane strain (Anderson, 1951).

The "Reches" model approaches brittle deformation on the assumption of the presence of pre-existing fractures. The issue of yield by fracture of an undeformed crust is not addressed by this model. The model therefore does not account for all the fractures in the deforming medium. The development of mode I extensional fractures, for instance, does not form part of the model. Such fractures may form conduits during intrusion of vertical dikes. The poly-axial model therefore, does not account for all natural conditions. Some fault systems are compatible with the classical Anderson model where conditions of plane strain prevail. The poly-axial model asserts that where a stress field acts in an environment of pre-existing fractures, the ones that are oblique to the principal stress directions will be re-activated. Fractures not oblique to the principal stress axes will remain inactive. The application of this model is considered in chapter 10.

3.4.3 Rift systems

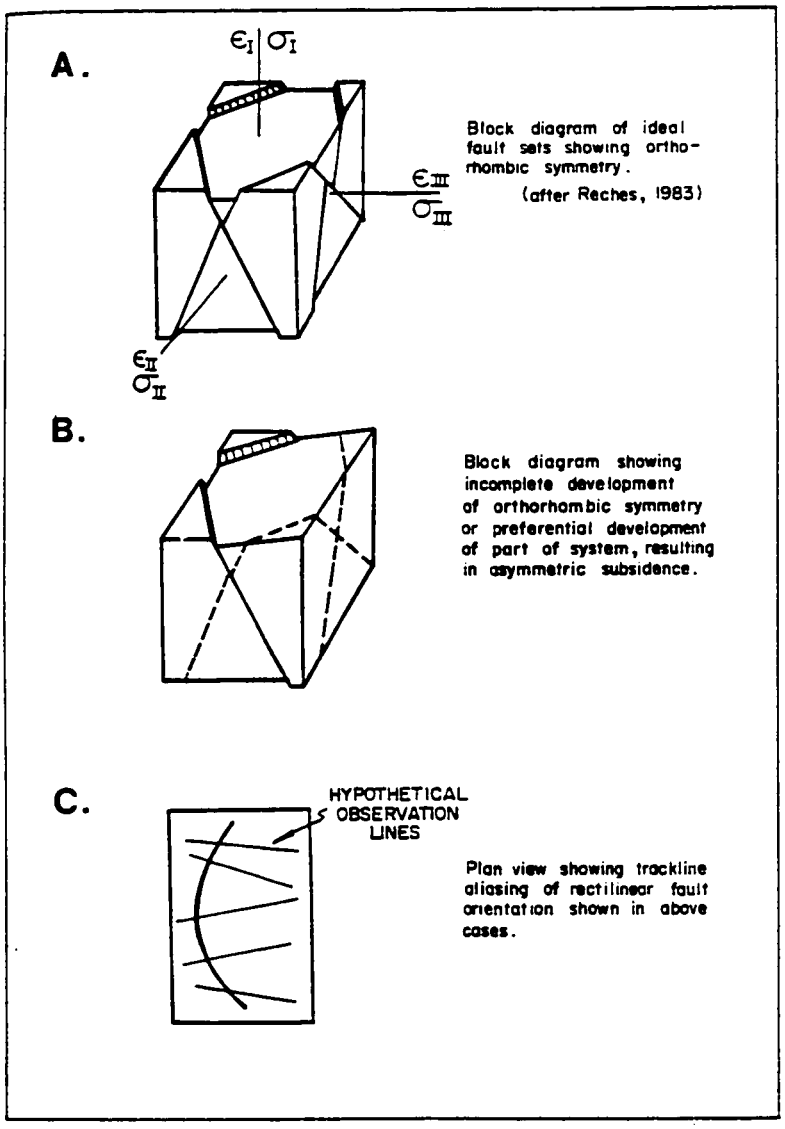

Figure 3.5: Creation of apparently curvilinear border faults by trackline aliasing of original orthorhombic fracture pattern. A rift zone forming over a dome on the earth's crust would incorporate this type of geometry. (After Rosendahl, 1987).

The system of faults given as an example in figure 3.4b and 3.5A consists of four sets of normal faults. The geometry and orientation of the bulk finite strain axes conform to a rift system. This model has been demonstrated in the East African Rift Valley by Rosendahl (1987). In figures 3.5B and 3.5C, the model is adapted to explain the apparent shape of a half-graben where movement along the fracture planes is incomplete in a poly-axial stress field. The complete and incomplete development of faults by this model has been used to explain the zig-zag pattern of faults in a number of areas dominated by normal faults. Examples are cited from the Basin and Range tectonic province of Nevada, the faulted regions in the states of Oregon and Utah in the United States, and the Rhein graben of Germany. In these regions multiple sets of normal faults are developed. The resulting rhomboid blocks are consistent with the 4 sets of normal faults predicted by the model. These patterns are not adequately explained by the plane strain model of Anderson (1951).

3.4.4 Strike slip faults

Strike-slip faults or wrench faults have been a subject of several significant publications over the past several decades (Moody and Hill, 1956; Tchalenko and Ambraseys, 1970; Harding, 1973; Wilcox et al, 1973; Woodcock and Fischer, 1986; Sylvester, 1988). Laboratory experiments simulating strike-slip faults have revealed the development of flower structures in map view and in vertical cross-sections (Cloos, 1955; Bartlett et al, 1981; Naylor et al, 1986; Mandl, 1988).

The map pattern of fractures at a locality of strike slip faulting was determined by Tchalenko and Ambreseys (1970) on the Dasht-e-Bayaz earthquake fracture zone in Iran. The pattern consists of Riedel fractures (Riedel, 1929 in Ramsay and Huber, 1987) in addition to the principal displacement fault and other subsidiary fracture sets (figure 3.6b). The main strike slip fault follows the principal displacement zone. Limited displacement occurs on the Riedel shears and other subsidiary fractures. The subsidiary fractures can become alternative surfaces of slip in a mature and anastomosing fracture zone. Experimental work (Bartlett et al 1981; Naylor et al, 1986) provided a three dimensional perspective to the geometrical pattern. The vertical cross-section cut perpendicular to the fault reveals a geometry resembling a flower structure that opens from a basal slip fracture upwards through a veneer of overlying rocks to the surface (figure 3.7C). The flower structure which shows uplift indicates that a compressive component is present. In such a case, the structure is transpressional. Where the structure shows subsidence, the structure is transtensional. Regional patterns of these kinds of fractures have been described in the San Andreas Fault system and other areas (Wilcox et al, 1973). The above geometries imply that where the fault system has been subjected to erosion to the point where the basement fault is exposed, the typical pattern formed in the now eroded veneer of sediments will not be apparent. The Riedel fractures have an Andersonian configuration that is predicted in homogeneous material yielding under a stress system. The displacement along these fractures is limited as most of it takes place along the principal

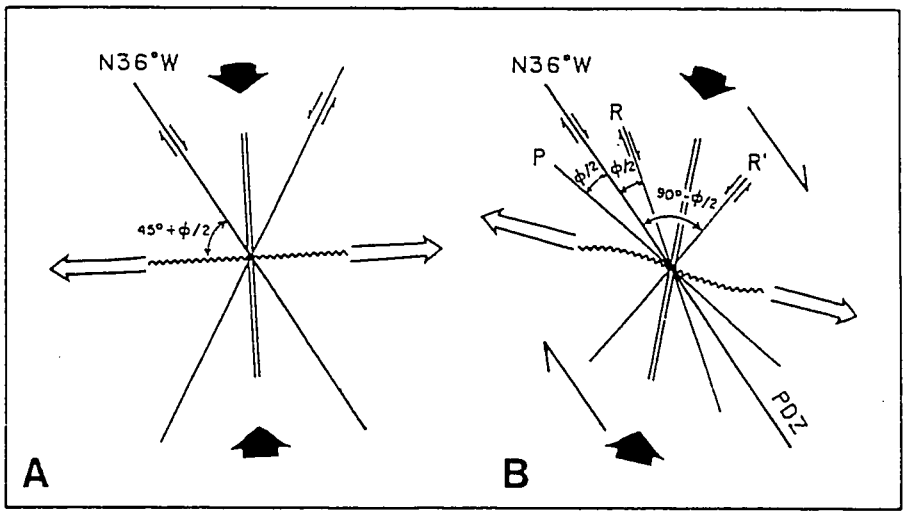

Figure 3.6: Plan view of geometric relations among structures according to two dimensional, strike-slip tectonic models for a vertical fault which strikes N36W. (A) Coulomb-Anderson model for pure shear, (B) Riedel model for right simple shear. Double parallel lines represent the orientation of extension fractures. The wavy line represents the orientation of fold axis and the strike of thrust faults. R and R' are synthetic and antithetic Riedel shears respectively. P represents secondary synthetic fractures. PDZ=principal displacement zone and ϕ=angle of internal friction. Short black arrows = shortening axis. Open arrows = axis of lengthening (After Sylvester, 1988).

Figure 3.7: Maps and cross-sections of specimen of Indiana limestone deformed by dextral shear in the laboratory. **A** shows the top of the deformed specimen slabs. **B** shows the bottom of the limestone specimen slabs. **C** shows cross-sections of flower structures in the deformed specimen. Details of experimental conditions are provided in the diagrams (After Bartlett et al, 1981).

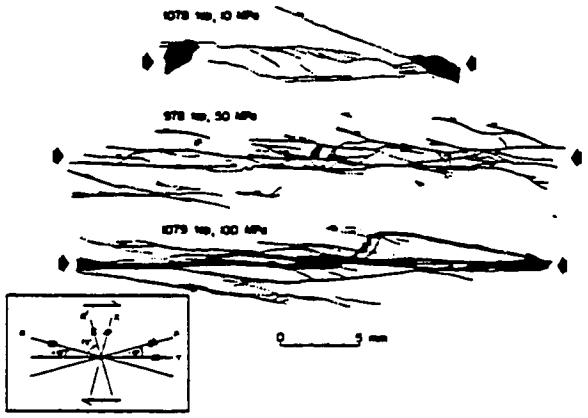

A Right-lateral, shear-zone fracture maps, top sections, of 0.5-cm thick layers of Indiana limestone deformed at 10- (Sp. 1078), 50- (Sp. 978), and 100-MPa (Sp. 1079) confining pressure, and taken to 0.46, 0.54, and 0.56-cm shear displacement, respectively. Solid lines indicate fractures along which there is separation; dashed lines are traces of gouge. Solid black areas indicate missing material (lost in thin section preparation). Bold arrows indicate orientation and location of sawcut in underlying forcing block. Boxed insert illustrates orientations and sense of shear for *R*-, *R'*-, *P*-, *X*-, and *Y*-shears in a right-lateral shear zone.

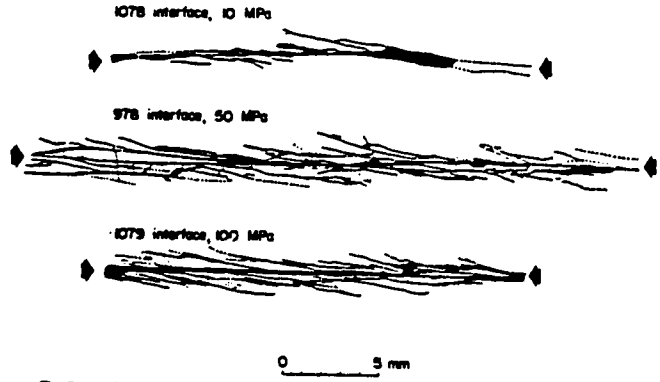

B Right-lateral, shear-zone fracture maps of interface sections of same specimens as in A. Lines of different character and arrows are defined in caption to A

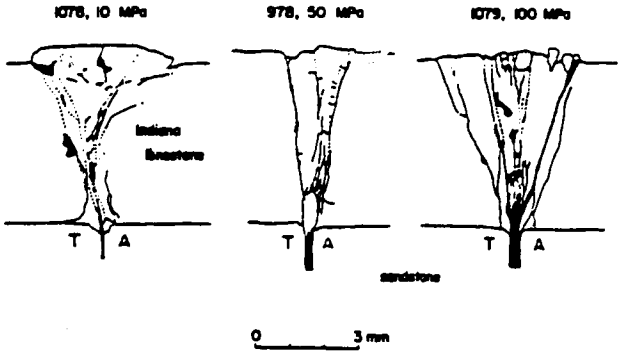

C Cross-section, shear-zone fracture maps of 0.5 cm of same specimens shown in A and B Sense of shear indicated by *T* (towards) and *A* (away). Line character same as in A

displacement zone. It has been noted that these patterns are scale dependent. The similarity of patterns observed at different scales has been examined by Moody and Hill (1956) and Tchalenko (1970). Strike slip faults that reactivate pre-existing fractures such as vertical joints and dikes may not necessarily display the patterns described by Tchelanko and Ambreseys (1970). This condition is discussed in chapter 8, for some of the major faults in the present study area.

3.4.5 Reverse faults

The pattern formed by reverse faults is better known from cross-sectional geometry (Boyer and Elliot, 1982). Because of details that cannot be readily discerned from surface mapping, a study of thrust faults commonly requires borehole and/or subsurface geophysical data for a more complete treatment. In rocks that are layered or exhibiting any form of horizontal planar anisotropy, reverse faults can form very shallow dips, lower than 10°. The characteristic pattern formed in map view consists of low angle faults, the trace of which is often irregular, varying in accordance with the ruggedness of the topography. This study will not dwell on the geometry displayed by thrust faults, which are developed to only a minor extent in the study area.

3.4.6 Oblique-slip faults

Oblique-slip is a more general form of faulting compared to the special types

described above. One could visualize this type of faulting as either normal faulting with a strike-slip component or reverse faulting with a strike-slip component. The former can be described as transtension and the latter as transpression. Sylvester (1988) observes that the most important factor governing uplift and subsidence along a strike slip fault is the bending geometry of the fault surface relative to the slip vector. The bends may have resulted from slip along non parallel faults that are part of a strike-slip fault pattern. Harland(1972), has defined transpression and transtension relevant for terrane in which folds are developed and terrane in which faults are developed. In an environment of brittle deformation, the most recognizable structures of transtension are normal faults that define a pull-apart basin or negative flower structure. Brittle structures of transpression are reverse faults and thrust faults or positive flower structures (Bartlett et al; Ramsay and Huber, 1987; Park, 1990).

PART 2

CHAPTER 4: THE GEOLOGY OF MOSHANENG AREA AND WEST OTSE

4.1 Introduction

Detailed geological mapping was carried out in two areas in southeast Botswana; at Moshaneng and at Otse as shown in figure 4.1 (box 2 and box 4). Exposure in these areas is relatively good for detailed structural studies. The larger area is around Moshaneng village where structures discussed in chapters 7, 8 and 9 were mapped in detail. The structures studied include mesoscopic and macroscopic joints, shear zones, tension gashes, faults, and folds. A peculiar development of fractures in the form of tension gashes and their relation to folded strata was investigated in a small area west of Otse village. These structures are discussed in section 4.3.3 of this chapter. The overall structural styles of these two areas is radically different; with gentle folds at Moshaneng and tight folds at Otse. The deformation of intraformational tension cracks is just as different in these two areas. These structures provide a means of comparing two mechanisms of progressive deformation; one mechanism familiar and well documented in the literature and a new mechanism proposed for the argillites near Otse.

Figure 4.1: Geological map of SE Botswana showing the location of detailed maps shown in figure 4.2 (box 2), figure 4.4 (box 4). The location of the regional geological map of the study (figure 6.5) is shown in box 1. Measuring station location maps figure 7.12 and figure 7.13 are shown by box 2 and box 3. Geological legend is the same as for figure 1.3.

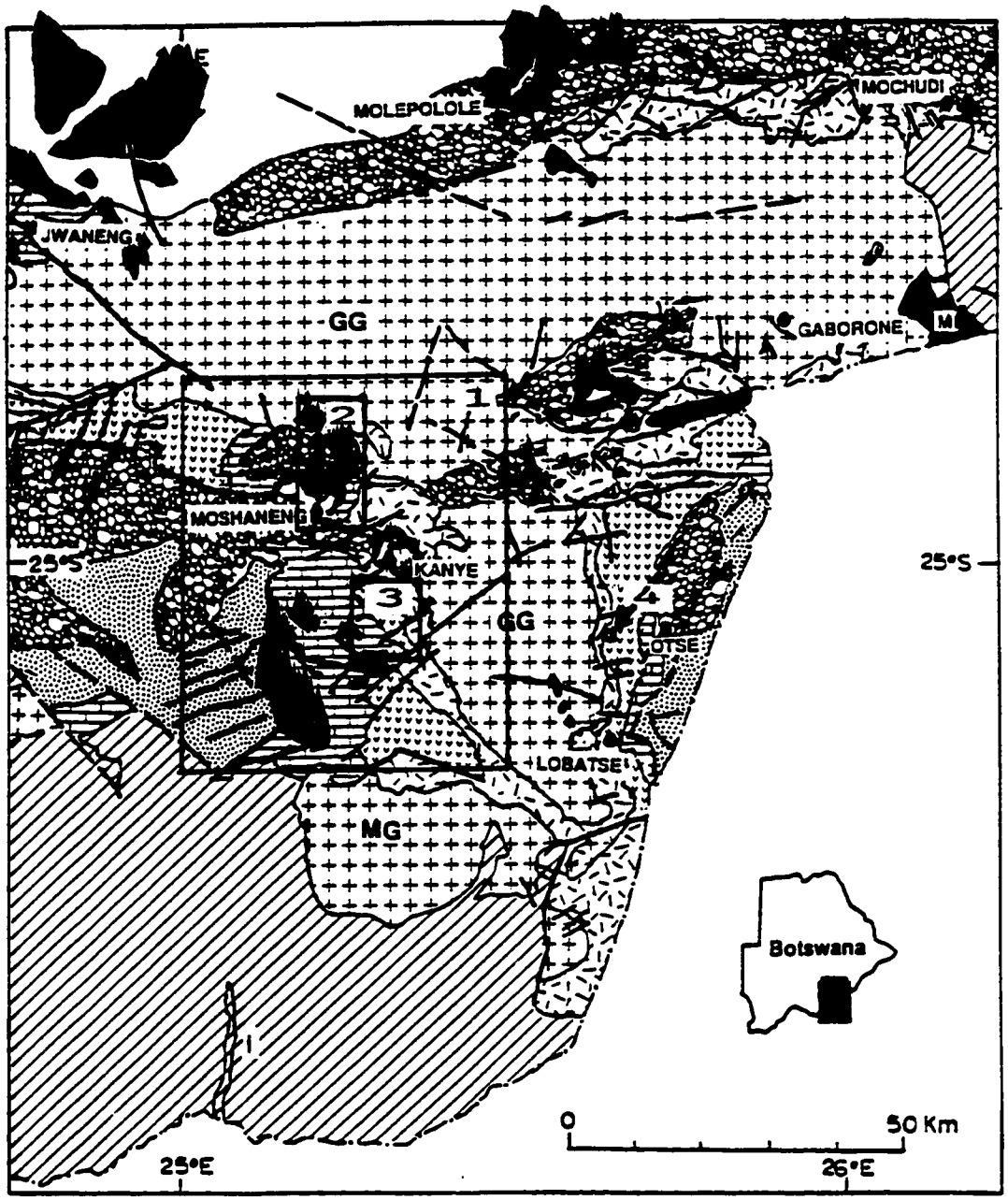
MOLEPOLOLE
MOCHUDI
JWANENG
GG
GABORONE
M
1
2
MOSHANENG
KANYE
25°S
3
4
GG
LOTSE
LOBATSE
MG
Botswana
0
50 Km
25°E
26°E

4.2 Moshaneng

4.2.1 Introduction

Moshaneng Village is located at latitude 24° 54' 30" south and longitude 25° 14' 20" east in southeast Botswana. The area of interest is approximately 120 km^2 as shown in **figure 4.2**. The basement, the layered supracrustals and associated intrusions display peculiar geological structure.

4.2.2 Previous work

Geological mapping around Moshaneng has been carried out by the Geological Survey of Botswana since 1949. The area has been of particular interest because of the presence of exploitable mineral deposits, chief among these being asbestos. Chrysotile asbestos was mined since the beginning of the 1900's up until 1965 (Aldiss et al, 1989). Other industrial mineral deposits include talc, brickearth and dolerite for construction. Showings of lead and zinc have been explored under prospecting licence in the early 1980's (Stalker, 1982).

In one of the early accounts of the geology of the Moshaneng area, Cullen (1955) described the joint pattern in Black Reef Quartzite as having a "brickwall" appearance. Reconnaissance geological mapping of Moshaneng and surrounding areas was carried out by Crockett (1971c, 1972a and 1972c) and Aldiss et al (1989).

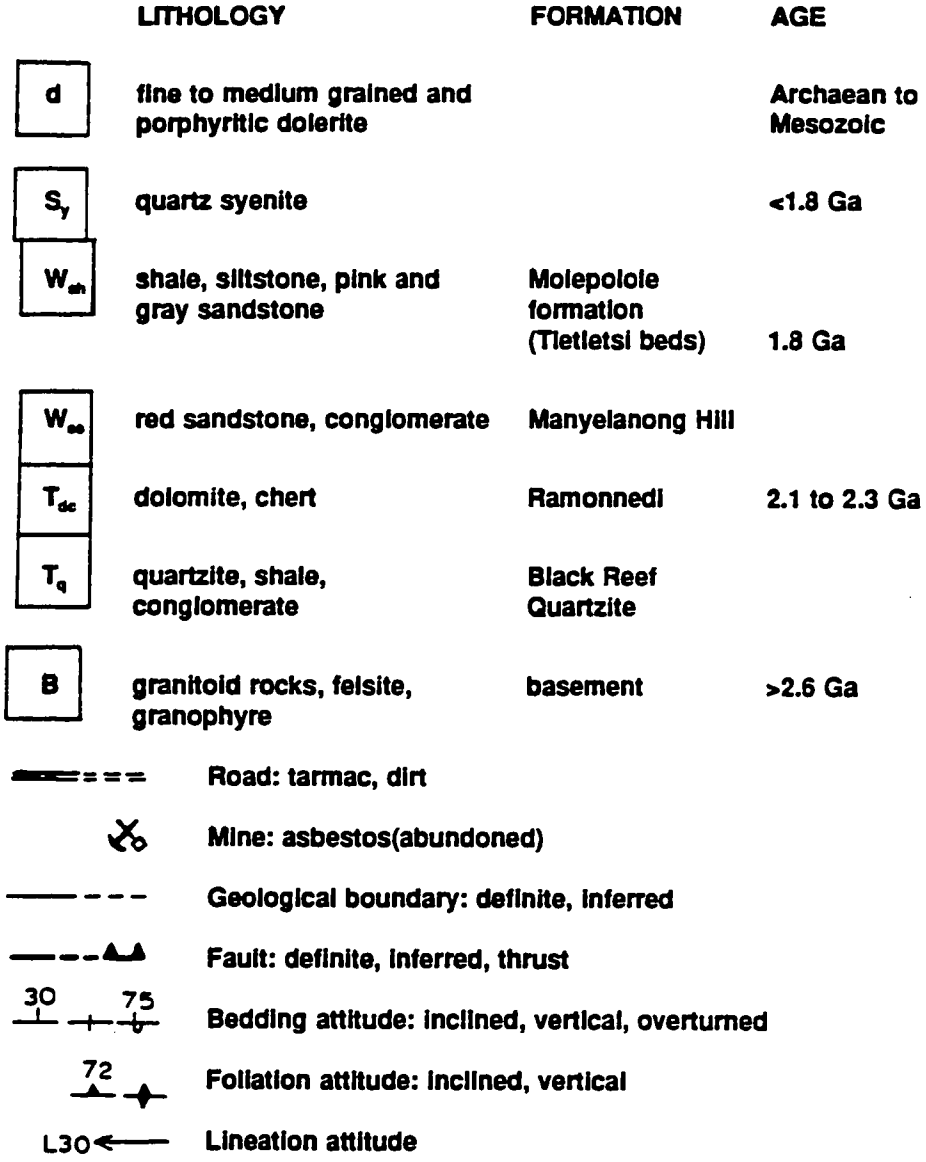

Figure 4.2: Detailed geological map of Moshaneng area. Location in southeast Botswana is shown by box 2 in figure 4.1.

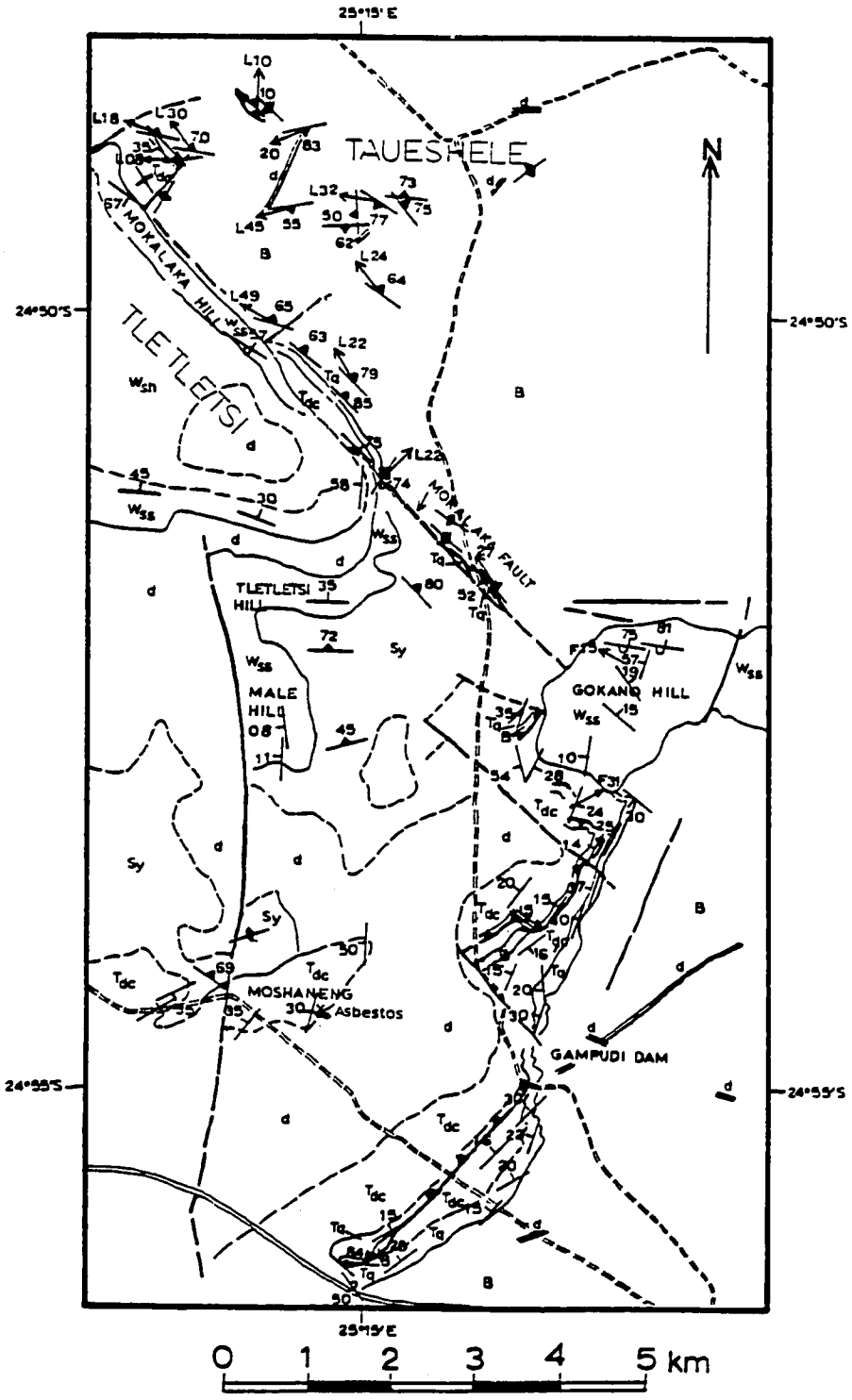
25°15'E
24°50'S
24°55'S
TAUESHELE
TLETLETSI
MOKALAKA HILL
MOKALAKA FAULT
TLETLETSI HILL
MALE HILL
GOKANG HILL
MOSHANENG
Asbestos
GAMPUDI DAM
N
0 1 2 3 4 5 km

Detailed petrographic descriptions are provided in the latter study. Various mapping exercises emphasizing petrography and stratigraphy have been undertaken by students of the Geology Department of the University of Botswana (Monngae, 1989; Moehadu, 1991).

4.2.3 Lithologic relationships and stratigraphy

The regional geology of SE Botswana discussed in chapter 1 incorporates rocks found in the Moshaneng area. The basement consists of Archaean granites, granophyres and felsite of the Gaborone Granite Complex and the Kanye Volcanic Formation. The pinkish, leucocratic, medium-grained, equigranular Kgale granite dominates the basement in the northeastern part of the map area, north of Gokano Hill (figure 4.2). Massive and porphyritic felsites of the Kanye Volcanic Formation occur just below the unconformity with the supracrustals along a 500m wide strip on the NE flank of Mokalaka Hill . Minor occurrences of this rock are also found around Taueshele. The basement in the southeast, south of Gokano Hill consists entirely of feldspar porphyry and felsite of the Kanye Volcanic Formation.

Transvaal Supergroup rocks around Moshaneng form part of the "Kanye Basin", which has been defined by Crockett (1972c). Directly overlying the basement is the basal Black Reef Quartzite Formation. This dark to light grey rock is typically gritty, with graded bedding and ripple marks. The base of the unit consists of discontinuous lensoid conglomerate pockets. The main quartzite unit is locally arkosic and grades

upwards into siltstone and shale at the top of the Formation. The quartzite unit consists of rounded quarts grains with a bluish tint and occasional pinkish feldspar. The quartzite is silica cemented, indurated and breaks across the grains, giving rise to smooth joint surfaces. The maximum thickness of the Black Reef around Moshaneng is about 15 metres. The Black Reef forms a topographic ridge that provides a relatively continuous outcrop. The unit is easily mappable on aerial photographs. The boundary with the basement is enhanced by the termination of east-north-east trending lineaments in the basement against the Black Reef as shown in figure 6.2.

Overlying the Black Reef Quartzite is the dolomite and chert sequence belonging to the Ramonnedi Formation (Aldiss et al, 1989). These unit is correlated with the Malmani Dolomite Sub-group of the Bushveld Basin (Button, 1973b). The dolomite and chert sequence normally occurs on plains with low relief outcrop. The dolomite is typically a dark grey, dense rock that is locally iron-rich. Cathodoluminescence examination reveals zoned carbonate crystals. Concentrations of specularite are locally developed. Stromatolite domes are common where dolomite and chert are thinly interlayered. The lower portions of the sequence are relatively chert free, characterized by massive dolomite in contrast to the upper Moshaneng member. This upper member consists of alternating chert and dolomite beds that range in thickness from 2 to about 30 cm. According to borehole records from previous work, the Ramonnedi Formation is at least 80 metres thick around Moshaneng (Stalker, 1982). A peculiar occurrence in the Moshaneng area is a chert breccia which occurs near the contact of dolomite and the overlying Waterberg sandstones. These deposits

are locally developed at the southern margin of Gokano Hill; their regional occurrence is shown in figure 6.5. Crockett (1972c) has suggested that the formation of the silica preserved in the breccia was related to volcanic activity. He proposes that brecciation occurred as a result the desiccation of precipitated silica gel exposed to the atmosphere during marine regression (Crockett, 1971c, 1972c). It is notable that the brecciation did not disrupt the original sedimentary banding. The evolution of this breccia is discussed in detail in chapter 7. The banded iron formation and the Pretoria Group described in section 1.5.2 and 1.5.3 are completely missing in the area around Moshaneng.

The Transvaal is overlain, with a distinctive angular unconformity by the Proterozoic red beds of the Waterberg Group. Coarse, purple to red poorly sorted sandstone and conglomerate form the lower part of the Waterberg in SE Botswana. The rock has a reddish ferruginous cement and breaks around the grains. These sediments belong to the Manyelanong Hill Formation (Key, 1983). Overturned beds of this formation along the Mokalaka ridge are more than 150 metres thick. Chert clast conglomerates occur at several horizons in this formation and are commonly one clast thick. These are probably terrace sheet deposits. The lower Waterberg in this area was probably deposited in an alluvial plain, separated from surrounding elevated terrains by active or juvenile faults. Thick accumulations of conglomerate of up to 23 metres are present at Kanye Village, a few kilometres to the southeast of the Moshaneng map area (Machacha, 1979). The clasts are mostly derived from the chert breccia and lower Transvaal rocks. In the Tletletsi area (figure 4.2), the middle part of the Waterberg succession consists of greyish to purplish red siltstone and shale with desiccation

cracks and mud rip-ups. These argillaceous sediments are overlain by thin-bedded, fine-grained pale pink quartzite. The overall thickness of these sediments is estimated at over 300 m within the Tletletsi syncline. Sediments similar to these are more extensively developed in the "upper" Waterberg at Molepolole (Jones, 1973b). It is suggested that the informal name *Molepolole formation* be adopted for these deposits until the type locality at Molepolole village is completely described.

4.2.4 Intrusions

4.2.4.1 Dolerite

4.2.4.1.1 Dikes

Dolerite dikes have intruded the basement complex and they could be of several ages. Many NE and ENE trending lineaments have been identified as dikes. Some dikes cannot be traced beyond the unconformity marking the base of Transvaal Supergroup rocks, e.g. near Gampudi dam (figure 4.2). These dikes are therefore considered to be of pre-Transvaal age. Dikes around Moshaneng display a variety of textures ranging from fine grained to porphyritic.

A fine grained dolerite in the basement to the east of Moshaneng has intruded a porphyritic felsite. A 5mm thick outer weathered shell is brown to grey. The freshly broken surface shows dark green randomly orientated needles of amphibole up to 4mm

long against a greenish grey fine to medium grained groundmass. In thin section, the rock consists mainly of altered laths of plagioclase and amphibole in about equal amounts. Accessory opaque minerals appear to be interstitial. The magnetic properties of this dolerite are described in chapter 5, sections 5.1.3 and 5.2.3.1.

Some porphyritic dolerite dikes have been identified parallel to the E-W, and WNW trend. Others have been identified parallel to the NE trend. A WNW trending porphyritic dolerite has intruded into the fine grained dolerite at a location just east of Gampudi dam (Figure 4.2). At Taueshele, porphyritic dolerite is not displaced by a post-Transvaal fault. This shows that the porphyritic dolerite dikes at these locations postdate the pre-Transvaal dikes and belong to a later generation. The weathered surface is greyish brown with grey phenocrysts of feldspar, about 10mm across, forming positive relief. The freshly broken surface is green and displays specks of pyrite. In thin section, the feldspar phenocrysts are altered and some show relict zonation. These are set in a groundmass of finer grained feldspar and amphibole. About 10% of the rock consists of opaque minerals. Some of the magnetic properties of this rock are given in chapter 5, section 5.2.3.2.

4.2.4.1.2 Sills

Dolerite has intruded the Transvaal and Waterberg Supergroup rocks, mostly forming sills. The rock consists mainly of plagioclase and pyroxene with about 5% opaque minerals. These opaques are probably magnetite as indicated by their effect on

the magnetic compass, and the magnetic detritus weathered from these rocks. The lower Transvaal dolomites have been partially metamorphosed to chrysotile asbestos by a dolerite sill. Moshaneng is a site of a now abandoned asbestos mine. According to previous work by Cullen (1955, p.8), serpentine and asbestos have been extensively developed along the top contact of the dolerite intrusion with the dolomite and chert. The bottom contact of the dolerite has remained relatively barren of such mineralization. Dolerite samples collected at the mine gave a K-Ar age of 1,110 ± 55 Ma (Jones and McElhinny, 1966, corrected by Cahen et al, 1984, quoted in Aldiss et al, 1989).

4.2.4.2 Quartz syenite

The quartz syenite is part of an igneous complex that consists mainly of quartz syenite associated with granite, diorite and gabbro. Field observations reveal that these rocks occur in peculiar hybrid forms. In figure 4.3A and 4.3B, a mosaic of basic rock blocks is invaded by leucocratic quartz syenite. Generally, the core of the complex consists of gabbro and diorite located about 1 km east of Male Hill. Surrounding this core are granite and quartz syenite that occur over a wider area as mapped (Sy) in figure 4.2.

Nowhere is the syenite seen in contact with the Waterberg rocks and therefore its age in relation to these rocks is unknown. The Moshaneng igneous complex may be coeval with the Segwagwa intrusion further south (see figure 6.5 for the location of

Figure 4.3A: Leucocratic quartz syenite invading a basic rock in a stream channel NE of Moshaneng Village.

Figure 4.3B: Leucocratic vein network of quartz syenite invading a gabbro near the core of the Moshaneng igneous complex.

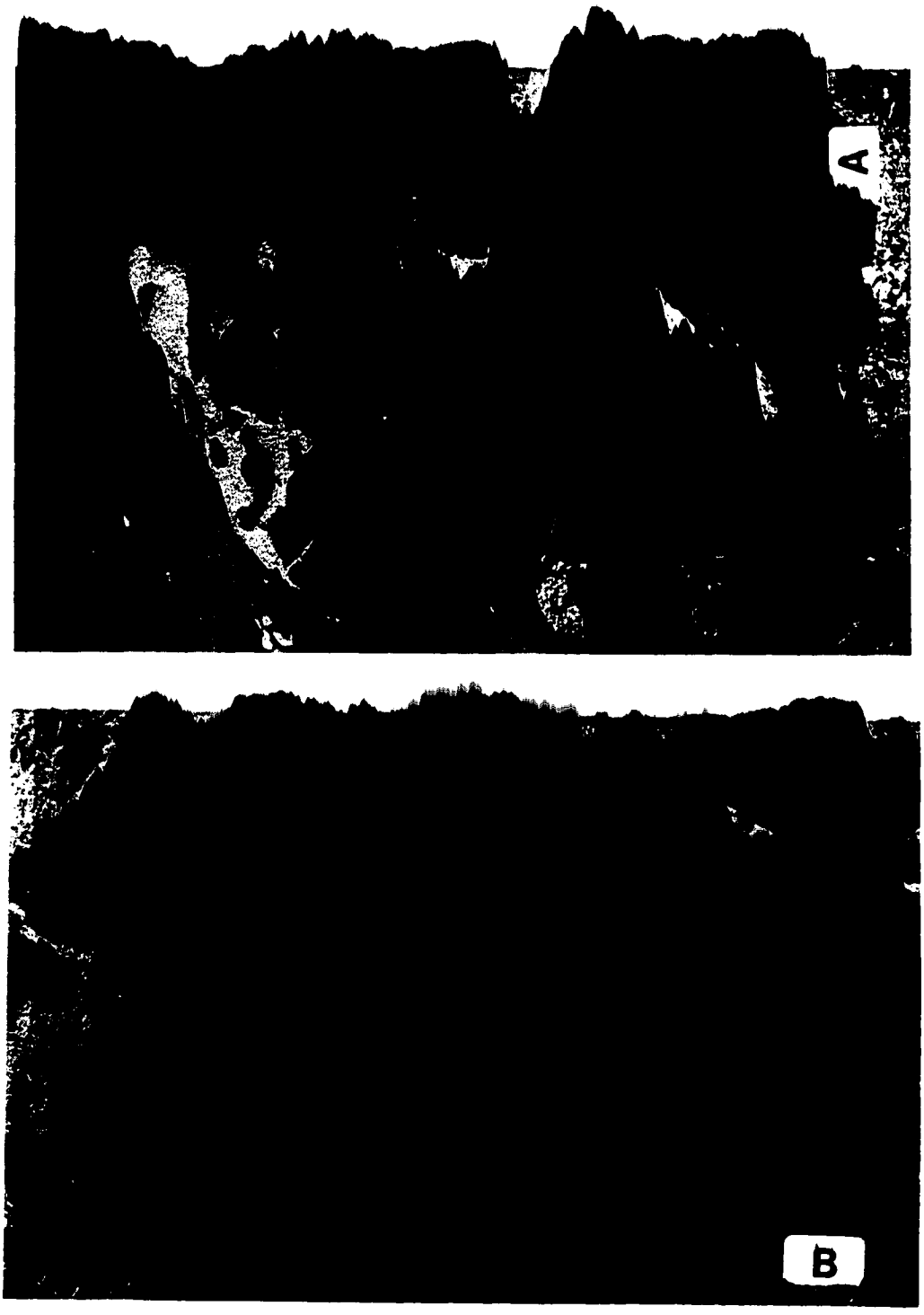
A
B

Segwagwa), which is similar in appearance but of a more mafic appearance. However, the Segwagwa syenite is intruded by dolerite. Three Rb-Sr whole rock and two K-Ar hornblende age determinations have been carried out on the Segwagwa syenite intrusion. Two of the whole rock ages were around 1,900 Ma., while the other one gave 910 ± 105. As all the samples were collected within 8 km of each other over the intrusion, they were assumed to be co-genetic (Key, 1977). The last much younger age was therefore thought to be erroneous. The two hornblende ages gave an age of 1,805 to 1,908. It has been suggested that an age of about 1,900 Ma for the syenites may typify them as a western extremity of the Bushveld Complex acid intrusions centred in South Africa (Key,1977; Tankard et al,1982).

4.2.5 Structure and tectonics

During the present study, detailed structural mapping was undertaken in the area around Moshaneng (figure 4.2). The tectonics of the Moshaneng area have always been enigmatic based on geological mapping by R.N.Crockett (1972a) and later by D.T.Aldiss et al, (1989). As indicated elsewhere, the Proterozoic sediments in Botswana have suffered little plastic deformation, but at Moshaneng vertical and overturned beds are displayed. The area has also been intruded by dolerites, granites and syenites. Crockett (1972a) has inferred the action of horizontal compression from the occurrence of thrust faults around Moshaneng. The thrust faults were thought to be the result of igneous intrusion (see section 2.2). The Tletletsi syncline in the northern

part of the Moshaneng area has been interpreted to indicate collapse of the crust into a graben-like feature. Aldiss et al (1989, p.130) have suggested that the collapse was into the magma chamber that produced the dolerite intrusions around Moshaneng. The Waterberg sediments and dolerite sill were folded over vertically displaced blocks in the basement in two monoclines that intersected to the southeast of the synclinal fold at Tletletsi.

It seems probable that the Moshaneng tectonics are related to a regional strike-slip fault. A hypothesis involving strike-slip faulting, transpression and thrust faulting is discussed further in chapters 8 and 9 for Tletletsi and surrounding areas.

The equi-granular Kgale Granite of the Gaborone Granite Complex that flanks the Tletletsi "syncline" contains a steeply dipping foliation. The fabric trends in a northwest direction. This foliation is absent as one moves away from the contact with the Waterberg rocks and into the main body of the granite. The fabric is aligned along a major lineament that can be traced for about 100 km along strike northwestwards towards Jwaneng (figure 1.3). This lineament is interpreted to be a strike slip fault to which some of the structures in eastern Moshaneng are parasitic. It is noted here that this structural trend is found in the Limpopo Mobile Belt further northwards, and in regions further to the south of the present area of study. The chronological bracket for movement along NW trending fractures around Moshaneng is discussed in chapter 6. It is interesting to note that the lineament that connects Gokano and Mokalaka Hill can be traced continuously through to the Jwaneng kimberlite province further northwest (see figure 1.3 for the location of Jwaneng). Are the alkaline intrusions of syenite and

kimberlite related to this lineament? A full account of the structural geology of Moshaneng and the surrounding areas is given in the remaining chapters of this thesis.

4.3 Otse West

4.3.1 Introduction

Outcrops of Nnywane Formation argillite of the Lobatse Volcanic Group (section 1.4) are located in an area about 11 km west of Otse Village (figure 1.4) at about 25° 03'S and 25° 40'E. A grid of 300 x 200 metres was cut in this thickly vegetated location at 10 metre intervals to facilitate detailed mapping. A structural map of a 20,000 m^2 area shown in figure 4.4 was produced. Folds of various shapes are developed in the argillites of the Nnywane Formation which belongs to the Ventersdorp Supergroup. The general geology of the area around Otse is incorporated in the reconnaissance map and district memoir of the Gaborone and Lobatse areas (Key, 1983). Other work has been undertaken for training purposes by geology students of the University of Botswana (Siamisang, 1987; Ratsoma, 1988).

4.3.2 Nnywane Formation argillite

The Lobatse Volcanic Group shales were deposited some 2.6 to 2.3 billion years ago. A general description of these rocks is given in chapter 1, section 1.4. For the

Figure 4.4: Geological map of folded and fractured argillite 11 km west of Otse Village (see figure 4.1 (box 4 for location in SE Botswana)).

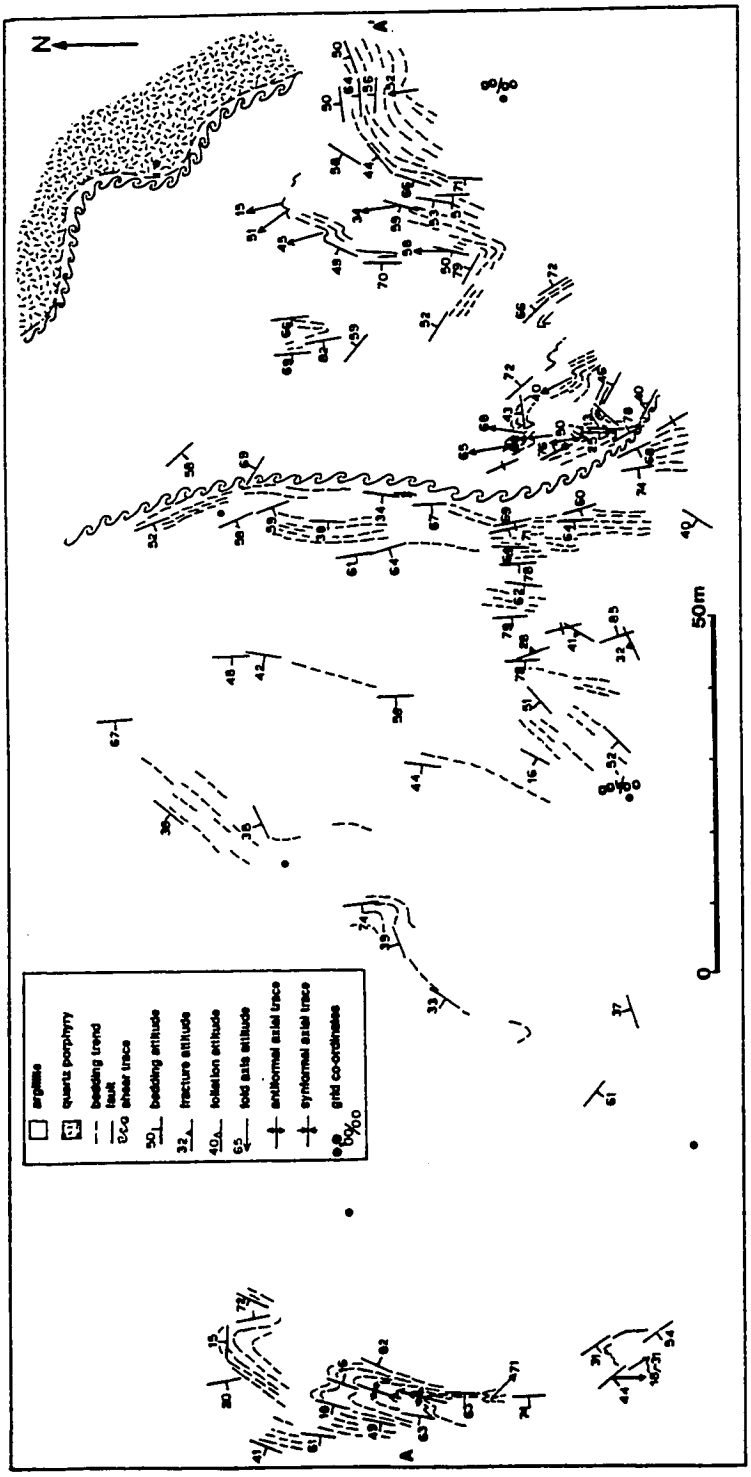
N
A
A'
50m
0
argillite
quartz porphyry
bedding trend
fault
shear trace
bedding attitude
fracture attitude
foliation attitude
fold axis attitude
antiformal axial trace
synformal axial trace
grid co-ordinates

most part, rocks of the Lobatse Volcanic Group succession displays open folds. Laminated argillites belonging to the Nnywane Formation, however, display some tight folds with a complicated pattern of tension fractures (figure 4.4, 4.5 and 4.6). The argillite displays fine laminations consisting of graded beds ranging in thickness from less than a millimetre to a few millimetres. A grain size of less than 30 microns shows that these dark grey sediments are siltstone, consisting mainly of quartz, sericite and other rock fragments. Contiguous with this rock is an intrusion of quartz porphyry belonging to the Plantation Porphyry Member of the Nnywane Formation. The argillite closest to the porphyry has spotted mineralization that decreases in abundance away from the intrusion, indicating contact metamorphism. In fresh samples, the mineralization is identified as andalusite, occurring in 1-2 mm long laths. In less fresh samples, the andalusite has been replaced by an opaque substance, probably due to alteration and oxidation.

4.3.3 Structure

Detailed data on the attitudes of bedding, fold axes, foliation and tension veins and cracks were obtained and some of these data were used to produce the structural map shown in figure 4.4. A very shallow foliation is developed in the argillite near the contact with the quartz porphyry. The quartz porphyry at the contact has been strongly sheared indicating a tectonic contact between the two lithologies.

Folds in these rocks vary from open types, some displaying box-like

Figure 4.5: Cross-section A-A' in figure 4.4 of the geology of Otse West. Folded extensional fractures are stylized on steep limbs below the footwall of the shear plane. The mapped section shows at least 32% shortening due to folding.

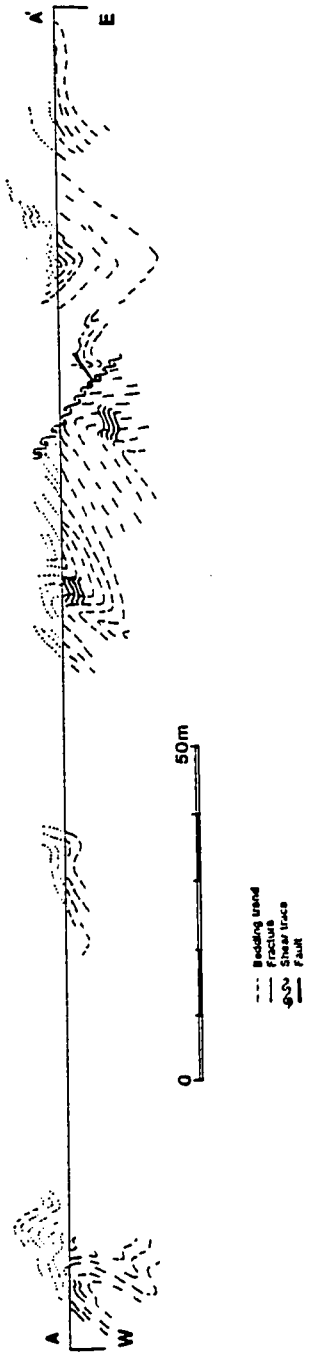
A'
E
A
W
50m
0
Bedding trend
Fracture
Shear trace
Fault

characteristics, to tight isoclinal folds (figure 4.6A and 4.7A). The dominant fold mechanism is buckling. Layer-parallel flexural slip occurred in discrete bedding plane surfaces which became infilled with secondary mineralization, mainly sericite, and probably also talc. The result gives the impression that the rocks are thickly bedded. Axial plane foliation has not been developed where this mechanism of folding is involved. The outer arcs of individual folded layers show tension cracks around the hinge areas. Contorted cracks form in the inner arcs. Heterogeneous simple shear and ductile flow probably affected the more tightly folded layers that show thinning in the limbs. Horizontal shortening by folding alone between A and A' in figures 4.4 and 4.5 is estimated to be at least 32%.

All the minor parasitic folds in the area of study have fold axes that trend N to NNW (mean azimuth of 350°). Folds in argillite to the east of the shear zone plunge to the north ranging from a shallow 15^ to a relatively steep 71°. Folds in the far west of the area plunge to the south (figure 4.8A). The fold axes are distributed along a vertical plane. These angular relationships suggest that folds on either side of the shear zone were contemporaneously formed under the same far field σ_1 direction.

The overturned fold in the western end of the area has a N-S trending horizontal fold axis (figure 4.8B). The overall fold is tight with an interlimb angle of 40°. Minor parasitic folds associated with this overturned fold plunge to the south as shown above. The middle portion of the study area is dominated by moderate dips to the west with a few steep near vertical dips. In figure 4.5 it is shown that these attitudes represent tight east-facing folds.

East of the shear zone a tight synform and small box-like antiform pair are exposed (figure 4.6A and 4.7A). The synform/ antiform pair of folds has a NW trending fold axis with a moderate plunge (328/50) (figure 4.8C). The dominant structure to the east of the shear zone however is an open synform. The attitude of this fold axis (340/40)(figure 4.8D) is similar to that of the synform/ antiform pair.

The disparity between the trend of the major folds (NW) and the minor folds (NNW-SSE) shows that the folding mechanism was non-cylindrical. This is also shown by the non-parallelism among the minor folds axes.

En echelon tension cracks were formed in the individual folded layers between the slip surfaces. These cracks were infilled with secondary mineralization, mainly sericite. In some locations, the tension cracks had become extended across primary layering slip surfaces and have been folded (figure 4.6B and 4.7B). It is apparent that with progressive deformation, tension cracks imparted a local anisotropy to the rock and nucleated new folds with continued buckling. These tension- crack- bounded layers are called "pseudo-bedding" in this study. The folds formed by the fractures are not the typical *S*-shaped sigmoidal tension cracks formed by the propagation of crack tips during simple shear deformation (Ramsay and Huber, 1983, p.24). The folds are buckled "pseudo-bedding" layers. These fractures were probably folded due to their rotation to higher angles with fold layer boundary and simultaneous thinning of the fold limb. The folded fractures were identified only in the near vertical layers below the footwall of the fault shown in figure 4.5, near the anticlinal hinge of tight folds. A schematic representation of this mechanism is provided in figure 4.9B.

Figure 4.6: **A** Folds in argillite within the Nnywane Formation of the Lobatse Volcanic Group, 11 km west of Otse Village. An open box-like antiform on the right is separated from a tight synform on the left by an inclined fault. Folding occurred mainly by buckling involving layer-parallel flexural slip along primary bedding surfaces. Slip surfaces are sites of secondary sericite in-filling, giving rise to apparent thick beds in otherwise finely laminated argillite. Gross fold geometry is non-cylindrical. The spiral note book provides a scale. See figure 4.7A for trace of structures described.

B En echelon talc-sericite-filled extension fractures in argillite. The left hand side of the photograph shows that the extension fractures have been folded. Trend of primary layering of the laminated siltstone is indicated by the Brunton compass. See figure 4.7B for trace of structures.


A
B

Figure 4.7: Trace structures described in figure 4.6A and B

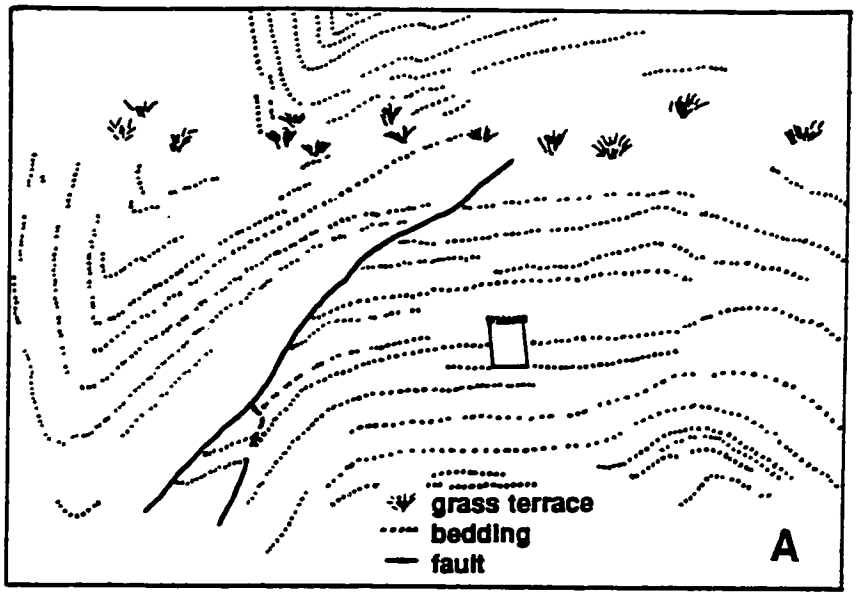
grass terrace
bedding
fault
A

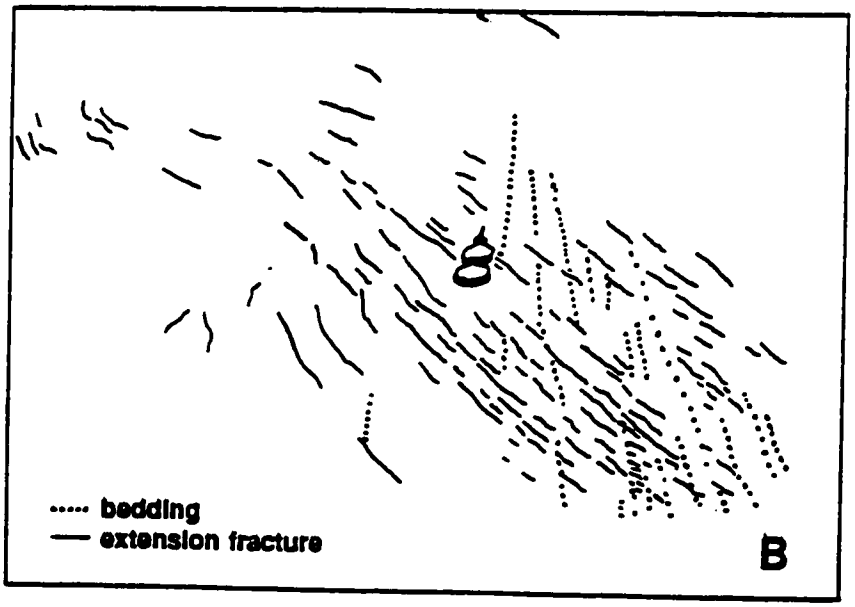
bedding
extension fracture
B

Figure 4.8: Stereographic projections of fold structures in the Lobatse Volcanic Group Argillite 11 km west of Otse Village. **A** Fold axes of minor parasitic folds. The north plunging axes were obtained in the hanging wall block of the shear zone mapped within the argillite (figure 4.3). The south plunging axes were obtained from the far west folds. **B** Poles to bedding of a horizontal, overturned, isoclinal antiform in the far west portion of the map area. Interlimb angle is about 40°. **C** Poles to bedding of a NW plunging antiform and synform pair shown in figures 4.6A and 4.7A. Fold axis is 328/50. These folds occur just to the east of the shear trace in figure 4.4). **D** Poles to bedding of the dominant NW plunging synform in the hanging wall block in the east of the map area. Interlimb angle is about 85° and fold axis is 340/40.

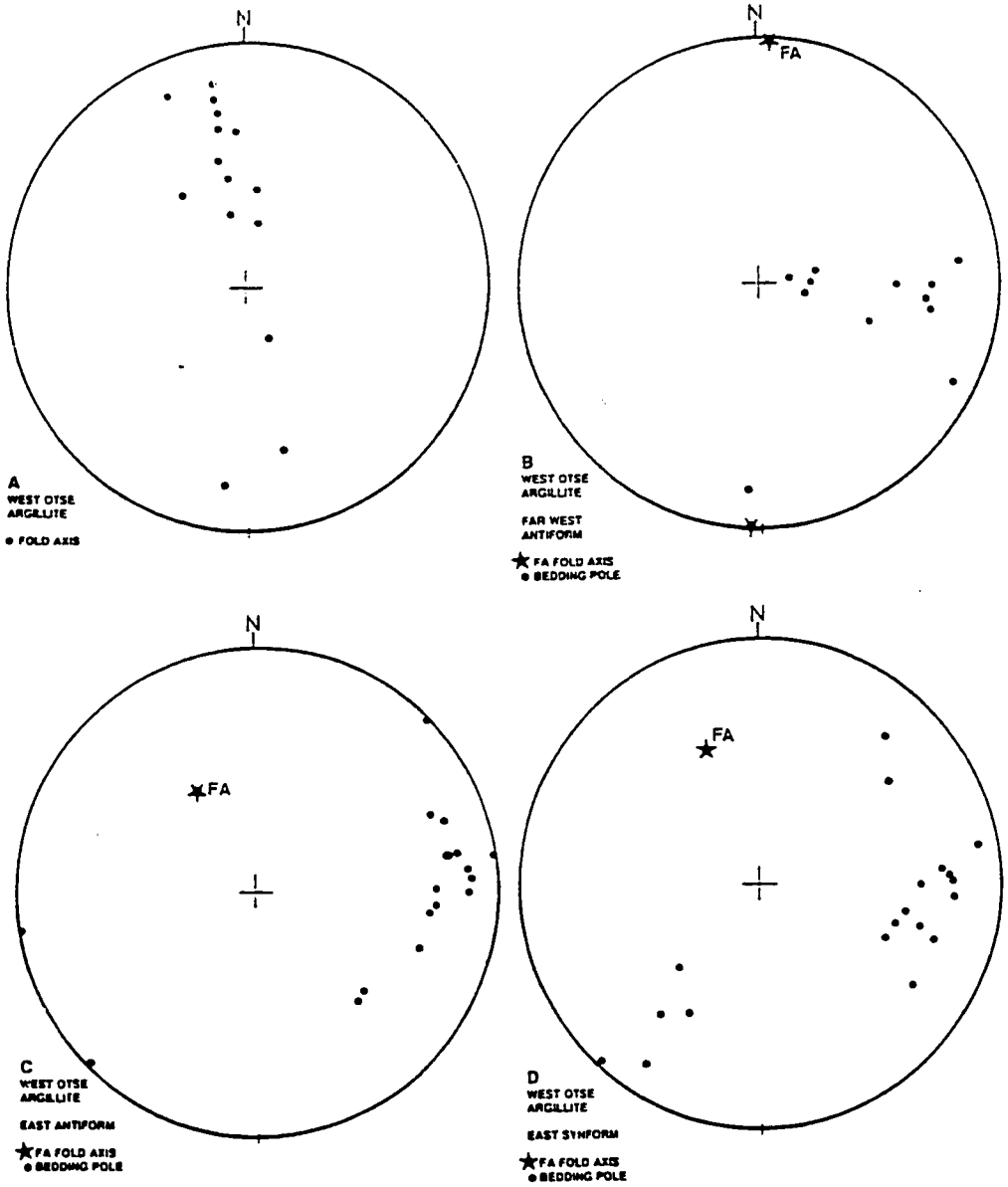
N
A
WEST OTSE
ARGILLITE
● FOLD AXIS
N
FA
B
WEST OTSE
ARGILLITE
FAR WEST
ANTIFORM
★ FA FOLD AXIS
● BEDDING POLE
N
FA
C
WEST OTSE
ARGILLITE
EAST ANTIFORM
★ FA FOLD AXIS
● BEDDING POLE
N
FA
D
WEST OTSE
ARGILLITE
EAST SYNFORM
★ FA FOLD AXIS
● BEDDING POLE

The geometry displayed by these structures demonstrates that mechanical properties of a rock may change during progressive deformation, giving rise to the coexistence brittle and ductile structures. In this case the deformational environment is dominated by plastic flow; but then brittle structures became intimately involved with the plastic deformation. The extent to which these mechanical changes influence the gross geometry of a folded sequence may be evaluated in this area.

The fracture\bedding intersection determined at three locations trends N to NNW, plunging gently from 08° to 33° (figure 4.9A). This orientation is similar to that of parasitic folds in the eastern part of the map area (figure 4.8A). The collinearity of the structures suggests that they were formed under the same stress field. The fold axis determined from the limbs of folded fractures trends NE with a moderate plunge of about 23°. The orientation differs from that of the bedding\fracture intersection, the parasitic folds and the larger folds.

Folding of the bedding planes was probably initiated before that of the fracture surfaces. This observation on the relative chronology of folding of the two layer types is supported by the greater severity of tight folding of the beds in contrast to that of the gently folded fractures. In addition, limbs that display talc and sericite-filled, bedding-parallel slip surfaces have not developed folded fractures. These latter limbs buckled by the bedding-parallel flexural slip mechanism. Such folds are shown in figure 4.6A. The middle part of figure 4.5 in which the folded fractures are developed dislplays tight folds.

The nucleation of folds along fracture surfaces and eventual buckling probably

Figure 4.9A: Great circles of bedding (solid lines) and fractures (dashed lines) in the West Otse argillite. The solid square symbol show the intersection of bedding and fractures at 3 locations(346\33, 350\38 and 360\08). The solid round symbol is the ß intersection of folded limbs (038\20 and 045\26) of fracture surfaces. Interlimb angle is about 120°.

Figure 4.9B: Schematic diagram of the mechanism of heterogeneous simple shear and ductile flow in the limb of a fold. **i)** Mode **I** tension gashes develop in the fold limb as deformation progresses. **ii)** Continued ductile flow and thinning in the fold limb induces buckling of the tension gash set which represents a new mechanical anisotropy in the rock, resulting in folded fractures.

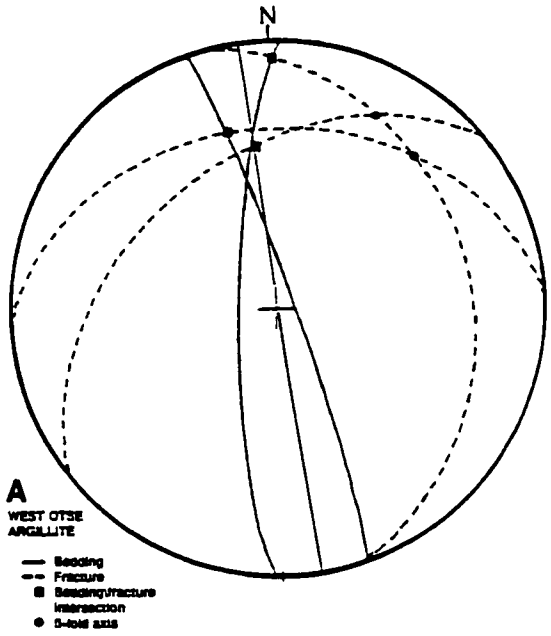
N
A
WEST OTSE
ARGILLITE
Bedding
Fracture
Bedding/fracture intersection
B-fold axis

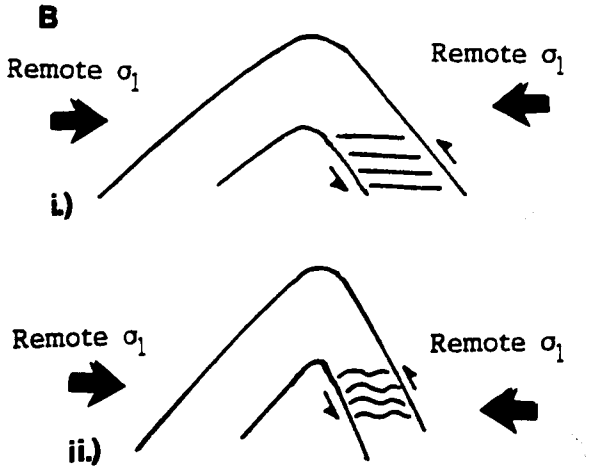
B
Remote σ_1
Remote σ_1
i.)
Remote σ_1
Remote σ_1
ii.)

occurred during progressive deformation under the same far-field stress system. The compatibility of the folds and the fractures supports this view. These structures can be regarded as having been formed at two different stages of progressive deformation. The fold trains formed by the folded fractures are irregular and cannot be traced as systematically throughout the argillite. They are mainly restricted to the exposures just below the thrust fault. The orientation of fold axes of the main folds were formed at the initial stages of deformation. The parasitic folds and the folded fractures were formed at a later stage in the deformation.

Faults were also developed during the deformation of these sediments. The fault near the central part of the map dips at 40° to the east and trends N to NNW. In figure 4.5, this east-dipping fault (shear trace) truncates a west dipping fault trace. It is inferred that the west dipping fault is an early dextral reverse fault. The east-dipping fault is a younger sinistral reverse fault. The two fault traces represent a conjugate system according to Andersonian geometry.

4.4 Conclusion

In Moshaneng, a regional fault, Mokalaka Fault, is mapped along the NE margin of the Tletletsi syncline. Strike-slip movement on this fault has given rise to parasitic structures such as thrust faults in the SE part of the area. Later reactivation caused dip-slip faulting in the NW portion. These features result from oblique total displacement on a fault that terminated in eastern Moshaneng. The recognition of

strike- slip motion provides new insight into the evolution of brittle type structures in SE Botswana. These types of structural associations and their interpretation are discussed in chapters 8 and 9.

Structural investigations in argillites of the Nnywane Formation of the Lobatse Volcanic Group indicate that the complex folding and fracturing are probably local phenomena. The deformation of intraformational tension crack sets into buckled folds differs from that normally encountered in incipient shear zones. The latter form of tension cracks are discussed in chapter 8. The style of tension fracture deformation is compared in the two areas. The west Otse argillites show that mechanical changes in rock can yield a close association of ductile and brittle structures during progressive deformation.

CHAPTER 5: GEOMAGNETICS

5.1 Magnetic surveys

5.1.1 Aeromagnetics around Moshaneng and Kanye

Areas around Moshaneng and Kanye fall within sheet 7: contour map of the reconnaissance aeromagnetic survey of western Botswana, compiled by Terra Survey (1976). These areas are shown in figure 5.1 which incorporates the northern portion of the present area of study. The contour map sheets are published at a scale of 1:500,000. The contours were drawn from data that was collected continuously along north-south flight lines spaced at 4 km. The flying height was 300m above ground. Datum is the International Geomagnetic Reference Field 1980, epoch 1986.0. minus 1,000 gamma. The total intensity of the earth's magnetic field is about 29,350 nT in SE Botswana. Inclination is -65°.

The ENE trending pre-Transvaal dike swarm proposed by Aldiss (1986) is not readily apparent on these maps. This is probably due to the scale of the map and the rather wide flight line spacing. Ground magnetic traverses across the proposed dikes in an area underlain by the Gaborone Granite and basement metamorphic rocks outside the present area of study yielded no response from such dikes (Aldiss, 1985 and

Figure 5.1: contours of total magnetic intensity of quarter degree sheet 2425C, a portion of sheet 7 of the reconnaissance aeromagnetic survey of western Botswana (Terra Survey, 1976). **M**=Moshaneng village, **K**=Kanye village and **Mh**=Mheelo Fault. Datum=International Geomagnetic Reference Field minus 1,000 gamma. Contour values are given in gamma; datum is International Geomagnetic Reference Field 1980, epoch 1986.0 minus 1,000 gamma. Contour interval is 50 gamma.

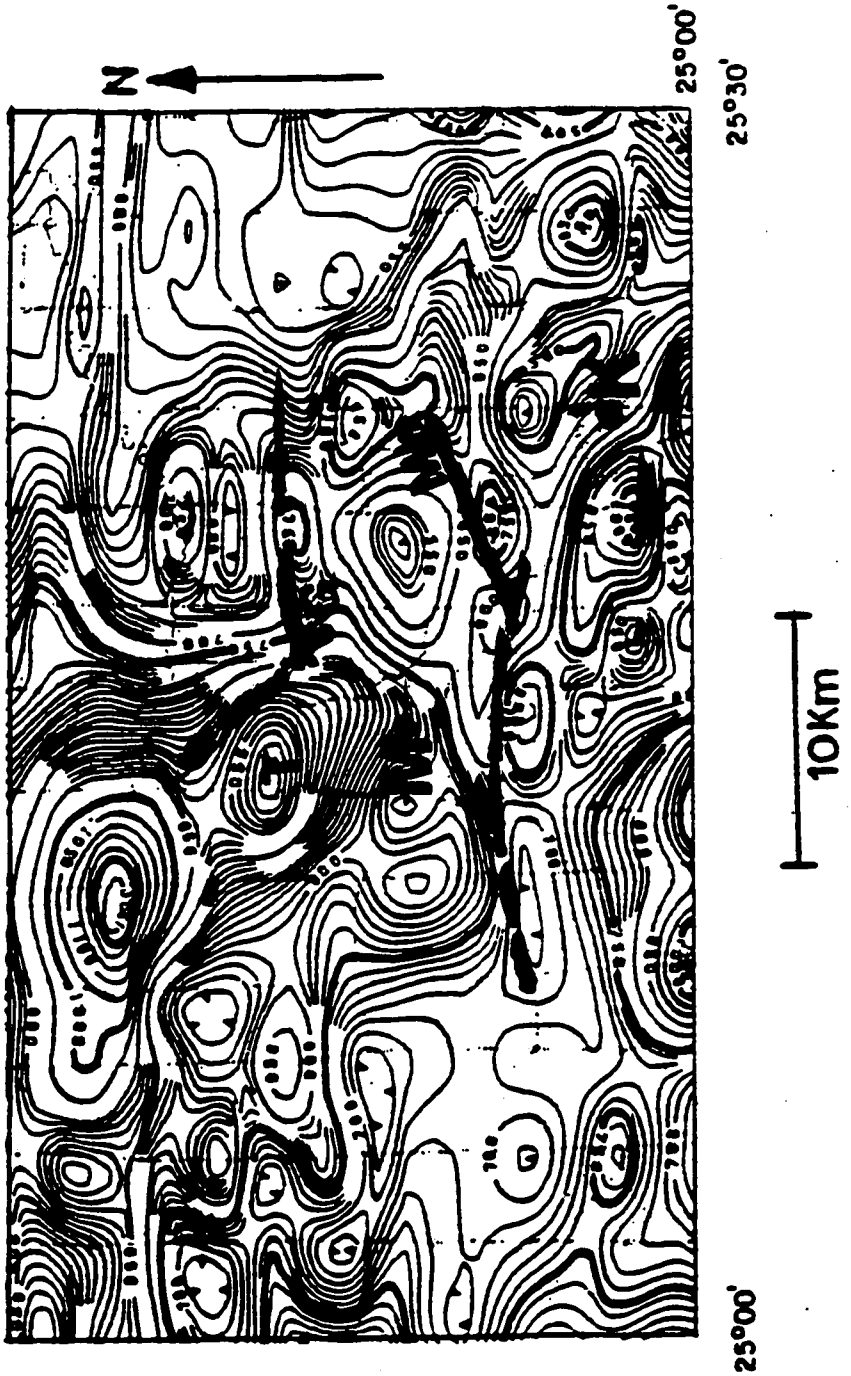
N
25°00'
25°30'
25°00'
10Km

1986). This lack of response has been attributed to deep weathering, hydrothermal alteration and lack of magnetic susceptibility contrast with the country rock.

The area of Archaean basement surface occurrence shows some magnetic relief; but the scale of the contour maps does not permit accurate comparison with surface lithologic variations. Some general correlations and comments are pertinent, however. The basement exposed in the area between Moshaneng (M) and Kanye (K) corresponds to low magnetic intensity values: lower than 550 gamma (figure 5.1). The magnetic high just south of the ENE trending Mheelo Fault (Mh), immediately NW of Kanye coincides with a dolerite sheet. A NW-SE trend in the magnetic anomalies in the SE quarter of figure 5.1 could be a reflection of the trend of lithological layering. The boundary between the Archaean basement and Proterozoic layered sequences follows this trend.

The area around Moshaneng is marked by an elliptical magnetic anomaly of >950 gamma centred on the Tletletsi syncline (T). The magnetic anomaly is probably associated with post-Waterberg dolerite intrusions. The northeastern flank of the anomaly is marked by a fault and monocline. A stronger anomaly of >1,300 gamma is located around Taueshele further north of the Tletletsi syncline.

An E-W trend in the magnetic contours is apparent. This trend marks post-Waterberg faults, some of which are associated with monoclines. The mapped fault on the northern flank of Gokano Hill (G) coincides with one of these trends (figure 5.1). The E-W faults and monocline to the south of Moshaneng that separate the Transvaal exposures to the north from the Waterberg to the south are also marked by a lineament

on the magnetic contour map.

5.1.2 Aeromagnetics south of Kanye

The area to the south of Kanye forms part of quarter degree sheet 2525A of the airborne magnetic survey of eastern Botswana (Stolberg, 1987). This survey was flown along north-south flight lines spaced at 1 km. Flight elevation was 150m above ground. Datum is the same as for sheet 7 above. The maps are published at 1:125,000 and can be more accurately related with the geology. The part of the study area represented on this map is shown in figure 5.2.

The ENE lineaments which are so prominent on aerial photographs (figures 6.1, 6.2 and 6.3) cannot be related to any feature of the magnetic contour map. This suggests that only a few of the lineaments are dikes; most of them are fractures.

In the eastern half of figure 5.2, a broad northwest trending ridge of positive magnetic anomalies corresponds to the distribution of the Kanye Volcanic Formation (KVF). The anomaly is horizontally displaced by about 4 km in a dextral sense along the Taupone Fault trace (TF). A ridge, 8 km further NE is not similarly displaced. This ridge has been mapped as medium grained Kgale Granite with exposures of finer grained Ntlhantlhe Microgranite along its axis further to the SE (Key, 1983). This suggests that the Taupone Fault does not continue much further in the NE direction. About 2.7 km northwest of the Taupone fault trace, the Kanye Volcanic Formation has again been displaced by about 0.5 km along another fault trace. The Nneneke Fault

Figure 5.2: Contours of total magnetic intensity of a part of quarter degree sheet 2525A of the airborne magnetic survey of eastern Botswana (Stolberg, 1987). The village of Kanye is given at the top of the map for comparison with figure 5.1. **MC**=Masoke Complex, **GG**=Gaborone Granite, **KVF**=Kanye Volcanic Formation, **TS**=Transvaal Supergroup, **VS**=Ventersdorp Supergroup, **TF**=Taupone Fault and **NF**=Nneneke Fault. Contour values are given in gamma; datum is International Geomagnetic Reference Field 1980, epoch 1986.0 minus 1,000 gamma. Contour interval is 10 gamma.

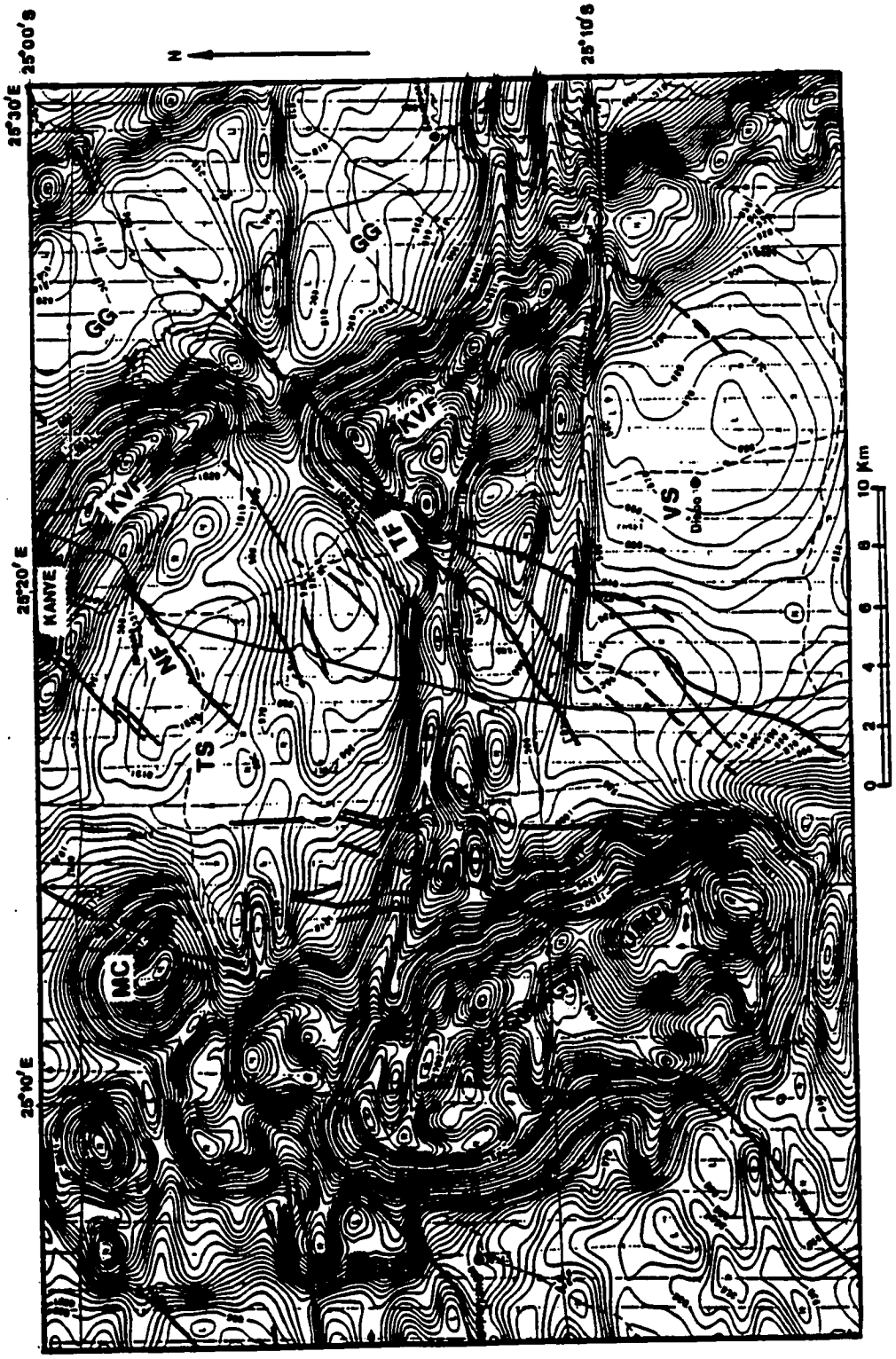
25°30'E
25°00'S
N
25°10'S
GG
GG
KVF
KVF
TF
KANYE
NF
TS
VS
Diabo
MC
25°20'E
25°10'E
0
2
4
6
8
10 Km

trace (NF), about 8.5 km northwest of the Taupone Fault displaces the Black Reef Quartzite by about 1.5 km (see figure 6.5); but does not displace the Kanye Volcanic Formation anomaly. This suggests that the Nneneke Fault does not persist much further in the northeast direction either.

In contrast to the KVF anomaly, the Gaborone Granite (GG) corresponds to regions of low magnetic relief and values of less than 860 gamma. The textural variety is mainly the Rapakivi Thamaga Granite. Areas of Transvaal Supergroup (TS) and Ventersdorp Supergroup (VS) surface occurrence are also characterized by low relief; but slightly higher total intensity with values greater than 860 gamma.

An E-W trending lineament revealed by SPOT imagery coincides with the southern boundary of a belt of aeromagnetic anomalies. This belt can be traced from the eastern boundary of the Segwagwa Complex for more than 25 km eastwards. The belt is about 7 km wide and consists of two positive E-W ridges with an intervening negative valley. A magnetic depression occurs where the southern boundary of the anomaly intersects the Kanye Volcanic Formation anomaly. At a location near the eastern margin of figure 5.2, porphyritic dolerite is exposed near the confluence of two rivers. It has been suggested that the E-W anomaly corresponds to a layered mafic igneous complex (Tombale, personal communication). The linear expression of this anomaly suggests the presence of dikes. The Kanye Volcanic Formation anomaly is displaced where the southern boundary of the belt intersects it, suggesting the presence of an E-W trending fault. This fault trend is post-Waterberg elsewhere in the study area. The E-W feature was probably formed later than the main movement on the

Taupone fault since neither this fault nor any of its branches displaces the feature. Another linear E-W positive magnetic anomaly can be traced from the northern lobe of the Segwagwa Complex, through the point where the Taupone Fault displaces the Kanye Volcanic Formation, to the eastern end of the Figure 5.2. The anomaly corresponds to a SPOT image lineament, but no exposures have been associated with it.

The Segwagwa and Masoke (MC) intrusions coincide with prominent positive magnetic anomalies with peaks >1,500 gamma. The southern part of the Segwagwa Complex anomaly has been sculptured by N-S trending faults on its eastern and western flanks. These faults probably controlled the igneous activity. The western limit of the Segwagwa intrusion is remarkably linear in the N-S direction and extends further north of the known surface distribution of the complex. This linear feature may indicate the presence of more major N-S trending, steeply dipping faults on the western flanks of Segwagwa.

5.1.3 Surface ground magnetic profile

The best exposure of one of the NE and ENE trending dikes in the study area is located about 10 km NNW of Kanye and about 6 km due east of Moshaneng (figure 4.1). Aerial photo lineaments parallel to this dike cut the Ventersdorp Supergroup age Lobatse Volcanic Group (2.6 Ga); but are overlain by the Transvaal Supergroup (2.3 Ga). The locality was chosen as the site for a ground magnetic traverse to determine

the contrast in total magnetic intensity between the dolerite dike and the Kanye Volcanic Formation. The exposed width of the dike at the site is about 50 m and it can be traced along discontinuous exposures for 3 km. The dike trends approximately 45°E. It consists of dark green fine grained dolerite with visible amphibole laths. The Kanye Volcanic Formation consists of feldspar porphyries set in a fine felsitic matrix.

The traverse was performed using a *SCINTREX* MP-2 portable proton precession magnetometer. A 200m profile was produced with readings of total magnetic intensity taken every 2m along a traverse with azimuth 135°E.

The magnetic profile is shown in figure 5.3. A negative anomaly, several hundred gamma below that measured over the Kanye Volcanic Formation was determined. The negative anomaly is consistent with magnetic susceptibility readings shown in table 5.1.

The magnetic profile was modelled using the Geosoft MAGMOD IBM programme. A best fit of the data produced the hidden magnetic body as shown in figure 5.4. This best fit model shows that the dike is buried some 9.93 metres below surface, is 90.2 metres wide and dips 79° to the south. This model is inconsistent with the ground observation that the dike is exposed at the surface. Several factors could account for this inconsistency, among them being 1.) The dike may not be magnetically homogeneous. 2.) The upper few metres of the dolerite may be heavily weathered or altered. 3) Closely spaced and thinner dolerite dikes may have intruded near the northwestern contact of the main dike while the MAGMOD programme can only model one dike at a time. The measured profile is noisy just to the northwest of

Rock type	Mean magnetic susceptibility $x10^{-6}$ c.g.s. units	Number of samples
Fine grained dolerite (dike)	71	14
Porphyritic dolerite (dike)	2487	8
Syenite (Moshaneng area)	760	1
Syenite (Moshaneng area)	918	1
Granite (Kgale Granite)	412	1
Granite (Kgale Granite)	4	1
Porphyritic granophyre (Kanye Volcanic Formation)	4381	1
Sheared granophyre (Kanye Volcanic Formation)	15	1

Table 5.1: Magnetic susceptibility of selected igneous rocks sampled from the Moshaneng area. The susceptibility was measured on cores of 1 inch diameter and 0.85 inch height.

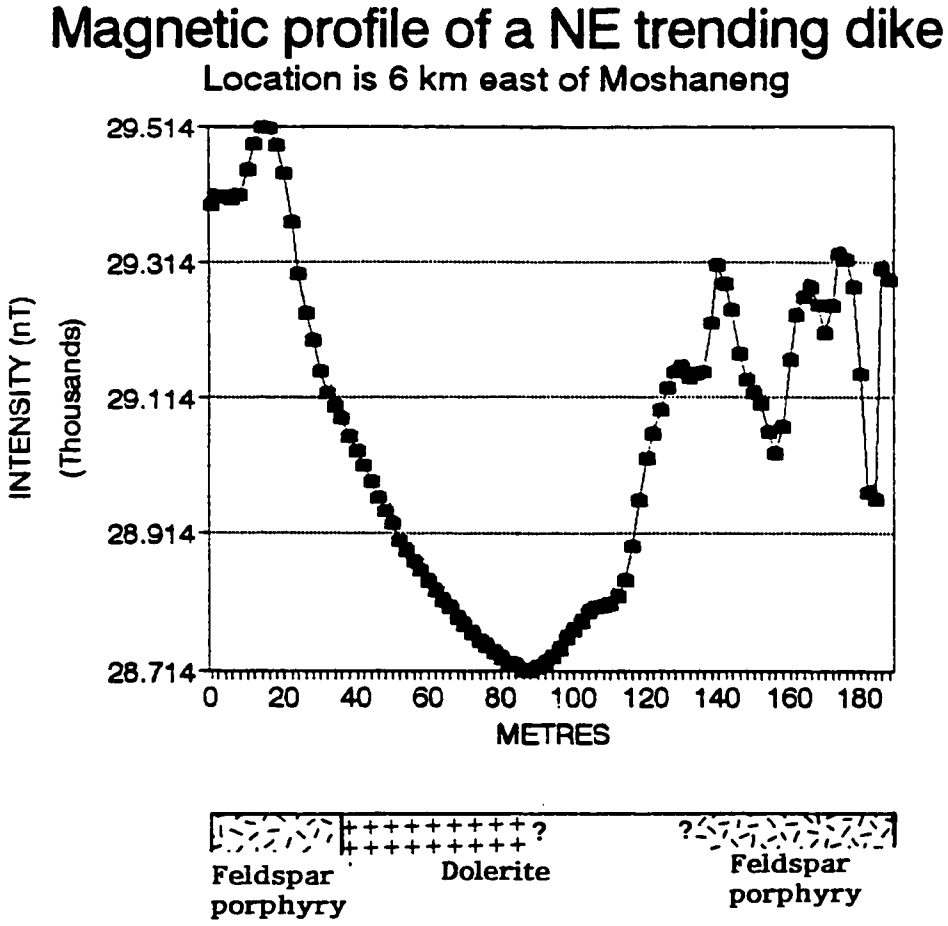

Figure 5.3: Total magnetic intensity profile over an exposed northeast trending dike, 10 km NNW of Kanye and 6 km east of Moshaneng.

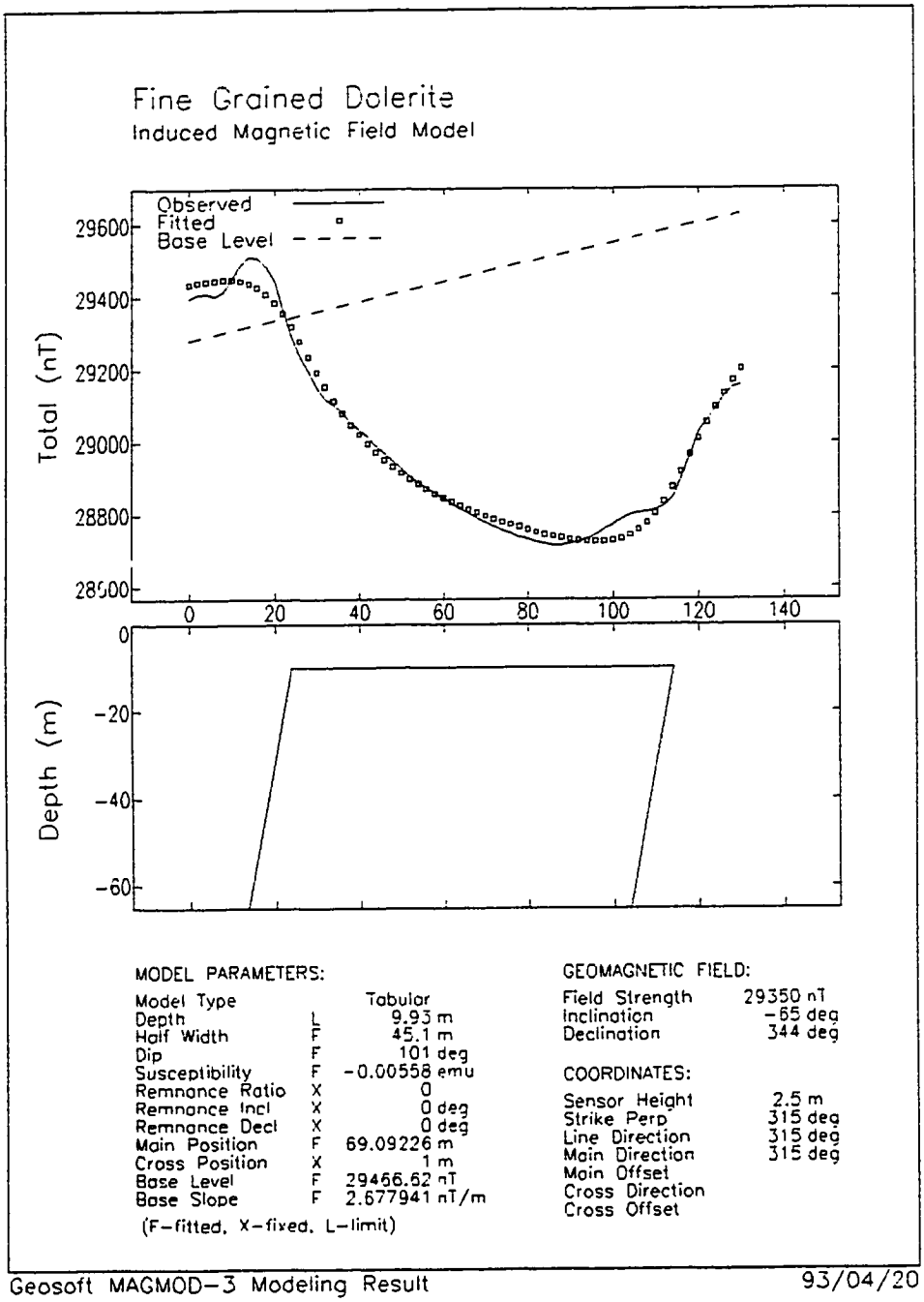

Figure 5.4: Model of the cross-section obtained from a ground magnetic traverse across an exposed northeast trending dike shown in figure 5.3. Section line orientation is 135 degrees east of north. The width of the dike is 90.2 metres and it dips 79° to the SE.

the main dolerite exposure. An alternative interpretation was obtained with the depth parameter fixed at 2.0 metres. The fitted profile does not make a perfect match with the observed profile, but the width and dip of the magnetic body (84.0 metres and 85° respectively) remained fairly similar to those in figure 5.4. The dip of the dike suggests that it was injected along a steeply inclined fracture. The dike was probably emplaced along a normal fault.

5.2 Palaeomagnetism

5.2.1. Introduction

Palaeomagnetic determinations were conducted mainly in an attempt to obtain a palaeomagnetic vector corresponding to the time of emplacement of the dikes that have intruded into the basement. Comparison with the polar wandering curve for the Kaapvaal Craton and other surrounding stable platforms would provide an indication of the age of the dikes sampled. The samples for palaeomagnetic determination were obtained from two of the best exposed dikes in the study area. One of the dikes chosen is the one from which the magnetic profile described above was obtained. Six oriented samples were collected from within a radius of 10m at a site on the dike. A second dike in the northern part of the study area was similarly sampled. The latter dolerite dike displays feldspar porphyries. At a location near Gampudi dam, porphyritic dolerite cross-cuts fine grained dolerite, revealing the greater relative age

of the latter. Table 5.2 shows all the data obtained by palaeomagnetic determinations.

5.2.2 Laboratory method

5.2.2.1 Sample preparation and measurements

A one inch diameter core was drilled into each sample and cut into cylinders such that the length to diameter ratio is about 0.85. A spinner magnetometer was used to measure the orientation and intensity of remnant magnetization in the sample in a zero ambient magnetic field environment. Each core sample was spun about 3 mutually orthogonal axes; spinning on each axis was started at two diametrically opposed positions such that a total of six spins were performed per measurement. The spin measurements were resolved by computer link to give the magnetic declination, inclination, intensity and A95 value of the sample. The sample declination and inclination values were corrected by rotation to the geographical vector orientation using field orientations and a basic program.

5.2.2.2 Thermal demagnetization

The core samples were thermally demagnetized at 50°C intervals. Demagnetization began at 300°C and ended at 650°C. The sample was heated at a constant temperature for 20 minutes. After each demagnetization, the sample was

	Temp	Declin	Inclin	Intensity	A95	Sample #	Temp	Declin	Inclin	Intensity	A95
MM39A	Raw	233 9	44 8	470 7	0 7	MM53	Raw	304 4	-59 2	5004 0	0 3
	300	235 6	45 2	279 7	0 7		300	307 6	-60 5	3282 5	0 4
	350	233 0	46 5	198 8	0 8		350	307 7	-59 3	2281 3	0 4
	400	233 9	46 1	181 4	0 8		400	306 5	-60 0	1632 3	0 5
	450	234 7	48 1	110 0	0 9		450	308 4	-62 1	1367 9	0 6
	500	228 7	50 4	83 6	1 1		500	311 8	-63 3	1036 7	0 6
	550	232 3	51 4	62 6	1 2		550	318 9	-66 9	808 2	0 8
	600	76 5	30 7	4 0	13 1		600	307 6	-51 9	61 5	3 4
	650	8 9	-35 3	3 5	10 6		650	244 2	-26 3	51 7	4 1
MM40A	Raw	267 9	-61 8	43 6	2 4	MM54	Raw	196 1	-21 4	17383 3	0 1
	300	271 7	-60 5	26 3	3 1		300				90 0
	350	272 6	-61 9	22 2	3 4		350	6 4	-11 0	3638 0	0 2
	400	167 0	-66 2	18 8	3 3		400	5 1	-13 4	2895 7	0 2
	450	265 6	-70 6	16 1	3 8		450	7 7	-8 5	2647 1	0 2
	500	255 1	-77 3	12 5	4 2		500	6 3	-8 9	2352 5	0 2
	550	300 6	-77 1	8 6	5 7		550	6 0	-11 8	1968 6	0 3
	600	46 6	35 1	7 0	5 3		600	32 2	1 4	344 6	0 7
	650	43 8	-36 8	3 9	9 6		650	108 7	21 7	120 5	1 0
MM41A	Raw	342 1	-43 9	37 1	2 7	MM55A	Raw	52 8	17 2	8149 1	0 1
	300	292 1	-11 4	14 4	3 2		300	309 0	22 0	1876 7	3 0
	350	275 5	-3 1	15 5	3 3		350	239 4	9 8	2805 0	0 3
	400	279 0	-11 5	16 8	2 9		400	237 7	0 3	1614 8	0 4
	450	238 0	-26 9	10 3	6 8		450	237 6	7 3	1303 8	0 4
	500	237 5	-40 6	8 1	7 6		500	238 3	6 1	1016 6	0 4
	550	252 9	-48 8	6 3	7 6		550	238 8	7 9	778 8	0 3
	600	285 9	-3 0	8 9	4 3		600	265 6	59 0	87 6	1 3
	650	257 3	-62 6	8 9	6 0		650	3 5	34 8	79 0	1 5
MM42	Raw	22 0	-51 3	91 5	1 8	MM56A	Raw	154 8	-50 3	11753 9	0 1
	300	21 1	-48 3	51 3	2 3		300	147 1	-2 1	10872 3	0 9
	350	21 3	-47 4	43 1	2 9		350				
	400	21 6	-45 5	35 2	3 1		400	159 4	-54 7	4822 7	0 2
	450	27 4	-43 9	31 4	3 5		450	163 6	-63 5	3406 2	0 3
	500	27 3	-45 8	27 8	3 5		500	158 5	-55 9	2490 0	0 2
	550	22 0	-42 7	19 3	4 5		550	160 5	-56 6	2157 2	0 3
	600	10 6	33 3	7 9	7 1		600	208 4	-87 8	73 7	1 7
	650	332 3	-20 7	8 9	6 4		650	153 1	-82 9	70 9	0 8
MM43A	Raw	290 0	-76 0	37 8	2 8	MM57	Raw	284 1	-30 9	51183 7	0 0
	300	240 4	-72 7	21 9	3 2		300				90 0
	350	237 1	-67 5	18 6	3 7		350				90 0
	400	233 5	-69 4	18 3	4 0		400				90 0
	450	184 6	-71 2	16 3	3 5		450	281 3	-29 1	20595 6	0 1
	500	179 4	-70 7	13 4	3 4		500	281 6	-30 4	14832 8	0 1
	550	310 4	-78 5	7 3	7 2		550	282 5	-31 9	12065 6	0 1
	600	346 2	-25 9	6 0	8 0		600	333 0	-15 9	254 6	0 5
	650	356 2	-74 6	11 1	4 0		650	3 1	-24 1	132 4	1 4
MM44A	Raw	295 2	4 7	35 8	2 0	MM58	Raw	264 3	57 1	31837 9	0 1
	300	278 1	8 1	17 6	4 2		300				90 0
	350	18 7	-49 7	14 2	5 9		350				90 0
	400	275 5	-5 1	10 8	5 7		400				90 0
	450	267 0	-24 5	7 2	7 3		450	260 5	57 1	11702 7	0 1
	500	282 6	-25 8	4 3	11 3		500	262 4	60 6	8648 6	0 1
	550	261 2	1 6	4 1	9 4		550	259 0	58 0	6565 0	0 1
	600	40 0	-48 0	1 4	24 3		600	33 1	60 5	231 0	0 9
	650	93 7	-75 9	5 9	9 6		650	37 4	37 9	202 9	0 9

Table 5.2: Results of palaeomagnetic determinations for 12 samples in the study area. Samples MM39 to MM44 were obtained from a fine grained dolerite dike. Samples MM53 to MM58 were obtained from a porphyritic dolerite dike. Thermal demagnetization was carried out at intervals of 50°C beginning at 300°C to 650°C.

cooled and the spin measurements were taken as above. The results for raw and demagnetised samples are shown in Table 5.2. The demagnetization curve in each of these plots can be divided into three parts: a steep portion between the raw and 300°C, a moderate portion between 300°C and 550°C and a shallow section between 550°C and 650°C. Thermal demagnetization ratio curves are shown in figures 5.7 and 5.10 for the fine grained dolerite and the porphyritic dolerite respectively.

5.2.3 Results

5.2.3.1 Fine grained dolerite

The palaeomagnetic vector orientations for the raw samples from the fine grained dolerite are given in figure 5.5A. The stereograghic projections for the orientation of palaeomagnetic vectors are from the lower hemisphere for positive inclination and from the upper hemisphere for negative inclinations. The magnetic vectors are scattered in three quadrants. No meaningful cluster can be discerned. After thermal demagnetization, a stable vector could be established at temperatures ranging from 350°C to 550°C. These determinations were obtained by the least squares lines method (Kirschvink, 1980), calculated by computer software. The orientations of these vectors are plotted in figure 5.5B. Samples MM40A, MM41A and MM43A cluster in the SW quadrant with orientations 247/-61, 233/-40 and 233/-67 respectively. The mean orientation for this cluster is 237/-57. Samples MM39A (234/+45) and MM42

Figure 5.5: Stereographic projections of the palaeomagnetic vector from the fine grained dolerite. Orientations with positive magnetic inclination are projected from the lower hemisphere. Negative inclinations are projected from the upper hemisphere. **A** shows vectors from six raw samples before thermal demagnetization. **B** shows vectors from demagnetized samples. These orientations represent the original natural remanent magnetic vectors. A cluster is formed by samples 40, 41 and 43 at 237/-57. Samples 39 and 42 are nearly collinear but mutually reversed.

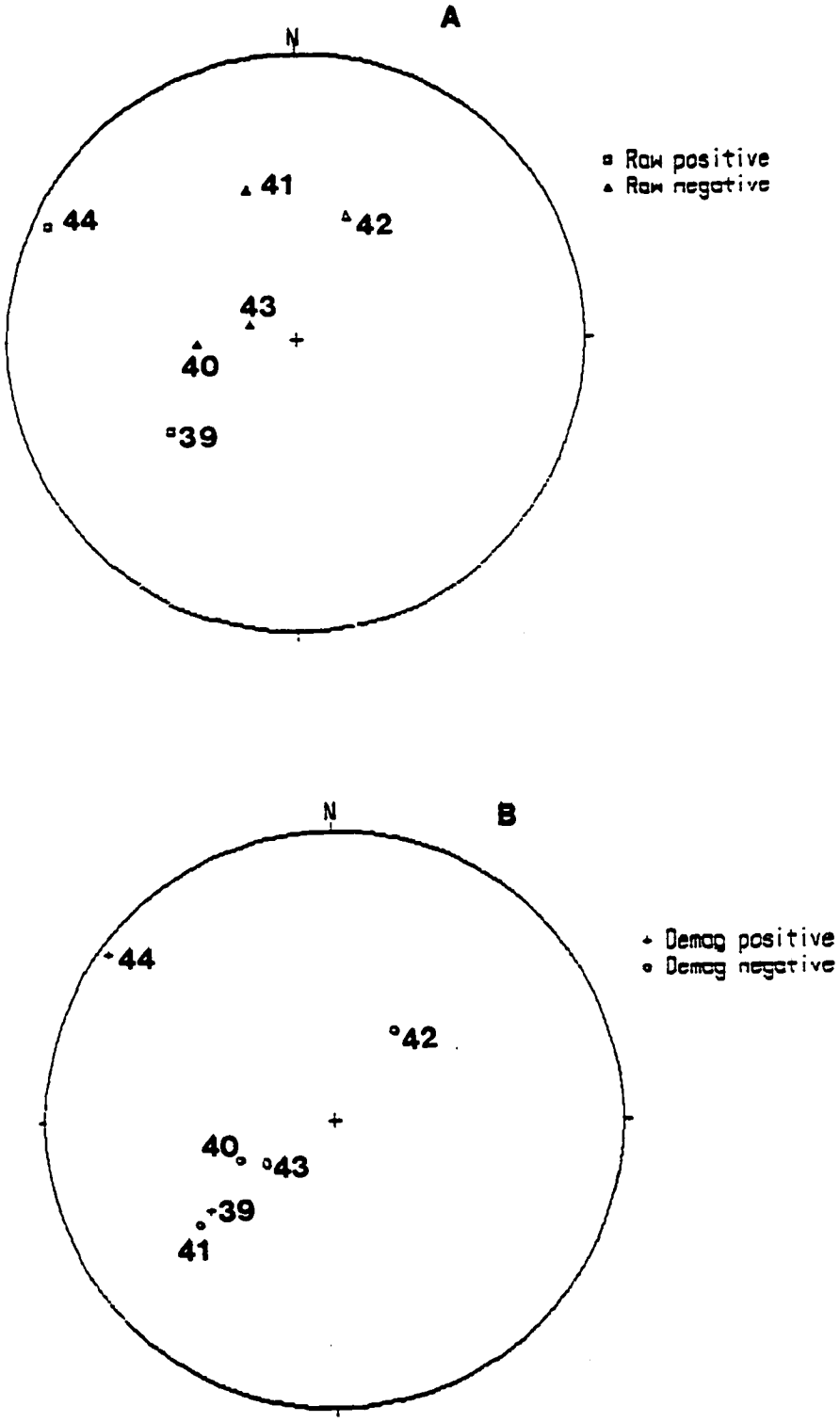
A
N
41
44
42
43
40
39
Raw positive
Raw negative
B
N
44
42
40
43
39
41
Demag positive
Demag negative

(35/-59) are virtually collinear with opposite signs. Sample MM44A has no relationship with any other sample. The cluster just mentioned has a similar orientation as the vector for the Great Dike of Zimbabwe which has a mean orientation of 216/-58.9 (Wilson et al, 1987). The Great Dyke is 2514 ± 16 Ma (Hamilton, 1977 in Hunter and Pretorius, 1981). The correlation implied in these results is by no means conclusive as it is not supported by statistical sampling. The radically deviant orientations shown by the other samples cannot be accounted for at the present time.

Thermal demagnetization has shown that samples from the fine grained dolerite have been affected by more than one component of palaeomagnetic remanence. However, sample MM39A appears to be an exception. At 471 x 10^{-6} e.m.u., it has the highest magnetic intensity among the samples from the fine grained dolerite. The orientation of the vector is virtually constant during demagnetization steps from raw to 550°C (figure 5.6A). The magnetization is destroyed at 600°C and the orientation is destabilized. This behaviour is consistent with magnetite (Curie point = 580°C) being the chief mineral responsible for the remanent magnetization. It is also consistent with the presence of one component of magnetization. Sample MM42 has the next highest magnetic intensity at 92 x 10^{-6} e.m.u. It is remarkably collinear with sample MM39A and appears to be reversely magnetized. Samples MM40A, MM41A, MM43A and MM44A show apparent overprinted components. The orientation migration patterns of samples MM40A and MM43A are comparable. The stereographic projection for sample MM40A in figure 5.6B shows that demagnetization followed a steep great circle from the raw state to 500°C. The distribution of the orientations indicates

Figure 5.6: Migration of the natural remanent magnetic vector orientation at successive stages of thermal demagnetization. The last point at which the arrowed line points is at 650°C. Each diagram A to F shows the migration of the orientation with a line that starts at the raw point, through 300, 350, 400, 450, 500, 550 600 to 650°C.

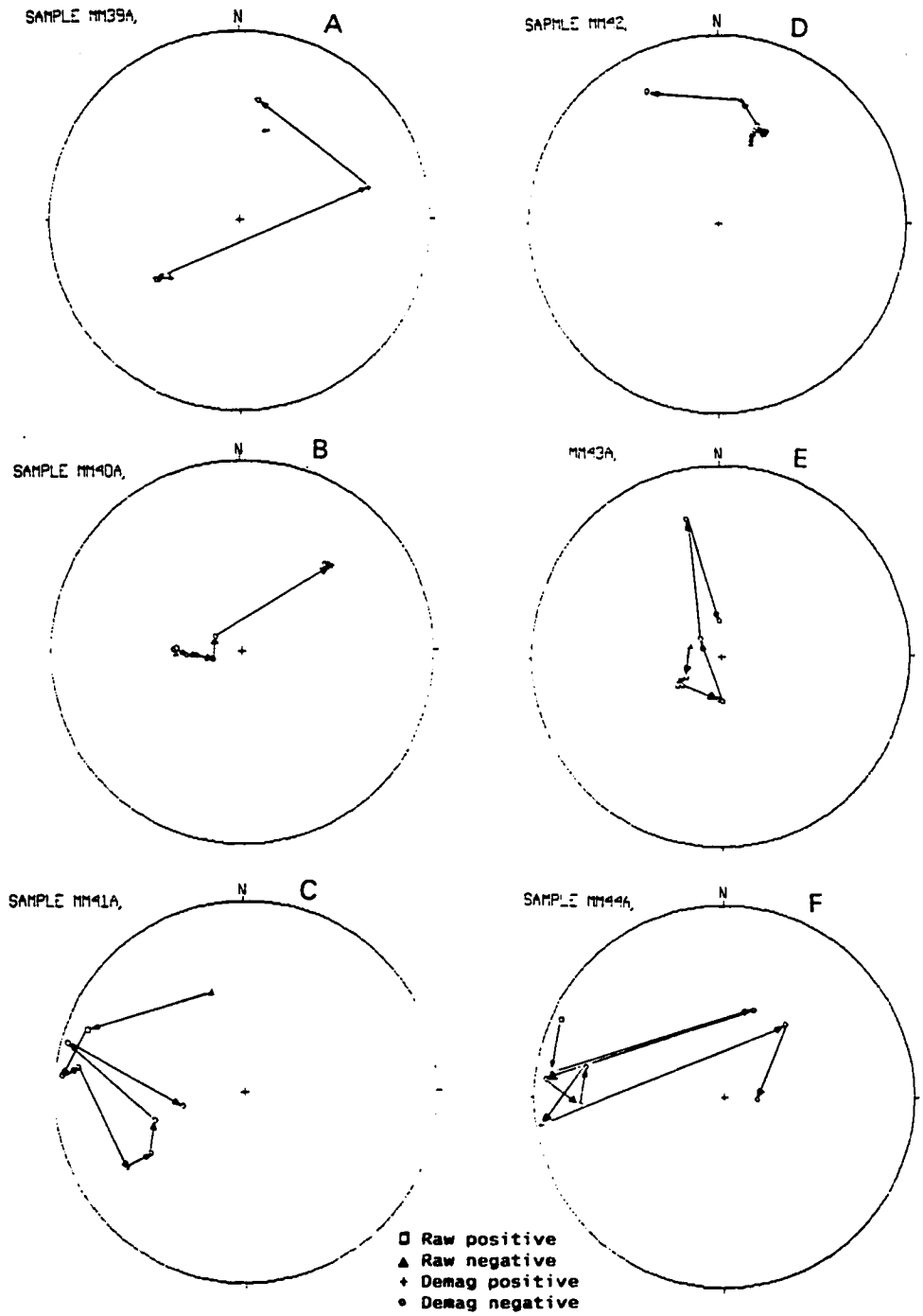
SAMPLE MM39A,
N
A
SAPMLE MM42,
N
D
SAMPLE MM40A,
N
B
MM43A,
N
E
SAMPLE MM41A,
N
C
SAMPLE MM44A,
N
F
Raw positive
Raw negative
Demag positive
Demag negative

overlapping components by the Hoffman-Day method (Piper, 1987). The demagnetization intensity ratio curve in figure 5.7 is linear from 300°C to 650°C. Sample MM43 in figure 5.6E also shows demagnetization that follows a moderately steep great circle from 300°C to 500°C. In this sample, two clusters are present: one at 300-400°C and another at 450-500°C. These indicate fairly distinct components of remanent magnetization. The distribution for samples MM41A and MM44A appear to be rather erratic. At about 350°C to 450°C, the orientations of samples MM40A, MM41A and MM43A, seem to cluster (figure 5.5B and 5.6).

5.2.3.2 Porphyritic dolerite

The orientations of palaeomagnetic vectors for the raw samples and thermally demagnetized samples are given in figure 5.8A and 5.8B respectively. Neither of the plots show any clustering of orientations. Thermal demagnetization orientations are given in figure 5.9A to 5.9F. Each of the samples from this dike show a strong consistent internal orientation from raw to 550°C. This behaviour demonstrates that the porphyritic dike has one component of natural remnant magnetization. The mineral responsible for the magnetization is magnetite with a Curie temperature of 580°C.

The raw samples from this dike are strongly magnetic as shown by the values in table 5.2. The lowest magnetic intensity raw value obtained is 4,823 x 10^{-6} e.m.u. and the highest is 51,184 x 10^{-6} e.m.u. The high remanent magnetism is probably responsible for the scatter of the orientation data. The field orientations were

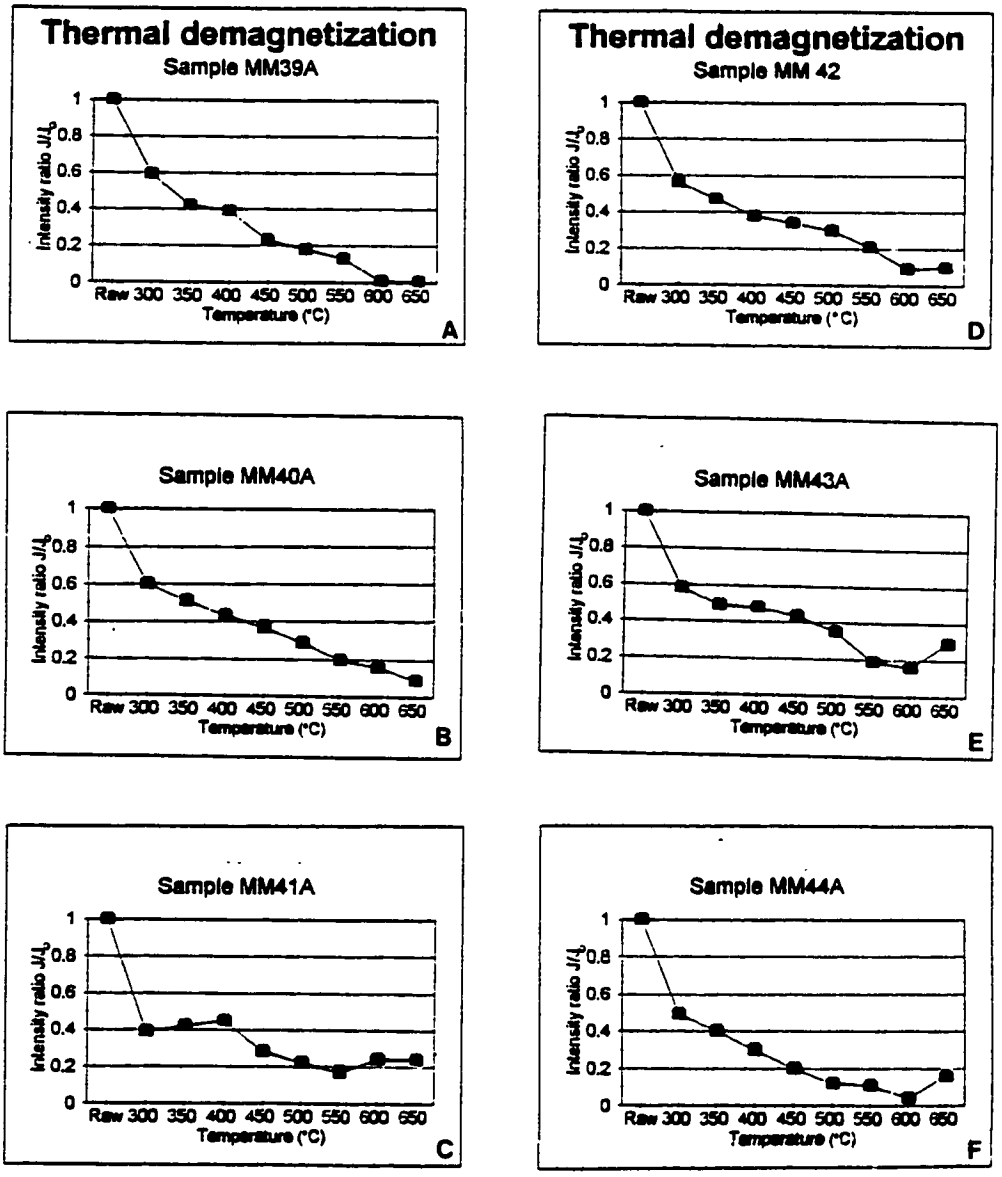

Figure 5.7: Thermal demagnetization intensity ratio plots for the fine grained dolerite.

Figure 5.8: stereographic projections of palaeomagnetic vectors from the porphyritic dolerite. The projection convention is the same as in figure 5.5. **A** represents the raw samples before thermal demagnetization. **B** represents the original natural remanent magnetization vectors. There is absolutely no clustering on either of the diagrams.

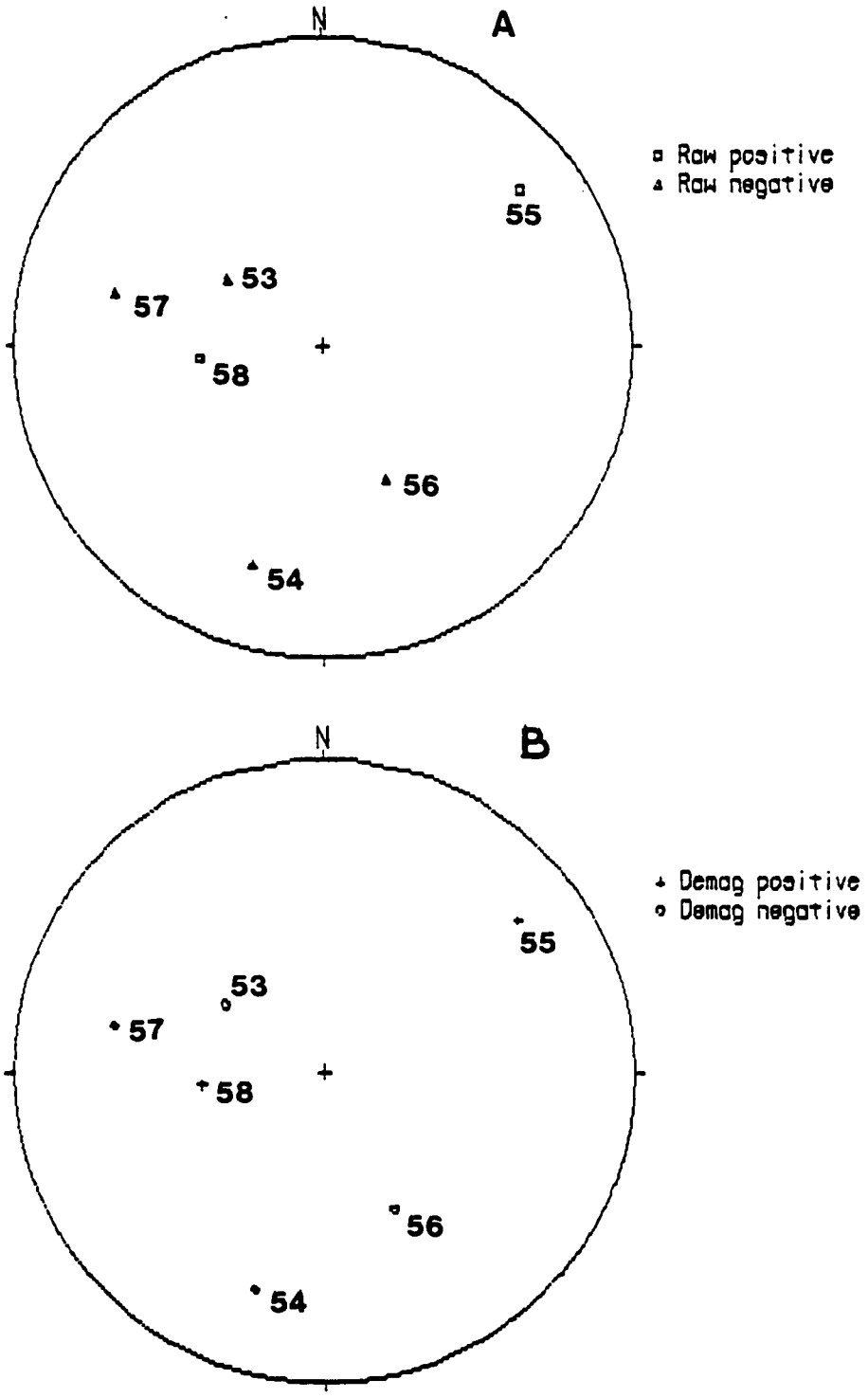
N
A
Raw positive
Raw negative
55
53
57
58
56
54
N
B
Demag positive
Demag negative
55
53
57
58
56
54

Figure 5.9: Migration of the palaeomagnetic vector orientation at successive stages of thermal demagnetization as in figure 5.6. In all the samples, the orientation is virtually constant. The vector only becomes unstable at 600°C.

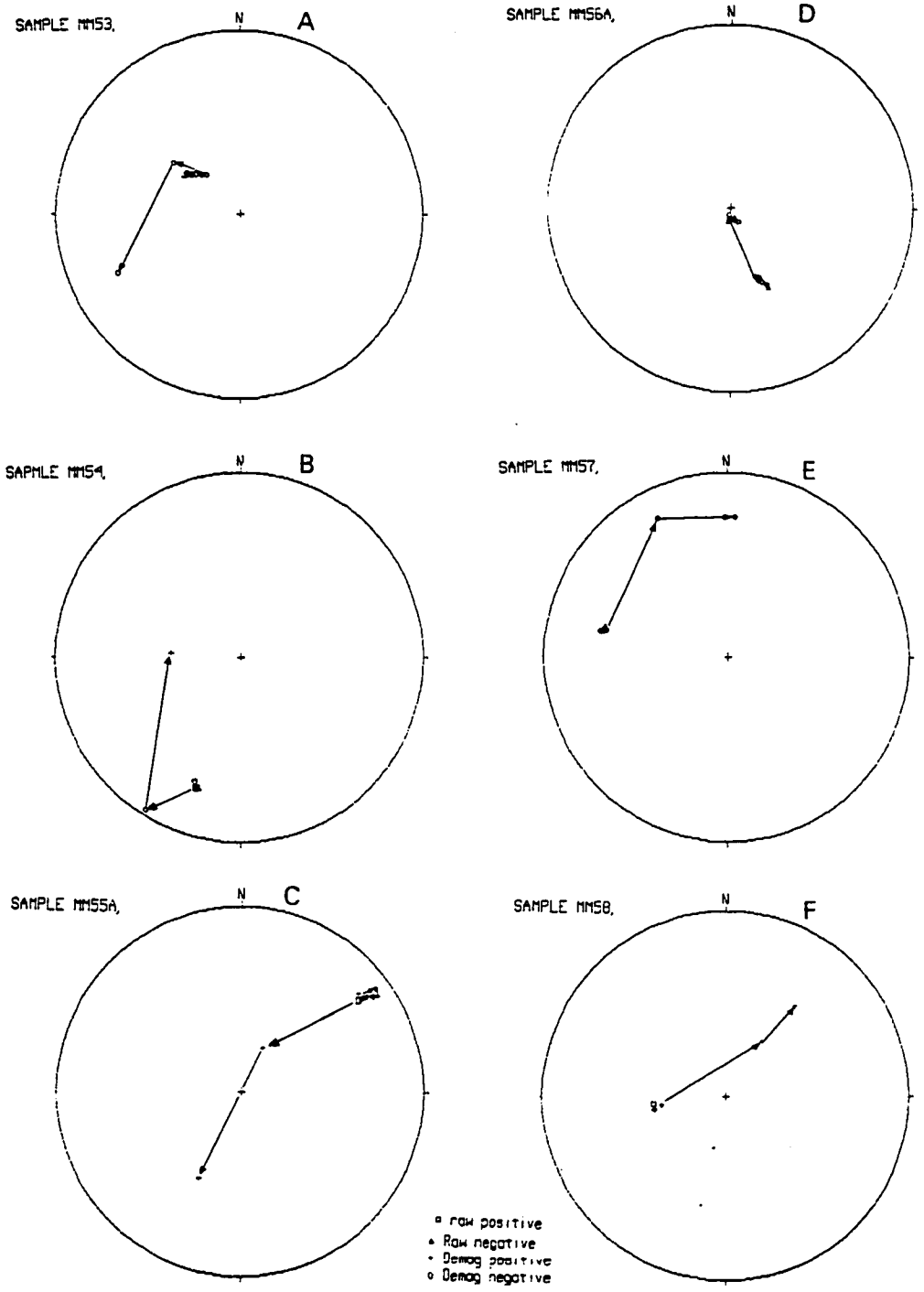
SAMPLE MM53,
N
A
SAMPLE MM56A,
N
D
SAPMLE MM54,
N
B
SAMPLE MM57,
N
E
SAMPLE MM55A,
N
C
SAMPLE MM58,
N
F
raw positive
Raw negative
Demag positive
Demag negative

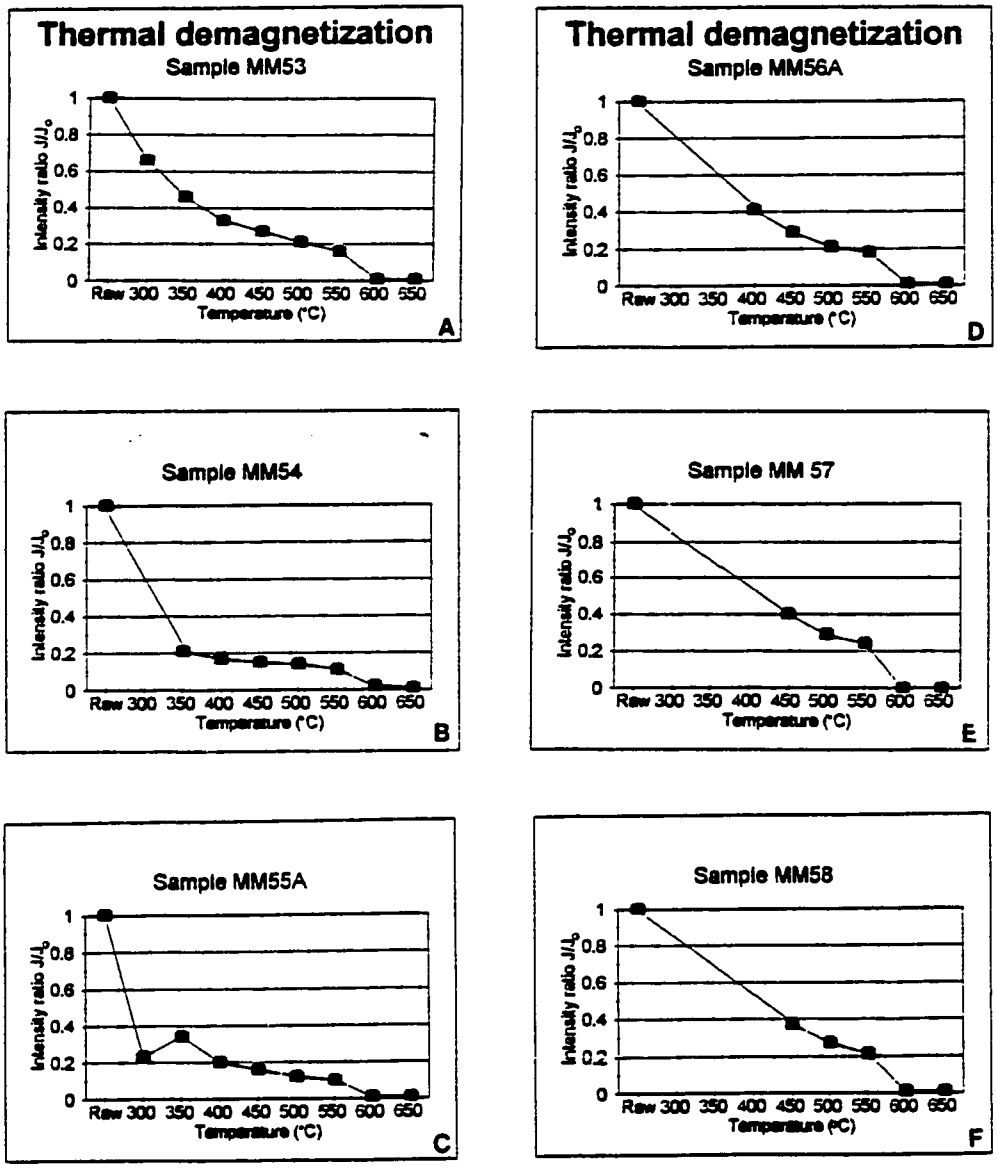

Figure 5.10: Thermal demagnetization intensity ratio plots for the porphyritic dolerite.

performed with a magnetic compass. It is also possible that some of the samples were obtained from moved blocks.

5.3 Conclusion

The NE trending set of faults south of Kanye, including the Taupone Fault, probably does not extend beyond the present area of study as strike slip faults. Horizontal displacements along these fractures preferentially affected the boundary between the basement rocks and the supracrustal deposits.

Pre-Transvaal ENE trending lineaments including those that have been identified as dolerite dikes do not form strong magnetic anomalies. This can partly be attributed to the low magnetic susceptibility of the dikes. It is also likely that many, if not most of the lineaments are fractures that contain no dike or vein material with significant magnetic susceptibility contrast with the country rock. The E-W trending, post-Waterberg dikes to the south of Kanye show strong linear magnetic anomalies. The 4 kilometre spacing of the existing aeromagnetic survey around Moshaneng cannot resolve these intrusions, if present, as anomalies in that area.

It has been suggested that the southern African Craton has remained as a coherent tectonic unit since the Archaean to the present time (Piper, 1987; Pretorius, 1979). The tentatively indicated palaeomagnetic vector correlation between the late Archaean to early Proterozoic dike near Moshaneng and dikes of similar age on the Zimbabwe Craton is consistent with the long-lived coherence notion. It is unlikely that

the fine grained dolerite could be of Karoo age. Results for the porphyritic dolerite cannot be interpreted at this stage.

CHAPTER 6: REGIONAL FRACTURE DOMAINS

6.1 Remote sensing media and interpretation

6.1.1 Aerial photographs

The regional lineament pattern shown in figure 6.1 is formed by undifferentiated fractures and dikes. The pattern was established from the interpretation of aerial photographs at scale 1:50,000. At this scale, aerial photographs yield the best resolution compared to other media described below. Figure 6.2 and 6.3 are copies of the contact prints produced from flight surveys carried out between 1988 and 1989. On this medium, joints are represented by the alignment of bushy vegetation and relatively dark tones that are discretely defined. Locally, in areas of rock outcrop, these lineaments are too closely spaced to be mapped individually. Dikes are characterized by the same features as joints but the dark tones are broader and marked by linear microtopographic depressions. Faults are represented by relatively light tones with diffuse boundaries and may be marked by discrete linear positive micro-topography along zones that have been silicified. Unequivocal ground truth identification of some lineaments is inhibited by lack of continuous rock exposure.

Figure 6.1: Fracture pattern map of the area around Kanye. Interpretation is based on black and white aerial photographs of scale 1:50,000 from flight surveys in May, 1982, October, 1988 and April, 1989.

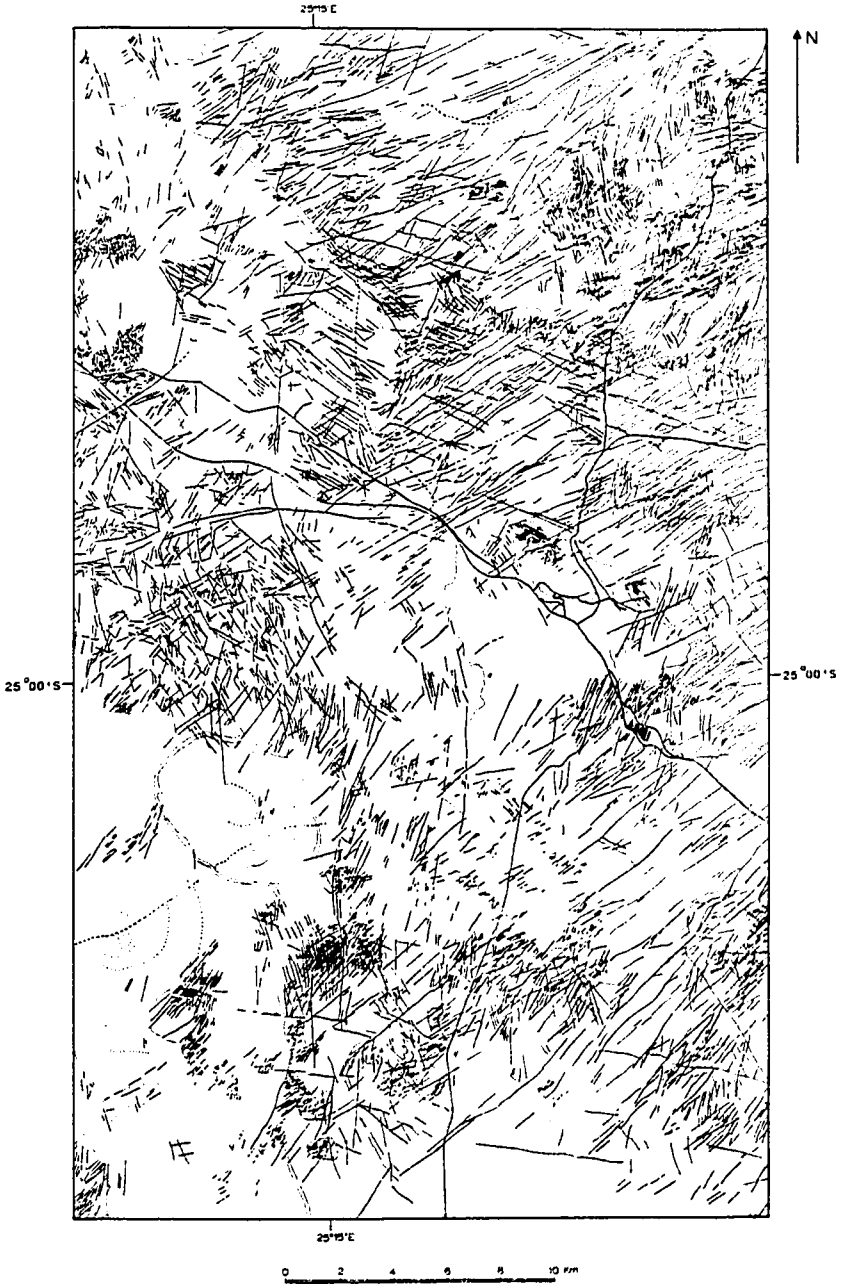
25°15'E
N
25°00'S
25°00'S
25°15'E
0 2 4 6 8 10 km

Figure 6.2: Aerial photograph of the area around Moshaneng. **M**=Moshaneng Village. **Go**=Gokano Hill. **Ga**=Gampudi Dam. **J**=Jwaneng Kanye Road. **1**=Unconformity between the basement and the Transvaal Supergroup. **2**=Unconformity below the Waterberg Group. **3**=Dolerite outcrop. The original contact print on which interpretation was carried out was at scale 1:50,000 from a flight survey in April, 1989.


1 km

Figure 6.3: Aerial photograph of the area around Taueshele and Tletletsi. **Te**=Tletletsi. **Ta**=Taueshele. **Mo**=Mokalaka Ridge. The original contact print is at scale 1:50,000 from a survey in October, 1988.

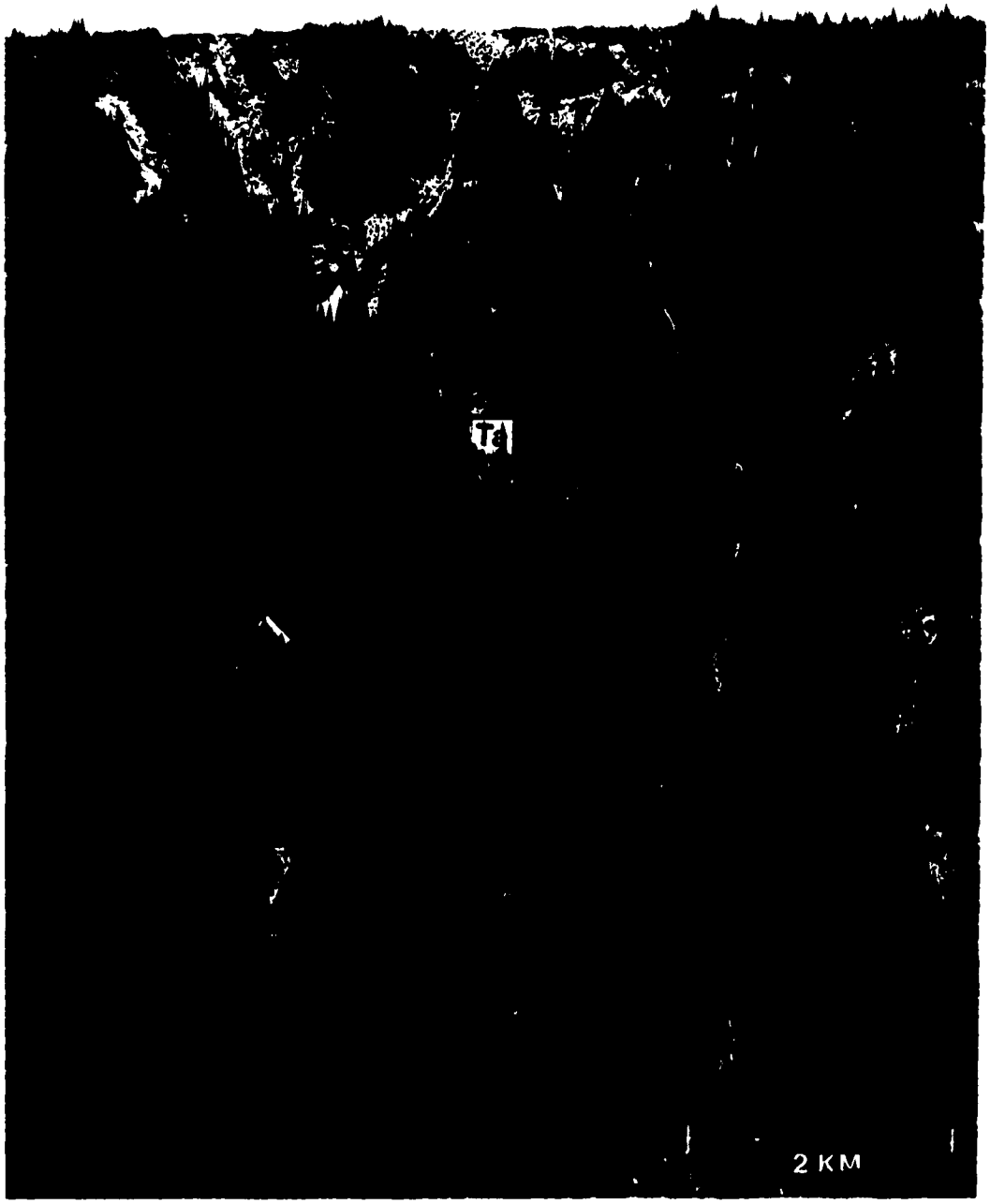
2 KM

6.1.2 SPOT imagery

The main advantage of SPOT (*System Pour l'Observation de la Terre*) imagery over aerial photography is its ability to show fractures as either soil moisture retention linear zones or lines of relatively healthy vegetation. The red false colour showing these characteristics is a signature of the infrared band. This signature is particularly useful in areas underlain by the dolomite and chert sequence to the south of Kanye (see figure 6.5 for the location of Kanye). The resolution of 10 x 10 m renders SPOT imagery as a satisfactory medium to resolve fractures at a scale of 1:125,000. This resolution is vastly superior to that of Landsat imagery which is 79 x 79 m. Landsat imagery interpretation was not used for this study because of its low power of resolution.

Notwithstanding its good resolving power and infrared false colour advantage, SPOT imagery yielded poor responsiveness in some of the terrane underlain by outliers of Waterberg rocks. It is probable that little or no moisture is retained in fractures where the Waterberg rock occurrences are high-perched compared to the surrounding terrane. The lineament pattern interpretation obtained from SPOT imagery is presented in figure 6.4. Due to the differences in the working scale and some of the responsiveness characteristics outlined above, generally more lineaments are revealed by aerial photographs than by SPOT imagery. Moisture retaining lineaments are, however, better enhanced in the SPOT image and therefore can be traced more continuously.

Figure 6.4: Fracture pattern map of the area around Kanye. Interpretation is based on a false colour SPOT image printed at a scale of 1:125 000. (Dated June 4, 1986).

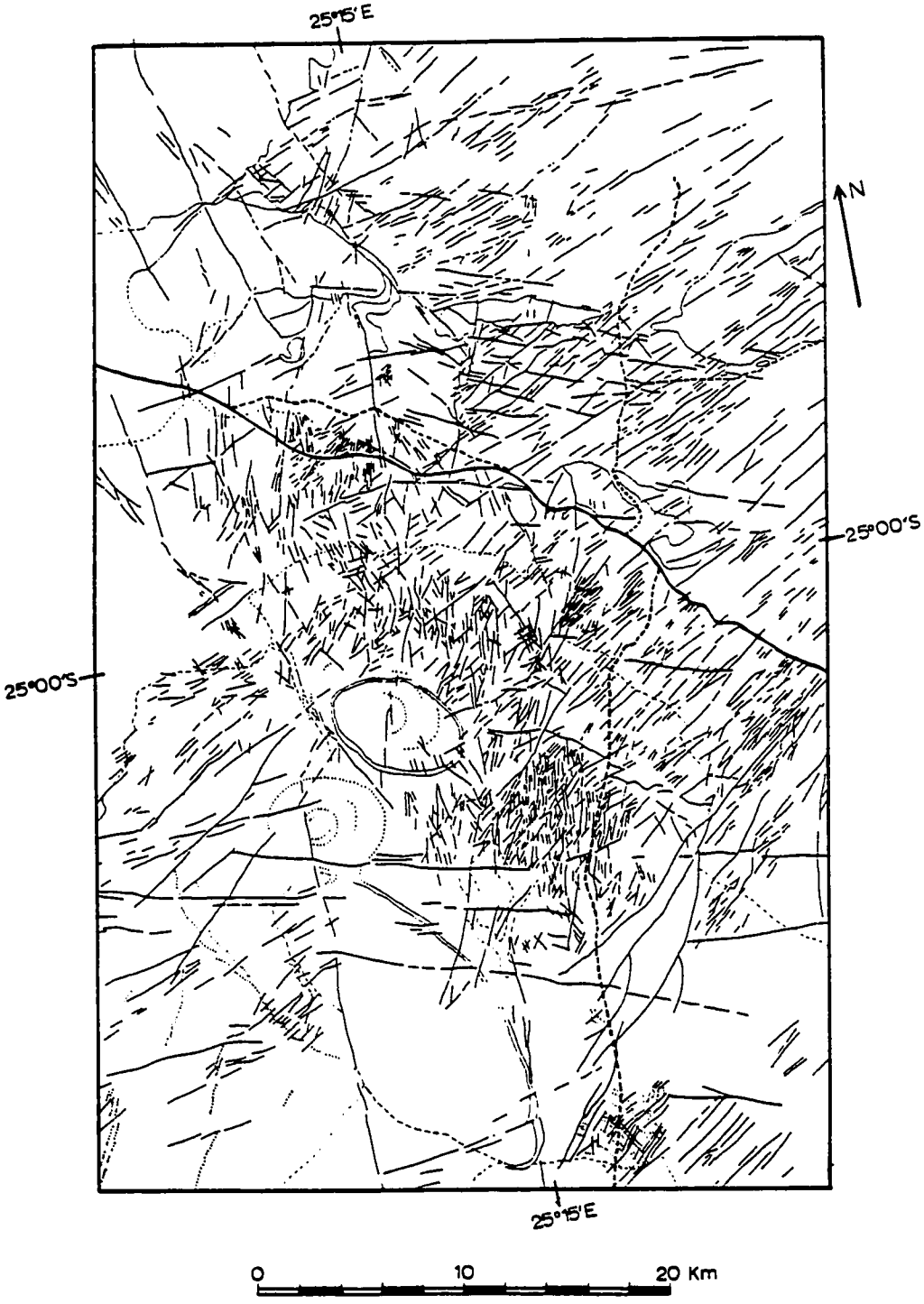
25°15'E
N
25°00'S
25°00'S
25°15'E
0
10
20 Km

Figure 6.5: Geological map of the area around Kanye (Adapted from Aldiss et al, 1989, Crockett, 1972b, Machacha, 1977, Tombale, in prep.).

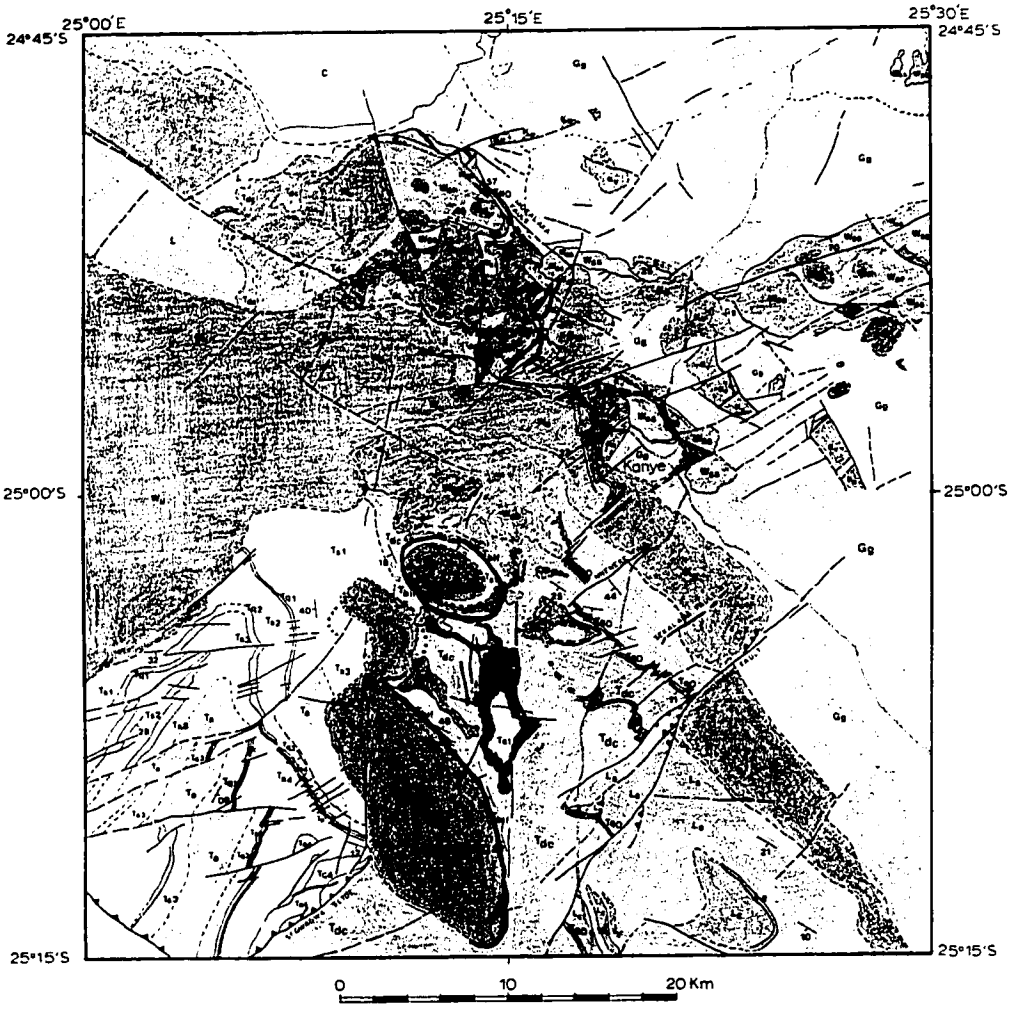
25°00'E
25°15'E
25°30'E
24°45'S
25°00'S
25°15'S
Kanye
0
10
20 Km

	LITHOLOGY	FORMATION/ STAGE	GROUP/SUB-GROUP	AGE
C	duricrust, sand	Kalahari beds	-	Cainozoic
	dolerite	undifferentiated		Archaean to Mesozoic
	syenite, granite, gabbro	Moshaneng, Masoke and Segwagwa Complexes		Late Proterozoic
	dolerite	Moshaneng Dolerite		1.1 Ga
W_{sh}	shale, sandstone	Molepolole formation	Waterberg	Mid-Proterozoic
W_{ss}	red sandstone, conglomerate	Manyelanong Hill		
W_{cb}	chert breccia	Kgwakgwe Hill Chert Breccia		
W_c	coarse clastics	undifferentiated		
T_{q4}	quartzite	Magaliesberg	Segwagwa (Pretoria)	Proterozoic
T_c	chert			
T_{s4}	shale			
T_{q3}	quartzite + shale	Daspoort		
T_a	andesite			
T_{s3}	shale			
T_{q2}	quartzite	Timeball Hill		
T_{s2}	shale			
T_{q1}	quartzite			
T_{s1}	shale			
	iron formation			
T_{dc}	dolomite ± chert	Ramonnedi	Taupone Dolomite	
T_{qO}	quartzite	Black Reef Quartzite		
L_c	conglomerate		Lobatse Volcanic	Late Archaean
L_g	graywacke			
L_s	shale			
G_g	granite		Gaborone Granite	
K	felsite	Kanye Volcanic		Archaean

Road
Geological boundary: definite, inferred
Fault: definite, inferred
30 Bedding attitude

6.1.3 Previous regional work with remote sensing media

Aerial photographs and Landsat imagery were routinely used in previous work for regional, reconnaissance, geological mapping of the study area (Crockett, 1972a, 1972b; Aldiss et al, 1989). However, only limited lineament interpretation was provided in these exercises. An evaluation of the use of Landsat imagery in SE Botswana for geological, geomorphological and land use interpretation was provided by Hutton (1978). The area of present study was included in the national remote sensing, geological interpretation (Mallick et al, 1981). Aldiss (1986) used aerial photographs to suggest the presence of a pre-Transvaal Supergroup dike swarm in SE Botswana.

6.2 Domain criteria

The area of study is shown as box 1 in figure 4.1. It covers a quarter degree or 30 minute area of about 2,750 km^2 in SE Botswana as shown on the geological map in figure 6.5. The rocks in this area are incorporated in the geological description of southeast Botswana provided in chapter 1. The area contains rocks that have been emplaced over a considerable period of geologic time. The earliest basement rocks, the Kanye Volcanic Formation were emplaced in the Archaean, some 3,000 million years ago. The youngest platform deposits, the Waterberg Group, were emplaced in the Proterozoic some 1,800 million years ago (see table 1.1). The rocks therefore straddle

the Archaean/ Proterozoic boundary, falling into two geologic time blocks that are tectonically distinctive. This area represents a period of major rock emplacement of more than a billion years, albeit with some breaks represented by distinctive unconformities. Brittle fractures have accumulated on these rocks from the time of their emplacement up to the present day. There has been virtually no ductile deformation since the late Archaean, such that brittle fractures formed since that time are still preserved in these rocks.

The initial criterion for demarcating domains rests in rock packages that are separated by the unconformities. The rock packages represent time blocks during which characteristic fracture development took place. The earliest of these packages is the Archaean basement, consisting of granites, granophyres and felsic volcanics. Above the basement are two Proterozoic platform cover sedimentary sequences; the Transvaal Supergroup at the bottom is separated from the Waterberg Group above it by an unconformity. Notwithstanding the great time interval of 100's of million years within each sequence and between sequences, the structures formed have been preserved largely in their original form and have not been significantly modified. The extent of repeated movements, however, within each demarcated time frame remains relatively obscure. Some of the movements could probably be interpreted from detailed stratigraphic mapping. Such mapping however is outside the scope of this thesis.

In this study, the principal criterion for defining tectonic domains within the time blocks is the fracture pattern as defined by the trend of fracture sets studied from aerial photographs, supplemented by SPOT imagery. For each block, photolineaments

were mapped from aerial photographs at a scale of 1:50,000. The photo interpretation was transferred to standard topographic sheets of the same scale for spatial integrity. A north-south and east-west grid pattern was used to measure the attitude of each lineament. These measurements were then used to compile orientation histograms and rose diagrams shown in figure 6.6 and 6.7 respectively. Standard procedure involved counting each lineament regardless of its length. This procedure can be criticized for its tendency to give prominence to short lineaments at the expense of longer ones in the frequency distribution.

The procedure described above was repeated for each of the rock packages that are divided by major unconformities. The rock packages have distinctive orientation patterns that could be delineated intuitively. Some of the rock packages show appreciable variations in their geographic distribution, warranting further delineation. These delineations produced the fracture pattern domains that are discussed below and shown in figure 6.7.

6.3 Basement

The basement has responded to stresses to yield a variety of macroscopic geological structures over at least 700 million years. The early complex ductile deformational history of the basement is beyond the scope of this study. Emphasis is placed on the development of brittle fractures which started to develop in Ventersdorp time. Probably due to the massive nature of the rocks in the basement, there is no

Figure 6.6: Lineament frequency histograms. The abscissa represents lineament orientations at 5° intervals from 0° to 180°. The ordinate represents frequency. N below is the number of fractures counted to calculate the frequency distribution.

A: Domain 1, north basement (N=694)

B: Domain 2, central basement (N=416)

C: Domain 3, south basement (N=451)

D: Domain 4, Moshaneng area; lower Transvaal Supergroup and intrusive suites (N=261)

E: Domain 5, Masoke area/Kanye south; lower Transvaal Supergroup (N=302)

F: Domain 6, Tletletsi and west Moshaneng area; Waterberg Group (N=100)

G: Domain 7, Gokano Hill; Waterberg Group (N=104)

H: Domain 8, Kanye area; Waterberg Group (N=130)

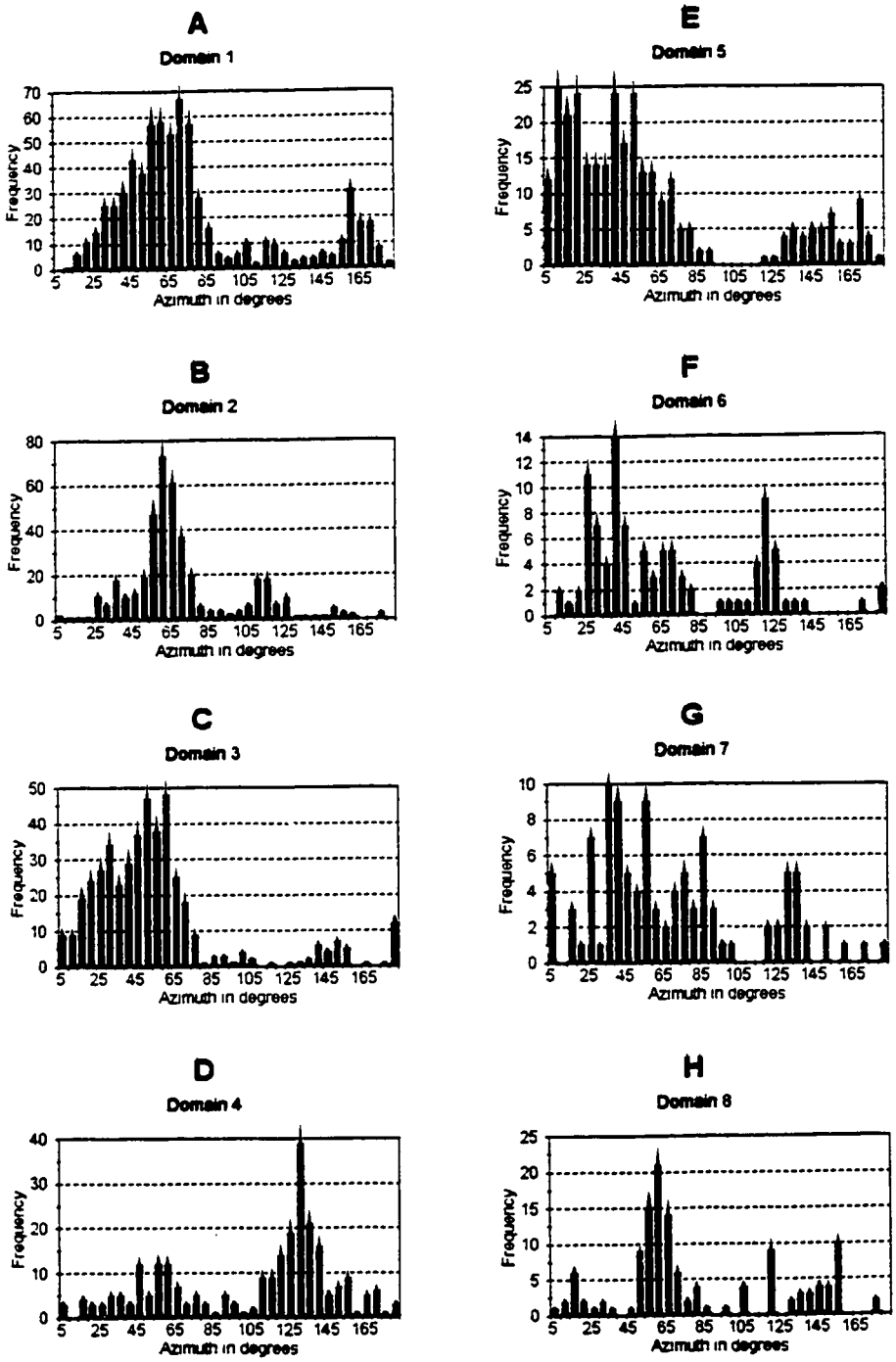
A
Domain 1
Frequency
Azimuth in degrees
B
Domain 2
Frequency
Azimuth in degrees
C
Domain 3
Frequency
Azimuth in degrees
D
Domain 4
Frequency
Azimuth in degrees
E
Domain 5
Frequency
Azimuth in degrees
F
Domain 6
Frequency
Azimuth in degrees
G
Domain 7
Frequency
Azimuth in degrees
H
Domain 8
Frequency
Azimuth in degrees

Figure 6.7: Tectonic domains and lineament orientation rose diagrams in the study area.

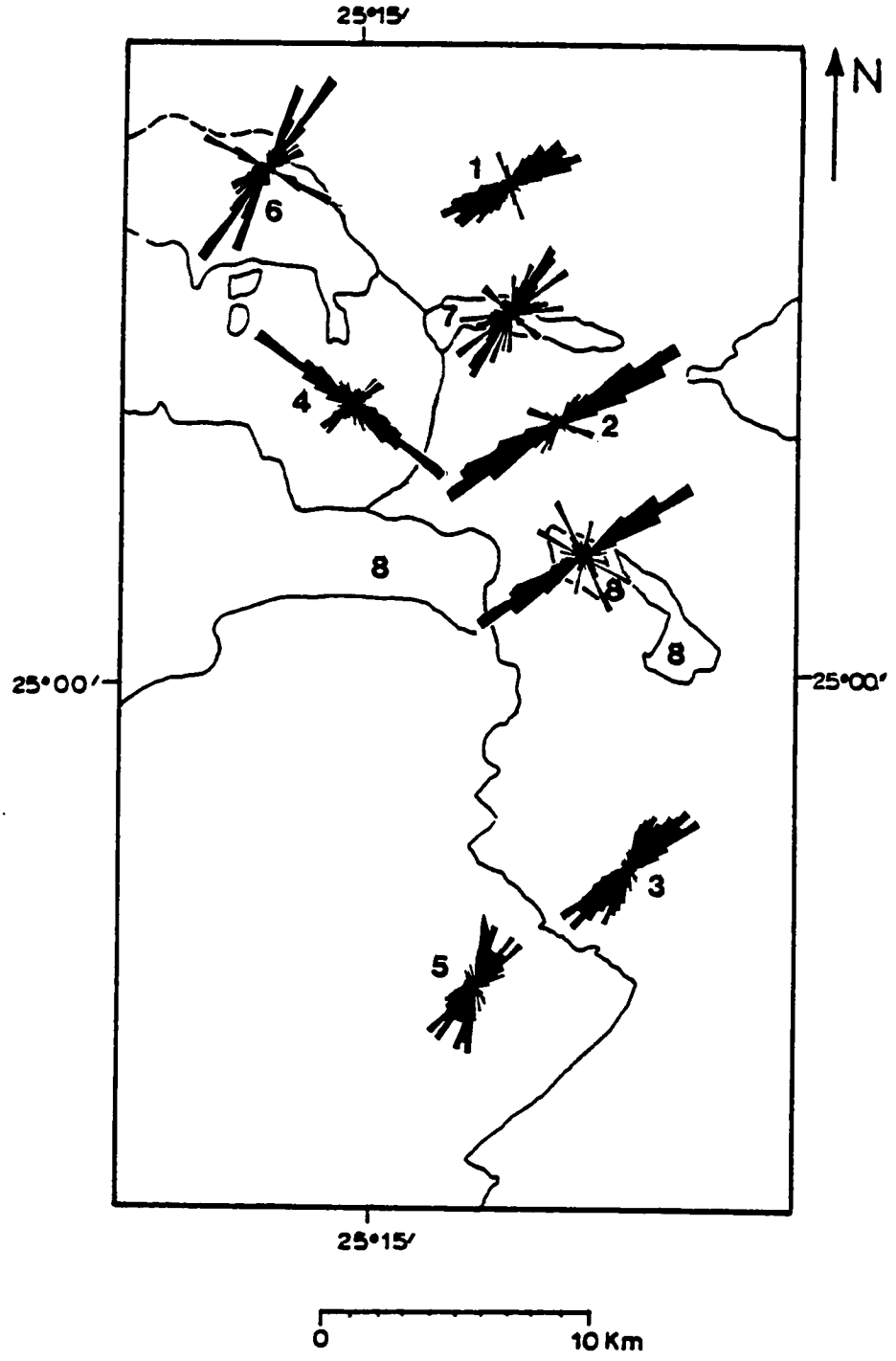
25°15'
N
1
6
7
4
2
8
9
8
25°00'
25°00'
3
5
25°15'
0
10 Km

record of folds of any distinction. Brittle deformation is represented by fractures, some of which have acted as sites for dike emplacement. Shear zones, breccia and silicification zones, fault planes and joints have been recorded and are discussed in detail in chapters 7 and 8.

The lineament pattern map does not differentiate any of the structures described above, so the lineaments represent zones or planes of mechanical discontinuity in the crust. A rigorous differentiation was not practical because at this scale of mapping, many of these structures are covered by superficial deposits, though mappable by remote sensing methods. Some of the lineaments are steeply dipping, and the dip direction can, in certain cases, be determined by the effect of the topography on the lineament trace.

The basement domain is characterized by lineament orientations that have peak ENE trends of 70° in the northern part, and 60° in the central and southern parts as shown in figures 6.6A, 6.6B and 6.6C respectively. The fractures show a fanning pattern. The fan has no recognizable structural apex, either within or outside the present area of study.

6.3.1 Domain 1 (northern basement)

The frequency distribution of lineament azimuths in domain 1 is shown in figure 6.6A. A peak at 70° defines the predominant trend of the lineaments. This trend invariably stops at the unconformity that separates the basement from the overlying

Transvaal Supergroup sediments. This is interpreted as a clear illustration of the pre-Transvaal age of lineaments of this trend. The basement/ platform interface along the NE flank of Mokalaka ridge (see figure 4.2 for the location of Mokalaka Hill) has been affected by major faulting and drag folding, such that the domainal boundary is not solely defined by the contrast in fracture pattern and chronology. The northern basement has two other minor fracture sets characterized by long fractures; a 45° set and a 115° set (see domain 1 in figures 6.6A and 6.7). The latter set is also well developed in the overlying Transvaal package in domain 4. The 45° set is only poorly represented in the overlying package. The foregoing implies that the ENE set is the oldest, developed before the Transvaal rocks were deposited, and the subsidiary sets were developed in post-Transvaal time. One NE trending 45° dike is displaced by ENE trending set 1 (70°) lineaments. This same ENE lineament displaces Transvaal rocks. These facts imply that some of the ENE trending lineaments were reactivated as faults in post-Transvaal times. The activity of the NE lineaments as faults is much more evident in the southern part of the study area, which is described in sections 6.3.3 and 6.4.2. A peak at 160°, defining a fourth set in the northern basement is an "artefact" of a large number of short fractures developed in the basement some distance from the basement/cover unconformity.

6.3.2 Domain 2 (central basement)

The azimuth frequency distribution for this domain is shown in figure 6.6B. The

central basement is dominated by a lineament set that trends 60° and truncated by the basement/ cover unconformity. Two subsidiary sets peak at 35° and 115° (figures 6.6B and 6.7). The 115° is also represented in the overlying Transvaal package and the 35° set is developed close to the unconformity but does not pass over it. Figure 6.1 shows the photogeological expression of the unconformity in eastern Moshaneng area. A dike near Gampudi dam traced in the basement does not continue beyond the unconformity into lower Transvaal sediments (see figure 6.2 for the location of Gampudi dam). This provides proof that this dike is of pre-Transvaal age. Many of the ENE 60° lineaments with a microtopographic depression have been identified as dikes in the northern and central basement areas; domains 1 and 2 respectively. Some of those with positive microrelief have been identified as silicified fault zones. A WNW 115° dolerite dike was identified on the ground in domain 2. A fault with the same trend can be traced from the basement, across the unconformity and onto the overlying Transvaal rock package. The latter structure is therefore clearly of post-Transvaal age. It is difficult to establish the relative age of the NNE trending 35° set.

6.3.3 Domain 3 (southern basement)

The southern basement includes rocks of the Lobatse Volcanic Group in addition to the Gaborone Granite Complex and the Kanye Volcanic Formation. In this area, the dominant fracture set trends 60 degrees with two prominent subsidiary sets at 30° and 150° (figure 6.6C and 6.7). The ENE 60° set mainly consist of faults that are

parallel to the Taupone Fault (see figure 6.5 for the location of the Taupone Fault and other NE trending faults). Displacement along these faults is most evident at the Black Reef Quartzite/ basement interface. The Taupone Fault and its family of parallel faults are mapped in an area where Waterberg rocks do not occur and therefore the upper limit of this faulting episode cannot be conveniently constrained. At Kgwakgwe Hill, a NE trending fault in the basement does not cut the basal Black Reef Quartzite of the overlying Transvaal sediment, providing unequivocal evidence for the pre-Transvaal age of the basement fracture. The 60° set and the 150° set appear to form an orthogonal system of master joints at certain locations of granite occurrence.

6.4 Transvaal

The lower age limit of the Transvaal Supergroup has been set at about 2,300 million years. The upper limit can be taken as the widely accepted age of the Waterberg Group sediments at about 1,800 million years. The geological history of these rocks may span up to 500 million years, but is probably less than this, considering the hiatus represented by each of the unconformities above and below. Continuous deposition of Transvaal sediments is from about 2,300 Ma to 2,100 Ma (Button et al, 1981). The Transvaal package consists of sedimentary sequences with a planar anisotropy in which mesoscopic folds can easily be developed in horizontally directed compressional stress fields. These rocks have been intruded by later igneous bodies, that are locally concordant. Geological structures preserved and recognized in

these rocks for this period of time include gentle folds in the layered sequences. In the Moshaneng area, the folds have a general NE trend and are positively pre-Waterberg because they do not affect rocks above the Transvaal/ Waterberg unconformity. A comprehensive joint survey in this domain indicates that well-developed mesoscopic fractures may be genetically associated with the folds. These associations are discussed in detail in chapters 7 and 9. A thrust fault, possibly formed contemporaneously with the folds, has been inferred near the eastern flank of the Moshaneng Transvaal exposures (figure 4.2).

6.4.1 Domain 4 (Moshaneng area, northern Transvaal Supergroup)

The domain defined around Moshaneng is dominated by a sharp lineament trend that peaks at 130° (figure 6.6D and 6.7). Faults and master joints are responsible for this lineament set. Around the Tletletsi syncline (see figure 6.1, and figure 4.2 for the fracture pattern and location of Tletletsi respectively), these fractures do not pass into the overlying Waterberg package. This could either be due to folding around the Tletletsi syncline, which may have obscured the linearity of the fractures or the these fractures are pre-Waterberg. Further westwards however, the fracture set is reproduced in the Waterberg, as it is also on Gokano Hill (figure 6.1 and figure 4.2). These facts could mean that the fractures were initiated post-Transvaal deposition, but pre-Waterberg deposition, with a reactivation in post-Waterberg times. This interpretation of fracture development in the post-Transvaal/ pre-Waterberg period is supported by

the non-displacement of Waterberg sediments by faults that displace Transvaal rocks around Gokano Hill (figure 4.2), e.g., Mokalaka Fault. Within the Moshaneng domain (domain 4), these fractures have affected layered sequences and massive igneous bodies. Such fractures continued to develop after the intrusion of the igneous bodies. The dolerite has been is dated at 1110 ± 55 Ma, a post-Waterberg age. A subsidiary fracture set trends 60 degrees; its mappable expression is restricted to occurrences of igneous bodies.

6.4.2 Domain 5 (Masoke area, southern Transvaal Supergroup)

Frequency distribution of fracture orientations in the southern Transvaal area near Masoke are dominated by peaks at 10° and 50° (figures 6.6E and 6.7). These lineaments have been confirmed on the ground to be parallel to joints developed mainly in the chert and dolomite sequence and in the chert breccia. A few of these lineaments represent major faults. The 50° lineament trend is parallel to the Taupone Fault and the other smaller faults that displace the lower Transvaal/ basement interface. Subsidiary fracture sets peak at 155° and 170°. On SPOT imagery, the area coincident with domain 5 shows up as the most densely fractured in the study area (see figure 6.4). The strong expression of these lineaments in this medium can be attributed to the false colour infrared signature that enhances the moisture retention properties of fractures in this area. A fracture set that trends about 90° is represented by few but fairly long lineaments, several kilometres in length. These lineament are

traced in figure 6.1, but have longer traces on the SPOT interpretation shown in figure 6.4. These lineaments do not produce a significant peak on the orientation frequency histogram (figure 6.6E). They cut across the post-Transvaal Taupone Fault without being displaced and the post-Waterberg Segwagwa Complex (see figure 6.5 for the location of the Segwagwa syenite intrusion).

6.5 Waterberg

The Waterberg is the youngest of the Precambrian platform rock packages that occur in the study area. In the Tletletsi region, these rocks have been thrown into a regional asymmetrical synclinal fold flanked by steeply dipping to overturned beds in the northeast and moderately dipping beds in the south. At Gokano Hill, the Waterberg beds are almost flat lying except for the western most part of the exposure which is also thrown into a syncline, with overturned beds in the north. Exposures in the central part of the study area are also more or less flat lying, except for steep dips in their northern margin. The steep dips are on limbs of drape folds, which have responded to differential vertical movement of the underlying basement. These forced folds are discussed in more detail in chapter 9. Mainly because the Waterberg is a thin veneer over the older rocks, it tends to show the lineament pattern of the underlying units that were probably reactivated at a later time that post-dates the Waterberg. Engelder (1985) suggests that extension joints are formed in response to a variety of processes that start early in the history of a basin and continue through uplift and unroofing. It is

herein suggested that the fractures in the Waterberg at Gokano were formed during uplift and unroofing, and the fractures formed in these platform beds are controlled by the pre-existing fracture pattern of the underlying rocks.

6.5.1 Domain 6 (Tletletsi area)

The Tletletsi area is designated domain 6. The fracture pattern in this domain is considered apart from other Waterberg areas because of the synclinal structure that makes this domain unique. The orientation frequency distribution is shown in figure 6.6F. A peak of lineament orientations occurs at 40°. This set of lineaments are due to joints which are developed on the southern limb of the Tletletsi syncline. Subsidiary sets are scattered at 20°, 75° and 120° (figures 6.6F and 6.7). The latter two directions are similar to those in the basement (domain 1) and the lower Transvaal (domain 4) respectively. These can be attributed to post-Waterberg reactivation of older fracture sets. This conclusion is supported by the fact that the fractures are not as closely spaced in the Waterberg as in the older rocks. Most of the basement lineaments that escaped reactivation stop at the basement/Waterberg unconformity.

6.5.2 Domain 7 (Gokano Hill)

The exposures at this locality show the most densely fractured location of the Waterberg occurrences on the aerial photo lineament interpretation map shown in

figure 6.1. The most dominant fracture set has a peak trend at 35° (figures 6.6G and 6.7). The frequency histogram is poorly defined around the dominant set. Notable modes are found at 85° and 130°. The fracture pattern is largely similar to that of the underlying northern (domain 1) and southern (domain 2) basement. The exception is a prominent east-west fracture set which is parallel to a silicification zone in the basement to the north, also parallel to the fold axis of a monocline on the northern end of the exposure. The lineaments correspond on the exposure to joints and some faults.

6.5.3 Domain 8 (Kanye area)

Lineament orientations in this group of exposures show a highly prominent peak at 60°. This set is parallel to the basement dominant set representing faults of the Taupone Fault set. Other distinctive subsidiary set are at 15°, 120° and 155° (figures 6.6H and 6.7). All of these sets are similar in orientation to fracture sets found in the underlying rock packages.

6.6 Discussion

A summary of the development of fractures in the study area is provided in **figure 6.8**. The Archaean basement developed ENE and NE trending fractures in pre-Transvaal times. Master joints and normal faults formed as the crust ruptured in a broad zone of extension that affected many parts of the Kaapvaal. Rifting conditions

Figure 6.8: Schematic illustration of the development of regional fractures in the area around Moshaneng. The vertical planes indicate the formation of fractures in the crustal block at different stages through geologic time.

A. Pre-Transvaal fractures develop in the Archaean basement. Master joints and normal faults rupture the crust under rifting conditions. Basic dikes are emplaced along steep fracture planes cutting rocks of the Gaborone Granite, Kanye Volcanic Formation and Ventersdorp Supergroup. The fractures are traced along ENE to NE trends. These developments are identified in domains 1, 2 and 3.

B. Deposition of the Transvaal Supergroup in epeiric basins. **T**= Transvaal Supergroup.

C. Post-Transvaal fractures affect all the rock types. New master joints and faults trend NW in domain 4 (figure 6.7). In this domain strike-slip faults show sinistral displacements. In domains 3 and 5 however, post-Transvaal fractures trend NE and faults display dextral displacement. Fault displacement occurs as a reactivation of pre-Transvaal fractures.

D. Deposition of the Waterberg Group mainly in fault controlled grabens. The faults are probably reactivated pre-Transvaal fractures trending NE to ENE.

E. Post-Waterberg reactivation of pre-existing faults affect mainly a thin veneer of Waterberg Group rocks. The fracture system in the Waterberg mimics that of the underlying rocks. These systems are apparent in domains 6, 7 and 8. The N-S to NNE trend in domain 5 is not shown in this diagram to avoid clutter. It probably represents new post-Waterberg normal faults.

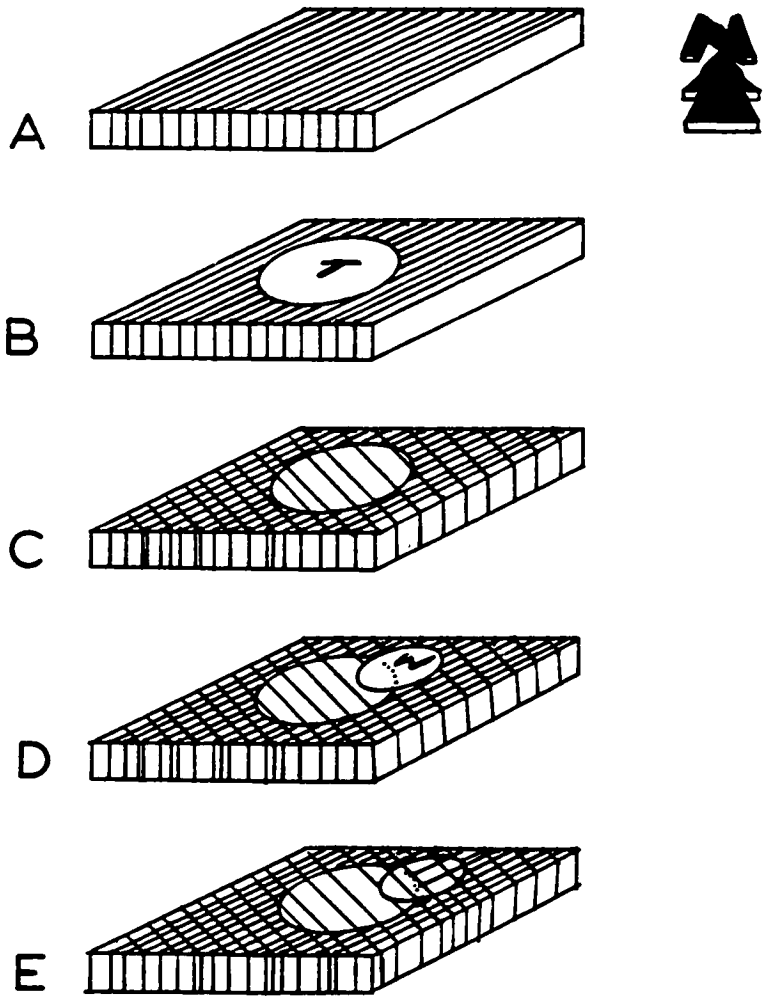
A
B
C
D
E

facilitated the emplacement of basic dikes along steep fracture planes cutting rocks of the Gaborone Granite, Kanye Volcanic Formation and Ventersdorp Supergroup. These developments occurred in domains 1, 2 and 3.

Transvaal Supergroup rocks were deposited on a subsiding crust that hosted epeiric basins. Post-Transvaal fractures affected all existing rock types. Master joints and faults trend NW in domain 4 (figure 6.7). Strike-slip faults in domain 4 result in sinistral displacements. In domains 3 and 5 however, most of the post-Transvaal fractures trend NE and faults display dextral displacement. These faults in the domains 3 and 5 are probably a reactivated pre-Transvaal fractures.

Deposition of the Waterberg Group occurred mainly in fault bounded grabens. The faults were reactivated fractures that had their origins in the pre-Transvaal. Post-Waterberg tectonics show continued reactivation of pre-existing fractures. The thin veneer of Waterberg Group rocks responded to basement instabilities by forming fracture patterns that mimic those of the underlying rocks. These systems are apparent in domains 6, 7 and 8. The N-S to NNE lineament trend in domain 5 represents new post-Waterberg fractures that affected a belt of terrane along a central strip of the area of study. Many of these fractures vertically displace all the rock types, but show no evidence of strike-slip displacement.

6.7 Conclusion

The basement was cut by ENE to NE trending fractures in pre-Transvaal times,

but probably after the Lobatse Volcanic Group rocks were emplaced. Some of these fractures became host to basic sheet intrusions. The ENE lineament trend in the basement is similar to the major axis of all the major Kaapvaal Craton depositional basins (see figure 1.2). The ENE and NE fractures in the study area were reactivated in the post-Transvaal. The reactivation was pronounced in the southern part, in the region of the Taupone Fault. Right-handed shear imparted a rotational bulk strain about a vertical axis. The Waterberg domain mimics the fracture pattern of the underlying lithologies where it directly overlies the basement.

CHAPTER 7: JOINTS

"According to the well-known 'theorem of minimum energy,' the equilibrium state of an elastic solid body, deformed by specified surface forces, is such that the potential energy of the whole system is a minimum. The new criterion of rupture is obtained by adding to this theorem the statement that the equilibrium position, if equilibrium is possible, must be one in which rupture of the solid has occurred, if the system can pass from the unbroken to the broken condition by a process involving a continuous decrease in potential energy"

Griffith, 1921

7.1 Introduction

In chapter 3 a joint was defined as a fracture along which no appreciable displacement has occurred (Ramsay and Huber, 1987; Hobbs et al, 1976; Price, 1966). Joints which have been filled with mineral matter are strictly veins, but are included in the following descriptions of the orientation and spacing of joints. Some joints show slicken-striae, indicating that some limited slip has occurred along the joint plane. Such slip however, has not produced appreciable displacement, hence the fractures still meet the definition of a joint.

Joints occur in all the rock types in the study area; but data acquisition was biased. Basement rocks, especially the Kanye Volcanic Formation, locally show high magnetic susceptibility of up to 4.0×10^{-3} c.g.s units and deflect the magnetic compass. Intrusive suites such as dolerite bodies and quartz syenite are also magnetic,

a factor that made it difficult to take a large number of orientation measurements from these rock types. Individual granitic exposures are relatively few and usually show a higher degree of weathering than other rock types. Therefore joint orientation data were mainly obtained from the layered sediments around Moshaneng.

In this chapter, geometrical aspects of joints in the study area are described. Some observations on the mechanical characteristics are presented and the role of joints in the development of chert breccia and karst in SE Botswana is examined. Exposures of stratigraphic profiles on which joint system patterns could be conveniently studied are limited to only a few metres or less. The patterns formed by traces of layer-parallel joints were therefore excluded due to poor or non-existent exposure. The following discussion will focus on bed-plan fracture pattern mapping and ground measurements of fracture orientations and spacing.

7.2 Joint architecture

In the area around Moshaneng, joint sets and systems in the layered sediments display a consistent angular relationship with the bedding plane. Joint planes are formed perpendicular to bedding. In all stereographic projections plotted from stations in layered rocks in **appendix A** , a great circle drawn as the mean bedding surface approximates a girdle through the poles to joints. Complications, arise where the beds are folded. A set of joints, however, is formed as a result of parting parallel to primary sedimentary layering (figure 7.1A). For these rocks, *bedding-normal* joints and

Figure 7.1A: Bedding-parallel parting planes in the Black Reef Quartzite at station 21. This rock consists mainly of graded beds with local occurrence of cross-beds. Bedding-parallel parting planes do not necessarily coincide with sedimentary structures. The tape in the foreground (white arrow) measures a layer that is 36 cm thick. The aggregate thickness to the tilted planar exposure in the middle ground is 101 cm.

Figure 7.1B: Plumose patterns on joint planes in the chert breccia unit near Kgwakgwe at station 82. The position of a horizontal axis along the middle of the joint plane is indicated by the large white arrow. Diffuse traces of wedge-like markings diverge from axis; becoming more pronounced at the edge of the joint surface (small white arrows). Propagation of the fracture edge was horizontal, from the right side of the photograph towards the left. En echelon fringe fractures are clearly visible at the top and bottom of the joint surfaces.


A
B

bedding-parallel joints become convenient descriptive terms. These types of joints are not exclusive in the area; variations occur under certain conditions which are discussed later in this chapter. Bedding-normal joints are truncated by bedding-parallel joints and vice versa (figure 7.2). The thickness of layers between bedding-parallel joints controls the spacing between bedding-normal joints. A relationship between fracture spacing and bed thickness was established by Price (1966), Ladeira and Price (1980) and Gross (1993). In these studies, however, no consideration was demonstrated for the effect of orientation i.e. cut effect (Ramsay and Huber, 1987).

Engelder (1985, fig.9a) has observed joint containment within coarser grained sandstone overlain by siltstone in Palaeozoic sediments of western New York State, U.S.A.. The spacing between joints is primarily a function of layer thickness. Layer thickness in turn can be controlled by lithologic type and thus different lithologic layers in a stratigraphic sequence will display different joint patterns.

Blocks of rock detached from outcrops of layered rocks have a brick-like morphology, rectangular or parallelepiped blocks being quite common. The architecture of joint planes at outcrop scale is diagrammatically illustrated in figure 7.2.

In massive rocks such as felsite, syenite, and granite, horizontal or near horizontal sheet joints have developed (figure 7.3A, figure 7.3B, and figure 7.3C respectively). Exposures of these rock types have a layered or locally contoured appearance due to the presence of these fractures. The aerial photograph in figure 6.2 shows a contour pattern of a hill of dolerite exposure. The contours are caused by

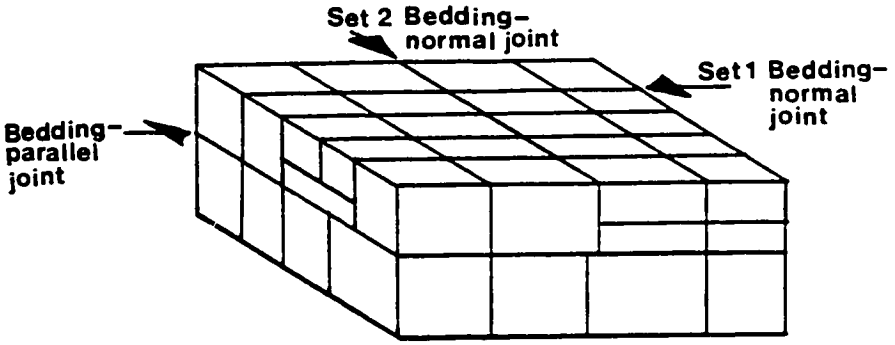

Figure 7.2: Schematic block showing the joint architecture in a homocline of the Black Reef Quartzite. The bedding surface displays two sets of bedding-normal joints. Each of the profiles shows one set of bedding-normal joints and the bedding-parallel joint set. The set 1 joints show a smaller spacing interval than the set 2 joints. The spacing interval between the bedding parallel joints is smaller in finer grained rock units within the same formation. The spacing between bed-parallel joints also contributes in defining the spacing between bedding normal joints.

Figure 7.3A: Station 46; three fracture sets in Kanye Volcanic Formation. The sets are virtually mutually orthogonal. The felsite at the measuring station is overlain by conglomerate a few metres above. The vertical fracture sets are congruent with the orthogonal system of the layered rocks of eastern Moshaneng (NB: the sets in figures 7.3A-3E are not necessarily defined as those in the layered units (section 7.3). The different symbols, however, show different sets)

Figure 7.3B: Station 54; Horizontal sheet joints in syenite. Three other sets of vertical joints were measured in the field. These sets are indistinct, unlike those developed in layered rocks (see NB in 7.3A).

Figure 7.3C: Station 73; An orthogonal joint system in granite. A slightly tilted SE-dipping sheet joint set is also developed (see NB in 7.3A).

Figure 7.3D: Station 74; NW trending conjugate joint sets in granite. A diagonal system is formed in vertical NE trending vertical section. The horizontal trend is similar to the regional Mokalaka Fault (chapter 8)(see NB in 7.3A).

Figure 7.3E: Station 76; sun azimuth fracture sets in Kanye Volcanic Formation felsite. NW trending fracture sets are parallel to a regional fracture set domain 4 (see NB in 7.3A).

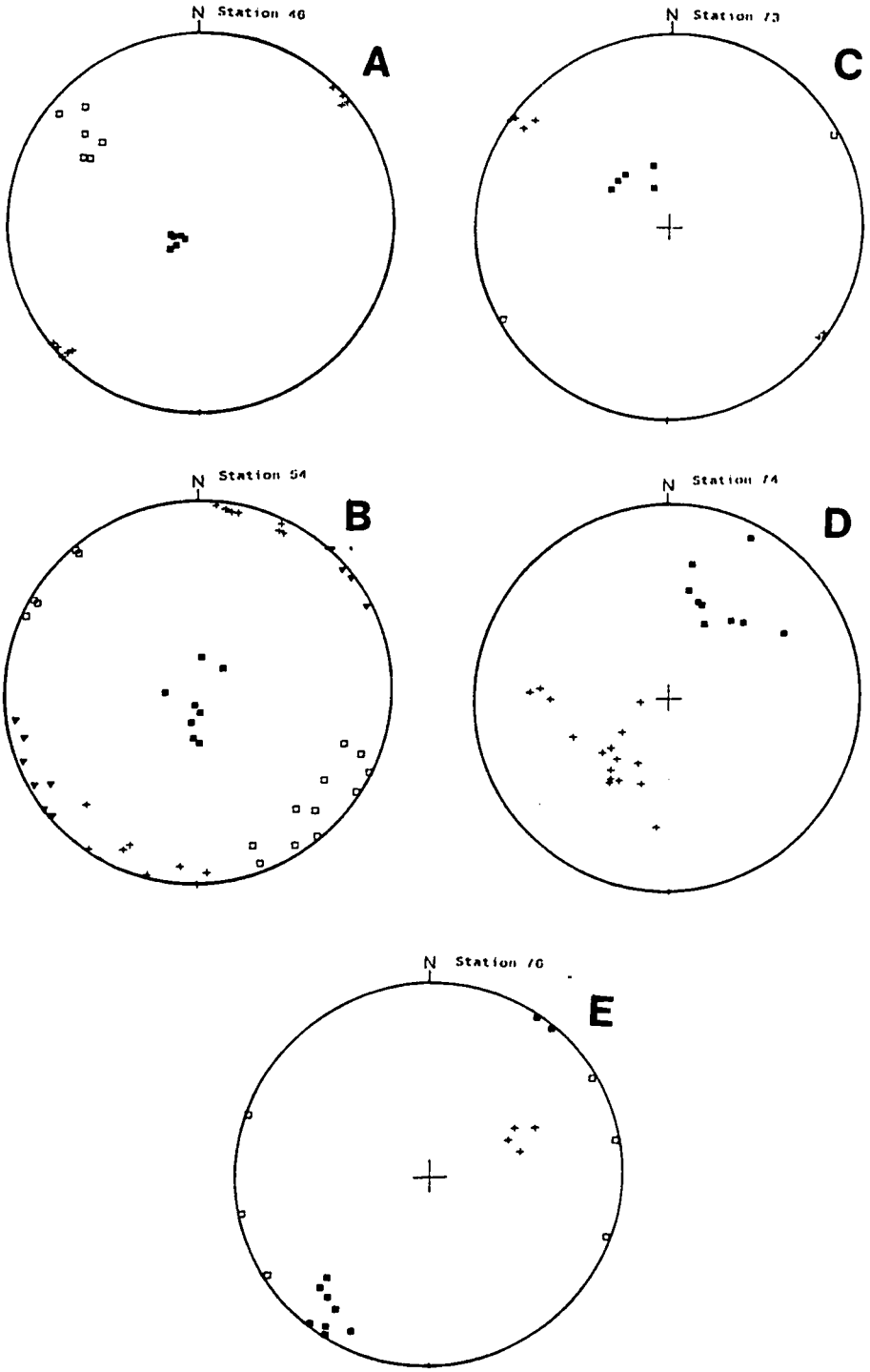
N Station 46
A
N Station 73
C
N Station 54
B
N Station 74
D
N Station 76
E

terraces formed at the intersection of sheet fractures and the topography. These sheet fractures assume a dome-like shape in some isolated kopjes and whale-back exposures. The joints have formed following uplift and stress release as overburden is removed (Price, 1966). These joints were probably formed during the post-Cretaceous landform development of SE Botswana.

7.3 Joint patterns

7.3.1 Orthogonal system

A joint system with orthogonal sets is the dominant pattern in the layered rocks. The best exposures occur on bedding surfaces of the Black Reef Quartzite of the Lower Transvaal Supergroup. The orthogonal system consists of remarkably consistent joint sets 1 and 2, as shown on the small scale map in figure 7.4 and the photographs in figures 7.5 and 7.6A. The stereographic projection for station 19 (figure 7.7B) shows an example of an orthogonal joint system. Table 7.2 shows that the average angular difference between sets 1 and 2 at stations 1 to 40 is 87°. In eastern Moshaneng the angular difference between these joints is >85°(but <90°). Joint set 1 has a strike line that is consistently parallel or sub-parallel to the strike of bedding i.e. the intersection of the set 1 joint plane and the bedding plane is approximately parallel to the strike of bedding. In table 7.2 the mean angular difference between the strike of bedding and the strike of set 1 at stations 1-40 is about 5°. The joint set 2 is

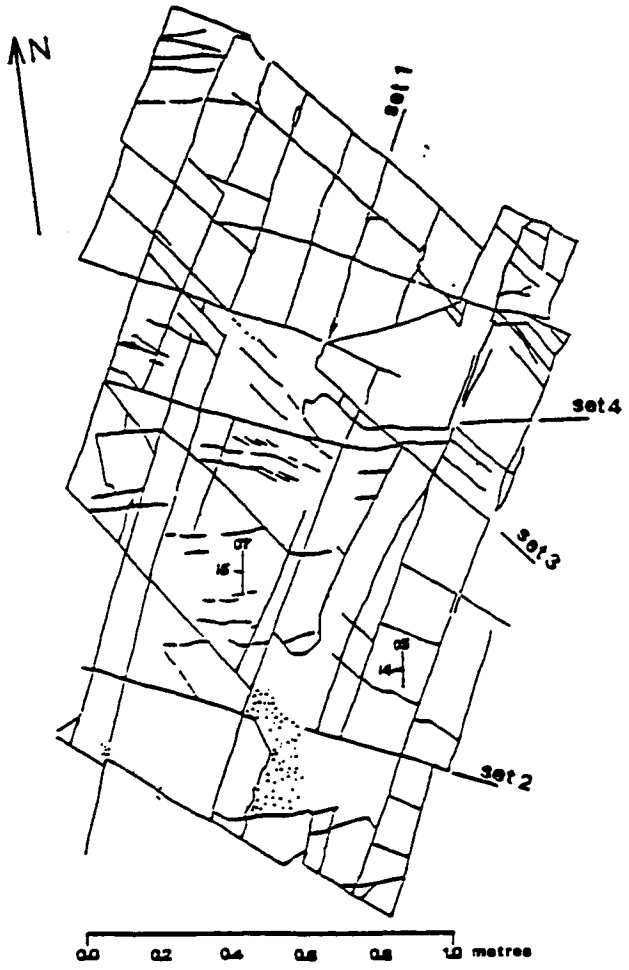

Figure 7.4: Map of the joint system on Black Reef Quartzite bedding plane at station 21 (see figure 7.12 for location and figure 7.7C for the stereographic projection). An orthogonal system consists of sets 1 and 2. Set 1 is the most closely spaced and has the closest trend to bedding strike. An apparent conjugate system is formed by sets 3 and 4. Set 3 is found at an acute angle, clockwise from set 2 and similarly, set 4, anticlockwise from set 2. The system does not reveal clear age relationships among the individual joint sets except for joint set 4. The large majority of set 4 joints are truncated by the other sets and many have terminations within blocks bounded by other sets. Many set 3 joints are truncated by sets 1 and 2.

Figure 7.5A: Joint system pattern on an inclined Black Reef Quartzite bedding plane. Three joint sets can be readily distinguished on this photo. The set 1 is parallel to the strike of bedding, and can be traced laterally across the photograph. The set 2 is orthogonal to set 1. Set 4 is nearly parallel to the hammer handle. The relative spacing among these joints is set 1< set 2< set 4.

Figure 7.5B: Two set joint system pattern on a Black Reef Quartzite bedding surface. The spacing is much closer than the three set system in figure 7.2A. The joint set 1 is approximately parallel to the hammer head and shows the closer spacing of the two in this photograph.

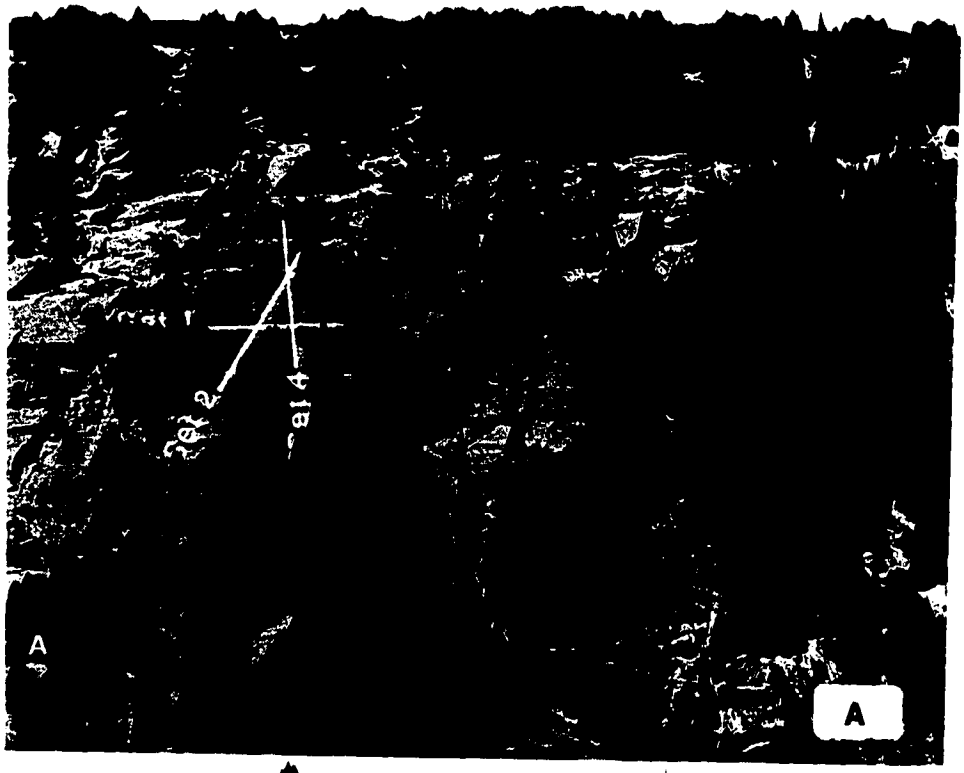
A

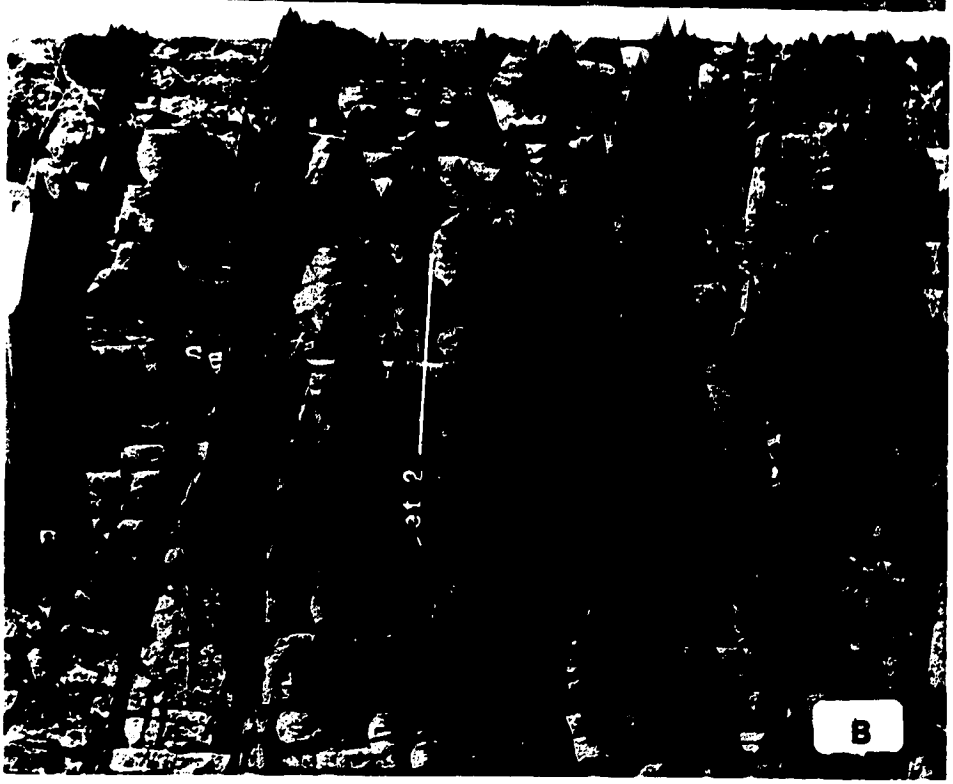
B

Figure 7.6A: Orthogonal joint system formed by sets 1 and 2. An apparent conjugate system is formed by sets 3 and 4. This photograph is obtained from station 21 and forms part of the map in figure 7.4.

Figure 7.6B: Quartz veins pattern on the bedding surface of Black Reef Quartzite. The set 1 veins have an attitude 033/67 at station 40. The vein quartz has been recrystallized and shows no fibres. Set 4 veins intersect set 1 veins at a high angle ≈65°. The set 4 veins are either truncated by set 1 veins or displace set 1 veins. These relationships show that the set 1 veins are older.

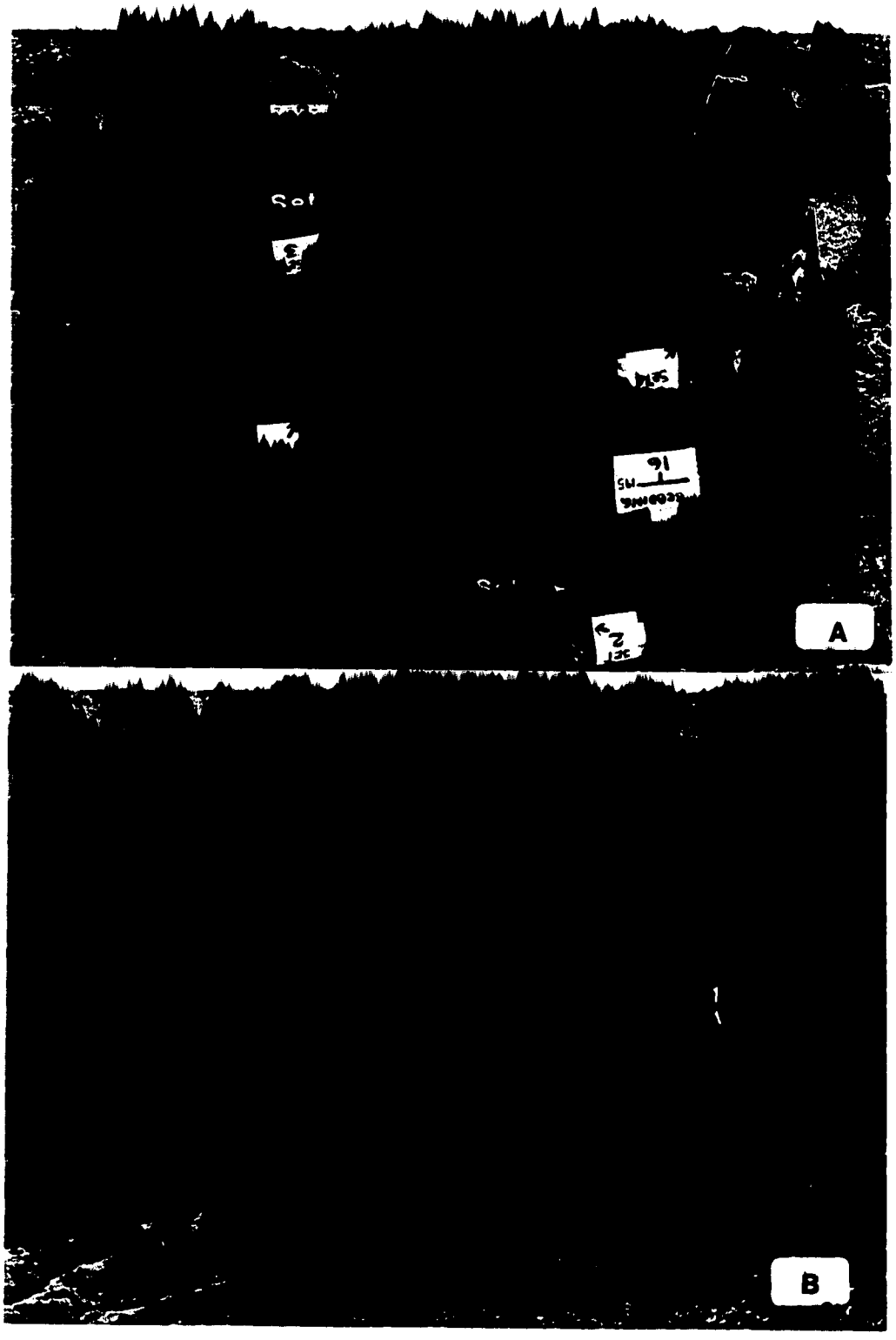
A
B

Figure 7.7A: Stations 1-10; Orientations of bedding and joints in the Black Reef Quartzite. The angle between the joint set 1 cluster and the bedding cluster is about 90 degrees. The intersection of the bedding plane and the set 1 joints coincides with the strike of bedding at about 018/00. Slicken striae in the bedding plane suggests flexural slip. Striae in the set 1 fractures suggests normal faulting. The mean attitudes of bedding and joint sets is given in figure 17.A.

• = bedding.
+ = set 1 joints
□ = set 2 joints
▽ = set 3 joints
▾ = set 4 joints
→ = slicken striae, with sense of slip
★ = fold axis
Girdle=mean bedding

Figure 7.7B: Station 19; Orthogonal joint system. Orientations of bedding and joints in the Black Reef Quartzite.

Figure 7.7C: Station 21; Orthogonal and diagonal joint systems. Sets 1, 2 and 3 are closely clustered. Set 4 is widely distributed.

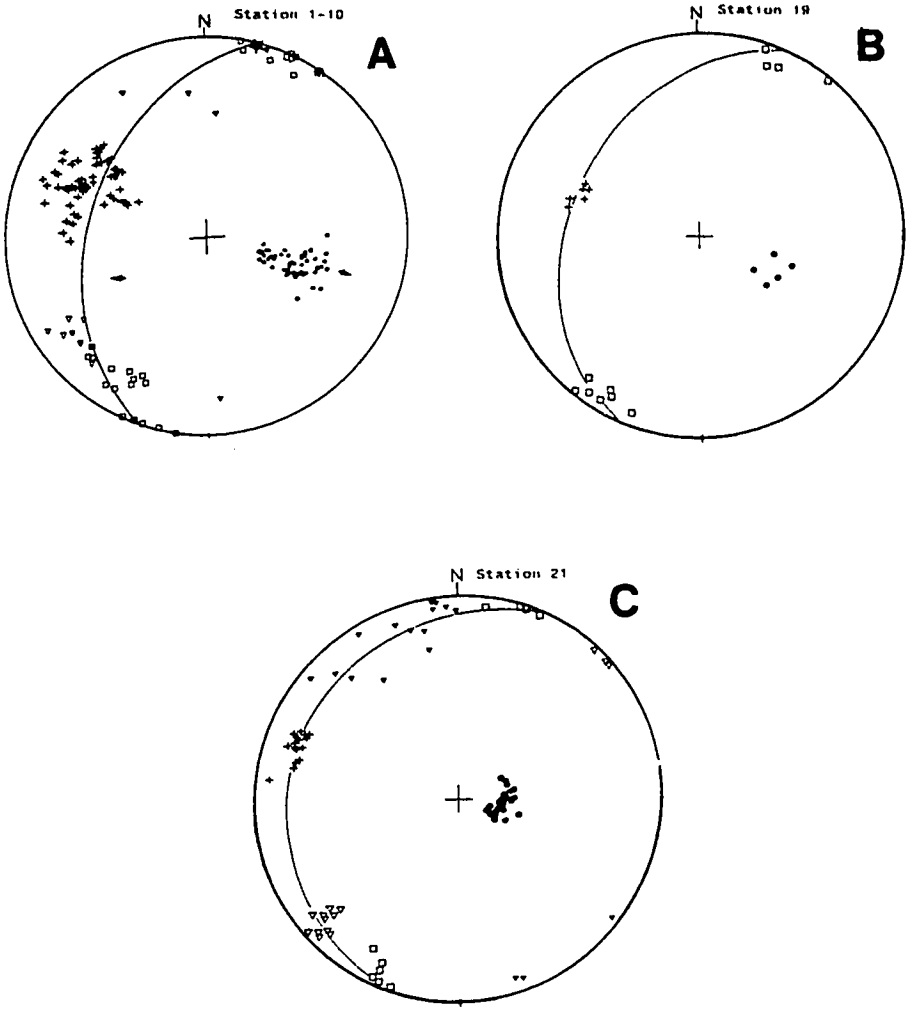
N
Station 1-10
A
N
Station 19
B
N
Station 21
C

Station	bed/ set	Eigen- vector 3		Number of readings	Average bed/ joint	
		Trend	Plunge		Strike	Dip
1-10	bed	108	51	50	198	39
1-10	1	296	33	53	26	57
1-10	2	206	8	33	296	82
1-10	3	233	18	7	323	72
1-10	4	358	14	6	88	76
22-24	bed	91	69	57	179	21
22-24	1	292	20	60	22	70
22-24	2	203	4	39	293	86
22-24	3	228	11	51	318	79
22-24	4	172	0	14	82	90
52-53	bed	119	86	39	209	4
52-53	1	299	1	51	29	89
52-53	2	221	0	25	311	90
53	3	237	11	10	327	79
1-40	bed	113	64	425	203	26
1-40	1	298	24	419	28	66
1-40	2	208	5	285	298	85
1-40	3	234	10	175	324	80
1-40	4	356	7	147	88	83

Table 7.1: Mean bedding and joint set attitude at stations in domain 4, east Moshaneng. The mean attitudes of bedding and joints are obtained by the calculation of the orientation of the maximum eigenvector, representing poles to these planar structures. A sample of these calculations is provided in appendix B.

Station	Strike line(s) Joint plane(j)	Angular difference(°)
1-10	bedding/set1(s)	8
1-10	set1/set2(j)	85
1-10	set2/set3(j)	26
1-10	set2/set4(j)	38
1-10	set3/set4(j)	64
22-24	bedding/set1(s)	13
22-24	set1/set2(j)	87
22-24	set2/set3(j)	25
22-24	set2/set4(j)	35
22-24	set3/set4(j)	60
52-53	bedding/set1(s)	0
52-53	set1/set2(j)	90
52-53	set2/set3(j)	20
1-40	bedding/set1(s)	5
1-40	set1/set2(j)	87
1-40	set2/set3(j)	25
1-40	set2/set4(j)	35
1-40	set3/set4(j)	60

Table 7.2: Angular difference between joints. Angular difference between the strike of bedding and joint set 1 in layered rocks of eastern Moshaneng (domain 4). These differences are based on the mean orientations given in table 7.1.

orthogonal to the joint set 1 and the bedding plane. Deviations from this rule occur where mesoscopic folds occur. Joint sets 1 and 2 rarely show joint terminations other than where they are truncated by other sets.

7.3.2 Diagonal system

Set 3 and set 4 joints form an apparent conjugate system. The joint set 3 is found at an acute angle clockwise from set 2 and set 4 is found at an acute angle anticlockwise from set 2. The stereographic projection at station 21 (figure 7.4 and figure 7.7C) provides a good example of a diagonal system superimposed on an orthogonal system. In this example, joint sets 1,2 and 3 have closely clustered poles to joint planes, demonstrating their consistent orientations. Joint set 4 has a rather broad spread in the distribution of orientations. Other sets are relatively rare and shall be named on local stations as they occur over the region. In table 7.1, the mean angular difference between sets 3 and 4 is 60°. At a few stations, the angular difference between these sets is up to 90°. Joint terminations are common in sets 3 and 4, especially set 4 as shown in figure 7.4.

7.3.3 Single set system

One set joint systems occur in the hinge areas of folded Waterberg sandstone. Joint terminations are common in this system. The joints are commonly quartz-filled

and display quartz fibres (figure 7.8A and 7.8B). The termination of one joint is commonly accompanied by the initiation of another adjacent joint. These kinds of terminations have been attributed to the interaction between joints (Segall and Pollard, 1983). Other terminations are characterized by bifurcations as shown in figure 7.8B.

7.4 Relative chronology of joint sets

In the majority of cases, joint sets 1 and 2 truncate other sets. Only in a few cases are sets 1 and 2 truncated by others. These relationships suggest that sets 1 and 2 are older than the others. The joint set 4 is invariably truncated by other sets. At station 40 (figure 7.6B), set 4 is either truncated by set 1, or it displaces set 1 joints. The displacement is dextral. At stations 21 (figure 7.4), en echelon fracture arrangement along set 4 also shows dextral shear displacement. These relationships show that set 4 joints have a shear aspect and are younger than set 1. The external stress field that was responsible for the formation of the joint system at each station was probably the same for each joint set. Mechanical conditions of the rock, and the variation of these conditions during progressive deformation probably account for the apparent chronology. These conditions and their effects are discussed later in this chapter. The orthogonal joint system is present in all the layered sediments suggesting a universal mechanism of formation. An examination of the stereographic plots of layered rocks in figure 7.7, 7.9, and 7.10 shows that the poles to joints plot on a great circle approximately coincident with the mean bedding plane. Joints developed in

Figure 7.8A: Vertical quartz veins in the Waterberg sandstone. At vein termination, an adjacent parallel vein begins. The quartz fibres in the main vein are perpendicular to the walls of the vein. These veins form part of a single set system.

Figure 7.8B: Branching set of veins in the Waterberg sandstone. The quartz fibres are virtually perpendicular to the vein walls; evidence for dilation as fracture walls moved apart. These fractures have strike-parallel traces in the limb of the Mokalaka monocline in the NE flank of Tletletsi syncline. Notwithstanding the bifurcations, these veins essentially a single set system.


A


B

Figure 7.9A: Station 59; Joint sets in south-dipping Black Reef Quartzite in domain 5 (figure 6.6). Bedding-normal joint sets are not as well defined as in domain 4. Quartz-filled en echelon tension gashes are developed at this exposure. The fracture set legend is the same as for figure 7.7.

Figure 7.9B: Station 61; Four sets of joints in south-dipping Black Reef Quartzite. Two superimposed orthogonal sets are well defined.

Figure 7.9C: Station 62; Three set system in south dipping Black Reef Quartzite. The orthogonal system is well-defined.

Figure 7.9D: Station 78; Three set system in west-dipping Black Reef Quartzite. Fractures are not congruent to the main part of domain 5 fracture system.

Figure 7.9E: Station 79; Three set system in southwest dipping dolomite and chert sequence.

Figure 7.9F: Station 80; Three set system in southwest dipping dolomite and chert sequence.

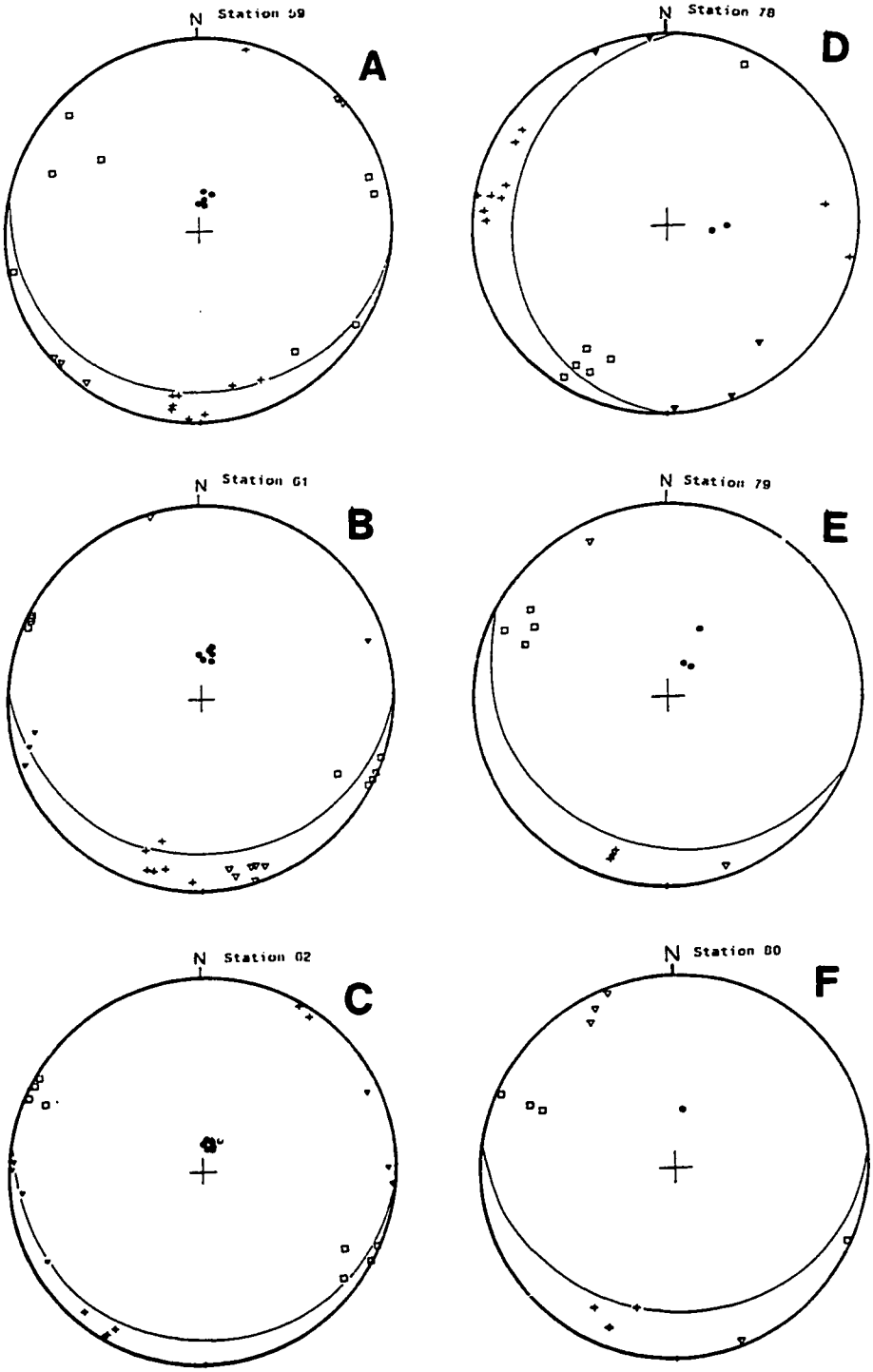
N Station 59
A
N Station 78
D
N Station 61
B
N Station 79
E
N Station 02
C
N Station 00
F

Figure 7.10A: Station 53; Four set joint system in dolomite. Exposure is in eastern Moshaneng.

Figure 7.10B: Station 55; Four set joint system in Waterberg sandstone. The closely clustered sets are belong to a minor domain on a local fold south of the Tletletsi Syncline.

Figure 7.10C: Station 58; Overturned fold and four sets of joints at Gokano Hill. One fold axis has attitude 286\08. A second fold axis about which the overturned monocline or drag fold is formed has attitude 080\00.

Figure 7.10D: Station 56; Four set fracture system in the Waterberg sandstone. The fractures belong to the same domain as in figure 7.10B.

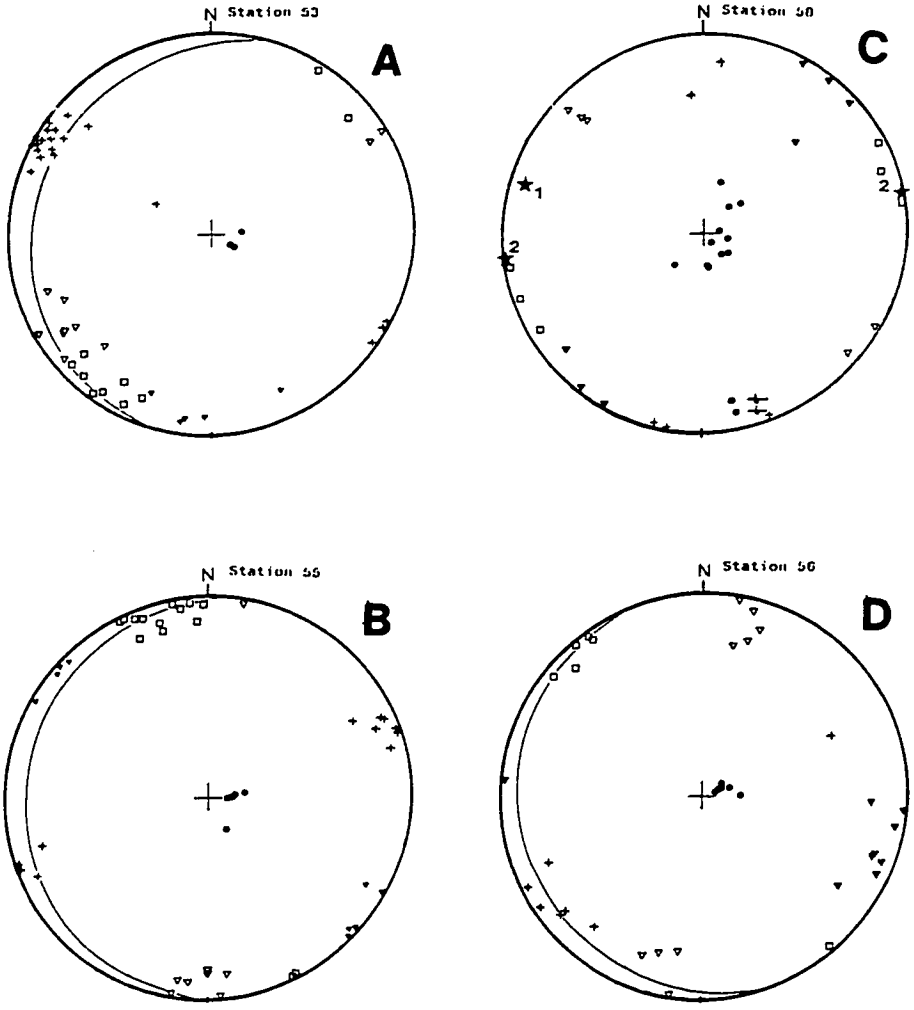
N Station 53
A
N Station 58
C
1
2
2
N Station 55
B
N Station 56
D

granitic or massive volcanic rocks do not fall on a such a girdle e.g stations 46, 73, 74 and 76 (figures 7.3). The anisotropy inherent in layered rocks therefore has a profound influence in the development of geometrical relationships of joint sets and layering.

7.5 Joint propagation

The propagation direction of joints can be inferred where plumose patterns on joint surfaces are preserved. In layered rocks, such patterns demonstrate that propagation is usually initiated at a layering interface or at an irregular object within a layer (Hogson, 1961; Price, 1966; Engelder, 1987; Ramsay and Huber, 1987; Pollard and Aydin, 1988). The point of origin of a joint is a locus of microscopic stress concentration. Such a point responds to a remote stress field stress, magnifying it locally until the tensile strength of the rock is exceeded (Engelder, 1987). After this initial process in crack formation, joint edge propagation in bedding-normal joints largely advances in a horizontal direction within a layer. In the study area, examples of horizontal propagation were recorded at Kgwakgwe, where plumose patterns on joint surfaces are preserved in chert breccia beds (figure 7.1B). At this locality, plumose markings branch away from a horizontal axis in each of the bedding-normal joint surfaces. This type of plumose pattern has been termed the S-type plume (Engelder, 1985; Engelder, 1987; Bahat and Engelder, 1984). Most of the exposed joint surfaces in the study area have, however, been eroded and now retain little of these plumose patterns. An absence of the plume patterns could also imply great speed

in joint propagation (Price, 1966, p.124; Segall and Pollard, 1983; Engelder, 1987). This relationship between plumose patterns and speed of joint edge propagation is a contentious one. Hackle marks in joints have been attributed to propagation speeds approaching that of sound or explosive rupture (Price, 1966; Atkinson, 1987). Hackle marks or conchoidal step structures and plumose marks sometimes coexist by some accounts (Price, 1966 p53; Ramsay and Huber, 1987, p660).

7.6 Correlation between regional lineament pattern and ground joint data

7.6.1 General

The regional lineament pattern shown in figure 7.11 presents only two dimensional trends and patterns. Three dimensional orientation data were obtained on ground measuring stations whose locations are shown in figure 7.12 and figure 7.13, box 1 and box 2 in figure 7.11 respectively. The spacing between bed-normal joints was also measured at these stations. True angular relationships between fracture planes and sedimentary bedding and between fracture sets are revealed by these data. Stereographic projections of the orientation data are given in appendix A. A summary of orientations obtain in eastern Moshaneng is given in table 7.2.

7.6.2 Domains 1, 2 and 3

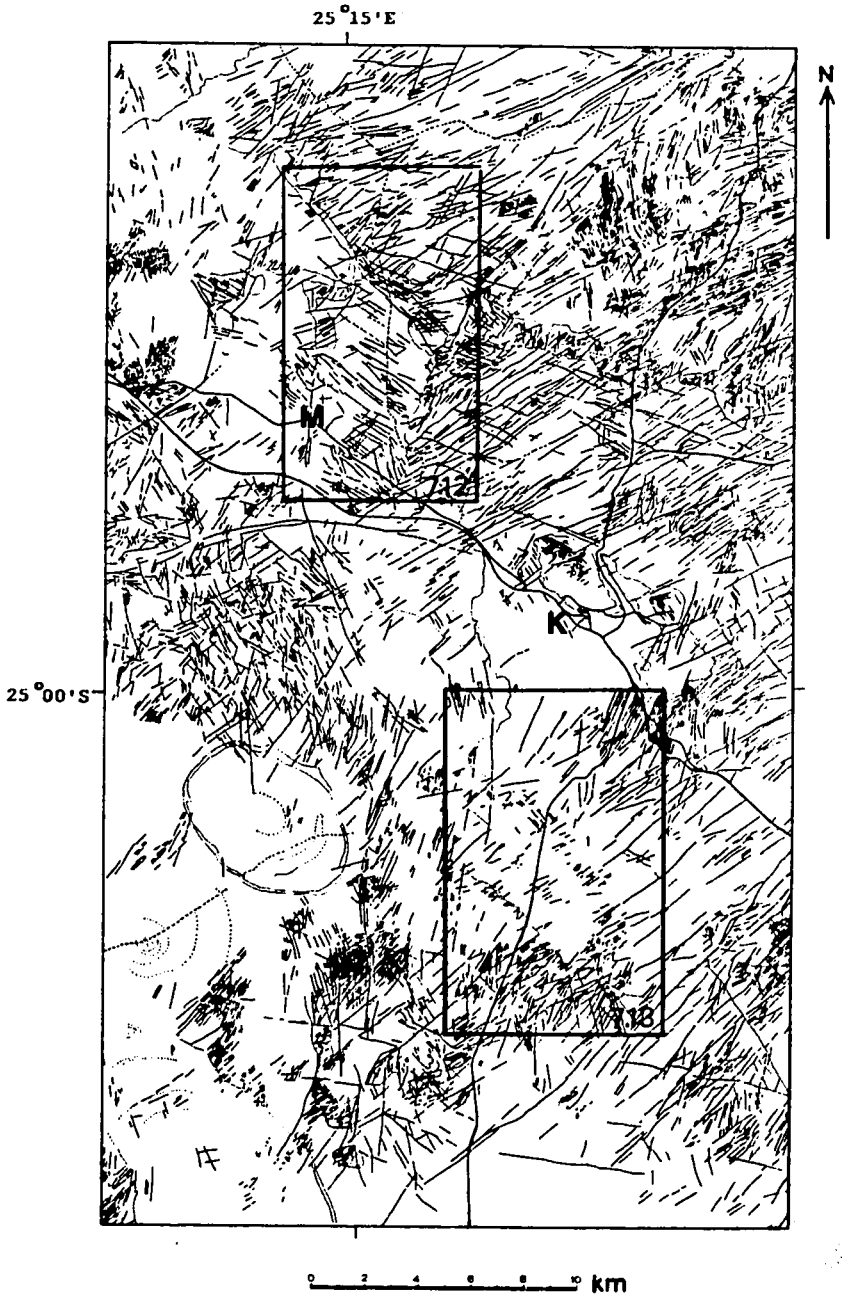

Figure 7.11: Regional lineament pattern interpretation of aerial photographs. The lineaments represent the trace of undifferentiated dikes, master joints and faults. **M**=Moshaneng, **K**=Kanye. The locations of figures 7.12 and 7.13 are shown.

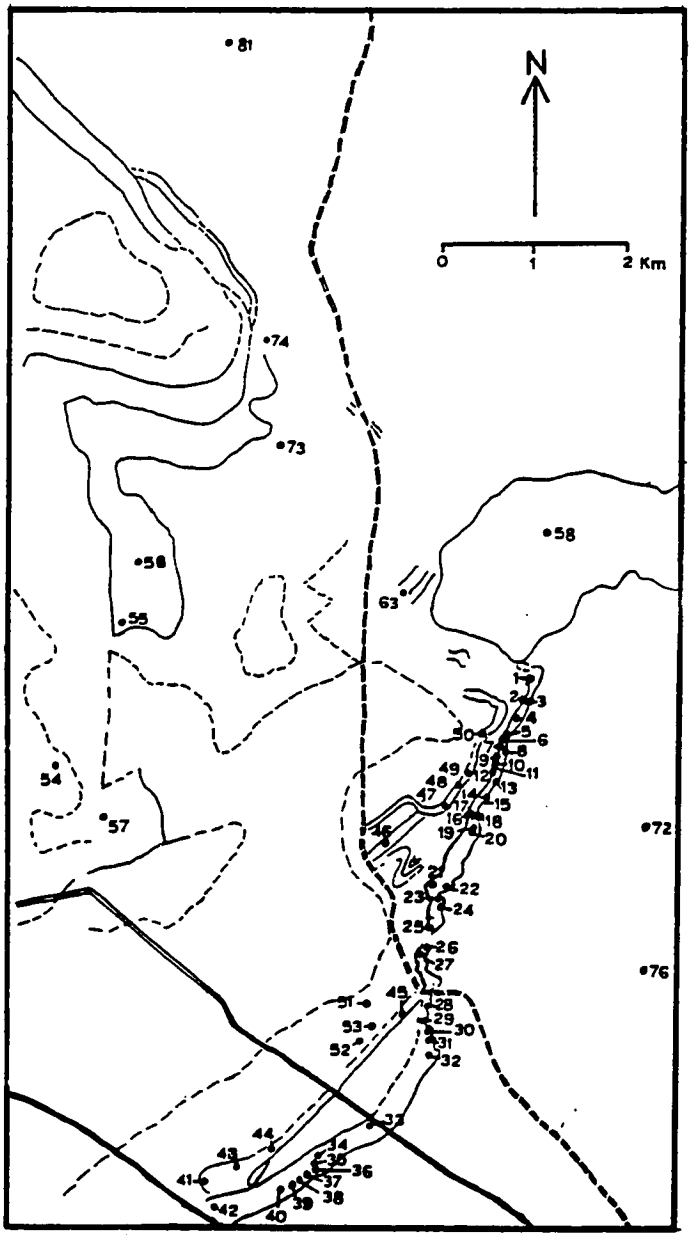

Figure 7.12: Distribution of joint data measuring stations around the Moshaneng area. **BRQ**=Black Reef Quartzite, **UQ**=Upper quartzite unit, **DC**=dolomite and chert, **W**=Waterberg sandstone, **Sy**=Quartz syenite, **D**=dolerite, **G**=Granite and felsic volcanic basement. The area covered by this map is shown on the regional lineament map in figure 7.7.

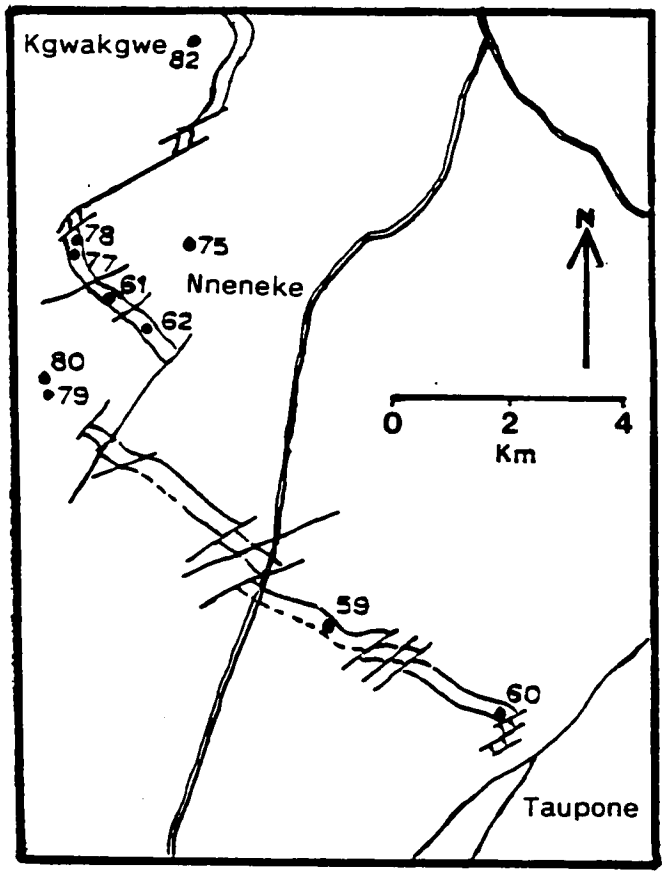

Figure 7.13: Distribution of joint measuring stations south of Kanye. **BRQ**=Black Reef Quartzite, **DC**=dolomite and chert, **LV**=Lobatse Volcanic Group sediments. The area covered by this map is shown on the regional lineament map in figure 7.11.

On the regional map, the basement in domains 1, 2 and 3 displays a ENE to NE trending lineament set. This set is interpreted to represent discretely defined dikes and fractures (section 6.3). There is a good correlation between the strike of joints at ground stations 72 and 81 (Appendix figures A62 and A71 respectively), which were obtained on dolerite dikes and the trend of NE lineaments mapped in figure 7.11 (see also figure 6.6). The relatively minor NW trend represents the strike of joints at station 76 (figure 7.3E or A66). No exposures revealing direct contact of dike and country rock were encountered. The highly fractured process zone that usually flanks these dikes (Delaney et al, 1986; Rogers and Bird, 1987) was therefore not observed.

7.6.3 Domain 4

Domain 4 (figure 6.6) consists mainly of stations which are on layered rocks comprising the Black Reef Quartzite and the dolomite and chert units (figure 7.12). A few stations are on massive granitic rocks. This domain is characterized by a dominant lineament trend of 130° (figure 6.7D) representing faults and master joints. The trend corresponds to that of the joint set 2 found in layered rocks throughout eastern Moshaneng. Between stations 1 and 40, joint set 2 has a mean trend of 128° that is correlated to the lineament trend of 130° (table 7.2 and figure 6.7D). Stations 46, 54, 73, and 74 are obtained from felsite, syenite and granite in this domain. The felsite (figure 7.3A) has a well developed near horizontal joint set. Two orthogonal vertical joint sets are similar to those in the layered rocks. The northwest trending vertical set

(mean strike = 312°) in this rock therefore is correlatable with the dominant lineament trend of 130° or 300°.

A fine NE trending photogeological fabric in eastern Moshaneng corresponds to the joint set 1. Individual master joints are not mappable at the interpretation scale of 1:50,000 used in this study. The orientation of this joint set is therefore not represented on the regional map. The lower Transvaal rocks in this area have been thrown into mesoscopic folds. The absence of master joints is in conformity with an observation made by Price (1966, p116), that master joints frequently fail to form in folds where there are thin interbedded competent and incompetent rock units. The Black Reef Quartzite consists of competent quartzite beds interbedded with thin argillaceous units. The dolomite and chert sequence also consists of a thin interbedding of dolomite and chert.

7.6.4 Domain 5

The area shown in figure 7.12 forms part of domain 5 (figure 6.6). The domain is dominated by lineament trends of 10°, 40° and 50° revealed by the interpretation of remote sensing data. These trends represent master joints and faults respectively (see figures 6.1 and 6.4). The dominant lineament trend of 10° may be correlated with the joint set 4 with a mean trend of about 355° at stations 61 (figure 7.9B) and station 62 (figure 7.9C, locations in figure 7.13). This correlation shows a slight discrepancy of about 15°. The 40° trend may be correlated with the joint set 2 with a mean strike of

about 30° at stations 61, 62 in the Black Reef Quartzite and stations 79 and 80 in the chert and dolomite sequence. There is a slight discrepancy of about 10° in this correlation. These discrepancies may be caused by the fact that ground data exclusively represents joints, and thus inherently biased while the remote sensing includes faults. The 50° trend on remote sensing data is not parallel to any of the joints measured in the layered sediments. This trend however, is parallel to the NE trending Taupone, Sekalaba, Nneneke and Kgwakgwe faults (figure 6.5).

7.7 Orientation analysis

7.7.1 Introduction

A statistical sample population of over 2,300 orientations was collected from outcrop at 82 observation stations. The location of the sampling stations is shown on figures 7.12 and 7.13. A station by station plot on a stereographic projection is given in appendix A. These were achieved by using the Rockware software "Stereo" for the statistical analysis and plotting of orientation data. In the following discussion, references will be made to these plots.

7.7.2 Joints in massive igneous units

Basement rocks, particularly the Gaborone Granite do not possess a strongly

developed primary layering at mesoscopic scale. The fracture pattern at exposures therefore does not conform to the orthogonal or diagonal systems recognized in the sedimentary units. Station 54 (figure 7.3B) is located on quartz syenite. A horizontal sheet joint set is developed. These are probably stress release sheet joints formed during uplift. Vertical joint sets in the syenite do not form as strongly clustered distributions as those described in units with marked primary layering at mesoscopic scale. Systematic patterns have, however, been recognized in massive units in regional studies elsewhere (Viak, 1984, Ronge and Ericsson, 1986). Larger scale layering of the crust is probably a controlling factor in the formation of regional joint patterns. Joints in some of the massive units follow the trend of regional lineaments. Station 74 (figure 7.3D) is located on a granite exposure close to the Mokalaka Fault on the NE flank of Tletletsi (see figure 4.2 and figure 7.12). The joints form a conjugate set on vertical profile. The strike of the joints is parallel to the regional fault. Joint sets in the Kanye Volcanic Formation at station 76 (figure 7.3E) are not closely clustered, but one set is parallel to the NW trending regional fractures. The vertical joint sets at station 46 (figure 7.3A) and station 73 (figure 7.3C) occur in Kanye Volcanic Formation felsite and granite respectively. The two sets of joints formed at these stations have trends consistent with those found in layered sediments within domain 4.

7.7.3 Joints in layered units

7.7.3.1 Black Reef Quartzite

The Black Reef Quartzite has the most continuous exposures, making it the most suitable unit for the orientation and spatial analysis of joints. This unit occurs along a NE trending ridge in the eastern part of Moshaneng and forms the basal unit above the basement-platform cover unconformity (figure 7.12). Joints in the northern part of the quartzite are open fractures with an aperture of >1 mm. Some of the joint surfaces belonging to set 1 have down-dip slicken-striae with a slip sense indicating small scale normal faulting (figure 7.7A). These structure may be joints that have been reactivated during later tangential displacement. Some mechanisms of fracture cleavage development result in the formation of normal and reverse faults at hinges of folds above and below the neutral surface respectively (Hobbs et al, 1976). Over these locations the spread in the dip of bedding is about 35°. This variation is a result of monoclinal flexure at these stations. Dips at the bottom of the dip slope are shallower than dips at the top of the dip slope. Stations 2 and 3 (figures A2 and A3 in appendix A) were taken at the shallower and steeper limbs respectively. This variation in dip is demonstrated at station 2 (figure 9.2A), where it is about 25°. A marked monoclinal flexure is also developed at station 31 (figure 9.3C), where the variation in dip is over 50°. Folds in the study area are fully discussed in chapter 9.

In the area shown in figure 7.12 the joints become increasingly quartz-filled from north to south. This trend generally corresponds to an increase in sediment grain size at measuring stations in the Black Reef Quartzite. From station 27 southwards, the joints are invariably filled with quartz. Quartz fibres are not apparent in the veins. The veins are probably non-dynamic secondary crystallization or recrystallization. At

station 31, bedding parallel parting surfaces are also quartz filled. En echelon tension gashes are aligned along shear zones parallel to the set 1 joints at this station. The trend of the tension gashes is parallel to set 4 joints, indicating local dextral shear displacement. These variations could be attributed to folds that occur at these exposures.

In the northeastern part of the exposures, the joint system is that of orthogonal sets formed by sets 1 and 2. In this region, between stations 1 and 10, the major structure consists of a gentle monoclinal fold with dips shallowing from east to west. The fold axis is parallel to the strike of the Transvaal sediments. Moving southwards, at stations 11, 12, 14 and 15, a diagonal system comprising of joint sets 3 and 4 is superimposed on the orthogonal system of sets 1 and 2. The diagonal system is particularly pronounced at station 18 (figure A18 in Appendix A). Moving further southwards, the angle between joint sets 3 and 4 is about 90°. An apparent second orthogonal system of joints becomes superimposed on the more pervasive joint sets 1 and 2. This geometry is demonstrated at station 21 (figure 7.7C). Two superimposed orthogonal systems are also found at stations 22 (figure A22) and 24 (figure A24). The presence of pre-existing west plunging folds at Gampudi dam, at stations 22, 23 and 24 (A22, A23 and A24) have caused the superimposition of two orthogonal joint systems. At these stations, joints are developed on three limbs of an anticline and syncline pair. At station 22 (figure A22), the strike of bedding is N-S, while that of set 1 is about 025°. All the joint sets however, are essentially perpendicular to bedding. The strike difference between set 1 (025°) and bedding (135°) is even greater at

station 23, where it is 70°. All the joint sets at this station are perpendicular to bedding. Similar relationships are apparent at locations of marked folding such as at stations 30 and station 31. The overlap of joint sets formed in different fold limbs complicates the pattern of joint set orientations. At station 33, the joint set 2 is not developed.

7.7.3.2 Joints in dolomite

The orientation of joints developed in the dolomite are shown in the plots for stations 52 and 53 (figure 9.3F or figure A52 and figure A53 in the appendix), located in the eastern part of Moshaneng area (figure 7.12). At station 52 minor open folds occur in these sediments (figure 9.4B). The orthogonal joint system persists with the development of other subsidiary joint directions. The detailed trends of elephant-skin weathering coincide with fracture trends. The weathering pattern is probably a detailed representation of the mesoscopic and regional fracture pattern in these rocks (figure 7.14).

There is no direct relationship that has been established between change in dips due to folding and the attitudes of joints. However, the station 52 plot shows that the set 1 fractures strike parallel to the fold axis (figure 9.3F). These geometric relationship suggests a genetic link between the two structures (see chapter 9).

Stations 79 and 80 (figure 7.9E and 7.9F) are located in the dolomite and chert sequence in the southern part of the area. Station 82 (figure A72) is located on the

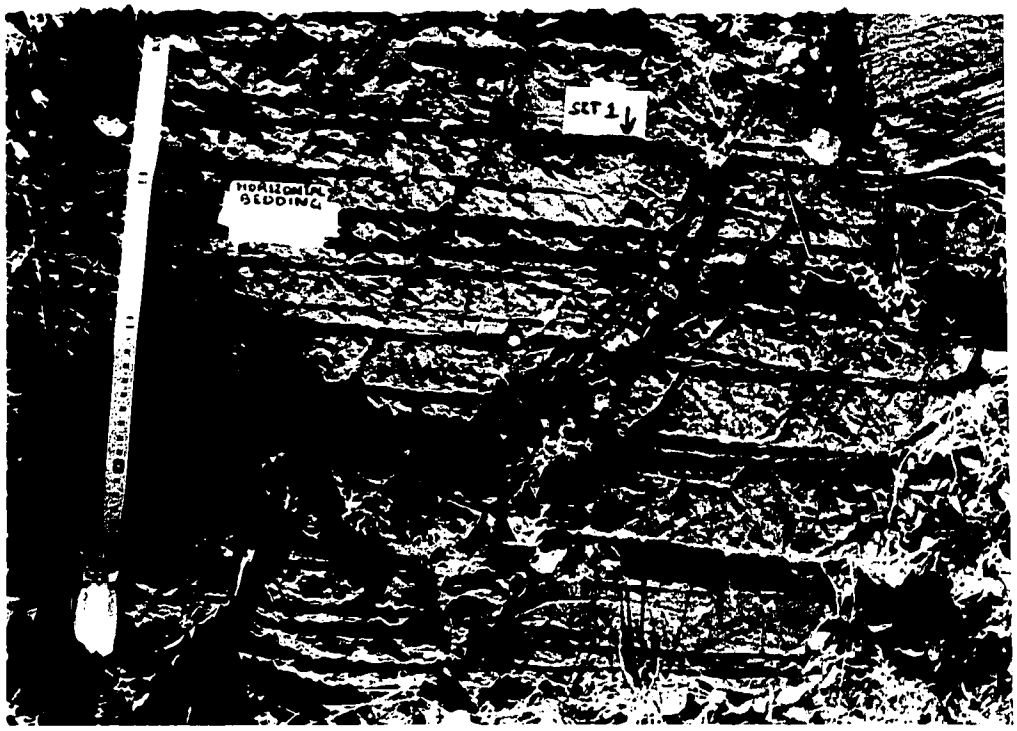

Figure 7.14: "Elephant skin" weathering pattern on dolomite, eastern Moshaneng. Red marks on measuring tape are 10cm apart.

chert breccia at Kgwakgwe Hill. Layering is irregular at mesoscopic outcrop scale. Gross post-collapse layering is however preserved (see figure 7.15A and figure 7.16). Nevertheless, the rock is well jointed with an orthogonal joint system and a subsidiary set as shown in figure A72. The NE and NW trends of the joints can also be identified on the regional map in figure 7.11.

7.7.3.3 Joints in the Waterberg

The joint system in the Waterberg sandstone is presented on stereographic projections for stations 55, 56 and 58 in figures 7.10B, 7.10D and 7.10C. A 4 set system is apparent from Male Hill (stations 55 and 56 in figure 7.12) where the sandstone beds are tilted at 10° to the west. An orthogonal system co-exists with a NE trending set. Whereas the NE trending set mimics fractures in the basement, the orthogonal set is consistent with the trend of the Tletletsi syncline.

A single set system of joints is found along the hinge zone of the monocline at Mokalaka Hill on the NW flank of Tletletsi syncline. These joints are typically quartz-filled and bifurcate. The branches suggest dynamic propagation (Segall and Pollard, 1983). No particular explanation is readily apparent that the Waterberg sandstone develops a single set system and the Black Reef Quartzite does not. Several factors may be speculated upon: one being that the Waterberg is less brittle and elastic behaviour is relatively diminished. The single set system could also have formed under confining pressure.

Figure 7.15A: Exposure of chert breccia observed on a south-facing cliff on Kgwakgwe Hill. The Cliff face is about 15 metres high. A modified stratigraphic layering of chert breccia and manganese-rich clay is preserved. The dark layers are mainly chert breccia cemented by silica. The lighter tones are mainly clay intermixed with breccia. The slump structures were formed during the collapse of chert beds following dissolution of dolomite, and have no tectonic significance. The near vertical fracture traces seen on the cliff are younger, probably post-Waterberg. This photograph is traced in figure 7.16.

Figure 7.15B: Fragments of chert in a silicified matrix in the lower parts of the Kgwakgwe chert breccia. The boundaries of the fragments are diffuse due to invasion of interstitial solutions, creating apparent matrix-supported breccia. The car keys provide a scale.

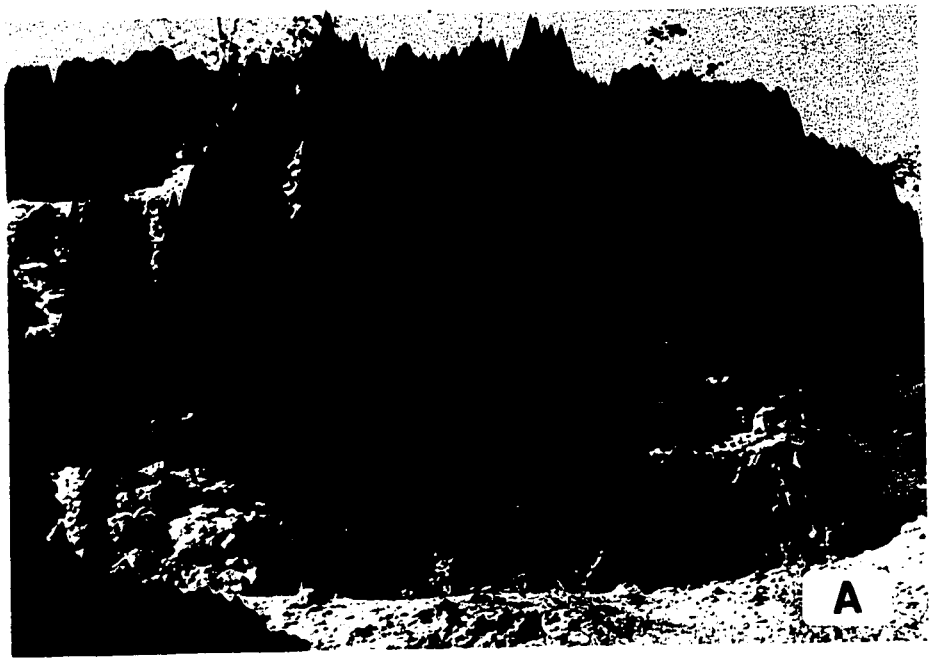
A

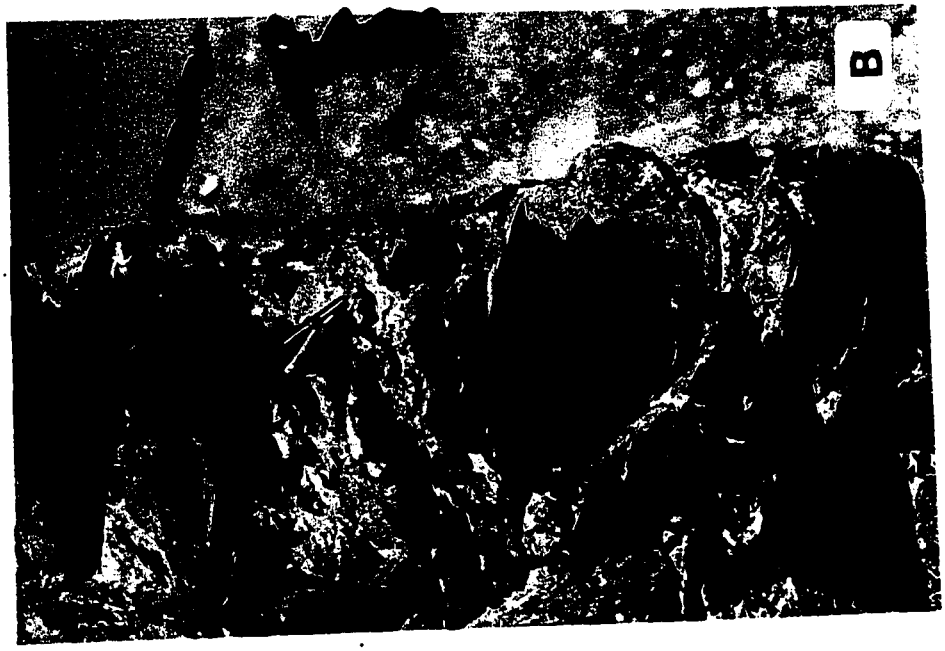
B

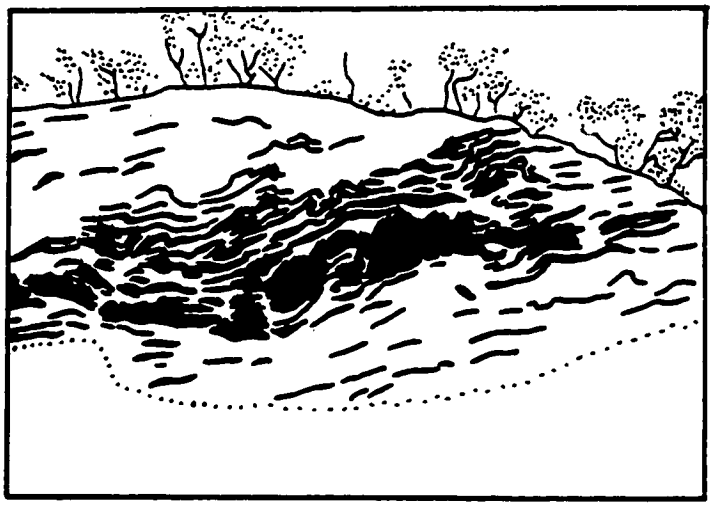

Figure 7.16: Trace of the chert breccia layers shown in figure 7.15A. The black are layers of silicified chert breccia illustrating contorted beds.

7.7.4 Relationship between layering and the principal directions of stress

The basic joint patterns in the study area are described in section 7.3. The orthogonal joint system is the basic system that forms in layered rocks when a stress field is imposed such that the σ_2-σ_3 or σ_1-σ_3 plane approximates that of layering. In conditions where folds already exist in the material, additional joint sets or other joint systems form. Disturbance of the basic rectiplanar joint sets can occur when perturbations in the stress field is induced by the presence of pre-existing faults (Rawnsley et al, 1992). In this case, the joints form in orientations that follow the perturbed stress trajectories in the vicinity of these pre-existing fractures. In the case of pre-existing folds, the joint sets meet at non-orthogonal angles. Diagonal patterns are typical in folded rocks (Maier and Mäkel, 1982). A mechanism for the formation of non-orthogonal joint sets is discussed by Rives and Petit (1990a and 1990b).

7.8 Fracture spacing

7.8.1 Introduction

It is generally regarded that spacing in sedimentary sequences is regular (Price, 1966 p.144) in contrast to granitic rocks where spacing is generally not uniform (Segall and Pollard, 1983). Previous work in other parts of the world has led to the assertion that thick layering is characterized by widely spaced joints and thin layering

by closely spaced joints (Ladeira and Price, 1981). The spacing of joints within a sedimentary unit may also be influenced by layer parallel parting surfaces. It is necessary to introduce the cur- effect, i.e. the cross-section on which the joints are observed. It can be shown that individual joint sets display a modal spacing characteristic by which the scatter of indiscriminate measurements can be reduced.

7.8.2 Results

Fracture density was determined for each fracture set identified in the field. Fracture spacing and density were measured for fractures longer than 1 metre, a convenient cut-off for outcrop scale observations. In the layered sequences, density and spacing were measured in the plane of bedding because all fractures were more or less perpendicular to bedding. Over 1,500 of these spacing measurements were taken over the stations shown in figures 7.12 and 7.13. It was not possible to obtain statistical data for fractures that formed parallel to the bedding because of lack of suitable exposure. Where possible, the thickness of bedding was noted at a data station; e.g., at station 21 (figure 7.1A), layers separated by bedding-parallel joints ranged from 40 to 25 cm. Contrary to other contentions, the spacing on joints on these layered sediments is not even, but shows a statistical distribution. Figure 7.17D summarizes the poles to bedding and joint sets from station 1 to 40 along the Black Reef Quartzite ridge in eastern Moshaneng. Table 7.3 gives the mean spacing for sets in domain 4. The more closely spaced set 1 has a mean strike of N028E for domain 4.

Figure 7.17: Mean attitudes of bedding and joints. Bedding is shown by a pole and great circle. Data is obtained from domain 4 in the eastern part of Moshaneng. See figures 6.6 and figure 7.13 for location. Numerical data is given in tables 7.1 and 7.2.

A: station 1-10.

B: station 22-24

C: station 52-53

D: station 1-40

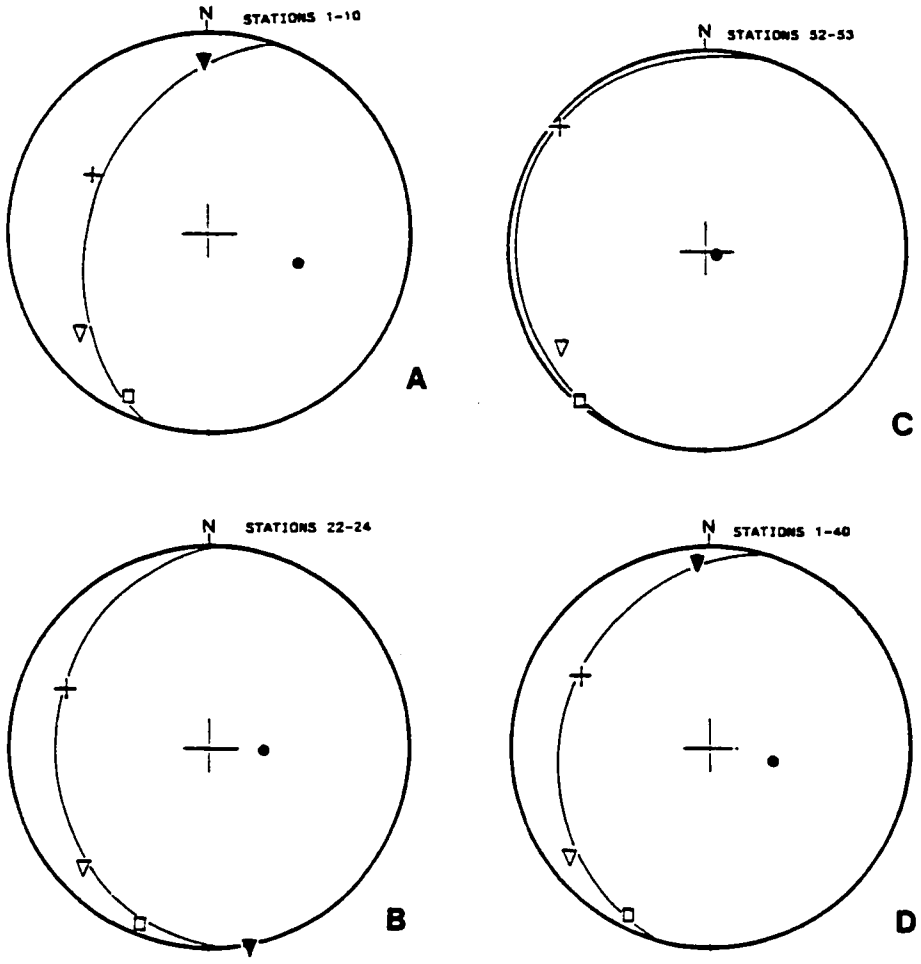

EAST MOSHANENG
(DOMAIN 4)
MEAN ATTITUDES

• = bedding
+ = joint set 1
▫ = joint set 2
▽ = joint set 3
▼ = joint set 4

The mode of fracture spacing is 20 cm (figure 7.18A) and the mean is 17 cm. Set 2 is at right angles to it, with a mode of 40cm (figure 7.18B) and a mean of 36 cm. Additional sets that are even more widely spaced occur. Set 3 has a mode of 40 cm (figure 7.18C) and a mean of 43 cm. Set 4 has a mode of 45 cm (figure 7.18D) and a mean of 51 cm. The spacing of joint sets 2 and 3 have the same mode (40 cm) and frequency histograms that are very similar (figure 7.18B and 7.18C). The sample population provided by the subdomains, e.g., stations 1-10 and stations 22-24 (figure 7.19) did not have significant data for the joint set 4 to provide frequency distributions. These subdomains represent a uniform dipping homocline and folded beds respectively. The more comprehensive analysis of stations 1-40 provided a frequency distribution for set 4 (figure 7.18D). Spacing for joint sets follows an order such that set1 < set2 < set3 < set4 (see table 7.3). This general rule is broken at stations 22-24, where set 3 (mean spacing of 29 cm) is more closely spaced than set 2 (mean spacing of 57 cm). The folds developed at these stations probably account for this anomaly. Variability of spacing from station to station is substantial: mean spacing for set 1 fractures at stations 1-10 is 24 cm, 14 cm at stations 22-24 and 8 cm at stations 52-53. These variations almost certainly can be controlled by measurements from units of comparable thickness (Gross, 1993). Exposures to enable such controls were however not available in the present area of study.

Examination of all the histograms in figures 7.18 and 7.19 shows that none of the spacing frequency distributions conforms to a negative exponential function. The comprehensive analyses in figure 7.18 also shows that the histograms are not normal

Figure 7.18: Domain 4 joint spacing frequency histogram. Data were obtained from exposures of Black Reef Quartzite in eastern Moshaneng.

A: Stations 1-40, set 1

B: Stations 1-40, set 2

C: Stations 1-40, set 3

D: Stations 1-40, set 4

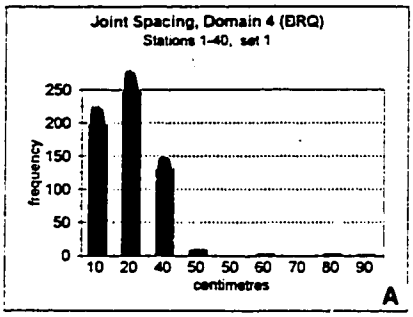
Joint Spacing, Domain 4 (BRQ)
Stations 1-40, set 1
frequency
250
200
150
100
50
0
10 20 40 50 50 60 70 80 90
centimetres
A

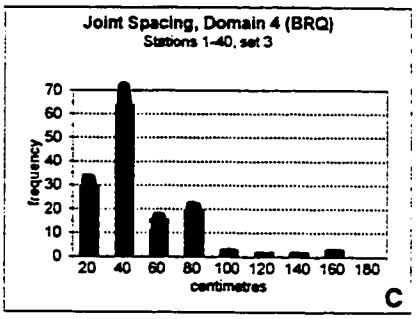
Joint Spacing, Domain 4 (BRQ)
Stations 1-40, set 3
frequency
70
60
50
40
30
20
10
0
20 40 60 80 100 120 140 160 180
centimetres
C

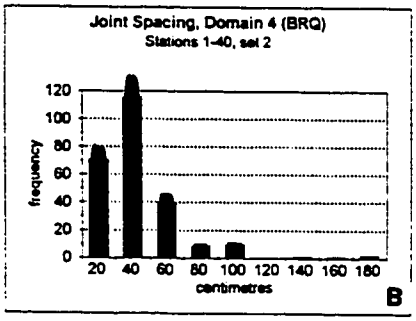
Joint Spacing, Domain 4 (BRQ)
Stations 1-40, set 2
frequency
120
100
80
60
40
20
0
20 40 60 80 100 120 140 160 180
centimetres
B

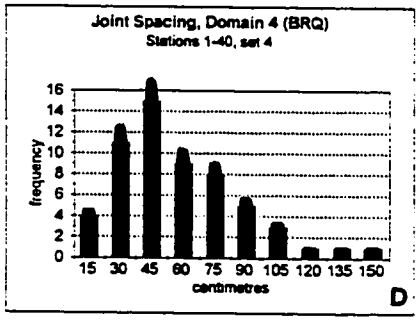
Joint Spacing, Domain 4 (BRQ)
Stations 1-40, set 4
frequency
16
14
12
10
8
6
4
2
0
15 30 45 60 75 90 105 120 135 150
centimetres
D

Figure 7.19: Joint spacing frequency histograms.

A: Stations 1-10, set 1 spacing frequency distribution.

B: Stations 1-10, set 2 spacing frequency distribution.

C: Stations 1-10, set 3 spacing frequency distribution.

D: Stations 22-24, set 1 spacing frequency distribution.

E: Stations 22-24, set 2 spacing frequency distribution.

F: Stations 22-24, set 3 spacing frequency distribution.

G: Station 52 and 53, set 1 spacing frequency distribution.

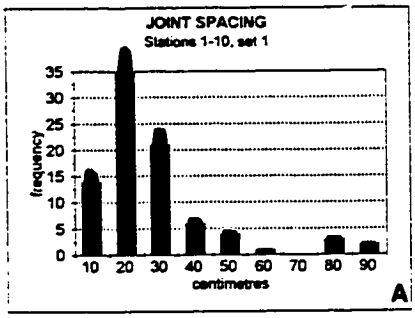
JOINT SPACING
Stations 1-10, set 1
frequency
0 5 10 15 20 25 30 35
10 20 30 40 50 60 70 80 90
centimetres
A

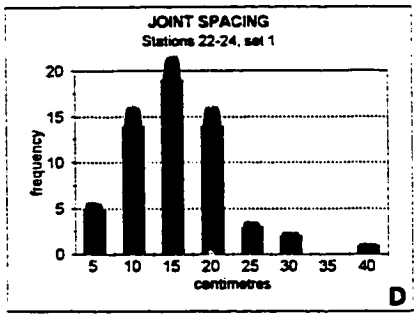
JOINT SPACING
Stations 22-24, set 1
frequency
0 5 10 15 20
5 10 15 20 25 30 35 40
centimetres
D

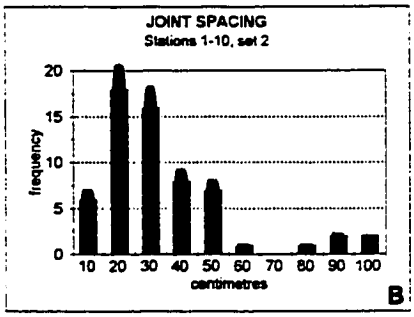
JOINT SPACING
Stations 1-10, set 2
frequency
0 5 10 15 20
10 20 30 40 50 60 70 80 90 100
centimetres
B

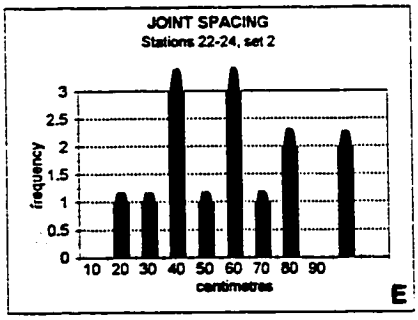
JOINT SPACING
Stations 22-24, set 2
frequency
0 0.5 1 1.5 2 2.5 3
10 20 30 40 50 60 70 80 90
centimetres
E

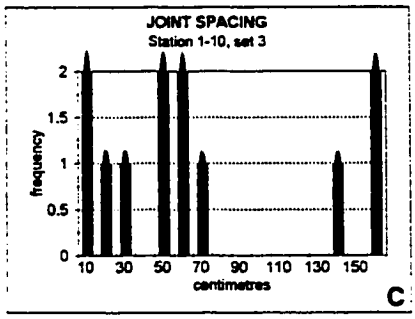
JOINT SPACING
Station 1-10, set 3
frequency
0 0.5 1 1.5 2
10 30 50 70 90 110 130 150
centimetres
C

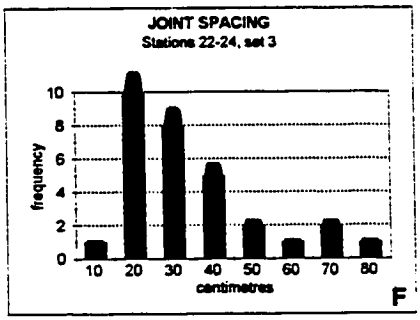
JOINT SPACING
Stations 22-24, set 3
frequency
0 2 4 6 8 10
10 20 30 40 50 60 70 80
centimetres
F

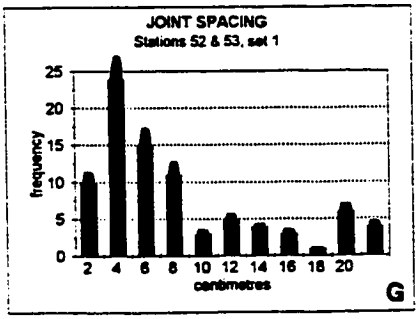
JOINT SPACING
Stations 52 & 53, set 1
frequency
0 5 10 15 20 25
2 4 6 8 10 12 14 16 18 20
centimetres
G

Station	Set	mean spacing(cm)	Standard deviation	Number of readings
1-10	1	24	18	86
1-10	2	31	21	61
1-10	3	84	82	13
22-24	1	14	6	58
22-24	2	57	26	14
22-24	3	29	17	31
52-53	1	8	6	63
1-40	1	17	11	593
1-40	2	36	28	251
1-40	3	43	37	141
1-40	4	51	30	58

Table 7.3: Mean spacing and standard deviation at joint measuring stations in domain 4, east Moshaneng.

distribution. The most likely shape that could be tested for these distribution is therefore the lognormal distribution or negatively skewed normal distribution. The interpretation of the frequency distribution in joint spacing is provided below.

7.8.3 Statistical considerations

Fracture spacing essentially provides a means of determining the size of fracture bounded blocks in a body of rock. The blocks are a function of the mutual orientation of fracture sets and the spacing between the fractures. The functions that describe fracture spacing are varied (Rives et al, 1992). The following are examples:

1.) $f(x) = \beta e^{-\beta x}$

2.) $f(x) = 1/\sigma V 2\pi e \left[\frac{(-\log(x)-m)^2}{2\sigma^2}\right]$

3.) $f(x) = 1/\sigma V 2\pi e \left[\frac{(-x-m)^2}{2\sigma^2}\right]$

Equation 1.) represents a negative exponential distribution, 2.) Log-normal distribution and 3.) normal distribution. σ=standard deviation. Histograms showing the distribution of fractures in the study area in figures 7.19 and 7.18 show that fracture spacing in the study area are closer to lognormal distribution or negatively skewed normal distribution. The exceptions shown in figures 7.19C and 7.19E may be due to insufficient and non-statistical data.

It has been suggested that fractures displayed in the field could reflect the evolutionary stage of the fracture system (Rives et al, 1992). The early stages conform to the negative exponential distribution. The log-normal distribution shows intermediate stages and the normal distribution shows advanced stage. The progression through these stages is a function of layer thickness and the extent of the strain. A relationship between fracture spacing and layer thickness is therefore influenced by such conditions as the fracture set chosen to characterize the spacing and the extent or stage of joint development in the rock.

In the study area, the spacing frequency distribution appears to have a lognormal or a negatively skewed normal distribution. According to the above theory, joint development in the area is at an intermediate or an advanced stage of development.

7.9 Joints and folds

At station 13, an open fold plunges 7 degrees towards 207 (figure 9.3D). A fracture set with a mean spacing of 23 cm trends parallel to the fold axis with another joint set (mean spacing of 14 cm) orthogonal to it. These joints are formed perpendicular to bedding. The dispersion of joint plane poles on the stereographic projection corresponds to that of bedding poles, in-keeping with the orthogonal relationship of joint planes to bedding. Another open-fold axis plunges 50 degrees towards 280. The relationship between the folding and the joints shows that there is

probably a genetic relationship between folds and joints. An open fold at station 20 is accompanied by a corresponding distribution of poles to fracture set 2. This is another example that demonstrates the variability of joint inclination according to that of bedding. It is possible that the joints were formed as a result of stress release of the folding episode during uplift. This type of mechanism has been inferred from a study of joints in the Appalachian Plateau, New York, U.S.A. (Engelder, 1985). A mechanism is required however to explain the process by which the joints are inclined in accordance with folds in the layered sediments such that the mutually perpendicular relationship is maintained.

Stations 22, 23 and 24 (figures A22, A23 and A24) are located on three limbs of a fold consisting of open, plunging anticline and syncline as shown on the combined stereographic projection for the three stations (figure 9.3E). Combining data from the three stations shows that the joint set 1 and less so set 2 remains closely clustered for all the stations. The joint set 3 is dispersed at the three stations. The joint set 1 has a distribution that does not vary in accordance to that of the folded beds, contrary observations at station 13 (figure 9.2D). This joint set however, is consistently perpendicular to bedding notwithstanding the change in strike of the beds. The joint sets 2 and 3 display increased dispersion with increased folding.

At station 30 (figure 9.3B), the Black Reef Quartzite has been folded into southwest plunging open folds. At this station an anticline-syncline pair is recognized. Typically, the folds have a limb that is steeply dipping to the south and has been relatively more eroded. A more gently dipping limb dips to the northwest. At station

31 (figure 9.2C), the folding is parallel to the strike of the beds with a southwest plunge. The folded structure here is a monocline. The joints have been filled with quartz and display en echelon patterns. The quartz fibres within the veins have grown perpendicular to the walls of the vein. The abundance of quartz veins decreases from set 1 through set 4 to set 2. Moving further southwards to station 32, the beds here show no interference folding. At this locality, a conjugate system of set 3 and set 4 joints becomes very prominent (figure A32). The angle between the conjugate system is bisected by the set 1 joints. The orthogonal complement of the joint set 1, set 2 disappears, reappearing further south at stations 33 and 35 (figures A33 and A35). Despite the folding, the orthogonal joint sets 1 and 2 maintain a consistent orientation. Neither of these joint sets are parallel to the fold axis. Remarkably, no other joint sets are developed at this locality.

The joint system in the layered sediments in domain 4 is very similar throughout the Moshaneng map area. Similarly, the joint system developed in domain 5 is internally consistent. The orthogonal system is little affected by minor folds. It is suggested that the joints were formed under local stress fields that were characteristic of each structural domain. The most dominant fractures formed in the layered rocks are formed parallel to the fold axis. This pattern is well defined under conditions of cylindrical folding. Where geometric and kinematic axes do not coincide,i.e. non-cylindrical conditions, due to the presence of F_1 folds, a complex array of fractures are developed by torque. At stations 22, 23 and 24 (figure 9.3E), the dominant cracks are developed parallel to F_2 fold axis. However, a set of fractures, set 4 is developed

parallel to the F_1 axis. Station 50 (figure A50) shows the presence of a minor fold with a NW plunge. The relationship between joints and folds was unambiguously established by Maier and Mäkel (1982). More recently, the mechanism of the formation of joints in folded layers was simulated in laboratory materials (Rives and Petit, 1990a and 1990b). The joint system formed in domain 4, in eastern Moshaneng consist essentially of 4 sets of joints, similar to those determined by in the Aywaille folds in Belgium (Maier and Mäkel, 1982). Most of the folds in the study area, however, are open and geometrical relationships such as those shown in figure 3.3 are tenuous (figure 9.3A, 9.3D and 9.3F). At the locations indicated, the joint set 2 is perpendicular to the fold axis of cylindrical folds. However, at stations 22-24, 30 and 31, none of the joint sets is perpendicular to the fold axis (figures 9.3E, 9.3B and 9.3C).

7.10 Mechanical considerations

7.10.1 Introduction

One of the most enigmatic problems in the study of joints has been to explain the formation of multiple sets. Joints are extensional fractures that form by the mode I displacement (Aydin and Pollard, 1988; Atkinson, 1987; Broek, 1982; Paterson, 1978). Under these conditions, fractures form in planes that are perpendicular to σ_3. In conditions where stress is concentrated at a point, the resulting fractures follow a

radial and concentric pattern. In contrast, blocks in which stress concentration points are far afield display evenly distributed and linear stress trajectories and a uniform fracture pattern. Pre-existing anisotropy and irregularities in the medium however, lead to perturbation of linear stress trajectories and the fracture pattern (Rawnsley et al, 1992; Barquins and Petit, 1992). The σ_3 trajectory can be traced through successive perpendiculars of contemporaneous fractures in the rock, provided that subsequent deformation has not displaced stress markers. Joints therefore can be used as palaeostress markers (Engelder and Geiser, 1980; Dyer, 1988). Rocks displaying multiple fracture sets imply a complex stress system (Price, 1966). Different sets of mode I fractures in the same rock unit are therefore formed in a sequence of deformational episodes. An aspect of the mechanism of such a sequence is outlined below. It is reasoned that 1) the formation of a joint set or sets changes the original elasticity of the bulk of the rock. 2) the joint patterns formed are controlled by the shape of the rock. i.e. joint patterns are controlled by a) planar blocks b) folded blocks. Where none of the principal directions of stress coincides with the layering in the rock, an orthogonal fracture system is unlikely to form. Such conditions probably prevail in regions of pre-existing folded rock over which a consistent far-field stress system is superimposed. Locally, the stress system may be perturbed to produce non-orthogonal stress systems.

At the earth's surface, where joints are commonly formed, $\sigma_3 \approx 0$ and has a vertical orientation, if the horizontal directions have $\sigma_N > 0$. This stress system is likely to produce horizontal sheet joints in homogeneous media such as certain massive

igneous intrusions. Where $\sigma_N<0$ or tensile in the horizontal directions, the joints are likely to be vertical. Away from any suture zone, the crust behaves in an elastic fashion (Turcotte and Schubert, 1982). The development of brittle fracture under these conditions is discussed below.

7.10.2 Elasticity

Hooke's Law is a linear relationship between stress and strain. It is represented by the equation:

$$4) \qquad \sigma_N = E\varepsilon$$

σ_N= normal stress, E= Young's modulus and ε= strain.

This relationship holds true under elastic conditions and before rupture of the material. At low stress levels and high strain rate, rock behaves elastically. The small amounts of strain involved in the formation of joints do not require high stress levels in the deforming material. The stress level, however must exceed the tensile strength of the material for failure to occur. Joints are formed in the relatively unconfined conditions prevalent in the upper 500m of the earth's crust. The elastic field is characterized by the coincidence of the principal directions of stress and strain (Turcotte and Schubert, 1982). Hooke's law is valid on the assumption that the stress and strain are measured in the same direction.

7.10.3 Mohr envelope

The Mohr envelope shows that for any material, the difference between σ_2 and σ_3 is relatively small under tensile conditions. At the earth's surface, σ_1=0, and plain strain conditions may be assumed for the horizontal or near horizontal plane. In layered rocks, near the earth's surface, such as those in the present study area, plain strain conditions are valid in the bedding plane.

The formation of cracks by mode I displacement decreases the amount of tensile stress perpendicular to the fracture plane. This relief of stress in one direction causes the relative rise of the amount of stress in a perpendicular direction. This means that immediately after the formation of a set of fractures the reduction of stress in the direction perpendicular the fracture plane may be sufficient to reverse the relative magnitudes of σ_3 and σ_2. Mode I displacement then affects fractures at right angles to the earlier formed fractures. It is reasonable to expect that the stress differential is greater under the initial failure conditions than after the reversal. The stress level however, must be sufficient to overcome the tensile strength of the rock. The spacing between the earlier formed fractures is closer than the later orthogonal set. These conditions give rise to the ubiquitous orthogonal system of fractures prevalent in layered sediments. This hypothesis has been validated in a laboratory setting where PVC plates, coated with brittle varnish were bent into cylindrical folds. During the generation of a fold by progressive bending, fractures were developed parallel to the fold axis. On unloading the stress, an orthogonal set was generated (Rives and Petit,

1990).

Shear fractures are formed when the differential stress is much greater. The Mohr envelope under shear failure conditions is nearly linear (figure 7.20A) and approximates the equation:

$$5) \qquad \tau=\mu\sigma_N + S$$

τ= shear stress, μ= coefficient of internal friction, σ_N= normal stress and S= is the cohesive strength of the rock.

At $\sigma_N=0$ the nature of the Mohr envelope changes drastically, and the curve changes form to approximate the equation:

$$6) \qquad \tau^2+4T\sigma_N-4T^2=0$$

T= Tensile strength of the rock.

This quadratic equation has the curve shown in figure 7.20B and shows that in approaching the tensile stress regime, the differential stress drops drastically and the shear stress approaches zero. It is in this area of the curve that extensional joints form. The latter relationship is the Griffith failure criterion that takes into account stress concentrations at the edges of microscopic cracks (Griffith, 1921). Compression tends to strengthen the rock whereas tensile stress weakens it. The Cohesive strength of the rock is therefore greater than its tensile strength given the same conditions. Due to

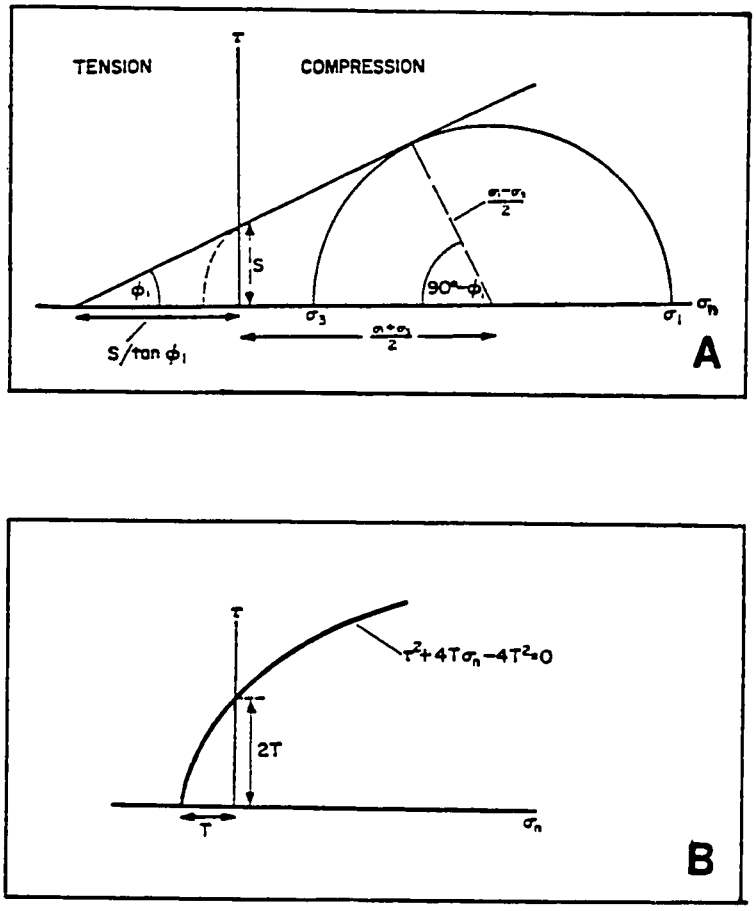

Figure 7.20: Mohr envelope showing areas of extension fractures and shear fractures. **A** The Mohr envelope follows a linear function representing the Navier-Coulomb criterion for brittle failure. ϕ_i=angle of internal friction, S=cohesive strength, τ=shear stress, σ_n=normal stress, σ_1=maximum compressive stress, σ_3=minimum compressive stress. **B** The Mohr envelope follows a curved function predicted by the Griffith criterion for brittle failure. T=tensile strength (After Price, 1966).

friction, tangential displacement across a fracture also requires more work compared to dilation. Tangential displacement often involves fractures across grain boundaries while dilation involves fractures around grain boundaries. Given the conditions near the earth's surface, the above factors account for the much greater number of joints than faults.

7.10.4 Finite strain

When rock is subjected to a stress field under elastic conditions, the total strain in the rock is, at any instant, the sum of the crack strain and the elastic strain (Segall and Pollard, 1983):

$$7.) \qquad \varepsilon=\varepsilon^c+\varepsilon^e$$

ε=total strain, ε^c=crack strain and ε^e=elastic strain.

The crack strain is accommodated by joint dilation and has no established relationship with the stress field. The elastic strain is recoverable according to Hooke's Law.

Before failure:

$$8.) \qquad \varepsilon^c=0 \text{ and } \varepsilon=\varepsilon^e$$

After rupture, crack strain increases and elastic strain decreases:

$$9.) \qquad \varepsilon_0^c \leq \varepsilon_f^c$$

$$10.) \qquad \varepsilon_0^e \geq \varepsilon_f^e$$

ε_0^c=initial crack strain, ε_f^c=final crack strain

ε_0^e=initial elastic strain, ε_f^e=final elastic strain

When 11.) $\varepsilon^e=0$, $\varepsilon=\varepsilon^c$

7.10.5 Implications of stress magnitude inversion on mode I stress loading

Orthogonal fracture sets are most likely formed in two phases of brittle rupture that closely follow one another. When this system of fractures is in place, any remnants of the stress field within the medium is dissipated by dilation across existing fracture sets. Equation 7.) in section 7.10.4 above provides components of strain in rock that deforms under elastic conditions. Before any cracks develop, conditions of equation 8.) prevail. It has been shown that once a fracture has formed, a region of stress relaxation is created in the immediate vicinity of the fracture (Segall and Pollard, 1983). Tensile stress cannot be transmitted across such a fracture and the elastic strain is therefore greatly diminished or absent in these zones. Figure 7.21A illustrates the distribution of the stress trajectories in the vicinity of a finite crack in two dimensions. An example of the distribution of mean normal stress around such a crack is provided in figure 7.21B (Pollard and Segall, 1987). Mean normal stress $\sigma = (\sigma_{11} + \sigma_{22})/2$, where σ_{11} and σ_{22} are principal normal stresses in the x_1 and x_2 directions. In figure 7.21, the co-ordinates are normalized by the ½ crack width. Crack strain develops at the expense of the elastic strain. The bulk modulus of

Figure 7.21A: Stress trajectories in the vicinity of a single planar mode I crack. View of cross-section with simple terminations in two dimensions. The longer tics are parallel to σ_3 and the shorter tics are parallel to σ_1. x_1 and x_2 are co-ordinates, normalized by a, the ½ crack width (After Pollard and Segall, 1987).

Figure 7.21B: Mean normal stress ($\sigma = (\sigma_{11} + \sigma_{22})/2$) in the in the vicinity of a single planar mode I crack. View of cross-section with simple terminations in two dimensions. Co-ordinates are as in figure 7.21A (After Pollard and Segall, 1987).

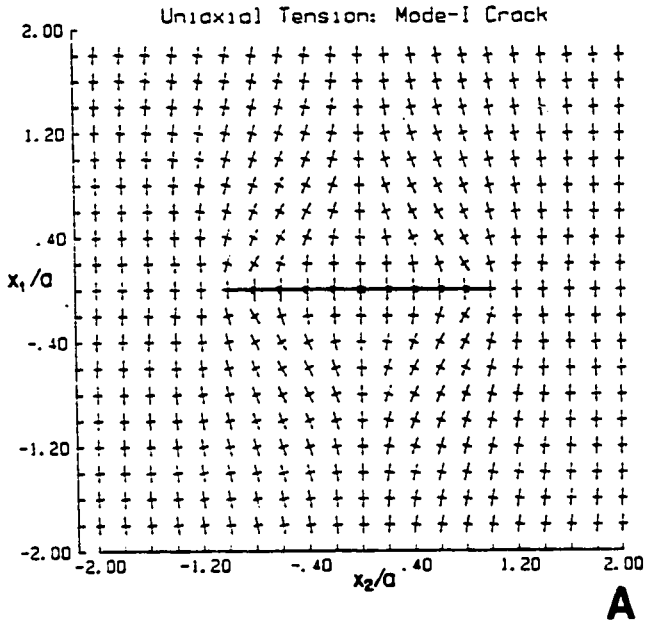
Uniaxial Tension: Mode-I Crack
2.00
1.20
.40
x_1/a
-.40
-1.20
-2.00
-2.00
-1.20
-.40
.40
1.20
2.00
x_2/a
A

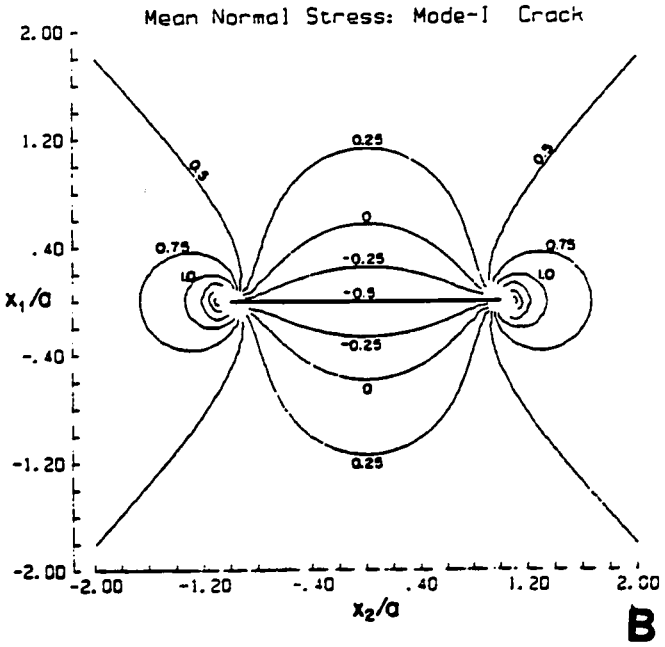
Mean Normal Stress: Mode-I Crack
2.00
1.20
.40
x_1/a
-.40
-1.20
-2.00
0.25
0.3
0
0.75
-0.25
1.0
-0.5
-0.25
0
0.25
-2.00
-1.20
-.40
.40
1.20
2.00
x_2/a
B

elasticity is therefore affected in the direction of σ_3. Tensile stress however, may still be transmitted parallel to the fractures. If the tensile stress parallel to existing fractures is greater than the pre-crack σ_3, a new σ_3 direction is formed. If the magnitude of the new σ_3 is still greater than the tensile strength of the rock, a new set of fractures are formed.

The processes described above account for the reversal in the relative magnitude of σ_2 and σ_3 and the formation of orthogonal sets of fractures. Normal microfaults may occur at the hinges or crests of folds when the stress system also induces buckling in the layers. The presence of down-dip slicken striae on set 1 joint surfaces in the study area provides testimony to this mechanism.

Engelder (1987), shows that rock that has the least amount of elastic strain has the closest fracture spacing. This observation supports the hypothesis given above. The above hypothesis is tenable for an orthogonal two set system. Diagonal systems will require a variation of the above mechanical conditions. Such variations can be exemplified by the fracture system at stations 22, 23 and 24 (figure A22, A23 and A24). In this case the interaction of kinematic axes and geometric axes hold the key to the development of the joint system. At particular locations two superimposed two-set orthogonal systems occur. Due to the presence of earlier folds, the far field σ_3 direction is oblique to the bedding or material anisotropy. The anisotropy induces the material to deform in a torque-like fashion. The fracture pattern produced by torque in layered material has been empirical determined (Rives and Petit, 1990a, 1990b). In these cases, Two sets of fractures are produced that are oblique to one another.

The formation of apparent diagonal joint sets is probably a result of mode II and mode III displacements. The interaction of the far field stress with the folded strata induces torque in the limbs of these folds. The set 4 fractures shown in figure 7.6B postdate and displace set 1 fractures. These fractures are therefore strictly microfaults although at the scale of mapping, they are included under joints. Thin quartz veins in these fractures show no trace of the fibrous growth associated with mode I extensional fractures.

It has been suggested by Price (1966, p.142) that joints are developed during the post-compressional phase. Any shearing movement during this phase would only dissipate the stress in the immediate vicinity of the shear fracture. Dissipation of stress through a wide area would require the formation of a large number of joints. This argument explains why there are a higher frequency of joints as compared to faults. One of the more significant findings of this study is that the joint density is greatest parallel to the main fold axes. These axes are perpendicular to the direction of now dissipated compression. This could indicate that these joints are mainly influenced by stress release.

When set 1 is not parallel to the fold axis, sets 3 and 4 become more strongly developed. The set 1 and 2 are exclusively formed when folding is cylindrical. These conditions prevail when the kinematic axes coincide with the geometric axes. Griffith (1921) and later Irwin (1958) accorded the crack its importance as a stress-concentrator in the initial stages of brittle deformation of cohesive media. It has been reiterated that pre-existing irregularities in rock will perturb the direction of the stress

field. This study shows that the orthogonal system of fractures is formed as a result of disturbance of the stress field resulting from the formation of the initial fracture set.

7.11 The role of joints in the creation of the chert breccia

7.11.1 Review of previous work

Exposures of chert breccia have been described and discussed at Moshaneng and other areas of southeast Botswana by a number of authors (Crockett, 1969; Crockett, 1972c; Key, 1983; Aldiss et al, 1989). Three main schools of thought have contended over the issue of the evolution of the chert breccia. Rabie(1958) proposed that the chert breccias south of Kanye are of tectonic origin. This early proposal has never received wide acceptance. Some workers (Vermaak, 1962; Gerrard, 1962; Cullen, 1965; Jones, 1965; Crockett, 1969) have argued that the chert breccia is a residuum left after chemical weathering of dolomite. The latest and third argument dwells on a suggestion that brecciation may be caused by rapid dehydration of a silica gel, parent to the chert (Crockett, 1972c; Aldiss et al, 1989). One of the main objections to the residuum theory has been that a crude layering is preserved, even across individual chert fragments. This is purportedly inconsistent with the notion of chert breccia collapsing into large caverns from which dolomite had been dissolved. The other objection to the residuum suggestion is that soft sediment structures are preserved in the chert breccia formation.

The controversy surrounding the evolution of the chert breccia has raged on, primarily because a detailed explanation of any of the proposed mechanisms has not been provided. The present study will support the residuum theory. The role of joints in the evolution of the chert breccia is brought into focus. A detailed explanation of the mechanism shows how crude layering and "soft sediment folds" came to be.

Mechanically fragmented solid material is commonly derived from a bulk parent that has undergone brittle failure. Such failure results from a prevailing stress system in the parent material such that the differential stress exceeds the cohesive strength or tensile strength of the material (equations 5 and 6 above respectively). At the initiation of brittle failure, some rocks displays characteristic fracture patterns that sculpture or shape fragments in rock that has lost primary cohesion. In cases where the fragments have not been transported for any significant distances, patterns of the parent rock may still be discerned in the fragmented rock as is the case with the Kgwakgwe chert breccia (figure 7.22A, 7.22B, 7.23A and 7.23B. The initial fracture pattern and spacing in the parent rock dictates the size of the breccia fragments. The Kgwakgwe chert breccia is an example of rock that consists of angular fragments derived from a cohesive parent rock.

7.11.2 Field description

In the southern part of Moshaneng area, and more extensively to the southwest of Kanye, i.e. the west central part of the study area (figure 6.5), exposures of chert

Figure 7.22A: Detail of mosaic chert fragments in a ferruginous matrix near the top of the Kgwakgwe chert breccia. The fracture sets preserved in the individual chert fragments are traced out and illustrated in figure 7.23A. At least 4 sets of fractures can be recognized in this portion of the chert breccia.

Figure 7.22B: Chert fragment mosaic near the top of the Kgwakgwe chert breccia. The detail is traced out in figure 7.23B. Three sets of fractures can be identified.


4
B


1
2
A

Figure 7.23: Detail of the chert breccia mapped from a vertical exposure at Kgwakgwe Hill. Fragments of chert breccia are the black fill, while the white is reddish brown siliceous cement. The breccia is the mosaic type consisting of variously sized fragments sculptured by fracture planes.A portion of the *ESTWING* geological hammer provides a scale.

A Unsorted angular fragments of chert. Large individual fragments **1**, **2** and **3** retain systematic fractures: set H, set V, set I_1 and set I_2. Set H and set V correspond to bed-parallel and bed-normal sets respectively. Sets I_1 and I_2 are inclined. Collapse following interstratal solution accounts for the fragmentation and rotation of fragments. Portions with small fragments have virtually lost the original systematic fracture pattern.

B Large individual fragment **4** displays set H, set I_1 and set I_2. The hammer portion is superimposed for scale.

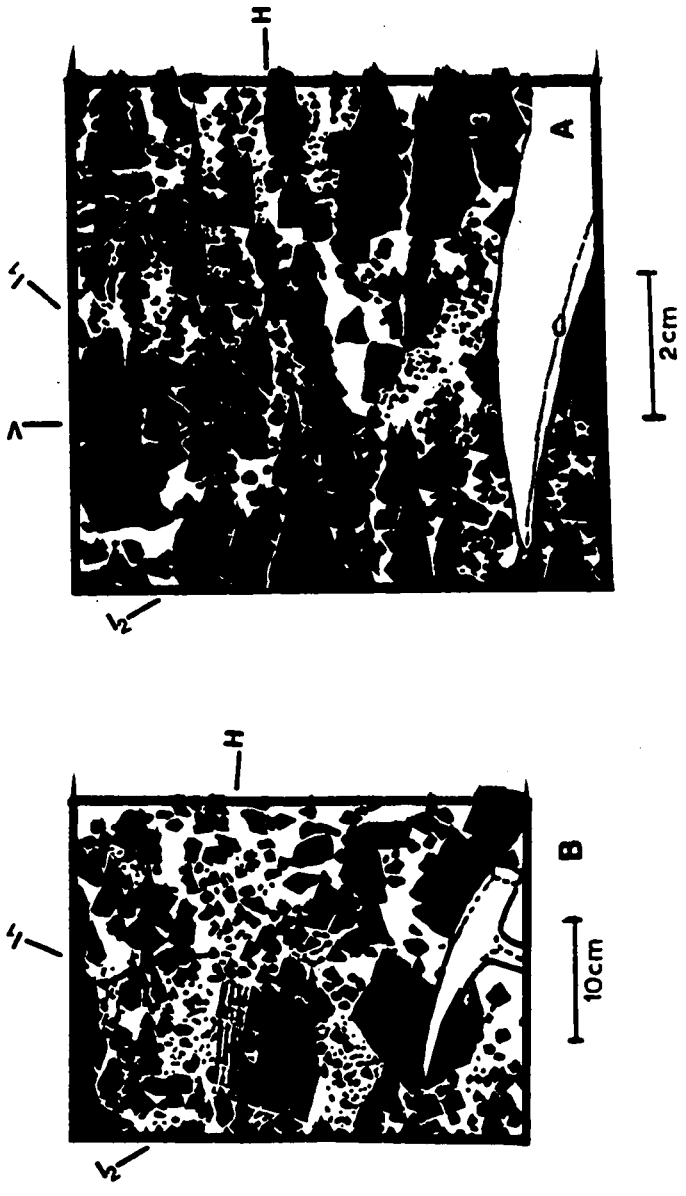
H
A
2cm
B
10cm

breccia occur. The chert breccia underlies low lying terrane. Significant exposure also occurs on hilly rugged terrane such as is found at Kgwakgwe and Dinakana Hills. The breccia consists of unsorted, angular chert fragments. The angularity of the fragments, particularly the large fragments demonstrates that there was virtually no transportation of the these fragments. The breccia is typically clast-supported, an observation that was also made on similar deposits to the east of the present study area (Key, 1983). The chert clasts are typically opaque and whitish. This contrasts with the translucent and grey colour of the chert beds in the dolomite and chert sequence. However, the weathered coating on the chert beds is opaque and whitish, similar to the breccia fragments. At Kgwakgwe Hill, the lower part of the chert breccia shows a high degree of silicification. The boundary of the fragments in this lower portion is diffuse, demonstrating a chemical interaction between the fragment and the cementing material (see figure 7.15B). The matrix becomes ferruginous as one moves up the chert breccia formation. In this upper portion, clastic sedimentation is apparent, shown by thin millimetre to centimetre thick horizons of red sandstone intercalated with chert breccia accumulations. Sections of the chert breccia are well exposed on cliffs around Kgwakgwe Hill. On these sections crude layering is apparent. Layers of silicified chert breccia are separated by Fe and Mn-rich clay horizons and lenses. The chert breccia layers are also laterally discontinuous The beds display folds, contortions and slump structures typical of soft-sediment deformation. Whereas some of the clay displays regular layering, some portions have been brecciated. These structures are shown in figure 7.15A. In many parts of the chert breccia, the fragments are arranged in a

mosaic (figure 7.24B, 7.22A and 7.22B), in which adjacent fragments have undergone little rotation and could be fitted together across the matrix. Some of the larger individual fragments retain a fracture system that can be correlated from fragment to fragment (see figure 22A, 22B, 23A and 23B). These joint systems are at least pre-Waterberg deposition in age. They were present during the formation of the chert breccia.

Exposures of dolomite interbedded with chert underlie areas of low, shallow slope, rounded ridges and hills which rise up to 20 metres above the surrounding terrane. On aerial photographs and on the SPOT image, these areas show up as light toned regions in contrast to just-dolomite beds, which are of a much darker tone and quartzite which shows a mottled medium toned expression. Dolomite underlies flat low lying areas characterized by dark brown soil while quartzite is found on continuous relatively narrow ridges.

The chert and dolomite interlayers occur in beds that typically vary between 30 and 10 centimetres in thickness. The chert horizons in the lower part of the chert/dolomite sequence are stromatolitic, changing to more massive beds as one moves up the sequence. In these massive beds the composition is a heterogeneous mixture of silica and carbonate. Weathered exposures have a porous "spongy" appearance. The carbonate has been eroded away or dissolved, leaving a porous residue of silica. At about the stratigraphic level where the "spongy" exposures occur, a thin clastic sediment horizon shows an impure arenaceous horizon consisting of angular fragments of chert. This litharenite demonstrates a period of clastic reworking

Figure 7.24A: Exposure of chert-dolomite-chert sequence. The remnant of fractured chert has been undermined by erosion of the underlying dolomite (section shown by the tape measure. The fracture-bounded chert fragments collapse into the voids once occupied by dolomite. This collapse breccia is then cemented by silica resulting in the chert breccia similar to that displayed in figure 7.15B.

Figure 7.24B: Detail of the chert breccia at Kgwakgwe Hill. The exposure surface is near vertical; facing NW. The view is perpendicular to fractures oriented 310/85. All the fragments are angular and show little or no transport effects. The cementing material is ferruginous, closer to the contact with the overlying Waterberg. Further down the chert breccia, the cementing material is increasingly siliceous.

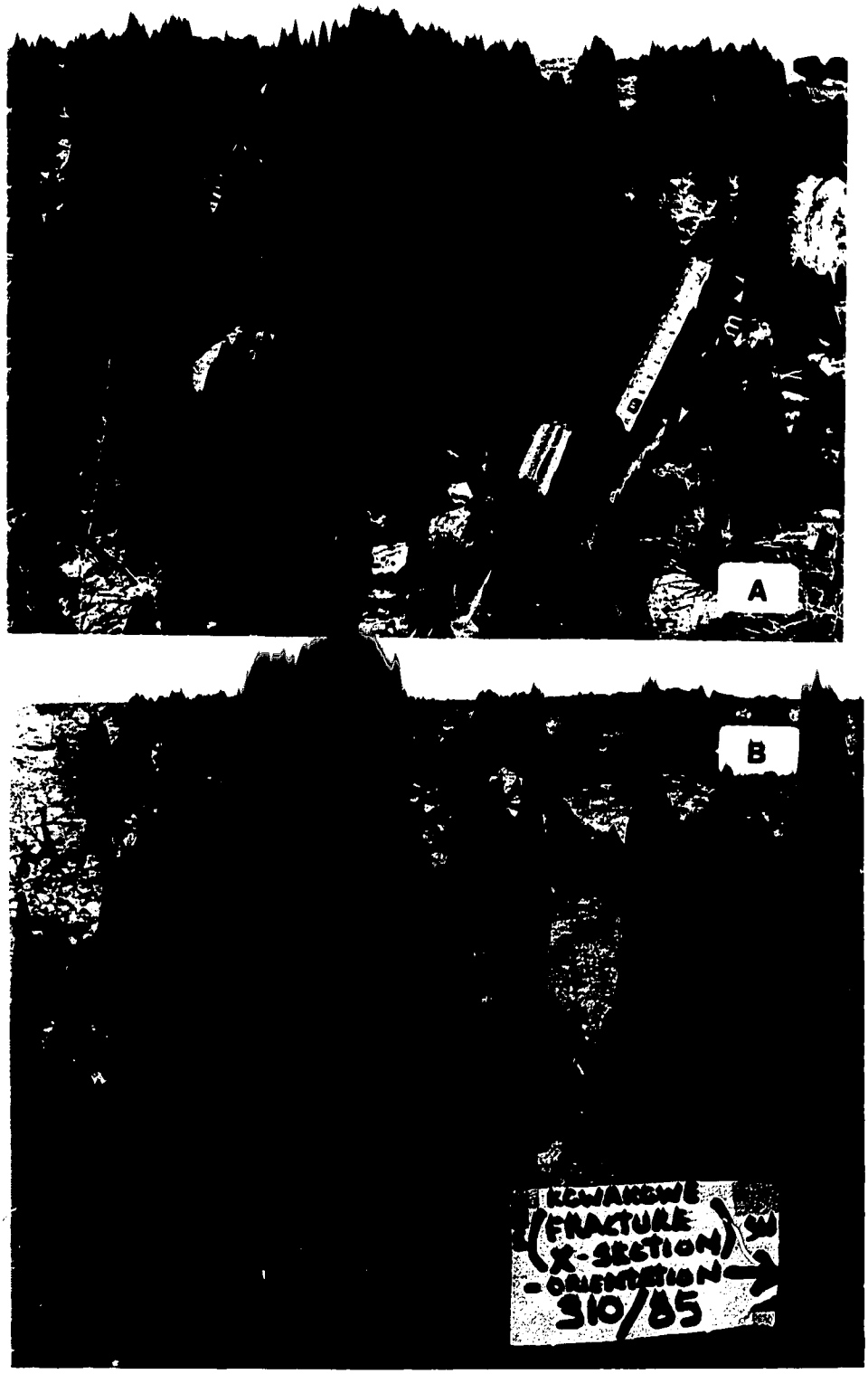
A
B
(FRACTURE
X-SECTION
-ORIENTATION
S10/85

intervening the process of chemical sedimentation.

The surface exposures of the dolomite and chert sequence in the Nneneke area to the south of Kanye show symptoms of the process of chert breccia development under present conditions. The breccia that eventually develops in this location will show relics of the present fracture system in these rocks.

7.11.3 Interpretation

The foregoing illustrates that carbonate rock was preferentially dissolved relative to chert by the following reaction:

$$CaMg(CO_3)_2 = Ca^{2+} + Mg^{2+} + 2CO_3^{2-}$$

Bedding-normal joints, with 1 to 2 centimetre spacing are developed in the cherty horizons. These joints are clearly visible on exposed bedding surfaces. The fracture sets mapped on the ground correspond to those that were interpreted on satellite imagery. SPOT-imagery shows that the dolomite and chert sequence is the most intensively fractured lithological unit in the study area. The dolomite below the chert dissolved as shown in figure 7.24A. The dissolution stage continues to occur under the present conditions of exposure which probably began in the post-Cretaceous. The chert collapsed into the resulting cavities as entire blocks that separated into mosaic fragments along joint planes (figure 7.22A and 7.22B and figure 7.23A and figure 7.23B. In this interstratal solution mechanism, successive portions collapsed over an

unspecified period of time, parting along fracture planes and accumulating as angular fragments. Some of these collapsed sediment preserved the original layering. The layers, however were only crudely preserved because the dissolution of the dolomite and the collapse of the chert into the ensuing cavities was not as even and regular as the processes that formed the layering. The layering would not be readily recognizable if the individual chert or dolomite layers were very thick. Chert breccia layers alternate with a clayey iron and manganese rich residuum. The sequence resulted in the formation of slumps that are clearly visible in figure 7.15A The interfragment space within the chert breccia was filled by silica rich solution that precipitated a cement, resulting in silicified chert breccia figure 7.15B. In this horizon, the fragmental outline is rounded and diffuse. Solutions apparently have reacted with these fragment during the cement forming process. In the upper portions of the chert breccia, more iron rich solutions precipitated, resulting in a more ferruginous cement. The sequence of breccia formation is illustrated in figure 7.25. These processes took place mainly during the period intervening the deposition of the Transvaal Supergroup and the Waterberg Supergroup. The relic fracture system displayed in these exposures was therefore formed in the pre-Waterberg period. Near the top of Kgwakgwe Hill, clastic sedimentation of red sandstone has started at the top of the chert breccia deposits.

The field observations elaborated above support a residual model for the evolution of the chert breccia rather than the model of the desiccation of an unlithified silica gel due to aerial exposure during marine regression that has been advanced in

Figure 7.25: Schematic representation of key stages in the development of the chert breccia. Intact strata undergo volume reduction due to interstratal solution of dolomite.

A. Intact buried beds of dolomite and chert within the Taupone Group (correlates with Chuniespoort Group).

B. Uplift and erosion bring beds into the brittle upper crust environment. Bed-normal and bed-parallel joints allows infiltration by groundwater.

C. Natural underground caverns are formed during dissolution of dolomite layers by ion-laden ground water. The caverns are formed near the water table.

D. The chert beds collapse into narrow caverns. Collapse of entire roof portions enables some preservation of the layering. The progressive nature of the process enables the individual chert beds to retain their identity.

E. Beds consisting of chert fragments are formed. These are interbedded with ferruginous and manganiferous clay residuum. The chert beds undergo silicification.

A

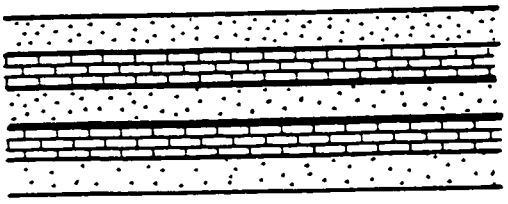

B

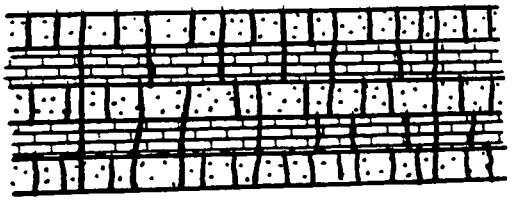

C

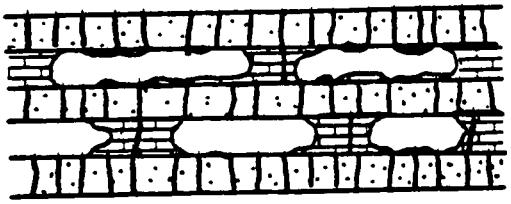

D

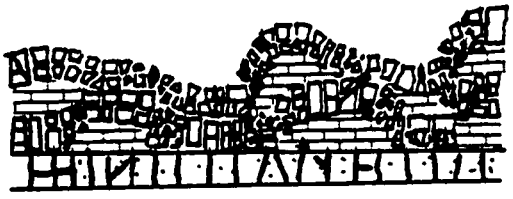

E

previous studies (Crockett, 1972; Aldiss et al, 1989). The notion of the dehydration of silica gel is intriguing, but lacks substantiation through a plausible analogy to a modern environment. The rectiplanar boundaries of fragments and their sharp intersections are untypical of desiccation cracks. The possibility that the chert breccia could be of tectonic origin has never received wide acceptance because of the distribution of the chert breccia and its lack of association with any zones of tectonic dislocation.

7.12 Joints and karst

The relationship between fracture patterns and karst in SE Botswana has been alluded to (Bons and Van Loon, 1985; Van Haren and Spaans, 1988). The presence of joints is considered to be crucially favourable for the development of caves (Jennings, 1985,p.18). Horizontal cave passages commonly follow the intersection between a bedding plane and a joint. Underground caverns have been encountered in boreholes in the study area (BGRM, 1986). In an area around Lobatse some 40 km further east of the present area of study, caves have been surveyed and mapped (Cooke, 1975). In that region, " the strike of the rocks is approximately NE-SW, with steep dips to the SE." The map indicates that the trends of the major cave corridors are similar to that of the primary lithologies. An orthogonal trend may be parallel to that of fractures. The horizontal attitude of some of the major corridors suggests that they were formed at the level of palaeo-water table. At least four level were surveyed indicating a

multistage process of cave formation. These corridors were probably formed at the intersection of bedding and fractures.

7.13 Conclusions

Conditions under which only one set of joints is formed may be considered to be the early evolution of the fracture system. At this stage, the rock still retains some elasticity and is essentially undergoing dilation. Fracture terminations are commonly observed and the relative movement on either side of the fracture is extensional, i.e., movement is perpendicular to the walls of the fractures. It is probable that the lateral and downward vertical propagation of these has not yet been limited by a truncating orthogonal set.

Virtually all the joints developed in the layered rocks are perpendicular to layering. This unambiguous relationship suggests that the primary anisotropy of the rock is a fundamental factor that controls the eventual architecture of the joints that form in it.

The elasticity is reduced as the fracture spacing decreases and the fractures propagate clear through the rock mass. A reversal in the magnitude of the principal stress initiates fracturing at right angles to the original direction.

The relationship between fracture spacing and bed thickness has been suggested by the work of Price and Ladeira (1980). This implies that for beds of a certain thickness, there is a limit to the spacing between fractures within that bed. This applies

to fractures that have cut cleanly through the whole thickness of the bed. Sedimentary units however develop bedding-parallel joints which further reduce the spacing between bedding-normal joints. This architectural development provides for high fracture densities especially in the near surface environment.

Segall and Pollard (1983) have mapped joints with a spacing frequency distribution that resembles a negative exponential function. The joints form a single fracture set in granitic rocks, which can be regarded as homogeneous media. Rawnsley et al (1992) have shown that the frequency distribution is dependent on the stage or level of joint development in the rock. The distribution evolves through a negative exponential distribution through log-normal distribution and finally normal distribution. Fracture development has probably reached saturation when the spacing shows a normal distribution. These conditions depend on the scale of observation. In this study, the scale of observation range from centimetres to metres (3 orders of magnitude). Perhaps where the fracture spacing has reached saturation, it may be possible to predict the thickness of the beds or layers involved in accordance to Ladeira and Price (1980).

The shape of fragments could be compared to the joint architecture of the same period. The comparison may however not be valid if there has been post-fragmentation fracturing. A study of several breccia sections could facilitate such an investigation.

CHAPTER 8: FAULTS AND SHEAR ZONES

8.1 Introduction

Faults were defined in chapter 3 (section 3.2.2). The study area is extensively affected by faults of all kinds (figure 6.5). Many of the faults are reactivated fractures, and some have been initiated along Archaean shear zones. Horizontal displacements along major faults, achieved by reactivation of pre-existing fractures, are more readily apparent in the southern parts of the study area than in the north (see figure 6.1 and figure 6.5). Faults were distinguished from other regional lineaments shown in figure 6.1 by ground evidence of slip, brecciation, silicification or displacement.

In this chapter, shear zones and faults in the study area are described by their spatial and angular distribution and by their chronological order. Local and regional fault patterns are examined. Small scale faults and shear zones are analyzed to provide their deformational significance.

8.2 Shear zones

8.2.1 General

The earliest evidence for the tectonic displacement of rigid blocks is shown by the occurrence of shear zones in basement rocks. Pre-Transvaal shear zones were probably initiated when these rocks deformed under ductile conditions. Consistent photogeological criteria for recognition of shear zones could not be established in the present area of study. Shear zones were therefore recognized from detailed ground mapping of foliation and lineation in the area around Moshaneng. They affected the Archaean basement, i.e. the Gaborone Granite and Kanye Volcanic Formation, and the overlying Proterozoic platform deposits.

8.2.2 Orientations

Shear zones have mostly steeply dipping foliation that is confined to relatively narrow strips of a few metres to less than 1 metre in width. At Taueshele (figure 4.2), southeast trending foliation is overprinted by an east-west trending foliation. Both foliations display steep dips of about 75° (figure 8.1). The east-west trending foliation is also marked by zones of silicification, formed in later brittle reactivation. Lineation measurements taken along the northeast flank of Tletletsi show slip attitudes with plunges that vary from a shallow 20° to a moderately steep 50° (figure 4.2) and indicate oblique slip. The variability of plunge indicates that movement on the shear zones was episodic. The most common foliation trend is northwest-southeast, with vertical or steep dips to the northeast (figure 4.2). These shear zones are relatively well developed on the northeastern flank of Mokalaka Hill. On this ridge the

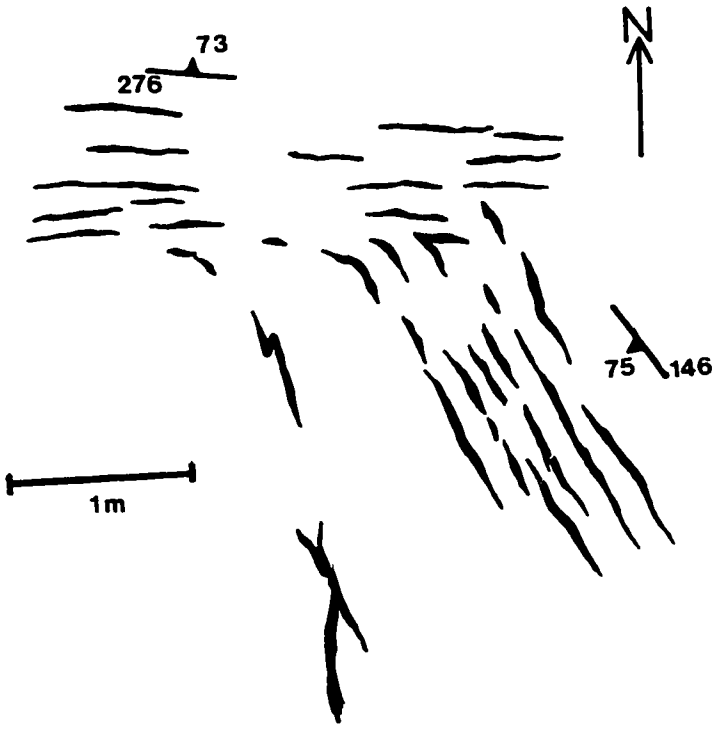

Figure 8.1: Silicified east-west trending foliation overprinting northwest trending foliation at Taueshele in Kgale Granite of the Gaborone Granite Complex. The E-W foliation is silicified due to later reactivation.

Waterberg sediments are steeply dipping or overturned, suggesting that the shear zone was reactivated as a fault in post-Waterberg times (see section 8.4.5).

Other possible shear zones are marked by foliation within the quartz syenite complex around the village of Moshaneng. The quartz syenite is probably of a post-Waterberg age. Isolated exposures show that the foliation trends ENE with steep to moderate dips to the north. These could also be zones of cataclastic deformation. This foliation is post-Waterberg in age and therefore not produced by Archaean ductile deformation.

8.2.3. Petrofabric

Shearing in the NE part of Moshaneng affects the medium crystalline Kgale Granite of the Gaborone Granite Complex and felsites of the Kanye Volcanic Formation. Most of the sheared granite is exposed in weathered outcrops that display a lot of secondary alteration and yield friable hand-specimens.

Petrographic examination of oriented thin sections from the flanks of Mokalaka Hill confirms the dominance of an oblique sense of slip. The northeast basement block has been uplifted relative to the southwest block of overturned platform deposits. Sheared Kgale Granite examined in thin section consists of quartz and feldspar in roughly equal amounts and a minor component of mica. Primary quartz crystals show undulatory extinction. The quartz and feldspar are fractured. Feldspar fragments are generally smaller compared to those of primary quartz. The two minerals are each

concentrated in bands marking a crude preferred orientation. Stringers of mica are concentrated along these bands, usually marking the boundary between quartz-rich and feldspar-rich bands. Cracks within feldspar and quartz grains are filled with mica. Many quartz grains are elongate ribbon quartz indicating dynamic recrystallization. The secondary recrystallized quartz does not display undulatory extinction. Coarse recrystallized quartz developed into elongate shapes are features of a blastomylonite. A thin section of sheared granite cut parallel to the lineation and perpendicular to the foliation shows that two directions of banding intersect at an angle of ≈25°. These bands represent ***S*** (*schistosité* or schistosity) and ***C*** (*cisaillement* or shear) planes. The ***S***-plane is truncated by the ***C***-plane. Most of the mica is aligned along the ***C*** (shear) plane. The ribbon quartz grew along the axis of maximum strain and the mica acted as a lubricant during slip along the ***C*** (shear) plane. The shear sense has been inferred as shown in figure 8.2A. The sense of shear and the lineation show that the NE basement block moved up relative to the Tletletsi syncline (See figure 4.2, 8.2A).

The Kanye Volcanic Formation felsite shows a microcrystalline groundmass with clusters of coarse quartz crystals. Oriented thin sections cut parallel to lineation and perpendicular to foliation were examined. The clusters show crude σ-structures with pressure shadow tails (Simpson and Schmid, 1983; Ramsay and Huber, 1987, p.633). The sense of shear in these rocks is shown by the shear couple in figure 8.2B. The shear sense in granite and felsite are consistent with each other.

8.3 En echelon cracks

Figure 8.2A: Photomicrograph of sheared Kgale Granite of the Gaborone Granite Complex (magnification x40). This quartzo-feldspathic rock shows *S-C* structures. Mica (**1**) is concentrated along the shear plane (*C* plane). Recrystallized quartz (**2**) is elongated along the schistosity plane (*S* plane). The two planes meet at an angle of ≈25°. The sense of shear is given by the shear couple. The specimen represents the NW trending shear on the NE flank of Tletletsi syncline.

Figure 8.2B: Photomicrograph of sheared Kanye Volcanic Formation felsite (magnification x40). This microcrystalline rock shows coarse elongate (**3**) and ribbon quartz formed during dynamic recrystallization. The coarse grained quartz clusters have been drawn into *S*-shaped σ-structures with pressure shadow tails (**4**). The sense of shear is shown by the shear couple and it is consistent with that found in the sheared granite. The specimen represents the NW trending shear on the NE flank of Tletletsi syncline.

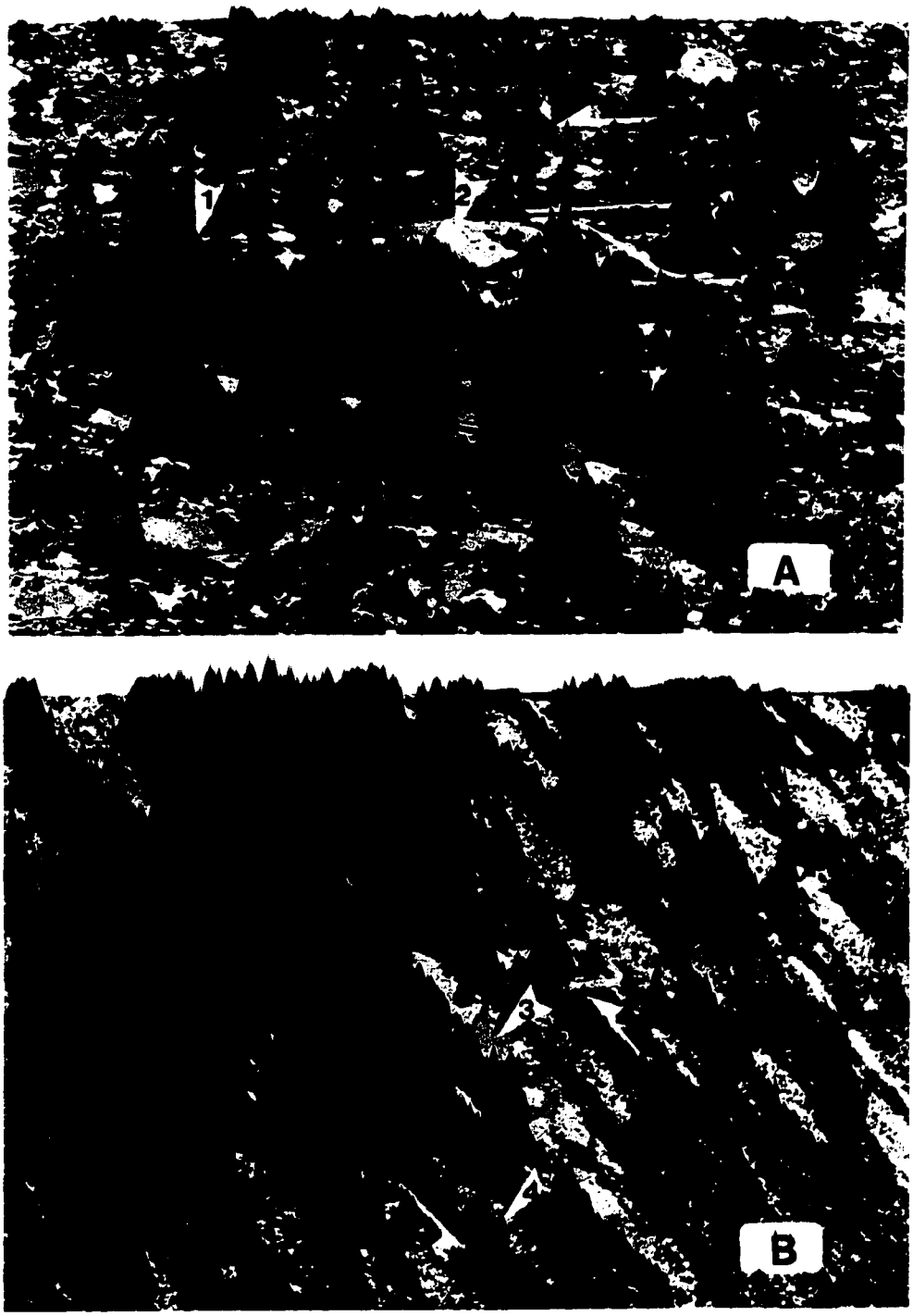
1
2
A
3
4
B

Incipient shear zones marked by en echelon cracks occur in some of the major rock types of the study area. They have been identified in the basement, Black Reef Quartzite and Waterberg sandstone. En echelon tension cracks mark incipient shear zones which did not develop a principal displacement zone. Features of these structures are described below.

8.3.1 Black Reef Quartzite

En echelon cracks and incipient shear zones are developed in the Black Reef Quartzite near the Taupone Fault (Figure 8.3A and 8.3B). The majority of these shear zones show dextral shear that is consistent with the horizontal displacement of the Taupone Fault. Sinistral incipient shears that trend 78°, with tension gashes that trend 40° are probably related to **R'** anti-Riedel shears (station 59). Alternatively this shear sense may indicate an additional episode of shearing with a shear sense that is opposite to that of the Taupone set of faults.

8.3.2 Waterberg sandstone

En echelon tension gashes and pinnate fractures are also displayed in the coarse sandstones of the Waterberg Group. Conjugate en echelon cracks were traced on an exposure 150 metres long on the NE limb of the Tletletsi Syncline (figure 9.1). The structures shown in figure 8.4A and 8.4B are representative of their geometry. They

Figure 8.3A: En echelon quartz veins along a linear incipient shear zone in the Black Reef Quartzite near the Taupone Fault. The en echelon arrangement diminishes towards the left of the photograph. The displacement across the near-vertical shear zone is dextral. Markings on tape are at 10 cm intervals.

Figure 8.3B: Quartz veins (joint origin) and quartz-filled en echelon tension cracks. Quartz fibres in the veins are perpendicular to the vein walls. The trend of the shear zone, quartz veins and quartz fibres provide a means of determining the movement sense and stress directions in the rock during the formation of these veins. Tension cracks have been rotated through 15° relative to joints outside the shear zone. The sense of shear is indicated by the shear couple. Markings on the tape measure are at 10 cm intervals. A structural interpretation is provided in figure 8.9B.


A

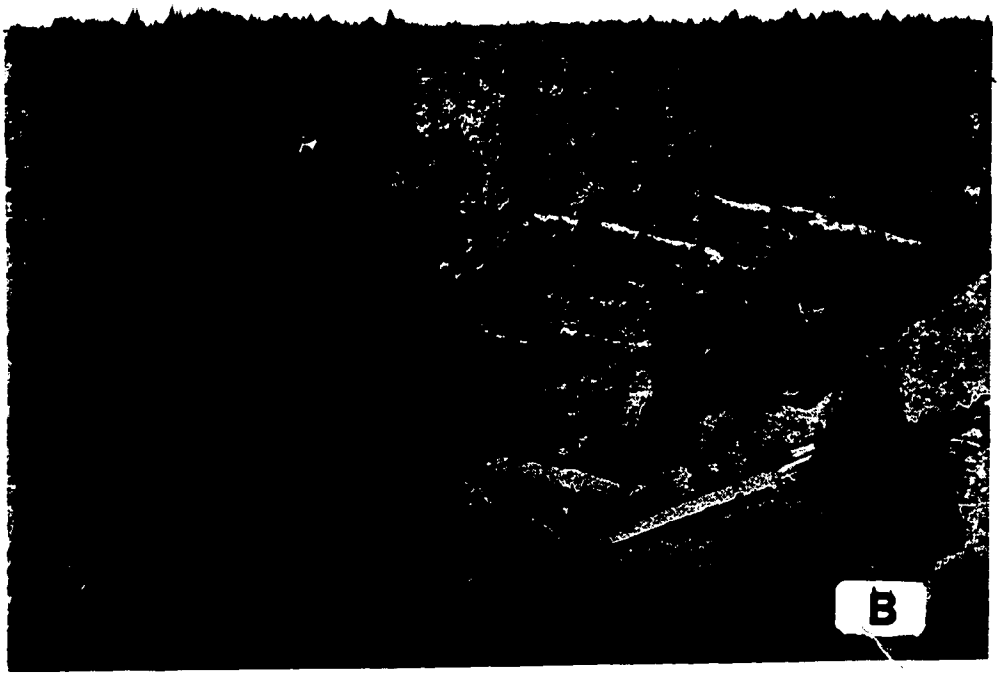
B

Figure 8.4A: Quartz veins originating from en echelon tension gashes and pinnate fractures. Quartz fibres are perpendicular to vein walls. At right-centre of the photograph, sigmoidal and rotated gashes are overprinted by later planar horizontal gashes. The measuring tape is held parallel to the trace of a reverse fault that is partially quartz-filled (see figure 8.4B for interpretation). These structures occur in the red coarse-grained sandstone of the Manyelanong Hill Formation of the Waterberg Group. The exposure occurs on the NE limb of the Tletletsi syncline, near the nose. The viewing surface has an attitude 193\73; the exposure is viewed looking east.

Figure 8.4B: Trace of veins and fractures in figure 8.4A. A set of 3 reverse faults dip towards the south. A reverse fault near the bottom left of the photograph dips towards the north; complementary as a conjugate shear to the set of three. Pinnate fractures flanking the fault traces are remnants of sheared en echelon tension gashes. En echelon tension gashes mark zones of incipient shearing typified by the conjugate shear couples **1** and **2**. Horizontal N-S compression is shown by the large arrows. Sinistral shears truncate dextral shears, demonstrating the younger age of the former.

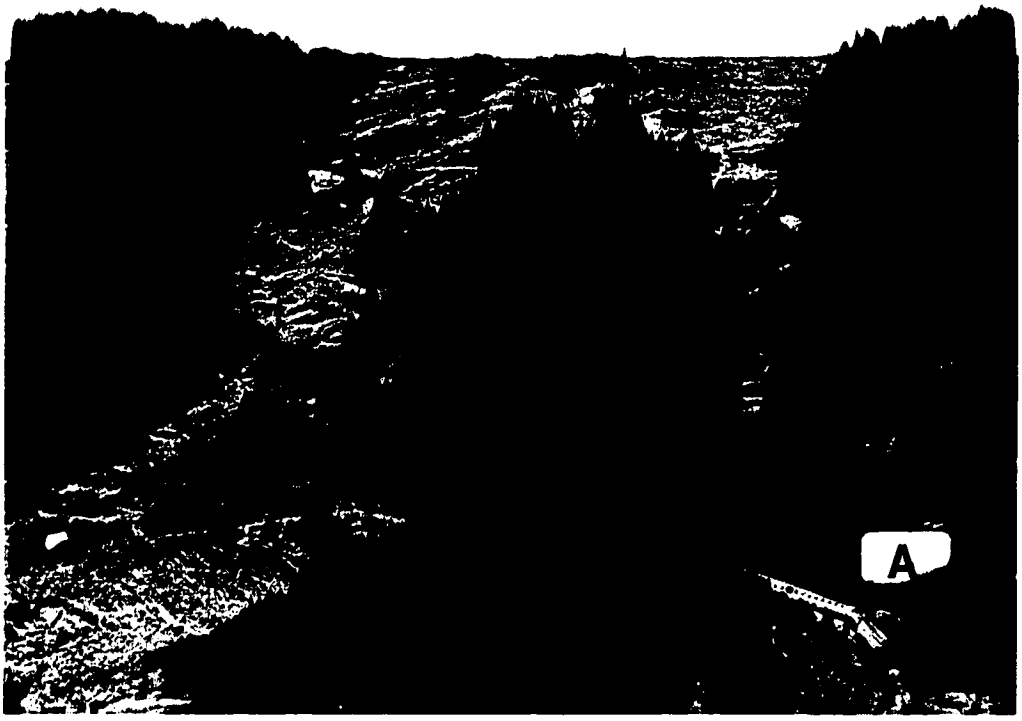
A

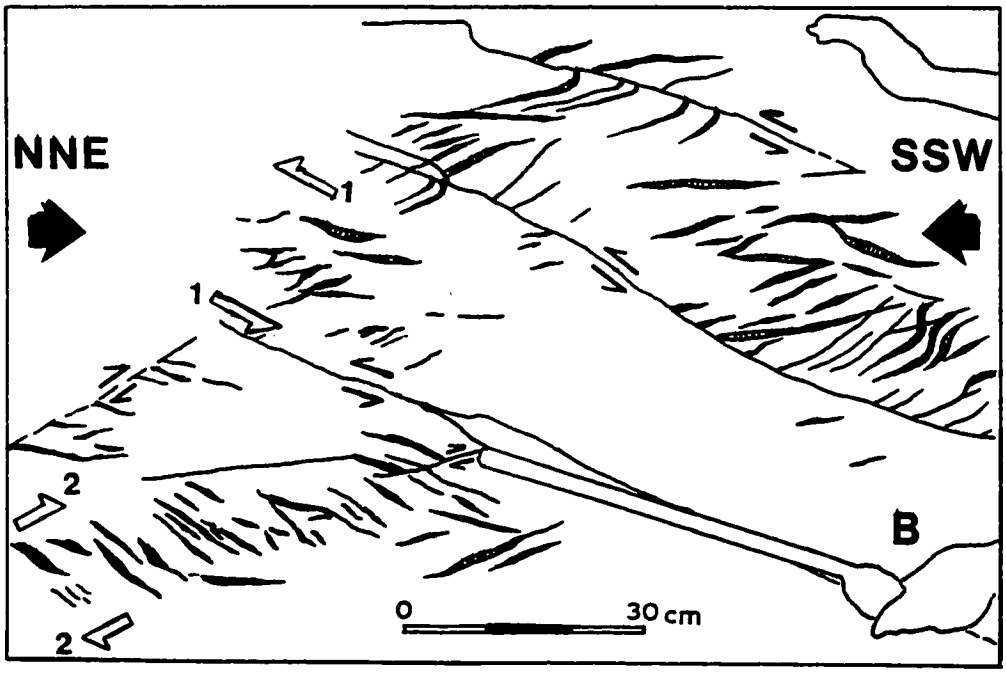
NNE
SSW
1
1
2
2
B
0
30 cm

indicate that a horizontal compressive stress acting in a NE-SW direction affected rocks on the NE limb of the Tletletsi syncline. Near-horizontal tension gashes formed an angle of about 30° with the shear plane (i.e. incipient shear zone or principal displacement zone)(figure 8.5A). The incipient shear zones along which these tension gashes developed dips to the SSW. Quartz fibres grew roughly perpendicular to the walls of the veins. A conjugate set of shear zones also developed in accordance with an Andersonian geometry (Anderson, 1951; Wilson, 1982). The en echelon tension gashes rotated away from the shear plane, some forming sigmoidal cross-sections as shear displacement continued (figure 8.4A and 8.4B). New horizontal tension gashes overprinted the earlier-formed sigmoidal and rotated gashes. The stress field eventually induced failure along individual incipient shear zones, resulting in sinistral shear within the SSW dipping shears. A principal displacement zone along each shear zone cut off the tension cracks and formed pinnate fractures (veins). The same process also affected the NNE dipping conjugate set of shears, but to a lesser extent. The shear sense on these latter ones is dextral. The number of sinistral shears exceeds that of dextral shears by a ratio of 3:2 (figure 8.4B and 8.5B). The amount of displacement along each shear cannot be determined. The development of principal displacement zones produced low angle faults. Bulk rotational finite strain is inferred solely from the number of shears of each displacement sense, and is shown schematically in figure 8.5B. The finite strain axes are non-coaxial with those of the far field stress.

The geometry of these en echelon veins does not accord with that formed by fractures and shears of a simple strike slip fault (Riedel, 1929 in Ramsay and

Figure 8.5A: Attitudes of reverse fault (100/38), tension cracks (300/03), slicken striae (240/27) and stress directions (σ_1=046/03, σ_2=136/26, σ_3=310/66) in the Waterberg sandstone on the NE limb of the Tletletsi syncline.

Figure 8.5B: Schematic stress and strain interpretation of the structures shown in figures 8.4A and 8.4B. Rotational bulk finite strain is postulated from the relative dominance of sinistral displacement over dextral by a ratio of 3:2. Finite strain axes (ε_1 and ε_3 are non-coaxial with the far-field principal stress directions (σ_3 and σ_1).

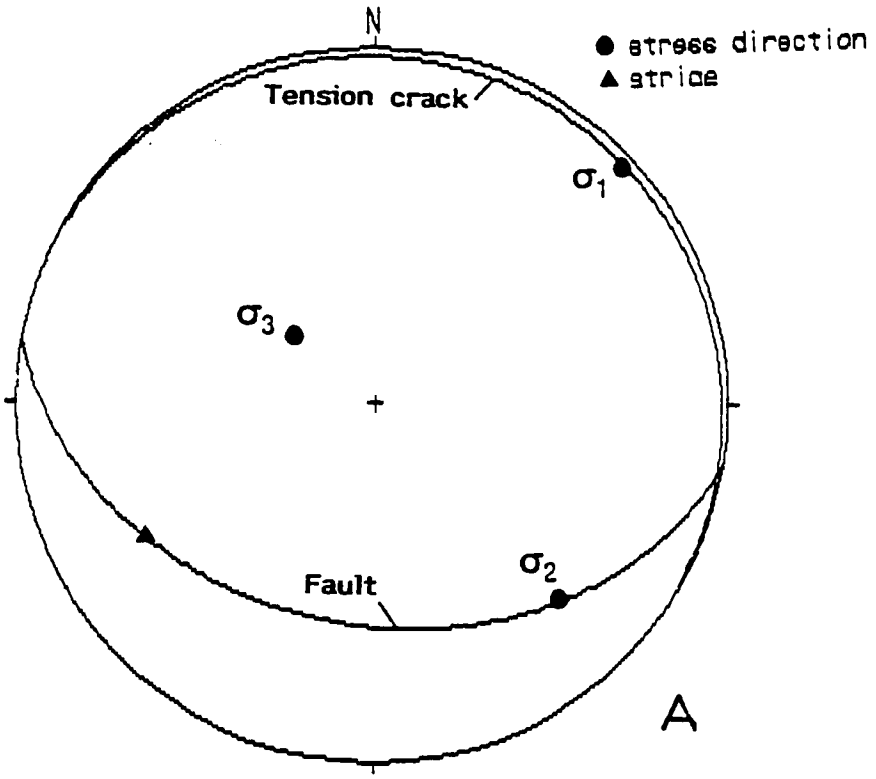
N
● stress direction
▲ strike
Tension crack
σ_1
σ_3
σ_2
Fault
A

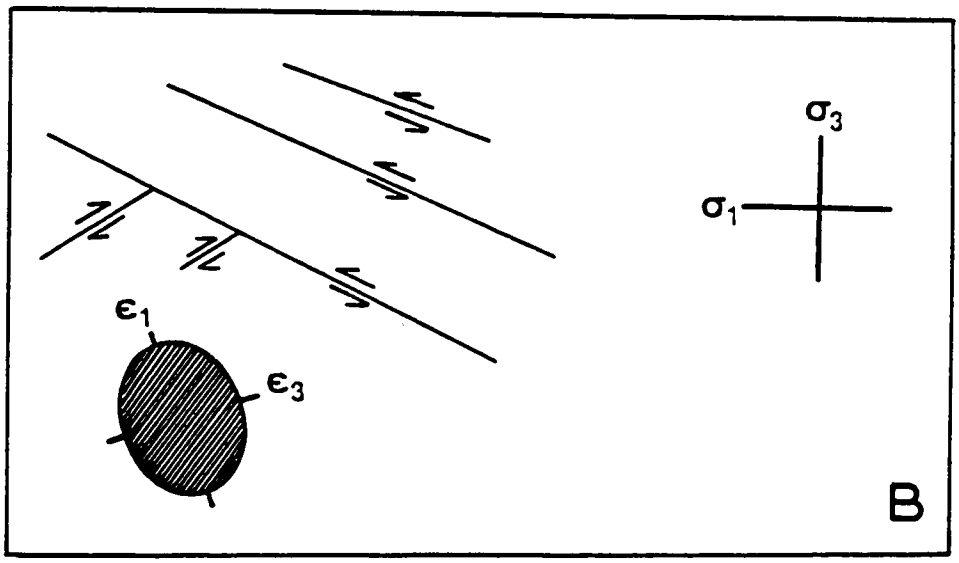
σ_3
σ_1
ϵ_1
ϵ_3
B

Huber,1987; Tchalenko and Ambraseys, 1970; Sylvester, 1988); but it is consistent with that of a conjugate system of faults (Anderson, 1951). An interpretation of the local stress field, prevalent during the formation of the tension cracks and the eventual slip along the faults is shown in figure 8.5A. The interpretation is made on the basis that slip along the fault plane occurs in the σ_1-σ_3 plane and that σ_2 lies in the fault plane. This interpretation reveals that σ_1 lies in the plane of planar tension gashes. The fringes of most of the sigmoidal tension gashes also have the attitude of the overprinting planar gashes. This geometry is consistent with the standard model on the development of en echelon tension cracks advanced by Ramsay and Huber (1983). The angle between the tension gash and the fault plane or principal displacement zone is about 30°.

8.3.3 Deformational significance

En echelon cracks occur along an incipient shear zone within the interior of a rock that is subjected to a remote stress field. The incipient shear zone probably develops as a discoid zone confined within the rock (i.e. structures are not initiated at a free surface). The deformed discoid portion undergoes mode II and III displacement in a manner similar to that of an elemental crack. The en echelon cracks within the deforming lens of rock however, are initiated by mode I displacement. The deforming lens may be complimented by a conjugate lens (Wilson, 1982) according to the Andersonian geometry. The conjugate shears are formed under the same stress system

but need not form simultaneously; one conjugate set may overprint an earlier formed set. A detail of non-systematic network of veins in Kgale Granite shows structures developed by superimposition of two shear senses (figure 8.6B and figure 8.7B). At this locality, pinnate veins formed during an early sinistral displacement are themselves displaced by a later set of en echelon veins with a dextral sense of displacement. An earlier NE trending shear zone (PDZ) with N-S trending en echelon veins (PV1) displays sinistral displacement. An overprinting, second, NE trending set of en echelon veins marking a N-S trending shear zone display dextral displacement. These structures are formed where a conjugate system of shear zones are coincident.

Within the shear zone bulk volume increase occurs (positive dilation). Figure 8.8B shows the widening of a shear zone from L_0 to L_1 as the tips of the tension gashes propagate. The gashes also rotate and dilate, resulting in net volume increase. Gaping or mineral-filled tension gashes in figure 8.8A also represent a net volume increase within the shear zone. In the Black Reef Quartzite, the tension cracks are quartz-filled and some have growth fibres preserved. The cracks make an angle $\leq 45°$ with the shear plane or principal displacement zone in accordance with standard models (Ramsay and Huber, 1983 p.50). Further shear movement results in the tension gashes rotating away from the principal displacement plane. Beyond 45°, the tension gashes develop a sigmoidal cross-section and deformation proceeds in a manner demonstrated in the Waterberg sandstone (section 8.3.2).

The en echelon cracks and associated shear zone display Andersonian geometry rather than a Riedel geometry. These structures are initiated within the confines of a

Figure 8.6A: Detail of the Taupone fault zone in Kanye Volcanic Formation felsite. The photograph is taken on a horizontal exposure. Quartz veins represent one set of faults and one set of pinnate fractures. Fault motion was strike-slip with dextral horizontal displacement. The structural interpretation is provided in figure 8.7A.

Figure 8.6B: Non-systematic vein network in the Kgale Granite. Three sets of veins are recognized. Two episodes of shear movement are distinguished. The episodes produced essentially opposite sense of shear movement in the rock. An interpretation of the structures is provided in figure 8.7B.


A


B

Figure 8.7A: Trace and interpretation of the salient features in figure 8.6A. The principal displacement zone (PDZ) trends NNE. The trend of the PDZ makes an angle of 45° with that of the one set of pinnate veins (PV). The relative orientations of the two vein sets demonstrates dextral displacement. The displacement is consistent with that shown by marker horizons on the geological map in figure 6.5.

Figure 8.7B: Trace and interpretation of the salient features in figure 8.6B. The trend of the principal displacement zone (PDZ) is NE, parallel to the silhouette of the *Brunton* compass. Secondary veins consist of pinnate veins (PV1, stippled pattern) that show an initial sinistral sense of movement (shear couple **1**). A second set of secondary veins consist of en echelon veins (PV2, stripped pattern). The shear sense associated with PV2 (shear couple **2**) is opposite to that of shear couple **2**. The second shear sense was probably superimposed on early formed structures during the incipient development of a conjugate shear. The displacement of PV1 veins along PV2 shows that the latter veins developed a shear aspect.

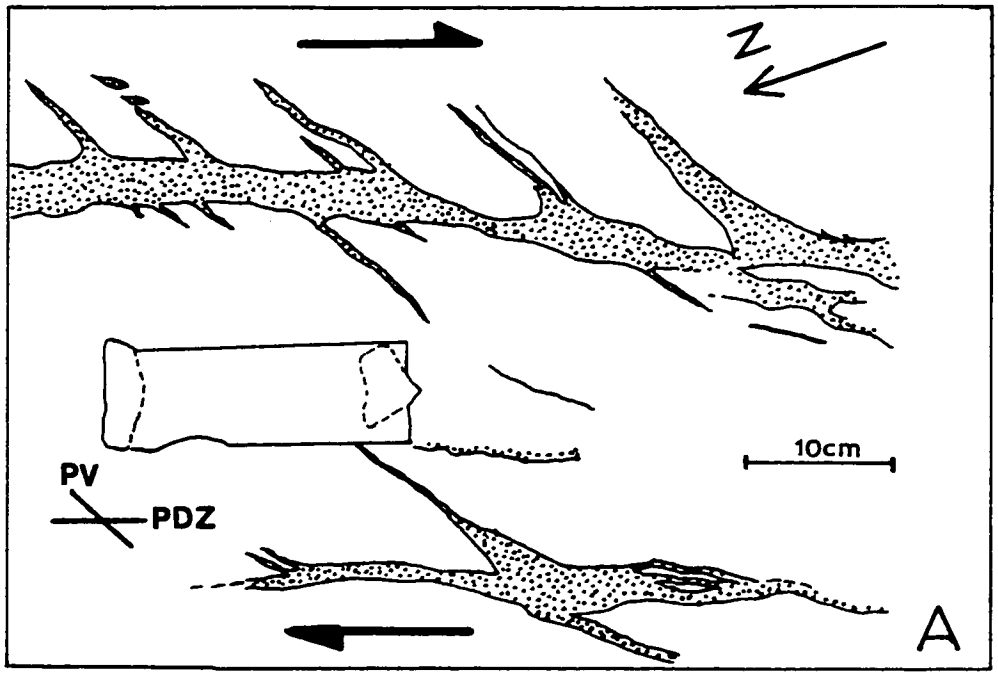
N
10cm
PV
PDZ
A

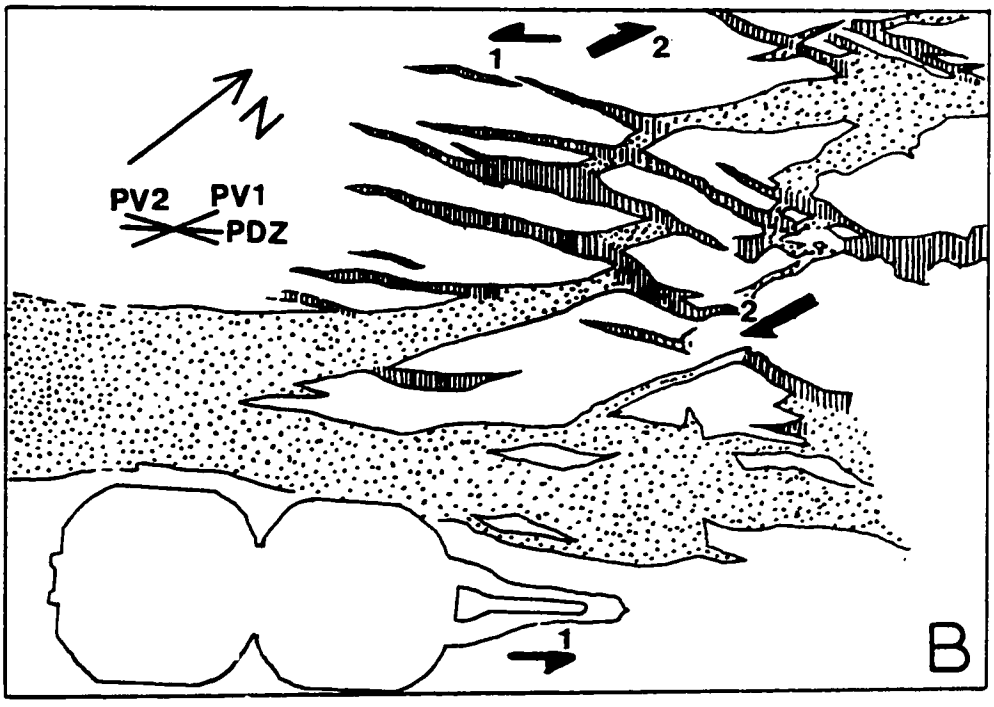
1
2
N
PV2
PV1
PDZ
2
1
B

Figure 8.8A: Perspective view of en echelon tension cracks marking a shear zone. The cracks which are commonly filled by vein material constitute bulk volume increase within the shear zone.

Figure 8.8B: Relationship between extension veins (joint origin) and en echelon tension veins. Within the shear zones, the tension veins are rotated to form a greater angle with the shear zone plane. The dilation direction of the tension cracks deviates increasingly from that of the extension veins outside the shear zone as shearing progresses. Volume increase is indicated in the cross-sectional width from L_0 to L_1.

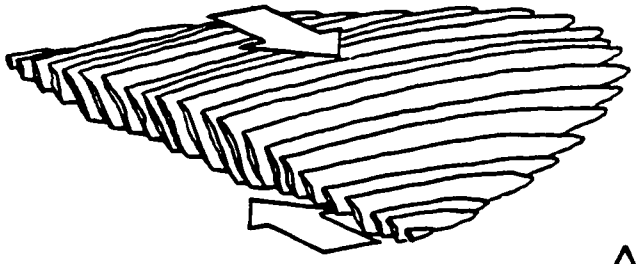

A

En echelon array of tension cracks in shear zone

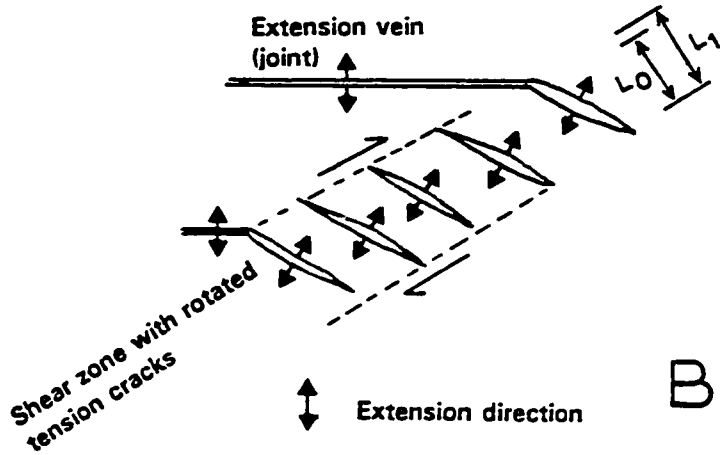

B

rock mass. So far, it has not been shown in the field or by experiment that incipient shear zones and en echelon cracks can be initiated at a free surface of a rock mass, the same way that Riedel shears and joints are formed. It seems that a favourable environment for the formation of en echelon cracks probably include confining pressure in an all-enclosing medium.

8.4 Faults

8.4.1 General

In addition to the ductile shear zones, other displacements of rigid blocks are indicated by the occurrence of breccia, silicification zones and slicken striae in faults that formed under brittle conditions. It is apparent that whereas earlier formed deformation was ductile in the deeper crust, later deformation was brittle, presumably when the same portion of the crust was uplifted to shallower levels. It has been suggested elsewhere that dilatant fractures nucleate shear zones (Segall and Simpson, 1986). The present study area provides evidence that suggests that shear zones nucleate brittle fractures. Such shear zones may be ancient basement ductile shears or incipient dilation crack-marked shears.

8.4.2 Basement faults

Silicification zones represent younger shear deformation in basement rocks. They are readily recognized on aerial photographs as positive relief lineaments that are not as thickly vegetated as lineaments representing dikes. The zones are oriented E-W, ENE and NE. On the ground, they are characterized by heavily veined zones and breccia. The original morphology of the breccia is often obscured by subsequent silicification. Some fault planes still have slicken striations preserved (figure 8.9A and 8.9B). Striations show that slip varied from strike slip, through oblique slip to dip slip within the same fault zone. These multiple slip orientations demonstrate a recurrence of movement in the same fault zone at different times.

Exposures of silicification occur on the northern flank of Gokano Hill, west of Taueshele and in the southeastern part of the Moshaneng area (see figure 4.2 for the location of these areas). In the last area, a 5 metre wide quartz reef has been developed in felsites of the Kanye Volcanic Formation. The reef has an attitude of 255/34. It consists of breccia that has been extensively silicified by a network of non-systematic quartz veins similar to those in figure 8.6B and 8.7B. Non-systematic vein network may results from the overprinting of fractures associated with one sense of shear by one or more fracture sets associated with some other sense of shear. This mechanism is described in section 8.3.3.

It is conceivable that a principal displacement zone developed in rock that failed in near-surface strike-slip fashion will eventually produce angular fragments in a fault zone. The intersection of Riedel R and R' fractures, principal displacement zone and other subsidiary fracture sets (figure 3.6B) will produce fragments. Rotation of such

Figure 8.9A: Strike-slip slicken striae on a fault surface in the Gaborone Granite. The location is at Taueshele in the northern part of the Moshaneng map area. The attitude of the fault 235/50. The slip is entirely horizontal; dextral displacement.

Figure 8.9B: Dip-slip slicken striae and quartz fibres on a normal fault surface in the Gaborone Granite. The location is at Taueshele in the northern part of the Moshaneng map area. The attitude of the fault is 303/56. The slip is strictly oblique, but mainly dip-slip; striae plunge 053/52.


A


B

fragments and further fracturing with continued displacement gives rise to breccia. Contemporaneous or subsequent introduction of silica between the fragments results in silicified fault breccia. Silicification zones have also been mapped in basement rocks in SE Botswana, but outside the present area of study (Key, 1983; Aldiss, 1989).

The majority of faults in the basement have a NE to ENE trend, parallel to main lineament trend shown in figures 6.1. This trend is also parallel to many dikes in the study area. There is evidence that shows that some of the faults were initiated in the pre-Transvaal period e.g. at Kgwakgwe, a NE trending zone of brecciation is terminated at the base of the Transvaal rocks. There are no exposures however, that reveal that any of the dikes have been sheared by these faults.

8.4.3 Syn-Transvaal tectonism

The lower Transvaal was deposited on basement that was already fractured. Local basal conglomerates in the Black Reef Quartzite are lensoid and variable in thickness. They were probably deposited in the vicinity of faults that were active during deposition. However, such conglomerates do not persist into the upper parts of the Black Reef Quartzite. The basin floor was undergoing stable subsidence for the greater part of lower Transvaal deposition. A single episode of basin floor instability is indicated by a thin horizon of coarse clastic sediments during the deposition of the dolomite and chert sequence. This horizon was mapped NE of Mokalaka ridge and south of Kanye. At the latter location, the horizon is about 10cm thick and consists of

angular matrix-supported chert fragments set in an unsorted sandy matrix. NE of Mokalaka Hill, the horizon is marked by consolidated porous sand.

The upper Transvaal is a succession of fine and coarse clastics (figure 6.5). Several episodes of transgression in the sedimentary sequence indicate basin floor oscillations or vertical displacements in Pretoria Group times.

8.4.4 Post-Transvaal faults

8.4.4.1 Previous work

Transvaal deposition stopped around 2.1 Ga and Waterberg Group deposits only began to be laid down about 1.8 Ga (Tankard et al). Structures in and outside the study area show that following the deposition of the Transvaal Supergroup, the Kaapvaal Craton in SE Botswana was unstable (Dietvorst, 1988, 1991 and Dietvorst et al, 1991). The instability probably started towards the end of upper Transvaal deposition (Crockett, 1969). According to previous work, tectonic activity affected basin areas much more than platform areas (Crockett, 1969, 1972). While vertical and detachment displacements are advocated in Crockett's work, horizontally directed forces and folds are emphasized by Dietvorst's work.

8.4.4.2 ENE to NE trending faults

Post-Transvaal ENE to NE trending fractures have their origins in pre-Transvaal, late Archaean to early Proterozoic events. Fractures of this trend are less numerous in the overlying platform deposits. This suggests that only some of the early-formed pre-Transvaal fractures were reactivated in post-platform deposit times. Faults traversing the Black Reef Quartzite are characterized by foliated and unfoliated breccia, and non-systematic quartz veins. The Nneneke fault south of Kanye exemplifies these features. Joint spacing observed on isolated exposures becomes more closely-spaced as fault zones are approached. The most prominent of these faults is the Taupone Fault. Features of this fault and others parallel to it are discussed below.

8.4.4.3 Taupone Fault

The Taupone Fault has the largest apparent horizontal displacement or separation (10 km) among the NE trending faults. Two other regional faults, namely Nneneke Fault and Kgwakgwe Fault are parallel to the Taupone Fault (figure 5.2 and 6.5). They are predominantly strike-slip with dextral sense of displacement. Figures 8.6A and 8.7A show a small scale fault in the Taupone fault zone displaying the dextral sense of displacement consistent with that of the regional map. Nneneke Fault has a horizontal displacement of about 1.5 km and Kgwakgwe Fault, a displacement of about 3.8 km (figure 6.5). The movement along these faults was a response to E-W directed horizontal compression as shown in figure 8.10 and figure 8.12.

One of the most striking characteristics of the Taupone fault is the fact that it

Figure 8.10: Interpretation of regional structures that constitute the Taupone Fault. Fault branches in the southwest end form a "dendritic" pattern that formed as a "flower" structure. The branches accommodated diminished components of the total displacement as the fault zone terminated southwestwards. The uplifted block was extruded upwards between oblique slip faults. The thrust and fold zone in the northeast formed in a region of transpression.

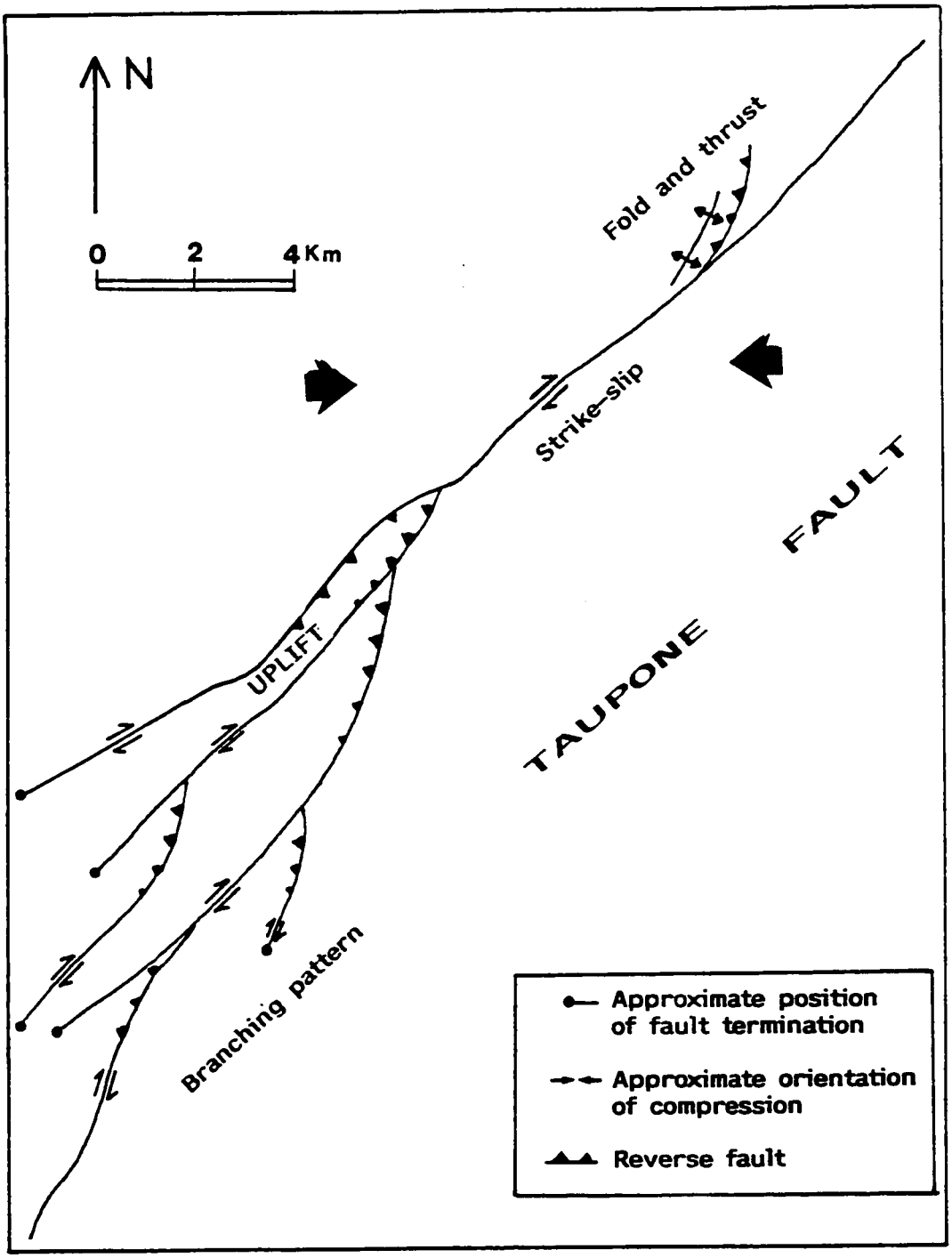
N
0
2
4 Km
Fold and thrust
Strike-slip
FAULT
TAUPONE
UPLIFT
Branching pattern
Approximate position of fault termination
Approximate orientation of compression
Reverse fault

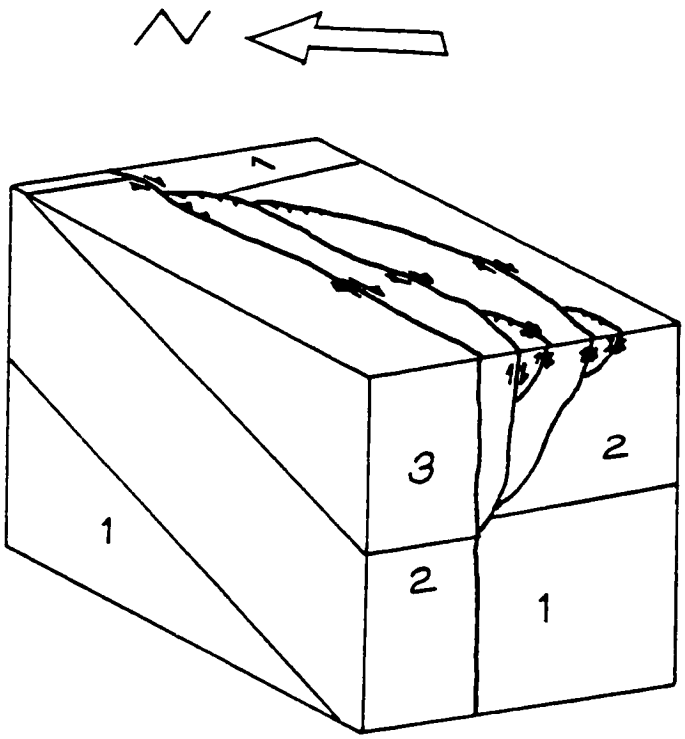

Figure 8.11: Schematic block diagram of the branching pattern of the Taupone Fault System. The dimensions on the diagram are not to scale; aspects of the vertical section being greatly exaggerated for illustrative purposes. **1**=basement, **2**=Lobatse Volcanic Group and **3**=Transvaal Supergroup. The diagram is based on "flower structure" models by Naylor et al (1986) and Woodcock and Fischer (1986).

bifurcates and then breaks into several branches when traced southwestwards from its displacement of the Black Reef Quartzite. It is apparent that the displacement along the fault decreases and eventually dies out southwestwards (figure 6.5 and figure 8.10). The attenuation of the displacement is taken up by the branches of this fault; thus the horizontal displacement on each of the branches is diminished compared to where the fault follows a single trace. The principle inherent in this type of termination is briefly described by Park (1989, p.6). These structures may develop by reactivation of existing fractures (Barquins and Petit, 1992).

The regional structural map and aeromagnetic data indicate that the Taupone Fault terminates southwestwards and northeastward within the study area (figures 5.2 and 6.5). The total horizontal length of the fault is about 30 kilometres. In the SW fault termination, the strain is dissipated in a zone of branches (figure 8.10). In the NE, diagnostic termination features are obscure, there is evidence that the fault does not displace pre-Transvaal magnetic anomalies (section 5.1.2). On the geological map in figure 6.5, the fault has an apparent horizontal displacement of 10 km and therefore a vertical displacement of about 1.94 km (calculated for 11° of dip of displaced Black Reef Quartzite near the fault, $V=H\tan\delta$, where V=vertical displacement, H=horizontal displacement and δ=dip of displaced strata) at the basement/ Transvaal Supergroup interphase. Minimum total slip is about 1.90 km. The horizontal displacement of the magnetic Kanye Volcanic Formation however, is about 3 km (see figure 5.2). That would produce vertical displacement of only 0.58 km. Considering the total length of the fault (30 km), a 10 km apparent displacement appears tremendously exaggerated.

Crockett (1971c) accounted for these displacements by suggesting that movement along the fault was active during Transvaal deposition. Coarse clastics that are normally associated with such syn-depositional activity are not, however, peculiarly developed near the fault.

A relationship between the maximum displacement, D and the maximum dimension of the fault surface in the direction normal to the slip direction, is given by:

$$\log P + \log D = 2\log W$$

where P = variable related to rock properties; namely, rigidity modulus, stress drop and slip increment (Walsh and Watterson, 1988). This relationship enables the determination of the fault width, given displacement, and vice versa. The horizontal displacement of 3 km of the Taupone Fault should yield a fault width of about 40 km according to the above relationships, assuming 30 GPa for the rigidity modulus on an intraplate fault (example calculated by Walsh and Watterson (1988)). The dimensions of the Taupone Fault within the study area do not strictly provide the width of the fault, but a cross-section of the length. These calculations however, still show that the observed limits of the fault within the study area are consistent with the observed displacements.

Transpression structures shown in figure 8.10 are represented by the fold and thrust zone in the NW side of Taupone Fault. These structures are formed as a result

of concomitant transcurrent motion and compression (Harland, 1971; Sanderson and Marchini, 1984). The total displacement combines components of vertical and horizontal displacements. These structures were formed as a response to post-Transvaal E-W compression that affected the study area. The pre-existing basement fracture along which strike-slip movement occurred probably approximated, but was not exactly aligned along, a principal displacement zone that would have formed had the prevailing stress system induced failure in unfractured basement. The resulting deformation was therefore not strictly that of plane strain, but that of transpression.

Fault branches on the SE flank of the fault disseminate the lateral bulk strain and displacement at the termination of the southwest end of Taupone Fault. In addition, these were subjected to uplift during strike slip movement. Shortening of the SE block was accommodated by reverse faults and lateral imbrication. The fault branches are especially prolific in shales of the Lobatse Volcanic Group (figure 6.5). Post-Transvaal strike-slip movement probably induced further failure to produce a flower structure in the overlying shales above a pre-existing basement fault. A block diagram of these structures is schematically shown in figure 8.11. Strike-slip movement accompanied by uplift provides a probable explanation for the displacements at the Taupone Fault. The block that is adjacent to the NW block across the main fault trace was subjected to the most uplift, while biocks further away southeastwards of the main fault trace had much less vertical displacement. The total regional horizontal component of the displacement along the fault is therefore about 3 km and not 10 km. Post-Waterberg vertical displacement may have further contributed

to the present total displacement, but this possibility remains to be investigated.

Bulk finite shear strain in the area east of Masoke and south of Kanye (between Kgwakgwe Fault and Taupone Fault inclusive) was produced by rotation about a vertical axis (figure 8.12). When plane strain is assumed, the angular displacement ψ is about 30° and **R**, the strain ratio is about 2.25. Rotation of the strain ellipse axis ω is 15.9° according to relationships given by Ramsay and Huber (1983). The angular shear strain is given by

$$\gamma=\tan\psi$$

The relationship between the angular shear strain and the rotation of the strain ellipse axis is expressed as

$$\tan\omega=\gamma/2$$

8.4.4.4 NW trending faults

The NW trending set of lineaments within domain 4 represents faults and master joints in the lower Transvaal sediments (see chapter 6 section 6.4.1). These domain 4 trends cannot be traced continuously into the area underlain by the Waterberg sediments in domain 6 suggesting that the fracture trends were developed mainly during the period intervening Transvaal and Waterberg deposition. The presence of some fractures of this trend in domain 6 however suggests reactivation in the post-Waterberg.

The fault extending northwestwards from Gampudi Dam (figure 4.2) is a tear

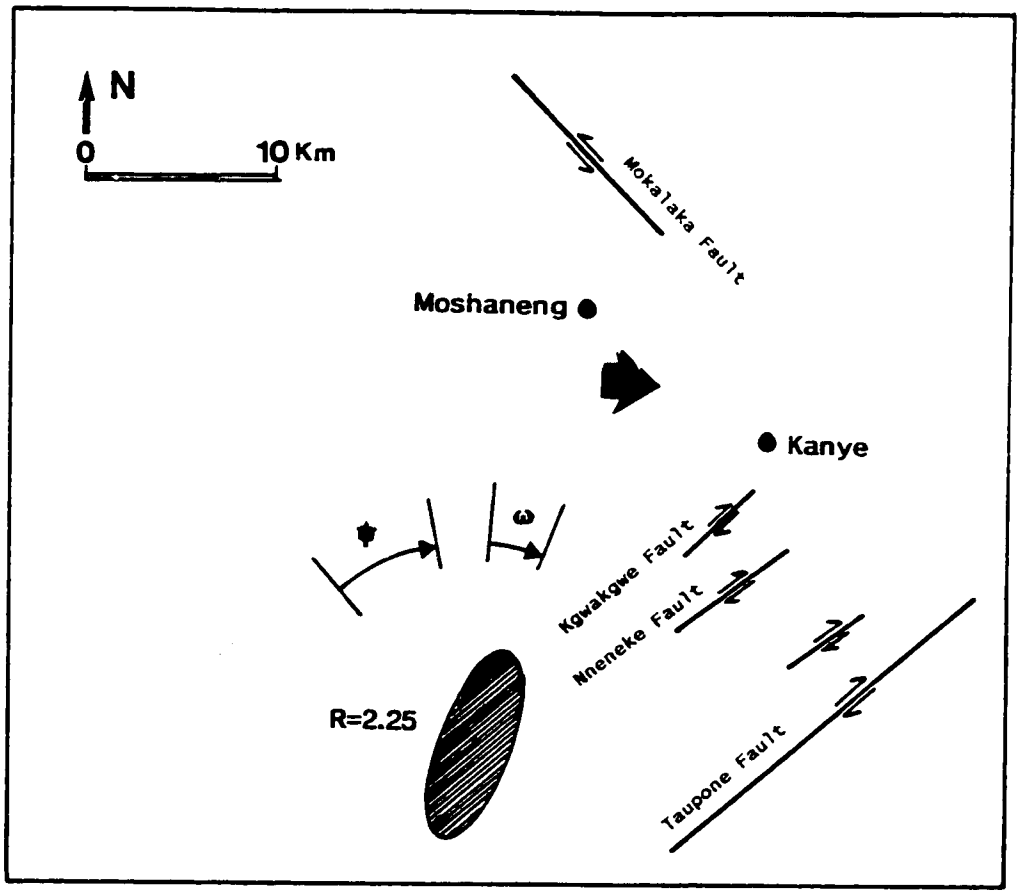

Figure 8.12: Bulk rotational finite strain south of Kanye and east of Masoke. The strain is estimated from the horizontal displacement along strike-slip faults. Plane strain is assumed. Shear angle ψ=30°. Shear strain γ=0.57, ω=16° and ellipticity R=2.25.◆=direction of post-Transvaal tectonic intrusion.

fault associated with the post-Transvaal thrust faults interpreted in eastern Moshaneng. Crudely foliated breccia along this fault has attitude 330/65. The Kanye Volcanic Formation/ Black Reef Quartzite contact shows a dextral horizontal displacement of 58 metres. This displacement is discussed further in section 8.4.5.2. Horizontal separation of the thrust fault along this tear fault is about 1.75 km. The NW trending faults around Gokano Hill in figure 4.2 probably had the same tear fault origin. The major fault from Gokano Hill towards Tletletsi (Mokalaka Fault) is discussed in section 8.4.4.5 below.

8.4.4.5 Mokalaka Fault

Mokalaka Fault was an active fault in the post-Transvaal/ pre-Waterberg period. During this time the fault acted as a sinistral tear fault. The faulting was contemporaneous with folding and thrusting of the lower Transvaal Black Reef Quartzite and dolomite around Moshaneng. Strike-slip imbricate blocks occur along the Mokalaka Fault midway between Tletletsi syncline and Gokano Hill (see figures 4.2 and 10.3. In these imbricates, detached blocks of Black Reef Quartzite were probably ripped from their main occurrences in the northwest and/or in the southeast. These detached blocks were probably formed by a mechanism similar to that of shunting strike-slip duplexes described by Woodcock and Fischer (1986). The blocks along Mokalaka Fault may be compared to exotic strike-slip duplexes. The quartzite in these imbricate blocks is recrystallized and brecciated. In the post-Transvaal/ pre-

Waterberg period, Mokalaka Fault complemented as a conjugate fault to the Taupone Fault. The block between these faults acted as a wedge driven eastwards akin to tectonic intrusion (figure 8.12). This fault cannot be traced southeastwards beyond Gokano Hill. The thrusts and folds developed in eastern Moshaneng are therefore part of the termination structures associated with Mokalaka Fault. The tectonism was in response to E-W directed compression. The compression was initiated in post-Transvaal times and could possibly have continued in the post-Waterberg. The far-field stress system that produced these structures is discussed in chapter 10.

8.4.4.6 Thrust faults

Thrust faults have been mapped in the eastern flank of Moshaneng area. The evidence for thrusting in this area is provided by the repetition of stratigraphy seen at the southern-most part of the area through to Gokano Hill in the central part of the area (the area shown in figure 4.2). Previous workers (Aldiss et al, 1989) have inferred that the quartzite that is interbedded with dolomite is the normal part of the stratigraphic sequence, and that the inlier of the Kanye Volcanic Formation and conglomerate beds associated with it is an exposed basement high (this is the inlier shown about 1 km NW of Gampudi dam on figure 4.2). These contentions are inconsistent with the relationships at the felsite inlier at the southern end of the map area near the tarmac road and the microgranite inlier mapped near Gokano Hill. When all the evidence is taken together, a thrust fault provides the best explanation for the

distribution of lithological units. A thrust fault is consistent with the folding of the Transvaal sequence (chapter 9) and a shortening episode directed in an E-W direction. The thrust fault described here is associated with a major NW tear fault, namely Mokalaka Fault. This association of structures was formed post-Transvaal and pre-Waterberg deposition. Waterberg sandstone deposits at Gokano Hill overly and are unaffected by these structures.

Dolerite intrusions associated with lower Transvaal sediments west of the thrust fault are paraconcordant. These post-Waterberg basic intrusions have reacted with the dolomite, producing serpentinization and chrysotile asbestos. These intrusions have been cut by post-Waterberg faults. Since evidence at Gokano Hill shows that post-Transvaal thrusting and folding are pre-Waterberg, the basic intrusions cannot be the cause of the thrusting in eastern Moshaneng. At the southern and northern ends of the thrust fault shown in figure 4.2, and at the inlier west of Gampudi Dam, the thrust plane cuts below the Transvaal/ basement unconformity. At other parts of the thrust fault, the thrust plane has been elevated to the upper parts of the Black Reef Quartzite. No slicken-striae or lineation evidence was encountered to infer slip along the thrust fault. Stratigraphic relations, however, indicate that the upper plate moved from west to east. The true nature of the thrust plane may be further investigated by core drilling.

Thrusts and tear faults mark the southeastern terminus of Mokalaka Fault in eastern Moshaneng. In the post-Waterberg, motion continued on the NE flank of Mokalaka ridge but with vertical displacement. At this point thrusting was arrested in the study

area.

8.4.4.7 Epidermal tectonics

The post-Transvaal/ pre-Waterberg structures in the eastern parts of the Moshaneng area are strongly suggestive of local epidermal tectonics. Shallow faults have been inferred in previous work from other parts of the lower Transvaal e.g. between Lobatse and Ramotswa further to the east and in the SW parts of the study area (Crockett, 1969, 1971c and 1972c). Some of these structures have been reported even further afield in the Rand area of South Africa (Parsons and Killick, 1990).

8.4.5 Post-Waterberg Systems

The final pattern produced by fault movement in post-Waterberg times is rather complex. Fractures that were created in pre-Transvaal and post-Transvaal times were reactivated. In addition new fractures were created in the post-Waterberg. Principles governing the character of fault patterns discussed in chapter 3 are used for reference in interpretation.

8.4.5.1 Reactivation of NW trending Mokalaka Fault

In the post-Transvaal, Waterberg deposits began accumulating in fault-bounded

grabens at about 1.8 Ga. These faults were initially formed in post-Transvaal times and a good example is the "graben" forming the Tletletsi Syncline. A basement graben was formed when the Mokalaka Fault developed dip-slip displacement along the northeast limb of the Tletletsi Syncline in post-Waterberg times. Complementary dip-slip displacement an E-W trending faults in the southern limb of the Tletletsi syncline completed a triangular graben that accumulated coarse clastic red beds. At this location, Waterberg sandstone and arkose were deposited over an unconformity above the lower Transvaal and basement rocks. Vertical displacement along Mokalaka Fault was greater around Tletletsi and then died down southward, terminating in the vicinity of Gokano Hill. With continued displacement monocline was developed at Tletletsi, but little of the displacement on this fault is seen at Gokano Hill. The fault may have moved as a hinge fault, with the blocks rotating on an axis normal to the fault surface with a small rotation angle.

Displacement along this fault is responsible for the truncation of the ENE lineament trends of the basement against the NE flank of the Tletletsi syncline (figure 6.1 and figure 6.3).

8.4.5.2 Reactivation of other NW trending faults

At station 25 (figure 7.8) near Gampudi dam (figure 4.2), the NW trending tear fault was reactivated in post-Waterberg times as a dip-slip normal fault (figure 8.13). The basement/ Black Reef Quartzite contact displays sinistral displacement of 58

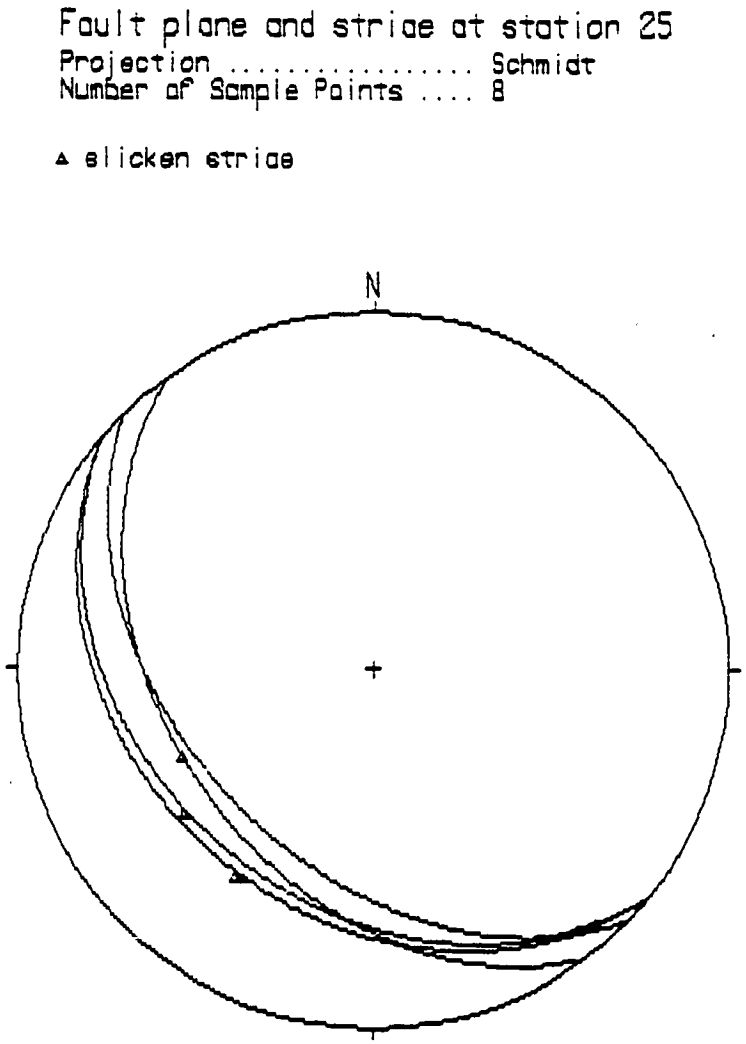

Figure 8.13: Fault and slicken striae attitudes at station 25 (see figure 7.8 for the location of the station). The sense of slip is that of a normal fault.

metres, vertical displacement of 33 metres). Slight variations in the attitude of individual fault surfaces and slicken striae indicate that the faulting was episodic.

8.4.5.3 N-S trending faults

The N-S fault trends are mainly phenomena of post-Waterberg times. These faults are mainly restricted to a belt of country that coincides or connects the syenite complexes of Moshaneng, Masoke and Segwagwa as shown by the SPOT image interpretation (figure 6.4) and the regional geological map (figure 6.5). Faults of this trend are virtually absent outside of the above mentioned belt. These faults always displace or cut through Waterberg rocks and there is no evidence that suggests they existed before Waterberg deposition.

The N-S fault west of Male Hill (figure 4.2) displaces post-Waterberg dolerite and Waterberg sediments. A N-S fault in the Moshaneng area displaces a syenite intrusion indicating that some of the fault activity took place post-intrusion. The western boundary of the Tletletsi Syncline (figure 6.5) is marked by a NNW trending fault which displaces Waterberg sediments and post-Waterberg intrusions.

Rocks from the northern lobe of the Segwagwa intrusion have an age of about 1900 Ma by Rb/Sr method. A N-S trending fault in the western part of the Segwagwa Complex (figure 6.5) displaces this lobe. Other N-S trending faults occur on the eastern flank of the Segwagwa Complex. These new post-Waterberg faults were probably formed as part of a rift system that was associated with the alkaline

intrusions at Moshaneng, Masoke and Segwagwa.

8.4.5.4 E-W trending faults

Post-Waterberg monoclines were formed as E-W, WNW-ESE, ENE-WSW and NW trending structures (see chapter 9). The monoclines were formed above basement fractures. The fractures are marked by crudely foliated and non-foliated breccia, non-systematic quartz veins and silicification. These features were observed at the northern flank of Gokano Hill (figure 4.2) in the central Moshaneng area around Tletletsi Hill and at the southern end of the Moshaneng area near the tarmac road that connects Jwaneng and Kanye. North of Gokano Hill uplift occurs north of the fault such that a south facing monocline is formed. At Tletletsi Hill downthrow occurs to the north, such that a north facing monocline is formed.

E-W trending faults are also encountered south of Kanye in the Kgwakgwe area and at the Segwagwa intrusion. The E-W trend is also shown by the magnetic contour maps. In figure 5.2, two E-W trending positive magnetic anomalies extend eastwards from the NE boundary of the Segwagwa Complex to the end of the map area. These anomalies are caused by dolerite dikes and fractures (see section 5.1.2).

8.4.5.5 Reches Model

Pre-existing fractures that were reactivated in post-Waterberg times around

Moshaneng mainly have NW and ENE directions. The main fault in the NW direction is Mokalaka Fault. A major ENE trending fault is the Mheelo Fault (figure 5.1). These represent the two of the trends of normal faults predicted by the Reches model for slip among randomly orientated pre-existing fractures (see 3.4.1)(Reches, 1978 and 1983).

8.4.6 Thrust fault of undetermined age

A thrust fault has been mapped in the Gaborone Granite basement at Taueshele (figure 4.2). The thrust plane at the river exposure is inclined about 10 degrees to the north. Down dip lineation and displacement sense determined on slicken striae show a southward movement of the upper plate in this region. Due to poor exposure, neither the extent, nor the age of the thrust could be ascertained.

CHAPTER 9: FOLDS

9.1 Introduction

This section discusses rock folds in the study area. Two types of folds are distinguished: 1) those formed when layered rocks buckled as a response to a remote stress field with a horizontal compressive axis, and 2) those formed when layered rocks responded to vertical fault displacement of the underlying basement, yielding drape folds.

The basement complex, comprising the Gaborone Granite and the Kanye Volcanic Formation, is mainly a massive unit, and generally does not display folds. The basement responded to stress loading mainly by displacement along faults. As shown in chapter 8, post-Transvaal/ pre-Waterberg faults were predominantly strike-slip. This gave way to dip-slip in the post-Waterberg. Discussions in this chapter will therefore focus mainly on Proterozoic platform units, namely, the Ventersdorp and Transvaal Supergroups and the Waterberg Group, which show folds that were developed mainly in post-Transvaal times. As with discussions of fractures in previous sections, folds will be discussed in terms of relative age, calibrated by the deposition of layered sequences.

Several episodes of folding are distinguished. A chronological hierarchy is

provided, together with the fold style for each deformational episode. Two broad time periods are recognized; namely, 1) the period between the deposition of the Transvaal and Waterberg rocks and 2) the period postdating the Waterberg Group.

9.2 Post-Transvaal/ pre-Waterberg

The post-Transvaal/ pre-Waterberg events produced open folds with westerly and southerly plunging fold axes. In the detailed map of the Moshaneng area shown in figure 9.1, the folds are best developed in the eastern parts of the area. This area is also the southeastern limb of the Moshaneng Synclinorium. The affected rock types in this area are mainly the Black Reef Quartzite and the dolomite and chert sequences of the lower Transvaal Supergroup. Small inliers of felsic volcanics and microgranite are also involved. The folds are generally open with interlimb angles that range from 110° to 150°. No penetrative cleavage was developed, not even in the argillaceous sediments that form a minor part of the Black Reef Quartzite.

Two fold episodes affected lower Transvaal rocks around Moshaneng Village in the post-Transvaal/ pre-Waterberg period. The first episode may be associated with regional thin-skinned tectonics and is designated F_1. The major structures developed are folds and thrust faults. A second episode of folding, F_2, resulted in the formation of open flexural-slip folds. Folds were also formed in upper Transvaal (Pretoria Group) rocks in the SW portion of the area shown in figure 9.2. The folds described in eastern Moshaneng area were developed before the deposition of the Waterberg

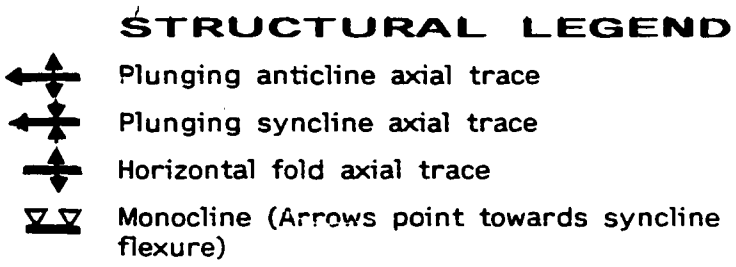

Figure 9.1: Structural map of Moshaneng area. Geological symbols are the same as those in figure 4.2.

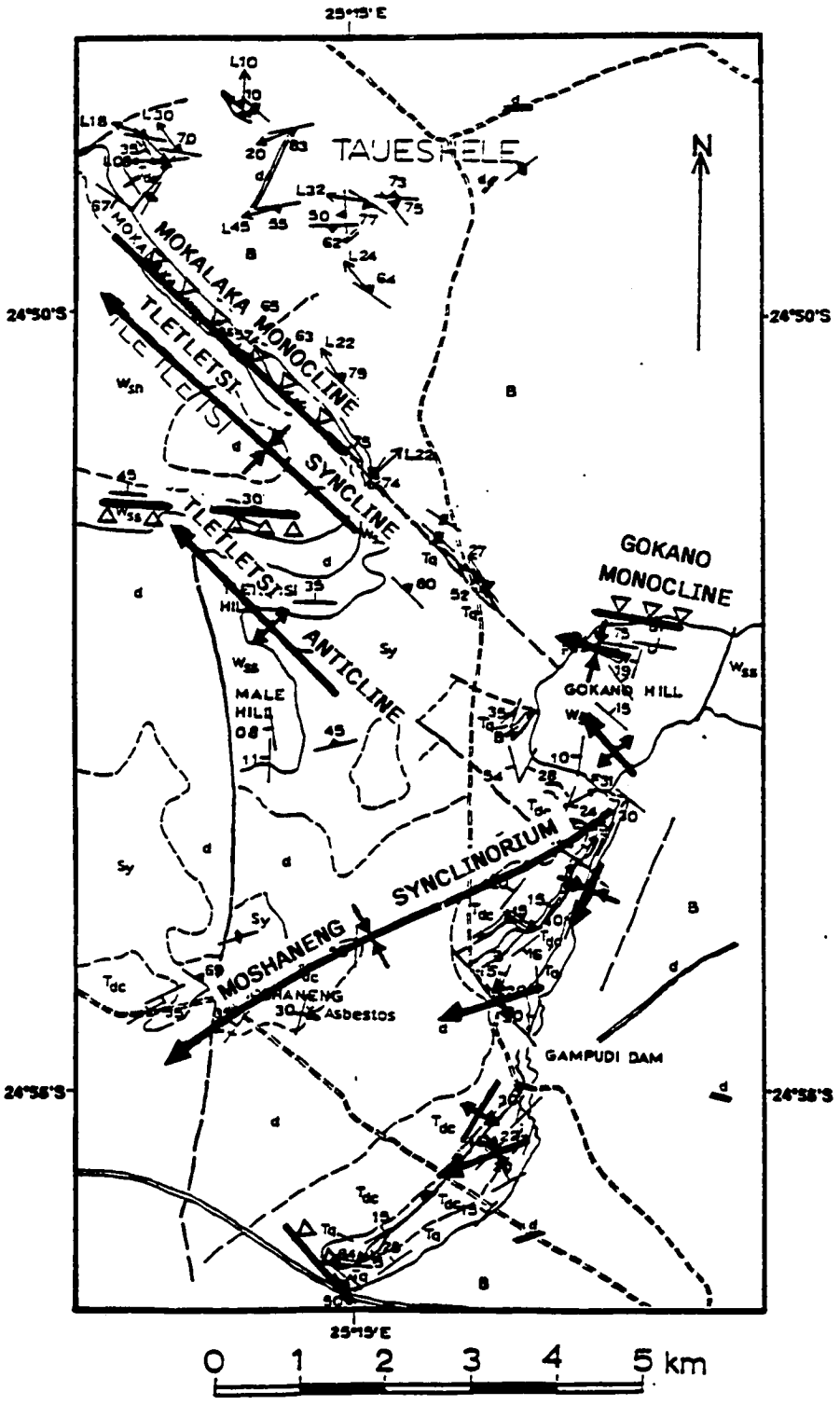
25°15'E
24°50'S
24°55'S
TAUESHELE
N
MOKALAKA MONOCLINE
TLETLETSI SYNCLINE
TLETLETSI ANTICLINE
GOKANO MONOCLINE
GOKANO HILL
MALE HILL
SYNCLINORIUM
MOSHANENG
Asbestos
GAMPUDI DAM
0 1 2 3 4 5 km

Figure 9.2: Regional structural map of the area around Moshaneng and Kanye , showing the major folds.

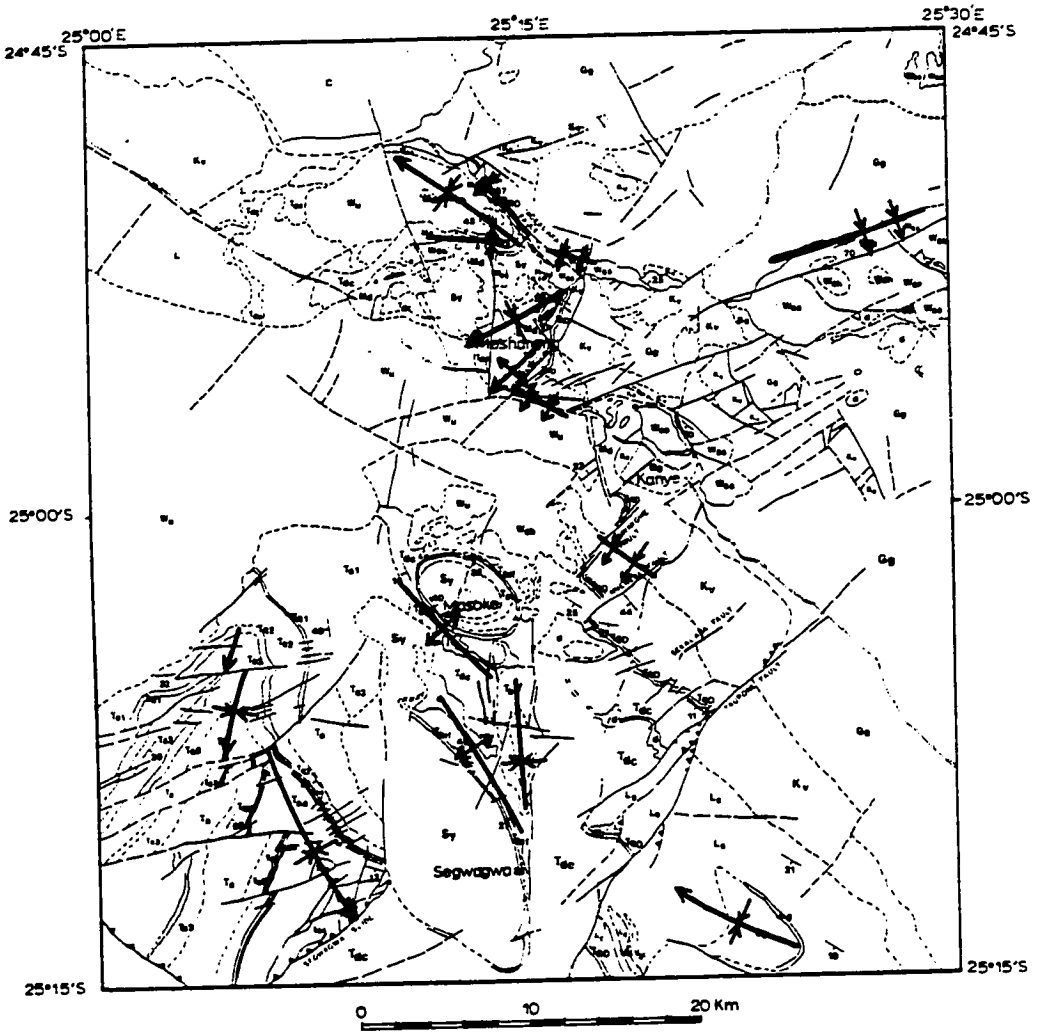

Fold axial trace with plunge direction: anticline, syncline

Monocline, arrows show facing direction

Group. These latter rocks overlie folded and thrusted Transvaal rocks with a distinct unconformity at the southern slopes of Gokano Hill (figure 9.1).

9.2.1 F_1

The area from the southern parts of Gokano Hill to Moshaneng village contains the axis of a southwest plunging synclinorium (figure 9.1). The variation in the plunge of minor folds just to the south of Gokano Hill indicates that the folds may be non-cylindrical near the hinge of the synclinorium. Some fold axes measured in dolomite plunge towards the northeast at about 30°. The Black Reef Quartzite at the fold hinge is bleached, brecciated and recrystallized. The plunges of fold axes forming part of the Moshaneng Synclinorium in the rest of the map area are consistently towards the southwest at about 25°. Stereographic projection of poles to bedding of the Black Reef Quartzite at stations 22-24, station 30 and station 31 are shown in figures 9.3E, 9.3B and 9.3C, respectively. These folds exemplify the character of F_1 folds. Stations 22-24 and station 30 are upright folds while station 31 is a monocline. From stations 22 through to station 30 in figure 7.8, F_1 folds display a vergence towards the south.

The definition of the Moshaneng Synclinorium is somewhat obscured by later post-Waterberg igneous intrusions, especially in its northern limb. The shape of the fold however is defined by the trace of quartzite units south of Gokano Hill. At Moshaneng village, igneous intrusions have disrupted primary layering in the chert and dolomite sequence. The sequence at Moshaneng Village is perched above a large

Figure 9.3: Legend of symbols:

- • = bedding
- \+ = joint set 1
- □ = joint set 2
- ∇ = joint set 3
- ▪ = joint set 4
- o = joint set 5
- ■ = joint set 6
- ★ = fold axis,1=F_1, 2=F_2

Figure 9.3A: Station 2; Monocline in the Black Reef Quartzite. The data were obtained from a synformal relic of the F_2 fold similar to that shown in figure 9.3D at station 13. Fold axis is 017/00.Interlimb angle is about 155°.

Figure 9.3B: Station 30; Anticline of a south-verging WSW plunging F_1 fold. Fold axis is 250/30. Orthogonal two set joint system apparently independent of folds. Exposure is in Black Reef Quartzite. Interlimb angle is about 110°.

Figure 9.3C: Station 31; Monocline in the Black Reef Quartzite. The data were obtained from an anticline flexure. Fold axis is 248/12. The fold is probably F_1. The orthogonal two set joint system is present and joint set 4. Interlimb angle is about 130°.

Figure 9.3D: Station 13; Monocline in the Black Reef Quartzite. An F_1 fold axis is 280/50. The geometry of the fold is shown in figure 9.4A. An F_2 fold axis is 207/07. Interlimb angle for the F_2 folds is 135°. The set 1 fractures are distributed in accordance with the orthogonal relationship to bedding.

Figure 9.3E: Stations 22-24; Anticline and syncline folds in Black Reef Quartzite exposed over 130 metres. The F_1 fold axis plunges 254/20. Three clusters show three limbs from each of the data stations 22, 23 and 24. Interlimb angle between station 22 and 23 is about 160° and between 23 and 24 is about 140°.

Figure 9.3F: Station 52; Horizontal folds in dolomite. The F_2 fold axis is 030/00. The joint set 1 distribution does not vary according to the orthogonal relationship with bedding. The folds are similarly to those shown in figure 9.4B.

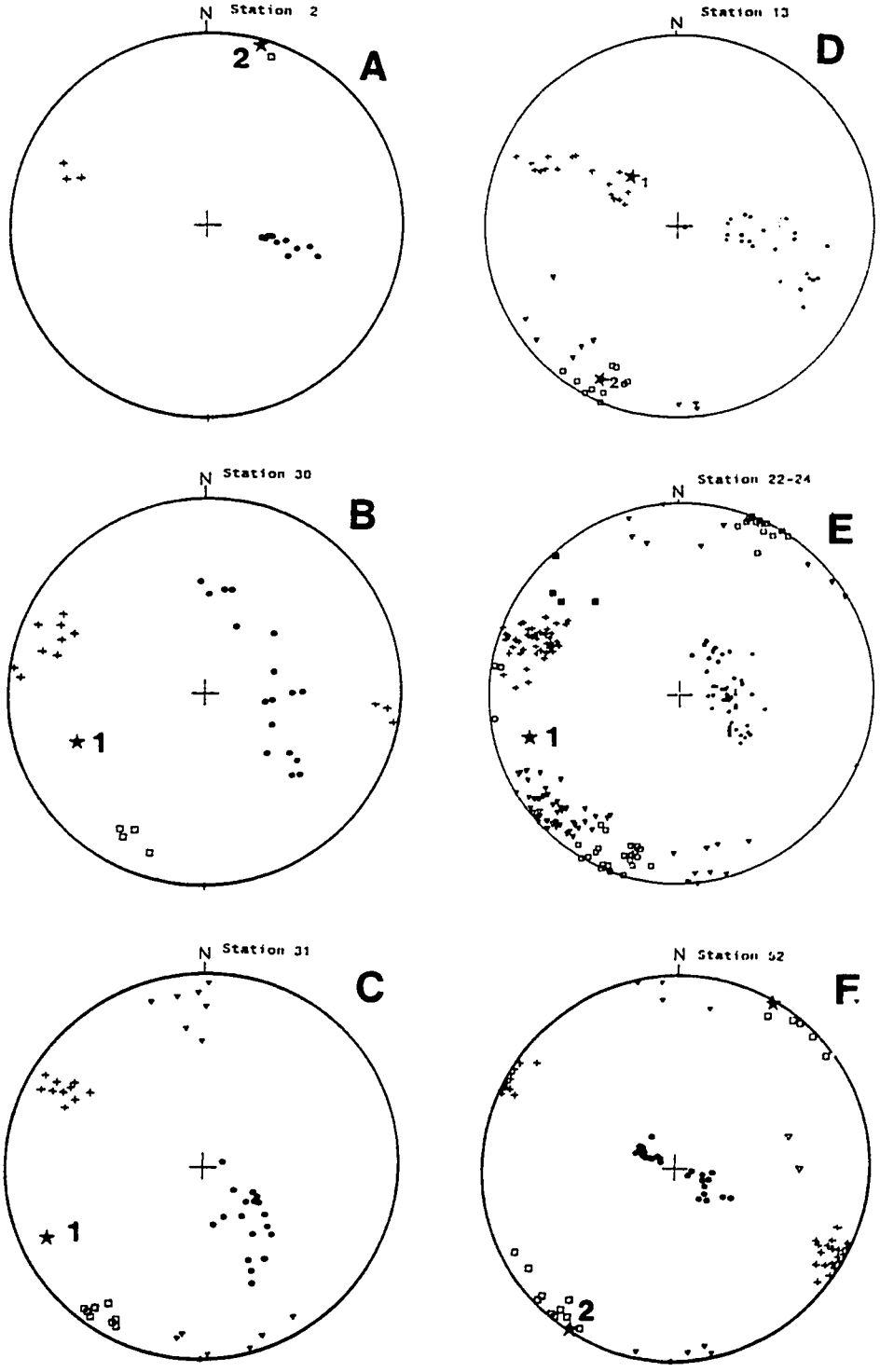
N
Station 2
A
2
N
Station 13
D
1
2
N
Station 30
B
1
N
Station 22-24
E
1
N
Station 31
C
1
N
Station 52
F
2

paraconcordant dolerite sheet that was emplaced to follow existing folds in the lower Transvaal rocks. Approximately 70 km west of these exposures, Tombale (1986) describes folds in Transvaal rocks in the Dikgomo-di-kae area, outside the present area of study. A series of NE trending folds in that area suggests that the stress field that give rise to those folds also probably produced the early F_1 folds around Moshaneng.

These folds are probably associated with the thrust faults described in section 8.4.4.6 in chapter 8 because both structures are constrained within the same period, and appear to be kinematically compatible. The deformational style was thin-skinned and did not involve the basement to any significant extent since none of these or similar structures have been recorded in the basement east of Moshaneng. The upper-most portion of the crust that consisted of layered deposits was transported in an ESE direction relative to an immobile lower crust comprising the basement.

9.2.2 F_2

Axes of F_2 folds trend NNE-SSW and are virtually horizontal. In the Black Reef Quartzite, slicken-striae developed in the bedding plane show that a mechanism of bedding parallel slip accounts for the development of these folds. Stations 2 and station 13 have fold axes 17/00 and 207/07 respectively and are examples of the F_2 folds (figures 9.3A and 9.3D). Folds at these stations are monoclinal flexures as shown in figure 9.4A. Station 52 is located in dolomite. The stereographic projection in figure 9.3F shows that the folds developed here are upright (vertical axial surface)

Figure 9.4A: Folded Black Reef Quartzite at station 13 in eastern Moshaneng. The monocline displayed by these beds has a horizontal fold axis of attitude 207/07 trending into the photo. This fold was produced by the flexural slip mechanism as shown by bedding parallel slicken striae. A second fold axis of attitude 280/50 is not obvious from this photo; but it trends laterally across the photo. These folds can be traced intermittently throughout eastern Moshaneng. Stereographic projection of structures at this location is given in **figure 9.3D**. The geological hammer in the middle ground provides a scale.

Figure 9.4B: Open, horizontal, upright, minor folds in the upper Quartzite of eastern Moshaneng. These folds have been mapped in the dolomite as shown at station 52 in figure 9.3F. The fold axis trends NE at about 030/00. The tape measure in the middle ground is extended 30 cm.


A

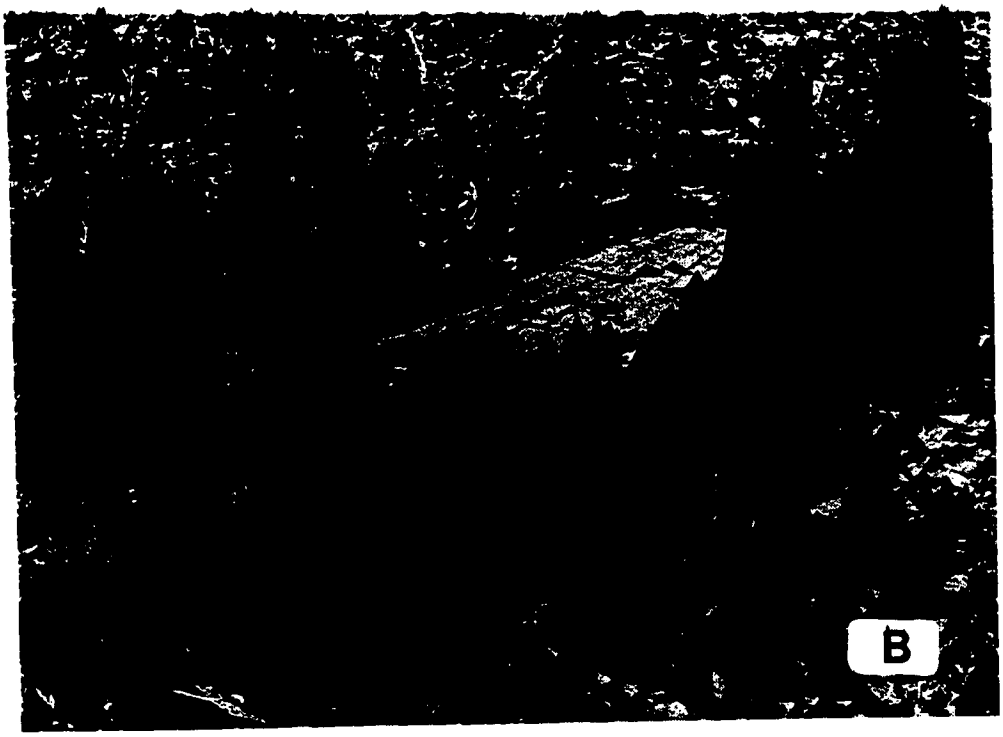
B

and the axis is horizontal (30/00). The fold style at station 52 is similar to the folds shown in figure 9.4B. At station 13 (figure 9.3D), the angular distribution of set 1 joints is consistent with that shown for J_2 joints in figures 3.3A and 3.3B. The cleavage pattern at this location is consistent with the development of parallel folds. Joints developed around the hinges of verging F_1 folds tend not to vary according to the variations of bedding. These relationships are shown at stations 22-24, 30 and 31 (see figure 9.3E, 9.3B and 9.3C respectively). This is in contrast to the relationship between bedding and joints shown at station 13 above.

9.2.3 Folds in the upper Transvaal

The upper Transvaal rocks belonging to the Pretoria Group are exposed in the southwestern part of the area shown in figure 9.2. These rocks have been thrown into a syncline with a southerly plunge. The syncline is broken by ENE trending cross-faults that have displaced the fold axial trace. The southern boundary of these rocks is marked by a slide surface (Segwagwa Slide in figure 9.2) which separates the upper and lower Transvaal rocks. The slide also separates distinctive structural styles; a folded allochthonous upper package is distinguished from an autochthonous lower package across the slide. Crockett (1972) has suggested that this tectonic boundary was formed when the upper Transvaal rocks slid above a low angle fault. He envisaged that the sliding took place during a catastrophic event, according to an interpretation similar to the one used for structures formed in the Ramotswa and

Lobatse areas much further to the east (Crockett, 1969). The epidermal character of the deformation is confirmed by the non-involvement of lower Transvaal rocks exposed to the east and to the south which remained welded to the basement. The upper Transvaal units were propelled on the Segwagwa Slide by gravity, forming a regional syncline in the process. The sliding may have been aided by the presence of high pore fluid pressure as suggested by Crockett (1969) for the Lobatse and Ramotswa areas.

Like the folds described in the Moshaneng area, the syncline developed in the Pretoria Group rocks was formed during the period between the deposition of the Transvaal and Waterberg sediments. The Waterberg sediments to the NW overly folded Transvaal rocks with an angular unconformity. It is not possible to assign these folds to either the F_1 or F_2 episodes recognized in lower Transvaal rocks around Moshaneng. However, it is very likely that the Moshaneng and Segwagwa epidermal episodes were contemporaneous.

9.3 Post-Waterberg

9.3.1 Monoclines or drag folds ?

Perhaps the most conspicuous structures formed in the post-Waterberg period are the drape or forced folds of platform-cover rocks, that developed over faulted and vertically displaced basement blocks. Similar structures are noted that probably formed

as a result of local crustal collapse in cauldron subsidence fashion. In most of these structures in the study area shown in figure 9.2, the top anticlinal flexure of the fold has been eroded and only the bottom synclinal flexure is preserved (see figure 9.5). Along the Gokano monocline, the synclinal fold was form by flexural slip. A portion of the top antiformal flexure is preserved to the northeast of Mokalaka Monocline as shown on the cross-section in figure 9.6. In this section, the deformation of the Black Reef Quartzite into drag folds is inferred as the basement fault gives way upwards to a drape fold in the overlying sediments. At Male Hill, (figure 9.1), bedding attitudes show that an open anticline of Waterberg strata exists to the southwest of the Tletletsi syncline. At this location, both the synclinal and anticlinal flexures of a monocline are preserved.

The cross-section in figure 9.6 demonstrates that both the Transvaal and the Waterberg layered sequences were involved in the drape folding. Nowhere do monoclines or drag folds involve only Transvaal rocks. This implies that these structures are exclusively phenomena of the post-Waterberg period. It also suggests that some monoclines may have broken into a fault through the inflection axis between the synclinal and anticlinal flexures. Subsequent erosion resulted in the preservation of only the synclinal flexure. The preserved synclinal flexure could therefore be a drag fold of layered sediments that have a faulted boundary with the basement; hence the discussion of monoclines does not necessarily preclude drag folds.

The minimum vertical displacement of the basement at Mokalaka ridge is at least 1,100 metres, considering that a total stratigraphic thickness of this amount is

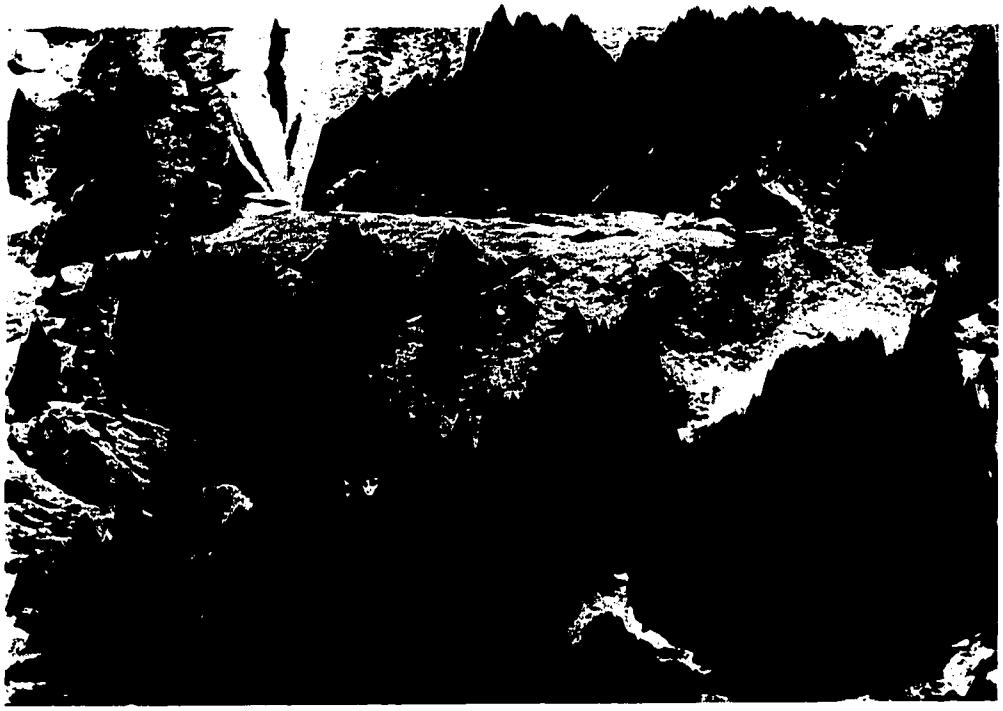

Figure 9.5: An exposed portion of the synclinal hinge of the monocline at Gokano Hill. Note the absence of the myriad of faults mapped at other folds of this type (Jamison, 1989). The mechanism of folding at this locality was by flexural slip.

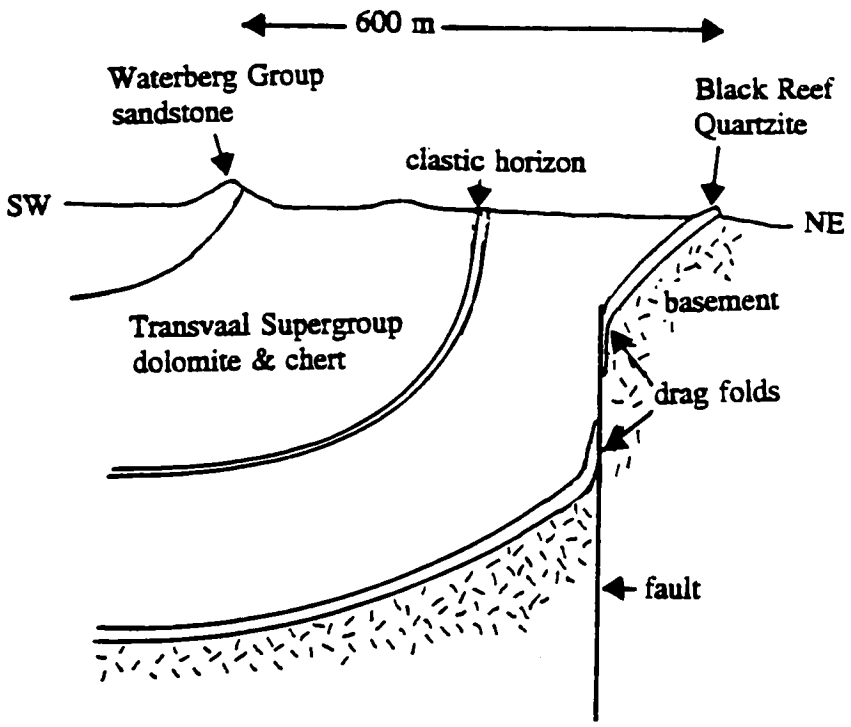

Figure 9.6: NE trending cross-section of a portion of a preserved monocline in the northern parts of the Mokalaka Monocline shown in figure 9.1. The occurrence of the basement fault and drag folds of the Black Reef Quartzite are inferred.

displaced. At the northern flank of Gokano Hill, where only the Waterberg is involved in the flexure a minimum vertical displacement of about 100 metres is obtained.

Dip slip, resulting in displacement along vertical or steeply dipping basement fractures, occurred in the post-Waterberg period as shown by the consistent involvement of the Waterberg sediments in these structures wherever recognized. On the geological map (figure 9.1), sites of these monoclinal flexures are marked by steeply dipping or overturned beds of the preserved synclinal flexure. The Mokalaka Monocline, the Gokano Monocline, and the southern end of the Moshaneng map area are typical examples of this type of structures (see figure 9.1). The monocline to the north of Gokano Hill shows that these folds are of a parallel type with slicken-striae on bedding surfaces. Along the NE flank of Mokalaka ridge, the Black Reef Quartzite and the dolomite and chert interlayers are exposed in lens-shaped sections sandwiched between the underlying basement and the overlying Waterberg sediments (see figure 4.2). The contact between the Waterberg and the underlying rocks is thus a horizontal view of a folded unconformity.

In the southeastern part of the map area (figure 9.2), Ventersdorp rocks have vertical dips near the contact with the Kanye Volcanics felsite southeast of the Segwagwa Fault. A NW-SE trending fracture zone has been mapped along this contact within the Kanye Vocanics. These structures suggest that Ventersdorp sediments were drape-folded over a fault trace in the Kanye Volcanics. The steeply dipping beds are therefore a part of a drag fold or a south-facing monocline. Monoclines involving the

Ventersdorp have not hitherto been reported in this area. The absence of younger formations at this isolated occurrence makes it difficult to assign a relative age to the structure. The preponderance of evidence in the rest of the study area however, suggests that the deformation, even at this locality, was probably formed in the post-Waterberg period.

Ventersdorp Supergroup rocks are exposed in the southeastern portion of the map area in figure 9.2. A regional NW plunging syncline is formed in conglomerate, greywacke and shales of the Lobatse Volcanic Group. This fold can only be designated as post-Ventersdorp. The lack of younger formations makes it difficult to constrain the upper time limit for the deformation using field data alone. This structural trend is similar to the Tletletsi Syncline in the northern parts of the Moshaneng area (figure 9.1). The presence of WNW-ESE post-Waterberg fractures and dikes just to the north of this fold (figure 5.2 and section 5.1.2 in chapter 5) and its trend suggests that it may be a post-Waterberg structure as well.

Other work outside the study area, e.g. around Molepolole, Thamaga and Mogonye (Key, 1983, Jones, 1973b) has revealed monoclines or drag folds similar to those found in the study area. South-facing monoclines are reported west of the present area of study in the Dikgomo-di-kae area (Tombale, 1986). They are also distinguished by the occurrence of steeply dipping or overturned Waterberg sediments. The Molepolole monocline is north-facing, suggesting that some of the basement blocks formed positive horsts between grabens that preserved Waterberg sediments. The trend of all these structures is parallel to that of pre-Transvaal extension fractures

and dikes. Pre-existing basement fractures were probably reactivated again in post-Waterberg times, giving rise to the monoclines or drag folds.

9.3.2 Cauldron subsidence

It has been suggested in previous work that the Tletletsi Syncline was formed as a result of the intersection of two monoclines (Aldiss et al, 1989). The NE limb of this structure consists of overturned beds of Transvaal and Waterberg sediments. The southern limb is formed by more gently dipping Waterberg beds. The core of the syncline is marked by an intrusion of dolerite which is probably concordant. The southern limb of the structure has also been intruded by concordant dolerite. It has also been suggested (Aldiss et al, 1989) that the Tletlesti Syncline is a depression that was formed when the supracrustals collapsed into the magma chamber that produced the dolerites.

The notion of cauldron subsidence is proposed to explain the structural basin that is marked by lower Transvaal rocks around Masoke (see figure 6.5 and 9.2). The banded iron formation that rims Masoke complex dips inwards towards the centre of the structure. The central part of the structure is occupied by Pretoria Group rocks and igneous intrusions of syenite and dolerite. It is proposed that a cynlindrical or cone-like central block within this structure collapsed into a magma chamber that produced the intrusion associated with this structure. The inwardly dipping banded iron formation defines a rim syncline that is probably draped over a ring fracture along

which cauldron displacement took place. The Segwagwa Complex was probably formed in a similar fashion. The oval shape of this complex and the satellite structure at its northern end suggests that several ring-like structures coalesced to form the Segwagwa Complex. East of Segwagwa complex, another oval, N-S trending, banded-iron-formation- rimmed, structural basin occurs (see figure 9.2). This structure probably has the same genetic origin as those of Masoke and Segwagwa. No surface exposures of syenite intrusion have, however, been identified at the structure.

PART 3

CHAPTER 10: SYNTHESIS

10.1 Tectonic evolution of southern Africa

The chronologies of deformational events in the crust of southern Africa are more readily recognized within the high grade and high strain mobile belts than the low grade and low strain cratonic nuclei which they surround. These nuclei have been compared to or equated with modern lithospheric plates or microplates (Windley, 1984, p61). In southeast Botswana, the 3.0 Ga Kaapvaal Craton is an Archaean tectonic nucleus surrounded by younger mobile belts or provinces (see figure 1.1). This simplified perception of the gross Precambrian geology is true only in general terms. For instance, the oldest rocks in southern Africa (about 3.8 Ga) have been identified within the Limpopo Mobile Belt, generally considered to host rocks younger than those in the Kaapvaal Craton. Many other examples may be quoted from the other mobile belts that have inliers older than the cratonic terranes (Tankard et al, 1982; Clifford, 1970). Tectonic events in the mobile belts, involving ductile deformation, have complementary, coeval events in the adjacent cratonic nuclei. The latter tectonic terrane will normally deform in a brittle fashion. Although extensive

geochronological data are not available for a rigorous correlation of such events, a general discussion here is still appropriate.

10.2 Limpopo Mobile Belt and Kaapvaal Craton

Tectono-metamorphic activity ceased by about 2.0 Ga in the Limpopo Mobile Belt to the north of the Kaapvaal craton. During the main initial phase of tectono-metamorphic activity in the Limpopo Mobile Belt, the Kaapvaal Craton was subjected to rifting, volcanism and sedimentation on sialic basement during Ventersdorp times (Burke et al, 1985). Ductile deformation in the Limpopo Mobile Belt resulted from convergence of and transcurrent displacement between the Kaapvaal and the Zimbabwe Cratons. The present study provides evidence that suggests that this type of rifting, sedimentation and igneous activity continued beyond Ventersdorp times up to post-Waterberg times. The Kaapvaal Craton of which SE Botswana forms a part, remained as a rigid block that has responded to stress mainly by fracturing and slipping along fracture surfaces since the Archaean to the present times. Old fracture surfaces were repeatedly reactivated to accommodate the bulk strain imparted to the earth's crust. Shear zones of Archaean age were reactivated under brittle conditions. Most of the strain of the present sub-continent was undoubtedly taken up by the high strain structures developed within the mobile belts. The cratonic blocks therefore constituted environments of relatively low strain levels. Although the Kaapvaal craton has remained as a relatively rigid crustal block since 3.0 billion years ago, it has been

rejuvenated at discrete times by additions from the mantle during igneous activity. Material from the surrounding mobile belt terrains was added to the downwarped intracratonic sedimentary basins.

10.3 Kheis Belt and Kaapvaal Craton

Events in the Kheis Belt along the western margin of the craton ceased by about 1.2 Ga (Tankard et al, 1982). Hartnady et al (1985) describe deformation of this tectonic belt between 2,100 and 1,760 Ma, the period post-dating the deposition of the Transvaal/ Griqualand West Supergroup and pre-dating deposition of the Waterberg/ Matsap Group. Several episodes of folding and shearing affected rocks of the Kheis belt including Griqualand West Supergroup rocks at the western margin of the Kaapvaal Province. Post-Griqualand West folds have broad wavelengths and trend NE. These are overprinted by post-Matsap or post-Waterberg high strain deformation. Post-Matsap, D1 deformation in the Kheis Belt produced tight folds with axes that trend N and NE. The D2 Namaquan deformation produced NW trending steeply inclined folds that increase in tightness westwards. The D3 event produced NE trending upright folds. This was followed by a minor D4 event. The D5 episode resulted in NNE trending, west dipping imbricate shears with the upward movement of the westward prisms (Stowe, 1979 in Tankard et al, 1982). The above demonstrates that the Kheis belt was zone of high strain with an E-W axis of shortening in post-Transvaal and post-Waterberg times. The deformation had a significant effect in the intracratonic

environment as shown by structures in the present area of study. These include the conjugate strike-slip faults exemplified by the Mokalaka and Taupone faults.

10.4 Kaapvaal Craton and younger mobile belts

10.4.1 1.0 Ga

Several nuclei and mobile belts, including the Kaapvaal were welded together to form the Kalahari Craton at about 1.0 Ga. The 1.0 Ga tectono-thermal event involved rocks of the Natal and Namaqua tectonic provinces that form the southern and southwestern boundaries of the Kaapvaal Province respectively (see figure 1.1 for locations).

10.4.2 500 Ma

The Kalahari Craton is surrounded by the continent-wide 500 Ma event of Gondwanaland. The absence of stratigraphic sequences equal to or younger than this age in the study area bars recognition of any tectonic activity coeval with this event in the intracratonic environment.

10.5 Chronology of regional brittle deformation in SE Botswana

10.5.1 Introduction

In SE Botswana, relative chronologies of intra-cratonic deformations are recognized using a number of remote sensing and field criteria. A compilation of lineament interpretations provided tectonic domains which are demarcated by boundaries of stratigraphic intervals (figure 6.6). These depositional intervals are used as a time frame by which tectonic events are described. The following is an outline of events recognized within the present area of study. 1.) Pre-Transvaal fracturing and dike emplacement. 2.) Post-Transvaal/pre-Waterberg fracturing, fault displacement and folding. 3.) Post-Waterberg fracturing, fault displacement, folding and igneous intrusion. Structural developments isolated in each of the stratigraphic intervals are correlated with events in the mobile belts.

10.5.2 Pre-Transvaal

The Transvaal Supergroup was deposited beginning about 2300 Ma (Tankard et al, 1982). Deformational events in the pre-Transvaal basement around Moshaneng incorporate the period postdating the emplacement of the Gaborone Granite. The minimum age for the emplacement of this granite is 2830 ± 10 Ma obtained by the U/Pb method on zircons (Sibiya, 1988). A diorite from the "West Kubung Complex", regarded as a component of the Gaborone Granite Complex has been dated at 2932 ± 250 Ma by a Rb/Sr errorchron (Aldiss et al, 1989).

Using petrological and geochemical criteria, Sibiya (1988) has argued that the Gaborone Granite was emplaced in an environment of plate convergence. An Andean-type volcanic arc setting for the emplacement of the Kanye Volcanic Formation and the Gaborone Granite has been suggested by Burke et al (1985). The time of emplacement of the granite (c.2.8 Ga) is significantly earlier than the peak of D2 deformation at 2.7-2.6 Ga, recognized in the Limpopo Mobile Belt. The Gaborone Granite Complex was therefore emplaced during an early phase of the deformational events that characterized the Limpopo Mobile Belt. The age difference between the Gaborone Granite and the peak of metamorphism in the Limpopo Mobile does not preclude a genetic or spatial association of these phenomena.

Rocks of Ventersdorp age are not exposed in the northern part of the study area. The basement consists of Gaborone Granite Complex and Kanye Volcanic Formation rocks. Dikes have intruded the Gaborone Granite within and outside the present area of study. In the Kubung area a few kilometres north of the area in figure 6.5, Sibiya (1988) has mapped steep to vertical dikes belonging to a "Late Mafic Dike Suite" that have a NE to E-W trend. At this location the dikes have been affected and displaced by a ductile shear zone. These were considered to have a genetic link with the emplacement of rapakivi granite and therefore probably of an earlier age to the post-Ventersdorp fracturing of the same trend.

Within the study area, brittle deformation of the basement resulted in the formation of steeply inclined ENE to NE trending fractures (figure 10.1). In the southern part of the study area, remote sensing evidence shows that fractures

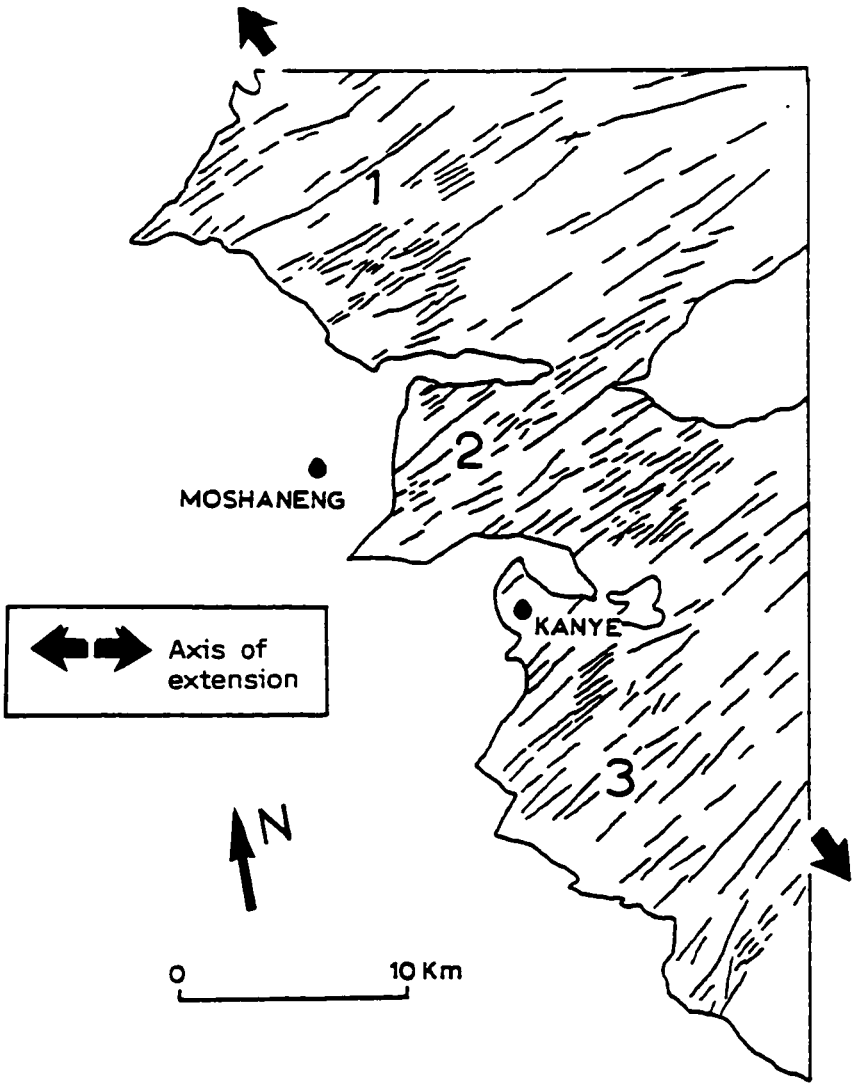

Figure 10.1: Nonpalinspastic map of the Pre-Transvaal initiated fractures and dikes in basement rocks. These are interpreted from major lineaments traced from SPOT imagery. These structures are probably modified and enhanced by reactivation in later geologic times. Domains **1, 2** and **3** are defined in figure 6.6.

belonging to the same set cut through Ventersdorp age sediments. The minimum age for fracturing and dike emplacement is therefore post-Ventersdorp deposition. Elsewhere, outside the study area, rifting and volcanism have been recorded as contemporaneous with sedimentation of Ventersdorp rocks (Burke et al, 1985). This rifting during Ventersdorp times (2643 ± 80 Ma) is reported further south in the Republic of South Africa. The rifting occurred as convergence was taking place in the Limpopo Mobile Belt beyond the northern margin of the Kaapvaal Craton. This convergence is marked by peak metamorphism 2.7-2.6 Ga. Rb/Sr and K/Ar dates between 2,000 and 2,600 Ma for the Gaborone Granite suggest that isotopic resetting occurred in this rock suite (Cahen et al, 1984, Sibiya, 1988). This resetting was probably caused by vulcanicity of the Ventersdorp. Because vertical dikes mapped mainly in the northern part of the study area are expressed as lineaments that cut through both the basement and the Ventersdorp deposits, the minimum age for these dikes is somewhere between 2600 Ma and 2300 Ma. The latter date represents the maximum age of the Transvaal sedimentation (Tankard et al, 1982). These dikes mark the period during which the Transvaal basin began to form. This period is also broadly coeval with the emplacement of the Great Dike of Zimbabwe at 2514 ± 16Ma (Hamilton, 1977 in Hunter and Pretorius, 1981). Tentative palaeomagnetic correlation suggests that some of the dikes around Moshaneng may be coeval with the Great Dike. This correlation is made on the premise that there has been little or no relative rotation between the Kaapvaal Craton and the Zimbabwe Craton since about 2,500 Ma (Piper, 1987). A pre-Transvaal dolerite dike swarm has been mapped in the eastern

Transvaal Province, east of the Bushveld basin (Fripp et al, 1980). It is entirely probable that these dikes are continuous with those mapped west of the Bushveld basin in SE Botswana. It has been suggested (Aldiss, 1986), that the emplacement of these dikes was spatially and temporally associated with the formation of the protobasin in which the lower Transvaal Supergroup Buffelsfontein (Buffalo Springs) sediments were deposited.

The gross structural grain of the Kaapvaal Craton is defined by the trend of the greenstone belts that are mainly exposed in the eastern parts of the Kaapvaal Craton in the Republic of South Africa. The Barberton belt in the southeast and the Murchison, Pietersburg and Sutherland belts in the northeast all have NE to ENE trends (Tankard et al, 1982). Shear zones developed around these greenstone belts also have an ENE trend (Fripp et al, 1980). Foliation in the Archaean basement to the south of Lobatse in SE Botswana also has a ENE trend (Key, 1983) (see figure 1.3 for the location of Lobatse). Pre-Transvaal fractures and dikes have a trend that is similar to that of the shear zones and the greenstone belts. The dikes and fractures are expressed as photo-lineaments that were brought into focus in a study by Aldiss (1986). In the east-central part of the study area, these lineaments occur in rocks as late as Ventersdorp age. The vast majority of the lineaments in the study area show no sign of folds, crosscutting shears or any type of ductile deformation. A notable exception are the deformed dikes reported by Sibiya (1988) in the Kubung area, just north of the present area of study. These are probably of an earlier age. Photogeological evidence suggests the fractures and dikes represented by these lineaments are post-Ventersdorp and pre-Transvaal in

age. There is little doubt that these lineaments represent a rifting episode that marked the proto-basinal stage of the formation of the Transvaal basin (see figure 10.2). This assessment is consistent with features such as the sediments developed beneath the Black Reef Quartzite at Tsele Hill, which have been equated with the Buffelsfontein Group in the central Transvaal (Aldiss, 1986; SACS, 1980). The lineaments probably represent steeply dipping normal faults and dikes (figure 10.2). Some of the dolerite dikes, such as the fine grained dolerite east of Moshaneng have a lower magnetic susceptibility than felsite of the Kanye Volcanic Formation (table 5.1). A ground magnetic traverse across an exposed dike shows a negative total magnetic anomaly relative to the Kanye Volcanic Formation (figure 5.3 and figure 5.4). Regional aeromagnetic contour maps show virtually no expression of these dikes (figure 5.1 and figure 5.2). Although it has been argued that all pre-Transvaal photolineaments represent a dolerite dike swarm (Aldiss, 1986), many of these features originated as fractures and may never have hosted basic dike intrusions. The secondary silica, non-systematic veins breccia along many of these lineaments demonstrate that many of them have remained as fractures rather than dikes. Reactivation of some of the fractures as strike-slip faults in the post-Transvaal and dip-slip faults the post-Waterberg is discussed in sections 10.5.3 and 10.5.4.

Pre-Transvaal tectonism probably included post-Ventersdorp folding which is displayed in the Nnywane Formation argillite just to the west of Otse. At this locality, thrusting and tight folding has affected these Ventersdorp age rocks. Comparable deformation has not been recorded within younger supracrustals. Regional Proterozoic

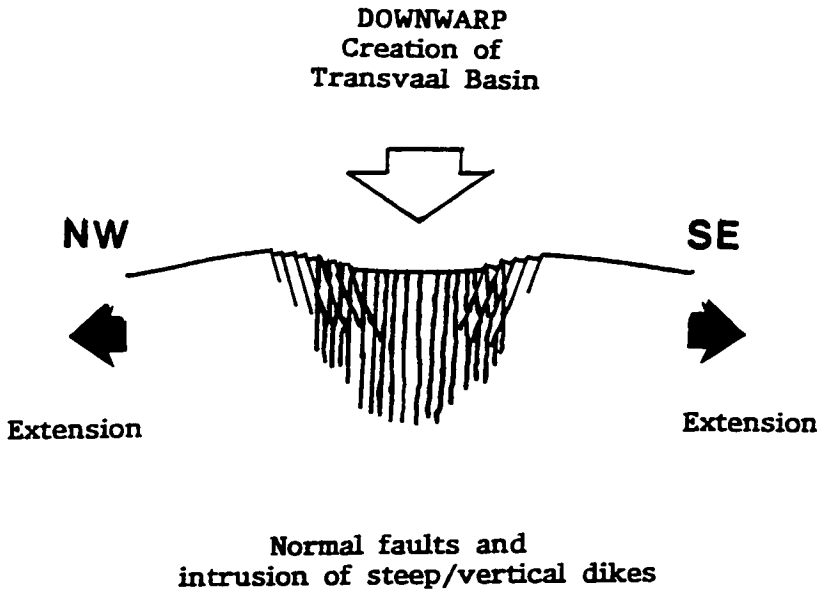

Figure 10.2: Schematic NW-SE cross-section across the Transvaal Basin during its formative stage. The accumulating deposits and early sill emplacements are omitted in this idealized diagram. The downwarp and extension produced crustal thinning and the intrusion of basic dikes in pre-, to early Transvaal Supergroup times.

folds in southern Africa and SE Botswana are discussed in studies by Dietvorst (1988, 1991), Dietvorst et al (1991) and Pretorius (1979, 1985).

The NE to ENE lineament direction was initiated in the pre-Transvaal period by NW extension (see figure 10.1). Basic dikes were probably emplaced into a thinning and subsiding crust that formed basins into which Transvaal sediments were deposited. (figure 10.2). The early proto-basinal Transvaal sediments are interlayered with bimodal volcanics in the Buffelsfontein Group in the west-central Transvaal Province of South Africa. A rift-controlled environment is favoured for these deposits (Tankard et al, 1982). It has been suggested by Aldiss (1986), that the pre-Transvaal dike swarm in SE Botswana is related to pre-Transvaal sedimentary deposits at Tsele Hill, near Mochudi, outside the present area of study (see figure 1.3 for the location of Mochudi).

10.5.3 Post-Transvaal/pre-Waterberg

The post-Transvaal tectonism was coeval with late ductile deformation in the Limpopo Mobile Belt. During this time, dextral shear zones were developing in the northern margin of the Limpopo Mobile Belt. In the Kaapvaal Craton, the Bushveld Igneous and Molopo Farms Complexes and their satellite intrusions were emplaced.

In the study area, the post-Transvaal/pre-Waterberg period is marked by epidermal tectonics and strike slip faults. Strike slip faulting occurred by slippage on pre-existing, pre-Transvaal fractures and shear zones within the basement. Figure 10.3

shows the salient post-Transvaal regional structures. These were formed mainly as a response to E-W compression. Where a veneer of sediments is not developed, the fault systems do not bear the typical signature pattern that is normally anticipated for these circumstances. Large scale or regional patterns described for similar systems (Tchalenko and Ambraseys, 1970; Sylvester, 1988; Cloos,1955) are not readily recognized in the present study area. The pre-existing fracture system locally realigned the stress field and displacement took place on these fractures without necessarily conforming to patterns customarily displayed during failure or primary rupture. The angular relationships conforming to the Mohr-Coulomb failure did not necessarily form under these conditions. Slippage occurred under a new set of rules that would govern bulk strain in a medium with an existing fracture system. A pre-existing basement fracture zone was traced through the overlying sediments along the Taupone Fault, however, and structures of primary rupture were identified within the sediments. The southwestward termination of this fault breaks into a dendritic branching pattern typical of a flower structure that forms under transpression.

It is conceivable that some of the Waterberg repositories were formed in pull-apart basins formed during post-Transvaal strike-slip faulting. The NW trending Mokalaka Fault (figure 6.5) in the Moshaneng area follows the trend of an ancient basement shear zone. This fault does not display patterns of failure or primary rupture. The Tletletsi Syncline (figure 9.1), was probably initiated as a pull-apart basin in the post-Transvaal, then continued to subside during Waterberg deposition and in the post-Waterberg.

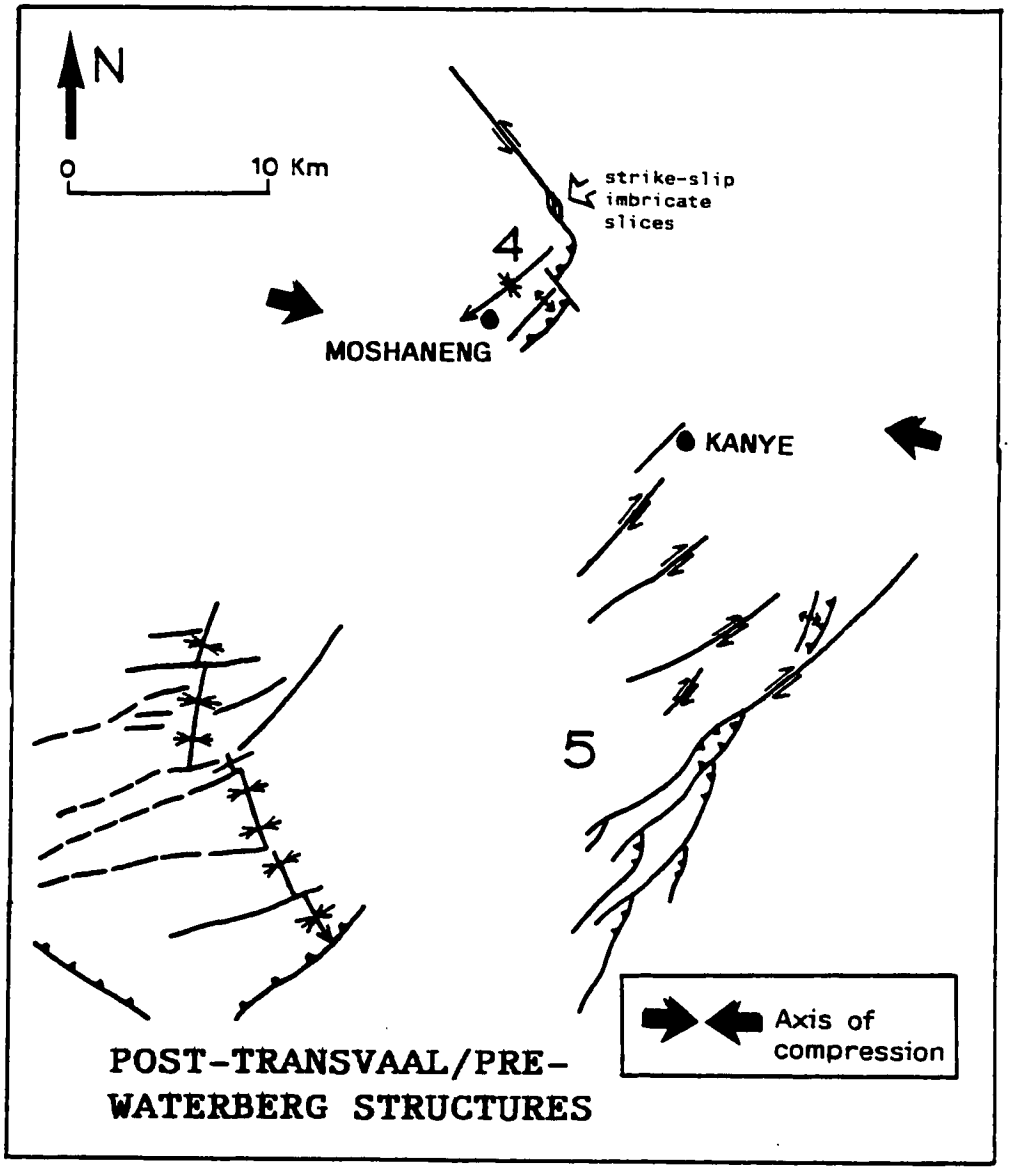

Figure 10.3: Salient regional structures of post-Transvaal/ pre-Waterberg time. E-W compression produced mainly strike-slip faults and reverse faults. These faults are probably modified by post-Waterberg reactivation displacements. Domains **4** and **5** are defined in figure 6.6.

Evidence of thrusting and faulting in the Moshaneng area supports an epidermal model advocated for post-Transvaal tectonics in the western margin of the Bushveld basin and in the Segwagwa area (Crockett, 1969, 1971c, 1972b). Post-Transvaal, SW plunging open folds at Moshaneng are associated with the thrust. These folds are conspicuous in the lower Transvaal sediments and involve the basement/Transvaal contact.

In the post-Transvaal, the Kaapvaal craton was subjected to E-W compression. At about the same time, the Kheis Belt at the western boundary of the Kaapvaal Craton was also undergoing E-W compression. It is therefore likely that the stress field that produced the high strain structures of the Kheis Belt was transmitted through the intervening terrane to produce low strain and mainly brittle structures in the present area of study.

Bulk rotational finite strain associated with a set of NE trending dextral faults is locally important in the area south of Kanye (figure 8.10). NW trending sinistral fractures such as the Mokalaka Fault and other parallel fractures around Moshaneng complement as a conjugate set.

The local rotational strain enhanced the planar anisotropy first developed during the pre-Transvaal rifting episode. The greater development of the NE trending fractures and a lesser development of the NW trending fractures may be directly related to the inherent vertical post-Transvaal anisotropy of the crust initially developed in the pre-Transvaal. Vertical NE to ENE trending planar discontinuities already existed to facilitate the rotational strain that was imparted to the Kaapvaal

Craton.

On a larger scale, bulk strain in the NW Kaapvaal Craton was mainly irrotational. The bulk crust deformed by pure shear displacement induced by E-W directed compression (see figure 10.3). The influences of E-W compression could account for the folding and thrusting that has affected Transvaal Supergroup rocks in the eastern flank of Moshaneng area.

10.5.4 Post-Waterberg

Post-Waterberg tectonism came at a time when tectonic activity had stabilized within the Limpopo Mobile Belt.

The chronological sequence of intracratonic events during this period may be evaluated by examining the relative ages of fractures and folds. Folds formed in the study area are mainly passive, having been formed as a response to rigid block, vertical or dip-slip displacement of the underlying basement. In the last section (section 10.5.3), it was established that reactivation of fractures has occurred in the post-Transvaal/pre-Waterberg period in this region. Waterberg rocks represent the last sedimentary package deposited some 1 800 million years ago. The post-Waterberg period therefore covers the latter 40% of the entire history of the earth. An absence of younger stratigraphic deposits and geochronological data inhibits resolution of tectonic events during this period. A record of such events only exists outside the map area. These include high strain crustal shortening in the Kheis Belt (c.1,200 Ma), the

Ghanzi-Chobe Fold Belt (c.850 Ma), the Damara Belt (c.500 Ma) and the Cape Fold Belt (c. 278-230 Ma)(Tankard et al,1982; Mortimer, 1984; Söhnge, 1983). These events may have possibly left a tectonic imprint on the intra-cratonic environment. A major extensional episode took place during the break up of Gondwanaland beginning in the Jurassic and continuing in Cretaceous Periods (Windley, 1984). WNW trending post Karoo dike swarms form a prominent structural feature in central Botswana (Mortimer, 1984; Reeves, 1978). The earth's crust in east and southern Africa forms part of the East Africa Rift System which is an extensional event that has been active since the Tertiary up to the present time.

Future work, entailing meticulous mapping and radiogenic isotope dating of igneous intrusions offers the best prospect of calibrating rifting and other tectonic events in the post-Waterberg. Dolerite dikes and sills, and syenite and granite bodies are fairly well exposed in the present area of study for this type of investigation.

The most recognizable and striking post-Waterberg tectonic activity involves rigid block, vertical displacements that gave rise to the development of monoclines throughout southeast Botswana. In the area of study and adjacent areas, the majority of mapped monoclines (including the Moshaneng lineament) are south-facing. It may be significant that the divide between the Kaapvaal Craton and the Limpopo Mobile Belt is presently marked by the Zoetfontein Fault with its downthrown block to the south (see figure 1.1 for the position of the Zoetfontein Fault). The latest displacement on this continental fault is of post-Karoo age (<200 m.y.). It is possible that the last

displacements on south-facing monoclines of SE Botswana are also post-Karoo. Considering that Karoo basic igneous intrusions and brittle deformation are recognized <50 km north of the study area and more distally to the west (Mortimer, 1984) and south (Tankard et al, 1982; SACS, 1980), all within the Kaapvaal Craton, it is virtually inescapable to infer that some of the post-Waterberg deformations in the study area belong to this period. Prime areas of investigation include the high positive E-W trending magnetic anomalies south of Kanye. In the central and northern parts of the Botswana, Karoo dolerite dikes are readily recognized by their linear magnetic anomalies.

In the study area, N-S trending faults that are unknown in the record of earlier deposits have affected Waterberg rocks. In figure 10.4, these faults are spatially associated with the alkaline complexes at Segwagwa, Masoke and Moshaneng. It is therefore probable that these intrusions were associated with a local rift zone marked by these N-S trending faults. Monoclines are recognized in the northern part of the study area. They trend NW and ENE and appear to follow the trends of fractures that were active in the pre-Waterberg times. These monoclines probably represent a reactivation of these earlier fractures. The geometry of the fractures conform to the Reches model. In this model, a system of four fracture sets hosts displacement in a triaxial stress field (see figure 3.4(b) and 3.5).

The syenite intrusions at Segwagwa and Masoke have been emplaced at or near the boundary of the lower Transvaal and the Pretoria Group. These intrusions particularly favour the top contact of the chert and banded iron formation horizon. On

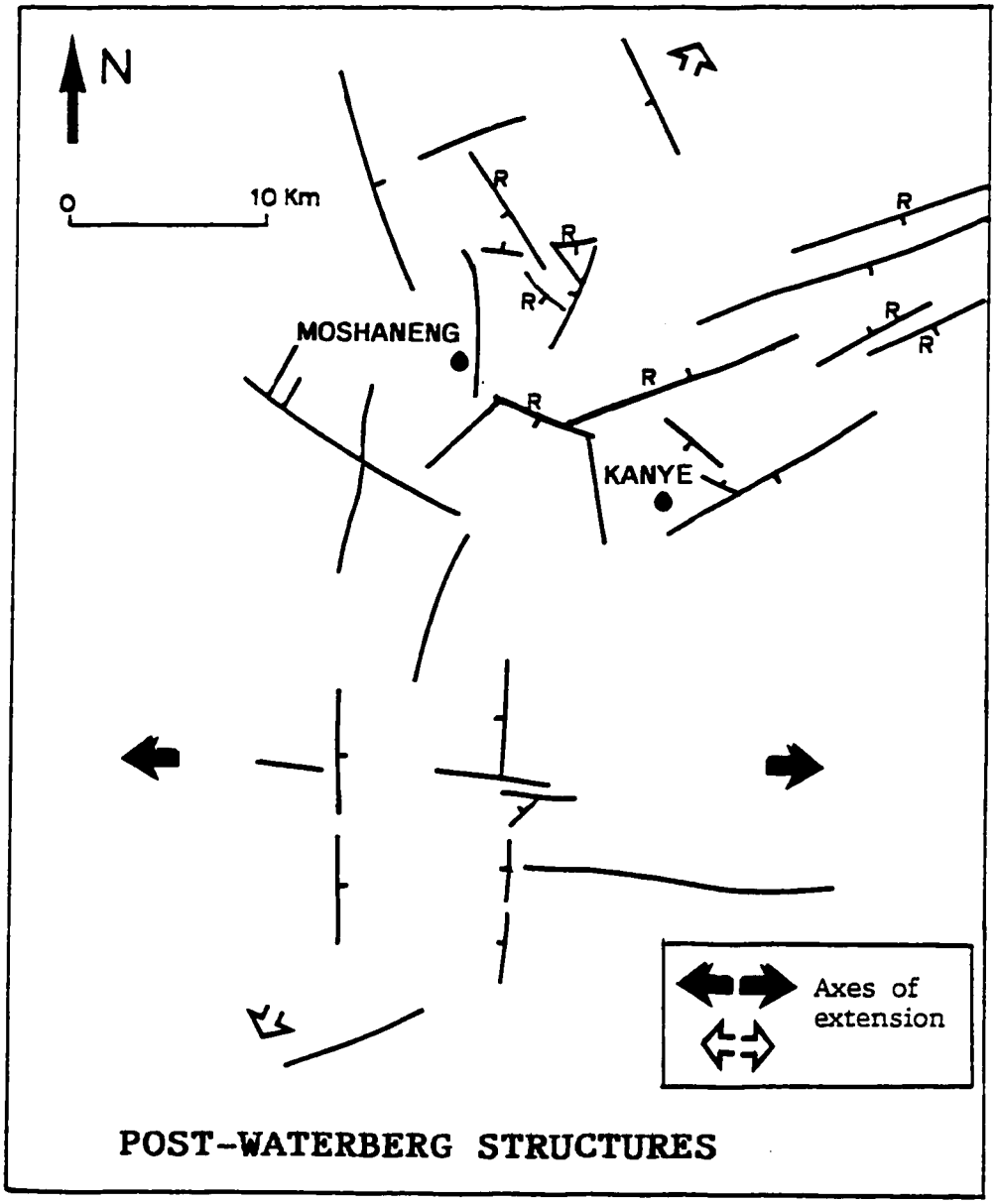

Figure 10.4: Salient regional post-Waterberg structures. Faults marked with **R** are reactivated fractures probably initiated in the pre-Transvaal. The unmarked fractures mainly trend N-S. They were initiated in the post-Waterberg. Reactivated fractures trend NW and ENE. They conform to the Reches model shown in figure 3.4(b) and figure 3.5 that is produced in a tri-axial stress field. The two axes of extension shown are not necessarily contemporaneous in this case.

the geological map, the shape of the intrusions has its long axis aligned along the strike of this boundary. The Segwagwa and Masoke chain of alkaline intrusions form an en echelon pattern to the southwest of Kanye (figure 6.5). At Moshaneng alkaline intrusions occur near the top of the lower Transvaal. This spatial association may be fortuitous, but it is possible that boundary between the lower and upper Transvaal rocks controlled the locus of these intrusions. The subsurface geometry of these complexes is unknown, but it is possible that they are paraconcordant. The presence of post-Transvaal and post-Waterberg dikes in SE Botswana has been inferred from photolineament studies (Aldiss, 1986). The interpretation of aeromagnetic contour patterns south of Kanye (figure 5.2) shows that dikes of post-Waterberg age actually intruded lower Transvaal rocks. Post-Waterberg dolerite sills intrude lower Transvaal and Waterberg rocks around Moshaneng and south of Kanye, around Nneneke. Reactivated fractures that cut through all the rocks, from basement through to the Waterberg were identified at many locations.

Other post-Waterberg dikes have been reported outside the present area of study, but in SE Botswana (Jones, 1973a; Stolberg, 1987; Emerman, 1991). Northerly trending dikes have been observed on photographs of ground underlain by weathered unexposed Modipe gabbro (Aldiss, 1986). The national aeromagnetic survey map shows a strong expression of these Pilanesburg dikes. This dike trend is however unknown in the present area of study.

The depositional basins for Waterberg sediments throughout SE Botswana are controlled by the ENE trending basement faults. Basal conglomerates in the Waterberg

sandstone around Kanye village support a syn-depositional tectonic model.

The Moshaneng, Masoke and Segwagwa syenite intrusion complexes are associated with regional north-south trending post-Waterberg Group faults (figures 6.3 and 6.5). Alkaline/felsic complexes associated with these faults suggest that the complexes were intruded through the fracture system. These faults have a linear expression indicating that they are probably steeply dipping. It is proposed that these faults mark a N-S trending rift system. The rift formed as a result of relative E-W extension (see figure 10.4). The extension probably facilitated intrusion of syenite complexes from Segwagwa, through Masoke to Moshaneng. It has been suggested that these intrusions may have been emplaced by cauldron subsidence (Aldiss et al, 1989). Such subsidence brought about the ring structures at Masoke and the northern lobe in the Segwagwa Complex (see figure 6.5). The main Segwagwa complex could have resulted from coalescence of a number of ring-like intrusions. The preponderance of dolerite sills along this zone of N-S faults also suggests a rifting environment. In the southern part of the study area, dolerite is virtually absent in the upper Transvaal sequences in the west, deemed to be outside the rift zone. A bimodal igneous suite consists of basic and alkaline felsic rocks. Dolerite constitutes the basic component and quartz syenite and granite constitutes the felsic component. At Moshaneng, the basic intrusion preceded the felsic intrusion.

10.6 Development of joints

10.6.1 Scope of the joint problem

One of the most enigmatic problems in structural geology has been the mechanisms by which joint systems form. A fairly comprehensive discussion of this issue is given in the book by Price (1966). Joint patterns have been studied extensively, but as Ramsay and Huber concede (1987), most of these studies have collected a large number of orientation measurements and offered less in a manner of definitive mechanisms.

A plethora of geological conditions will give rise to the formation of joints. The structures may develop at practically any stage in the history of the rock (Price, 1966; Suppe, 1985; Hatcher, 1990). Unconsolidated sediments are capable of developing joints. Joints may develop during tectonism. They may also develop much later when the main episode of tectonism has long subsided or during uplift. Some joint types develop due to cooling after igneous emplacement. Exfoliation type joints may result from near-surface temperature differences. These are but a few of the conditions that cause the formation of natural joint systems. Competent rocks which show no sign of any other type of deformation are always cut by joints. These structures, the most ubiquitous near the earth's surface, are still perhaps the least understood.

10.6.2 Mechanical requirements for joint formation

The mechanical requirements under which joints form provide a perspective by

which some useful comprehension is derived. Some important conditions that are favourable for the formation of joints include 1.) A tensile stress field, or a suitable stress ratio that can overcome the tensile strength of the rock 2.) relatively high strain rate that will permit brittle fracture, and 3.) relatively low temperatures to preclude plastic deformation and favour elastic behaviour. Generally, these conditions prevail near the earth's surface; dominantly in the upper 500 metres.

A number of factors seem pertinent for developing any joint system or architecture. These include the internal homogeneity or inhomogeneity of the deforming medium; its anisotropy; the overall geometry of deforming medium, i.e. presence or absence of folds, and the proximity of the fractures to material boundaries during their formation. The inherent planar anisotropy of layered rocks provides an unambiguous control on the architecture or relative geometrical relations of the joints that form in them.

10.6.3 Anisotropy

10.6.3.1 Primary anisotropy

In all the layered rocks of the study area, joints form perpendicular to primary sedimentary layering. On a regional scale, this rule always applies, despite the variability of the orientations of the bedding plane. The regional tilt of the Black Reef Quartzite exposures for areas around Moshaneng (figure 7.8) is towards the NW. This

is a markedly different tilt for areas to the south of Kanye (figure 7.9), which is towards the SE. The orientation of bedding in the Waterberg also varies from that of the Black Reef Quartzite, but the orthogonal relationship of bedding and joints is maintained. Orientations in the joint system at different locations abide by the rule of orthogonality to bedding even though there is nothing to suggest that the joints formed under varying remote stress fields, nor that they formed during different geological times. Since joints form perpendicular to the σ_3 direction, it follows that during the time of joint formation, this principal stress direction locally is parallel to bedding, notwithstanding the orientation of the remote stress field.

On a local scale, fracture orientations obtained at individual stations on the limbs of local mesoscopic folds show this orthogonal relationship unambiguously. The bedding strike is parallel to one joint set at most of the measuring stations in the study area. However, in limbs of folded layers a strike difference of the two planes occurs. This does not alter the orthogonal relationship of joints and bedding.

10.6.3.2 Secondary anisotropy

The formation of one set of joints in the rock produces a new planar anisotropy that controls the development of the subsequent joint set or sets. The new direction of σ_3 becomes parallel to the intersection of primary and secondary anisotropy, consisting of bedding and the newly formed joint set, respectively. This mechanism gives rise to the two set orthogonal joint system typical of layered rocks. Figure 10.5 is a schematic

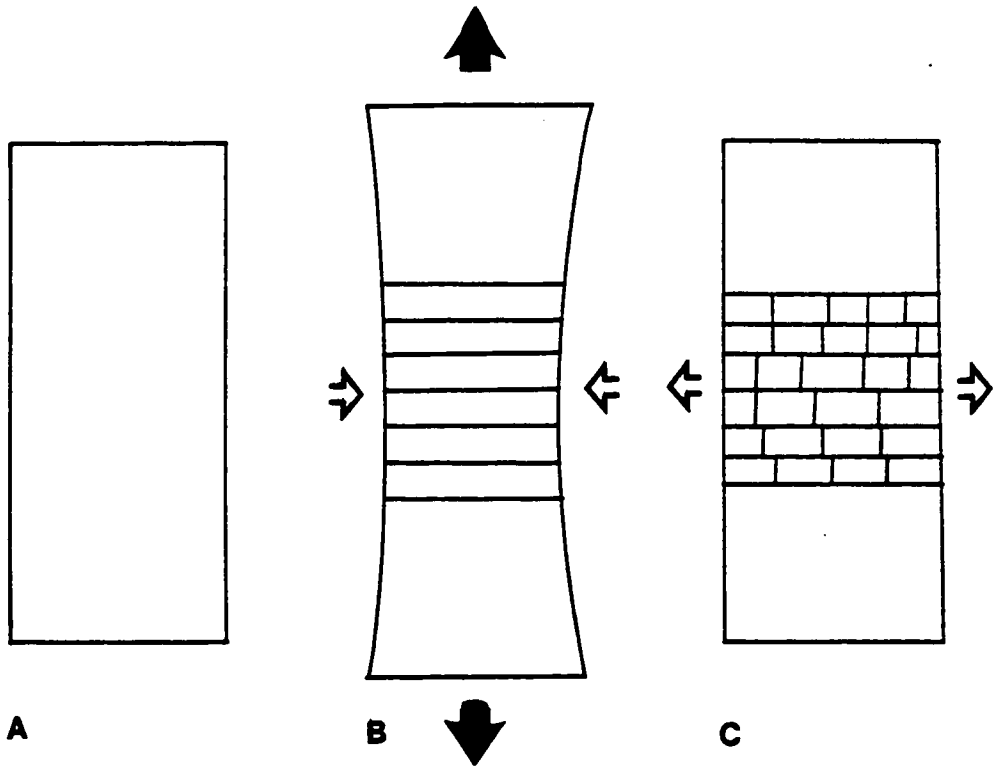

Figure 10.5: Effect of visco-elasticity in a plate.

A: Initial undeformed state.

B: Elongation in tensile stress and formation of set 1 fractures. σ_3 direction is along the axis of large arrows. Contraction is in perpendicular direction.

C: After the formation of set 1 fractures, stress cannot be transmitted through these fractures. New σ_3 direction is parallel to set 1. Set 2 fractures form. System reaches equilibrium. No remote stress transmitted through system.

(Graphic illustration adapted from Rives and Petit, 1990)

illustration of this mechanism by which an orthogonal two set joint system forms under elastic conditions. The formation of an orthogonal system of joints during folding has been explained by Rivet and Petit (1990a). The mechanism involves the bending of a visco-elastic plate. During folding, the plate undergoes traction elongation while contracting perpendicularly. When the traction stops, the plate tends to recover its initial form which produce a traction orthogonal to the initial traction.

Variations to the system occurs especially where folds occur. Diagonal joints are typical of folded rock layers (Maier and Mäkel, 1982). In the present study area, diagonal joint systems are superimposed on the two set orthogonal joint system with consistent angular relationships.

The diagonal fracture system, formed perpendicular to bedding in the Black Reef Quartzite may have formed at the initiation of buckling. This geometry would be in accordance with the classical mechanism where the fractures are conjugate strike slip faults. If the folding is principally cylindrical, an orthogonal fracture system develops with the dominant fracture set parallel to the fold axis. The more widely spaced complementary fracture set is formed perpendicular to the fold axis. When non-cylindrical conditions prevail, torsional forces act on the deforming layers (Rives and Petit, 1990a and b). Such a stress system may be induced by layers that have been previously folded about a different axis. The fractures formed meet at oblique angles. When the elastic component of the strain is released during uplift, a diagonal fracture system will form. This scenario is very likely in the folded beds at Moshaneng. Under relatively high confining pressures, verging folds were formed in parts of the Black

Reef Quartzite during the post-Transvaal/pre-Waterberg period. During a later phase, still in the post-Transvaal, cylindrical folds were formed in parts of the Black Reef at an axis which met at a high angle with the earlier fold axes. The geometry was non-cylindrical causing some of the folded layers to experience torsional forces. In those portions of the rock where the two fold systems are superimposed, an orthogonal fracture system is superimposed with a diagonal fracture system. The relative dispersion of fracture sets around stations 22-24 accords with brittle deformation caused by the interference of non-parallel fold axes. The development of more than two sets (orthogonal system) is a result of non-cylindrical folding.

10.6.4 Spacing

Hancock (1985) asserts that the evolution of a complete joint pattern involves the progressive infilling of increasingly smaller blocks and in some settings, the attitudes of older joints controls those of younger ones. The formation of joints is therefore the initial stage of quasi-static fragmentation. The initial fractures are widely spaced and the more maturely fractured blocks reflect relatively close spacing. Statistically, the evolution of fracture spacing begins with a negative exponential distribution function. At this stage, there are zones with a large number of closely spaced intervals separated by few wide spacings. This progresses through the lognormal distribution which is an intermediate stage that may progress to the most mature systems that display normal distribution. At this stage fracture spacing

approaches even spacing throughout any particular domain. The fracture pattern developed in the quartzite at Moshaneng is at the lognormal, intermediate stage.

10.7 Elasticity

Joints are formed during deformation taking place under elastic conditions. It has been observed by Turcotte and Schubbert (1982 p.104), that one of the fundamental postulates of plate tectonics is that the surfaces of the plates comprising the lithosphere do not deform significantly on geological time scales. The lithosphere behaves elastically. The continental lithosphere, especially displays such behaviour for a very long period of time. The Kaapvaal Craton is an Archaean lithospheric plate that has behaved elastically since the Archaean. Deformation has been brittle with rupture or fracturing before the onset of plastic behaviour. It is on this premise that the regional structure of this crustal block was examined.

10.8 Current stress field

The current stress field in Botswana is inferred from borehole overcoring data. Botswana is dominated by a NW-SE and N-S oriented maximum horizontal stress direction (Zoback, 1992). Normal faults show an active extensional stress regime. The Okavango Swamps panhandle in northern Botswana represents this regime. This implies that optimal orientation for open fractures is NW-SE. Fractures at right angles,

NE-SW are probably closed. Open fractures that are capable of contributing to the permeability of the rock are found in the top 80m below the surface (Von Hoyer, 1982).

10.9 Tension gashes

Tension gashes are structures that form in confined zones that are undergoing simple shear deformation. Sigmoidal tension gashes develop by propagation at the margin concomitant with the simple shear deformation. These type of structures are developed in the low strain environment typical of rocks around Moshaneng and Kanye. In these rocks, tension gashes are developed within incipient shear zones. The structures themselves are brittle fractures. In the area around Otse, a contrasting style of the deformation of tension gashes is presented. Tension gashes that formed in the limbs of folds in argillaceous rocks have been folded near anticlinal hinges of these folds. The folds developed by buckling of layers separated by tension gashes. Development of tension gashes appears to be favoured by an environment of semibrittle to ductile deformation at confining pressures higher than for those for joint development.

10.10 Significance of study

This thesis should set the stage and provide direction for future research in

brittle fractures in southeast Botswana. It is shown in this study that a long-lived tectonically stable environment has accumulated and preserved brittle fractures for more than 2.5 Ga. Fractures are of particular application to the understanding of fluid storage and conductivity in the outer portion of the earth's crust. Management of underground water resources in fractured rock is particularly important for economic activities in Botswana.

CHAPTER 11: CONCLUSION

The chronological development of regional brittle fractures in SE Botswana can be described for three periods that are divided by major stratigraphic breaks. These breaks occur at the basement/ supracrustal unconformity and between the Transvaal Supergroup and Waterberg Group rocks. The fracture pattern within each stratigraphic package is distinctive, enabling definition of tectonic domains. The first period is pre-Transvaal Supergroup time, represented by rocks below the basement/ Transvaal Supergroup unconformity. Only the brittle aspects of the deformation are considered during this time. The second period is constrained by the time of the production of unconformities bounding Transvaal Supergroup rocks. The third period is subsequent to deposition of Waterberg Group rocks.

During the first period, NE to ENE trending fractures were formed, and dikes of the same azimuth were emplaced in the pre-Transvaal basement of SE Botswana. These late Archaean to early Proterozoic structures are located in the NW portion of the Kaapvaal Craton for the present study. They probably correlate with NE trending dikes emplaced in the eastern parts of the craton. These developments took place concurrently with orogenic activity within the Limpopo Mobile Belt and the emplacement of the Great Dike of Zimbabwe. The orientation of pre-Transvaal structures follows that of earlier ductile structures formed in pre-cratonic times. The

development of the pre-Transvaal fractures and dikes constitutes one aspect of the initial phase of formation of the Bushveld and North Cape basins. The depo-axes of these basins also follow the NE to ENE trend of earlier Archaean structures. These early structures controlled regional displacements in subsequent deformations.

Post-Transvaal times were marked by the establishment of E-W directed compression. The remote stress with this principal axis of maximum stress probably affected the high strain Kheis Belt at the western margin of the Kaapvaal Craton as well. Dextral displacement occurred along pre-existing NE to ENE fractures. Locally, rotation about a vertical axis produced simple shear in the vicinity of Taupone Fault and other parallel faults south of Kanye. The Taupone Fault shows features of regional termination by the development of branches or "flower structures". Transpression caused reverse faults and uplift of sliced blocks along this regional fault zone. It is possible to trace the variations in structures formed along this strike slip fault from a reactivated basement fault to new ruptures in the overlying supracrustals. In basement rock, the fault follows a planar zone or linear surface trace. In the supracrustals however, the fault ramifies upwards into branches, defining a flower structure. The classical models of these fracture patterns are derived from laboratory experiments (Cloos, 1955; Naylor et al, 1986) and structures formed in the recent geological time (Tchalenko and Ambreseys, 1970). The patterns along the Taupone Fault also show that these models apply to structures formed in the Proterozoic.

On a scale that incorporates areas around Moshaneng, bulk strain in the study area is less rotational because of the presence of conjugate sinistral strike-slip faults.

The largest among these is the Mokalaka Fault, which forms the main zone of displacement north of Moshaneng and is marked by a major termination that gives rise to folds and thrusts east of Moshaneng.

The period preceding deposition of Waterberg Group rocks was marked by general peneplanation. The erosion of the Ramonnedi Formation carbonate and chert sequence probably produced underground caverns similar to the karst features currently produced in suboutcrop areas of these rocks. A pre-Waterberg joint system probably facilitated the fragmentation of the chert layers to produce the Kgwakgwe Chert Breccia Formation.

The redbed sediments of the Waterberg Group were deposited when all tectonic activity had ceased in the Limpopo Mobile Belt. Depositional basins in SE Botswana were mainly controlled by ENE to NE trending fault-bounded basins. The faults were probably reactivation by displacement along pre-existing faults. Coarse syntectonic deposits were developed in the basal Manyelanong Hill Formation.

In the post-Waterberg period, new N-S trending faults are spatially associated with the alkaline complexes at Moshaneng, Masoke and Segwagwa. The faults probably define a rift zone that formed in the post-Waterberg period. It has been suggested that some of the alkaline complexes intruded during cauldron subsidence (Aldiss et al, 1989), probably as ring structures.

ENE and NW trending fractures were reactivated during an episode of NE-NW extension. Vertical displacement on these faults could be modelled by the Reches model of tri-axial stress. Basement fractures were displaced along four sets of fractures

according to the Reches model. The model is derived on the premise that displacement occurs on pre-existing fractures. Waterberg and Transvaal sediments, draped over these faults, were either thrown into monoclines or into drag folds. The relative timing between the NE-SW and the E-W extensions is uncertain, but it seems likely that the E-W extension happened first, and facilitated emplacement of the syenite complexes. The NW and ENE trending faults, produced during NE-SW extension were probably activated during the Karoo. E-W dikes intruded during this period, forming prominent regional magnetic anomalies.

Joints in layered rocks of the study area are classified into 3 basic systems: namely, 1.) the single set system, 2.) the two set orthogonal system 3.) the two set diagonal system. On most exposures in the study area, the orthogonal and diagonal systems are superimposed. Classically, this type of pattern is described for folded strata (figure 3.3a and figure 3.3b). Joints are tensile fractures with an architectural arrangement that is primarily influenced by the planar anisotropy of the rock. The remote stress is important in controlling the orientation of the initial joint set.

Tension gashes are formed in media that are undergoing simple shear deformation. They form as brittle cracks in incepient shear zones in the Black Reef Quartzite and the coarse arenites of the Waterberg Group. In argillites of the Lobatse Volcanic Group, tension gashes form in the limbs of of folds. The tension gashes are folded by heterogeneous simple shear in the Waterberg arenites; and by buckling in the Lobatse Volcanic Group argillites.

REFERENCES

Aldiss,D.T.,1985, The geology of the Phitshane area: Geological Survey of Botswana, Bulletin 28, 106p.

Aldiss,D.T.,1986, The chronological significance of the pre-Transvaal Sequence dolerite dike swarm in south-east Botswana: Transactions of the Geological Society of South Africa,**89**,325-334. Author's Reply to discussion, p.419-420.

Aldiss,D.T., Tombale,A.R., Mapeo,R.M.B. and Chiepe,M.,1989, The geology of the Kanye area: Geological Survey of Botswana, Bulletin 33, 170p.

Anderson,E.M.,1905, The dynamics of faulting: Transactions of the Edinburgh Geological Society,**8**, 387-402.

Anderson,E.M.,1951, The Dynamics of Faulting: Oliver and Boyd, 183p.

Anhaeusser,C.R. and Wilson,J.F.,1981, The granitic-gneiss greenstone shield: in D.R.Hunter (editor), Precambrian of the Southern Hemisphere: Elselvier, Amsterdam, 423-499, 882p.

Atkinson,B.K.,1987(editor), Fracture Mechanics of Rock: Academic Press, Toronto, 534p.

Aydin,A. and Nur,A.,1982, Evolution of pull-apart basins and their scale independence: Tectonics,**1**,91-105.

Aydin,A. and Reches,Z.,1982, Number and orientation of fault sets in the field and in experiments: Geology,**10**,107-112.

Babcock,E.A.,1973, Regional jointing in southern Alberta: Canadian Journal of Earth Science,**10**, 1769-1781.

Bahat,D. and Engelder,T.,1984, Surface morphology on joints of the Appalachian Plateau: Tectonophysics,**104**, 299-313.

Bartlett,W.L., Friedman,M. and Logan,J.M.,1981, Experimental folding and faulting of rocks under confining pressure: Part IX,wrench faults in limestone layers: Tectonophysics,**79**,255-277.

Barquins,M. and Petit,J.-P.,1992, Kinetic instabilities during the propagation of a branch crack: effects of loading conditions and internal pressure: Journal of Structural Geology, **14**, 893-903.

Bons,C.A. and Van Loon,J.A.W.M.,1985, Water resources evaluation of a dolomite ground water basin in Southeast Botswana: Institute of Earth Science, Free University, Amsterdam (Unpublished).

Bothe,H.W., 1971, Final geological report, Kanye manganese, Botswana Exploration and Mining Co. Ltd: Geological Survey of Botswana, CR 10/2/1 (Unpublished).

Boyer,S.E. and Elliot,D.,1982, Thrust Systems: American Association of Petroleum Geologists Bulletin,**66**, 1196-1230.

Broek,D.,1986, Elementary engineering fracture mechanics: Kluwer Academic Publishers, Boston, 516p.

Bureau de Recherches Geologiques et Minieres(BRGM),1985, Hydrological survey of Kanye and Molepolole area;structural study: Agence d'interventions a l'entranger,Orleans,France (Unpublished).

Bureau de Recherches Geologiques et Minieres(BRGM),1986, Hydrological survey of Transvaal Supergroup dolomite in the Kanye area; final report volume 1, 86 BWA 020 EAU: Department of Water Affairs, Botswana, Ministry of Mineral Resources and Water Affairs (Unpuplished).

Bureau de Recherches Geologiques et Minieres(BRGM),1988, Kanye dolomite groundwater basin, hydrogeological investigation, resources assessment and development project; phase II, main report, volume 1, TB 10/1/85-86: Geological Survey of Botswana, Ministry of Mineral Resources and Water Affairs (Unpublished).

Burke,K.,Kidd,W.S.F., and Kusky,T.,1985, Is the Ventersdorp rift system of southern Africa related to a continental collision between the Kaapvaal and Zimbabwe cratons at 2.64 Ga ago? : Tectonophysics,**115**, 1-24.

Button,A.,1973a, The depositional history of the Wolksberg protobasin, Transvaal: Transactions of the Geological Society of South Africa: **76**, 15-25.

Button,A.,1973b, The stratigraphic history of the Malmani Dolomite in the eastern and northeastern Transvaal: Transactions of the Geological Society of South Africa,**76**, 229-247.

Button,A.,1976, Stratigraphy and relations of the Bushveld floor in the eastern Transvaal:Transactions of the Geological Society of South Africa,79, 3-12.

Button,A., Pretorius,D.A., Jansen,H., Stocklmayer,V., Hunter, D.R., Wilson,J.F., Wilson,A.H., Vermaak,C.F., Lee,C.A. and Stagman,J.G., 1981, The cratonic environment,chapter 9, in Hunter,D.R.(editor), Precambrian of The Southern Hemisphere: Elsevier, Amsterdam, 501-639,882p.

Cahen,L., Snelling,N.J., Delhal,J., and Vail,J.R., 1984, The geochronology and evolution of Africa: Clarendon Press, Oxford, 512p.

Chaoka,T.R., 1988, The geology, petrology and geochemistry of the Kannye Volcanics and Nnywane Formation: Ramotswa area, South East Botswana: M.Sc. thesis, Memorial University (Unpublished).

Clifford,T.N.,1970, The structural framework of Africa, in T.N.Clifford and I.G.Gass (editors), African Magmatism and Tectonics: Oliver and Boyd, Edingburgh, 1-26, 461p.

Cloos,1955, Experimental analysis of fracture patterns: Bulletin of the Geological Society of America,66, 241-256.

Cooke,H.J.,1975, The Lobatse caves: Botswana Notes and Records,7, 29-34.

Crockett,R.N.,1969, The geological significance of the margin of the Bushveld Basin in Botswana: Phd thesis, University of London. (Unpublished).

Crockett,R.N,1971a., The rocks of the Ventersdorp System of the Lobatse and Ramotswa areas,Republic of Botswana; their possible origins and regional correlation: Transactions of the Geological Society of South Africa,74, 1-24.

Crockett,R.N.,1971b., Some aspects of post-Transvaal System tectogenesis in southeastern Botswana with particular reference to the Lobatse and Ramotswa areas: Transactions of the Geological Society of South Africa,74,211-235.

Crockett,R.N.,1971c., Brief explanation of the geology of the Kanye area (quarter degree sheets 2425c and 2525A): Geological Survey of Botswana, RNC/55/71, 10p (Unpublished)

Crockett,R.N.,1972a., Geological map of the Kanye area (QDS 2425C) at 1:125,000: Geological Survey of Botswana.

Crockett,R.N.,1972b., Geological map of the Mmathethe area (QDS 2525A) at 1:125,000: Geological Survey of Botswana.

Crockett,R.N.,1972c., The Transvaal System in Botswana:Its geotectonic and depositional environment and special problems: Transactions of the Geological Society of South Africa,75, 275-289.

Crockett,R.N. and Jones,M.T.,1975, Some aspects of the geology of the Waterberg System in eastern Botswana:Transactions of the Geological Society of South Africa,78, 1-10.

Crockett,R.N. and Key,R.M.,1989, Commentary on "Early Precambrian basement uplift and block faulting along the western margin of the Bushveld Complex, southeastern Botswana(Eugene J.L.Dietvorst)": Journal of African Earth Sciences,8, 127-129.

Cruikshank,K.M., Zhao,G., and Johnson,A.M.,1991, Analysis of minor fractures associated with joints and faulted joints: Journal of Structural Geology,13, 865-886.

Cruikshank,K.M. and Aydin,A., 1993, Fracture patterns in Entrada Sandstone, Salt Valley Anticline, Arches National Park, Utah: Geological Society of America Annual Meeting; Abstract with Programs, Boston, Massacusetts, p.A-279.

Cullen,D.J.,1955, Preliminary report on the geology in the vicinity of the Moshaneng asbestos mine: Geological Survey of Botswana, DJC/3/55, 30p, (Unpublished).

Davies,R.K. and Pollard,D.D.,1986, Relations between left- lateral strike-slip faults, and right lateral monoclinal kink bands in granodiorite, Mt. Abbot quadrangle, Sierra Nevada, California: in Wang,C. (editor), Internal Structure of Fault Zones: Birkhauser, Boston, 177-201, 373p.

Delaney,P.T.,Pollard,D.D.,Ziony,J.I., and McKee,E.H., 1986, Field relations between dikes and joints: emplacement processes and paleostress analysis: Journal of Geophysical Research,91, 4920-4938.

Dietvorst,E.J.L.,1988, Early precambrian basement uplift and block faulting along the western margin of the Bushveld Complex, SE Botswana:Journal of African Earth Sciences,7, 641-651.

Dietvorst,E.J.L.,1991, Instability and basin formation on the Kaapvaal Craton, southern Africa: Journal of African Earth Sciences: Journal of African Earth Sciences,13, 359-365.

Dietvorst,E.J.L., De Vries,J.J., and Gieske,A., 1991, Coincidence of well fields and tectonic basins in the Precambrian shield area of southeast Botswana: Ground

Water, 29, 869-877.

Dyer,R.,1988, Using joint interactions to estimate paleostress ratios: Journal of Structural Geology,10, 685-699.

Emerman,S.H.,1991, Correlation of a dyke swarm in southeast Botswana with the Pilanesberg dyke swarm, South Africa: Journal of African Earth Sciences, 12, 525-531.

Engelder,T.,1982, Is there a genetic relationship between selected regional joints and the contemporary stress within the lithosphere of North America?: Tectonics,1, 161-177.

Engelder,T.,1985, Loading paths to joint propagation during a tectonic cycle: an example from the Appalachian Plateau, U.S.A.: Journal of structural Geology,7, 459-476.

Engelder,T,1987, Joints and shear fractures in rock, in Atkinson,B.K.(editor), Fracture Mechanics of Rocks: Academic Press Geological Series.p27-69, 534p.

Engelder,T, and Geiser,P.,1980, On the use of regional sets as trajectories of paleostress fields during the development of the Appalachian Plateau, New york: Journal of Geophysical Research,85, 6319-6341.

Ericsson, L.O., Ronge, B.,1986, Correlation between tectonic lineaments and permeability values of crystalline bedrock in the Gideå area: technical report 86-19 for SKB (Swedish Nuclear Fuel and Waste Management Co.) (Unpublished).

Ferguson,J.,1973, The Pilanesberg Alkaline Province, southern Africa: Transactions of the Geological Society of South Africa, 76, 249-270.

Fischer,M.P., Gross,M.R., Engelder,T., and Greenfield,R.J., 1993, Stress distribution around fractures in layered media: implications for joint spacing in bedded sedimentary rocks: Geological Society of America Annual Meeting; Boston Massacusetts, A-279.

Fripp,R.E.P., van Nierop,D.A., Callow,M.J., Lilly,P.A., and du Plessis,L.U.,1980, Deformation in part of the Archaean Kaapvaal Craton, South Africa: Precambrian Research,13, 241-251.

Fueten,F.,1992, Tectonic interpretations of systematic variations in quartz c-axis fabrics across the Thompson Belt: Journal of Structural Geology,14, 775-789.

Gould.D. and Rathbone,P.A.,1985, The geological structure of the Molopo Farms, in D.G. Hutchins and A.P.Lynam (editors), The Proceedings of a Seminar on the Mineral Exploration of the Kalahari, October, 1983: Geological Survey of Botswana Bulletin 29, 160-186, 364p.

Grady,D.E. and Kipp,M.E.,1987, Dynamic rock fragmentation, in Atkinson,B.K. (editor), Fracture Mechanics of Rocks: Academic Press Geological Series.p429-475, 534p.

Griffith,A.A.,1921, The phenomena of rupture and flow in solids: Philosophical Transactions of the Royal Society, SerA221, 163-198.

Groshong,R.H.,1976, Use of the four axes universal stage in rock deformation analysis: Cities Services Oil Company, technical report #53 (Unpublished).

Gross,M.R., 1993, The origin and spacing of cross joints: examples from the Monterey Formation, Santa Barbara Coastline, California: Journal of Structural Geology,15, 737-751.

Gross,M.R. and Engelder,T.,1991, A case of neotectonic joints along the Niagara Escarpment: Tectonics,10, 631-641.

Gurney,J.J.,1990, The diamondiferous roots of our wandering continents: South African Journal of Geology,93, 423-437.

Hancock,P.L.,1985, Brittle microtectonics:principles and practice: Journal of Structural Geology,7,437-457.

Hancock,P.L. and Engelder,T.,1989, Neotectonic joints: Geological Society of America Bulletin,101, 1197-1208.

Harding,R.R. and Snelling,N.J.,1972, Age determinations carried out on rocks from Botswana by the O.G.S. during the period 1963-1972: Isotope Geology Unit,Institute of Geological Sciences Report.72-5,11p.

Harding,T.P.,1973, Newport-Inglewood Trend,Carlifornia-an example of wrench style of deformation: American Association of Petroleum Geologists Bulletin,57,97-116.

Harland,W.B.,1971, Tectonic transpression in Caledonian Spitsbergen:Geological Magazine,108,27-42.

Hartnady,C.,Joubert,P.,and Stowe,C.,1985, Proterozoic crustal evolution in southwestern Africa: Episodes,8, 236-244.

Hatcher,R.D.,1990, Structural Geology: Principles, Concepts, and Problems: Merrill Publishing Company, Toronto, 531p.

Hobbs,B.E., Means,W.D. and Williams,P.F.,1976, An Outline of Structural Geology: John Wiley and Sons, New york, Toronto, 572p.

Hogson,R.A.,1961, Classification of structures on joint surfaces: American Journal of Science,259, 493-502.

Hubbert,M.K. and Rubey,W.W.,1959, Role of fluid pressure in mechanics of overthrust faulting: Bulletin of the Geological Society of America,70,115-166.

Hunter,D.R.,1974a, Crustal development in the Kaapvaal Craton,I. The Archaean: Precambrian Research, 1,259-294.

Hunter,D.R.,1974b, Crustal development in the Kaapvaal Craton,II. The Proterozoic: Precambrian Research, 1,295-326.

Hunter,D.R.,1991, Crustal processes during Archaean evolution of the southeastern Kaapvaal province: Journal of African Earth Sciences, 13, 13-25.

Hunter,D.R. and Halls,H.C.,1992, A geochemical study of a Precambrian mafic dyke swarm, eastern Transvaal, South Africa: Journal of African Earth Sciences, 15, 153-168.

Hunter,D.R. and Reid,D.L.,1987, Mafic dyke swarms in southern Africa: in H.C.Hall and W.F.Fahrig (editors), Mafic Dyke Swarms: Geological Association of Canada Special Paper34, p.445-456, 503p.

Hunter,D.R. and Pretorius,D.A.,1981, Structural Framework: in D.R.Hunter (editor), Precambrian of the Southern Hemisphere, Elselvier, Amsterdam, 397-422, 882p.

Hutton,S.M.,1978, An interpretation of Landsat imagery of southeast Botswana and a review of the practical uses, merits and disadvantages of the imagery: M.Phil thesis, Open University, 166p. (Unpublished)

Irwin, 1948, Fracture Dynamics: in Fracturing of Metals, Cleveland, Ohio: American Society of Metallurgists,p147-166.

Jackson,J. and McKenzie,D.,1983, The geometrical evolution of normal fault systems: Journal of Structural Geology,5, 471-482.

Jaeger,J.C.,1962, Elasticity, fracture and flow: with engineering and geological

applications: John Wiley and Sons, New York, 208p.

Jamison,W.R.,1989, Fault-fracture strain in Wingate Sandstone: Journal of Strutural Geology,**11**, 959-974.

Jamison,W.R. and Stearns,D.W.,1982, Tectonic deformation of Wingate Sandstone, Colorado National Monument: American Association of Petroleum Geologists Bulletin,**66**, 2584-2608.

Jennings, 1985, Karst Geomorphology: Blackwell, Glasgow, 293p.

Jones,M.T.,1973a, Geological map of Mochudi area (QDS 2426A and part of QDS 2426C) at 1:125,000: Geological Survey of Botswana.

Jones,M.T.,1973b, Geological map of Molepolole area (QDS 2425B) at 1:125,000: Geological Survey of Botswana.

Kent, J.T., Briden, J.C., and Mardia, K.V.,1983, Linear and planar structure in ordered multivariate data as applied to progressive demagnetization of palaeomagnetic remanence: Geophysical Journal,**75**, p.592-621.

Key,R.M.,1977, The geochronology of Botswana: Transactions of the Geological Society of South Africa,**80**, 31-42.

Key,R.M.,1983, The geology of the area around Gaborone and Lobatse, Kweneng, Kgatleng, Southern and South East Districts: Geological Survey of Botswana, District Memoir 5, 230p.

Key,R.M.,1986, Discussion on"The chronological significance of the pre-Transvaal Sequence dolerite dike swarm in south-east Botswana": Transactions of the Geological Society of South Africa, **89**, p.419.

Key,R.M. and Wright,E.P.,1982, The genesis of the Gaborone rapakivi granite complex in southern Africa: Journal of the Geological Society of London,**139**, 109-126.

Kirschvink,J.L.,1980, The least-squares line and plane and the analysis of palaeomagnetic data: Geophysical Journal of the Royal Astronomical Society,**62**, 699-718.

Ladeira,F.L. and Price,N.J.,1980, Relationship between fracture spacing and bed thickness: Journal of Structural Geology,**3**, 179-184.

Law,R.D., 1986, Relationships between strain and quartz crystallographic fabrics in the

Roche Maurice quartzites of Plougastel, western Brittany: Journal of Structural Geology, 8, 493-514.

Lock,N.P. and Carney,J.N., 1991, A window into "basement" rocks in southwest Botswana: inferences from borehole chip samples: Botswana Journal of Earth Sciences,1, 23-41.

Logan,J.M.,Friedman,M. and Stearns,M.T.,1978, Experimental folding of rocks under confining pressure: Part VI, Further studies of faulted drape folding, in Matthew III,V.(editor), Laramide Folding Associated with Basement Block Faulting in Western U.S.A.: Geological Society of America Memoir 151,79-99.

Machacha,T.P.,1977, The geology of Diabo area: Geological Survey of Botswana, TPM/1/77, 15p, (Unpublished).

Machacha,T.P.,1979, The origin of the Kanye conglomerate: Geological Survey of Botswana, TPM/6/79, 2p, (Unpublished).

MacKinnon,P.,1988, A study of echelon fracture sets in the Killarney Igneous Complex, Killarney, Ontario: M.Sc. thesis, McMaster University, 164p, (Unpublished).

Maier,G. and Mäkel,G.H.,1982, The geometry of the joint pattern and its relation with fold structures in the Aywaille area (Ardennes, Belgium): Geologie Rundschau, 71, 603-616.

Mallick,D.I.J., Habgood,F. and Skinner,A.C.,1981, A geological interpretation of Landsat imagery and air photography of Botswana: Institute of Geological Sciences, London, Overseas Geology and Mineral Resources Number 56, 35p.

Mandl.G.,1988, Mechanics of tectonic faulting: models and basic concepts: Elselvier, New York, 407p.

Matthew III,V.,1978, Laramide folding associated with basement block faulting along the northeastern flank of the Front Range, Colorado, in Matthew III,V.(editor), Laramide Folding Associated with Basement Block Faulting in Western U.S.A.:Geological Society of America Memoir 151,101-124.

McCoss,A.M.,1986, Simple constructions for deformation in traspression/transtension zones: Journal of Structural Geology,8, 715-718.

McElhinny,M.W.,1966, Rb-Sr and K-Ar age measurements on the Modipe Gabbro of Bechuanaland and South Africa: Earth Planetary Science Letters,1, 439-442.

McElhinny,M.W. and Briden,J.C.,Jones,D.L. and Brock,A.,1968, Geological and geophysical implications of palaeomagnetic results from Africa: Reviews of Geophysics,6, p.201-238.

Moehadu,O.,1991, The geology of the area around Moshaneng: B.Sc. Thesis, University of Bostwana (Unpublished).

Monngae,J.,1989, The geology of the area around Moshaneng: B.Sc. Thesis, University of Botswana (Unpublished).

Moody,J.D. and Hill,M.J.,1956, Wrench fault tectonics: Bulletin of the Geological Society of America,67, 1207-1246.

Mortimer,C.,1984, Geological Map of the Republic of Botswana (1:1,000,000): Geological Survey of Botswana.

Naylor,M.A., Mandl,G., and Sijpesteijn,C.H.K.,1986, Fault geometries in basement-induced wrench faulting under different initial stress states: Journal of Structural Geology,8, 737-752.

Nickelsen,R.P., and Hough,V.D.,1967, Jointing in the Appalachian Plateau of Pennsylvania: Geological Society of America Bulletin,78, 609-630.

Park,R.G.,1989, Foundations of Structural Geology: Blackie, Glasgow and London,148p.

Parker,J.M., 1942, Regional systematic joints in slightly deformed sedimentary rocks: Geological Society of America Bulletin,53, 381-408.

Parsons,C.F. and Killick,A.M.,1990, A reassessment of the structure of the dolomite inliers southeast of Westonaria: South African Journal of Geology; 93, p.438-442.

Paterson,M.S.,1978, Experimental Rock Deformation; The Brittle Field: Springer-Verlag,New York,254p.

Piper,J.D.A.,1975, The palaeomagnetism of Precambrian ingneous and rocks sedimentary rocks of the Orange River Belt in South Africa and South West Africa: Geophysical Journal,40, p.313-344.

Piper,J.D.A.,1987, Palaeomagnetism and the Continental Crust: Open University Press, Miton Keynes, 434p.

Pollard,D.D. and Aydin,A.,1988, Progress in understanding jointing over the past

century; Geological Society of America Bulletin,100, 1181-1204.

Pollard,D.D., Saltzer,S.D. and Rubin,A.M.,1993, Stress inversion methods: are they based on faulty assumptions?: Journal of Structural Geology,15, 1045-1054.

Pollard,D.D. and Segall,P.,1987, Theoretical displacements and stresses near fractures in rock: with applications to faults, joints, veins, dikes, and solution surfaces, in B.K.Atkinson (editor), Fracture Mechanics of Rocks: Academic Press Geological Series.p429-475, 534p.

Pretorius,D.A.,1979, The crustal architecture of southern Africa: Alex. L. du Toit Memorial Lectures No.13(Delivered, 1973 - Published, 1979): The Geological Society of South Africa, Annexure to Volume 76, 60p.

Pretorius,D.A.,1985, The Kalahari Foreland, its marginal troughs and overthrust belts, and the regional structure of Botswana, in D.G.Hutchins and A.P.Lynam (editors), The Proceedings of a seminar on the Mineral Exploration of the Kalahari, October, 1983: Geological Survey of Botswana, Bulletin 29, 294-319, 364p.

Price,N.J.,1966, Fault and Joint Development in Brittle and Semi-Brittle Rock: Pergamon Press,Toronto,176p.

Price,N.J. and Cosgrove,J.W.,1990, Analysis of geological Structures: Cambridge University Press, New York, 502p.

Rabie,L.,1958, Geological field report on the first investigation into the manganese ore possibilities in the Bangwaketsi native reserve, Bechuanaland Proctectorate, Report to Johannesburg Consolidated Investment Co. Ltd. (Unpublished).

Ragan,D.M.,1985, Structural Geology: An introduction to Geometric Techniques: John Wiley and Sons, New York, 393p.

Ramsay,J.G., and Graham,R.H., 1970, Strain variations in shear belts: Canadian Journal of Earth Science, 7, p.786-813.

Ramsay,J.G., and Huber,M.I.,1983, The Techniques of Modern Structural Geology;vol.3;Strain Analysis: Academic Press, Toronto, 307p.

Ramsay,J.G., and Huber,M.I.,1987, The Techniques of Modern Structural Geology;vol.2;Folds and Fractures: Academic Press, Toronto,700p.

Ratsoma,W.,1988, The geology of the area around Otse: B.Sc. Thesis, University of Botswana (Unpublished).

Rawnsley,K.D., Rives,T. and Petit J.-P., 1992, Joint development in perturbed stress fields near faults: Journal of Structural Geology,**14**, 939-951.

Reches,Z.,1978, Development of monoclines: Part I, Structure of the Palisades Creek branch of the East Kaibab Monocline, Grand Canyon,Arizona, in Matthew III,V.(editor), Laramide Folding Associated with Basement Block Faulting in Western U.S.A.: Geological Society of America Memoir 151,235-271.

Reches,Z.,1983, Faulting of rocks in three-dimentional strain field II. Theoretical analysis: Tectonophysics, **95**,133-156

Reches,Z. and Dieterich,J.H.,1983, Faulting of rocks in three-dimensional strain fields I.Failure of rocks in polyaxial, servo-control experiments; Tectonophysics,**95**, 111-132.

Reeves,C.V.,1978, Reconnaissance aeromagnetic survey of Botswana, 1975-1977: Final interpretation report, Terra Survey, Ltd., Geological Survey of Botswana, 199p.

Rives,T. and Petit,J-P.,1990a, Experimental study of jointing during cylindrical and non-cylindrical folding: in Rossmanith, H.P.(editor), Mechanics of Jointed and Faulted Rocks: Proceedings of the International Conference on Mechanics of Jointed and Faulted Rock/Institude of Mechanics /Technical University of Vienna/ 18-20 April,1990. p.205-211.

Rives,T. and Petit,J-P., 1990b, Jointing and folding: An Experimental approach: C.R. Acad. Sci. Paris,**t.310**, Serie II, p.1115-1121.

Rives,T., Razack,M.,Petit J-P. and Rawnsley,K.D.,1992, Joint spacing: analogue and numerical simulations: Journal of Structural Geology,**14**, 925-937.

Rogers,R.D. and Bird,D.K.,1987, Fracture propagation associated with dike emplacement at the SKaergaard intrusion, East Greenland: Journal of Structural Geology,**9**, p.71-86.

Ronge,B. and Ericsson,L.O.,1986, Correlation between tectonic lineaments and permeability values of crystalline bedrock in the Gideå area: Technical Report 86-19, Swedish Nuclear Fuel and Waste Management Co.

Rosendahl,B.R.,1987, Architecture of the continental rifts with special reference to east Africa: Annual Reviews, Earth and Planetary Sciences,**15**,445-503.

Rutter,E.H.,Maddock,R.H.,Hall,S.H. and White,S.H.,1986, Comparative microstructures of natural and experimentally produced clay bearing fault gouges: in

Wang,C.(editor) Internal Structure of Fault Zones: Birkhauser Verlag, Boston,3-30, 373p.

Sanderson,D.J.,and Marchini,W.R.D.,1984, Transpression: Journal of Structural Geology,6,449-458.

Secor,D.T.,1965, Role of fluid pressure in jointing: American Journal of Science,263, 633-646.

Segall,P.,1984, Rate-dependent extensional deformation resulting from crack growth in rock: Journal of Geophysical Research, 89, 4185-4195.

Segall,P. and Pollard,D.D.,1983, Joint formation in granitic rocks of the Sierra Nevada: Geological Society of America Bulletin,94, 563-575.

Segall,P. and Simpson,C.,1986, Nucleation of ductile shear zones on dilatant fractures: Geology, 14, 56-59.

Sengör,A.M.C. and Burke,K.,1978, Relative timing of rifting and volcanism on earth and its tectonic implications: Geophysical Research Letters, 5, 419-421.

Sharma,P.V.,1986, Geophysical Methods in Geology: Elsevier, Amsterdam, 442p.

Sheperd,J., and Huntington,J.F., 1981, Geological fracture mapping in coalfields and the stress fields of the Sydney Basin: Journal of the Geological Society of Australia,28, 299-309.

Siamisang,T.,1987, The geology of the area around Otse: B.Sc. Thesis, University of Botswana (Unpublished).

Sibiya,V.B.,1988, The Gaborone Granite Complex Botswana,southern Africa: an atypical rapakivi granite-massif anorthosite association: PhD Thesis, Free University Press, Amsterdam.

Sibson,R.H.,1977, Fault rocks and fault mechanisms: Journal of the Geological Society of London,133, 191-213.

Simpson,C. and Schmid,S.M.,1983, An evaluation of criteria to deduce the sense of movement in sheared rocks: Geological Society of America Bulletin,94, 1281-1288.

Söhnge,A.P.G., 1983, The Cape Fold Belt-perspective, in A.P.G.Söhnge and I.W.Hälbich (editors), Geodynamics of the Cape Fold Belt; Special Publication No.12: Geological Society of South Africa 184p., p.1-6.

South African Committee for Stratigraphy (SACS),1980, Stratigraphy of South Africa, Part 1 (Compiler, L.E.Kent) Lithostratigraphy of the Republic of South Africa: South Africa Geological Survey Handbook 8, 690p.

Stalker,A.D.,1982, Final report on Moshaneng prospecting licence 2/81, vol.1 and 2: Geological Survey of Botswana Report, CR 39/2/3 (Unpublished).

Stearns,D.W.,1978, Faulting and forced folding in the Rocky Mountain Foreland, in Matthews III,V.(editor), Laramide Folding Associated with Basement Block Faulting in Western U.S.A.:Geological Society of America Memoir 151,1-37.

Stearns,D.W.,1967, Certain aspects of fracture in naturally deformed rocks, in Riecker,R.E.(editor), Rock Mechanics Seminar, Bedford,Massachussetts;Air Force Cambridge Research Lab;97-118, 594p.

Stolberg Ingenieurberatung GMBH, 1987, Report:Interpretation of the airborne magnetic survey of eastern Botswana 5105.11.14.017: Geological Survey of Botswana, 77p, annexes and maps.

Suppe,J.,1985, Principles of Structural Geology: Prentice-Hall, 537p.

Swanson,M.T.,1989, Sidewall ripouts in strike-slip faults: Journal of Structural Geology,**11**, 933-948.

Sylvester,A.G.,1988, Strike-slip faults: Geological Society of America Bulletin,**100**,1666-1703.

Tankard,A.J.,Jackson,M.P.A.,Ericksson,K.A.,Hobday,D.K., Hunter, D.R., and Minter,W.E.L.,1982, Crustal Evolution of Southern Africa; 3.8 Billion Years of Earth History: Springer-Verlag,New York,523p.

Tchalenko,J.S.,1970, Similarities between shear zones at different magnitudes: Geological Society of America Bulletin,**81**,1625-1640.

Tchalenko,J.S.and Ambraseys,N.N.,1970, Structural analysis of the Dasht-e-Bayaz(Iran) earthquacke fractures: Geological Society of America Bulletin,**81**,41-60.

Terra Surveys Ltd, 1976, Reconnaissance Aeromagnetic Survey: Republic of Botswana: Sheet 7, Contour map: Geological Survey of Botswana.

Thatcher,W. and Hill,D.P.,1991, Fault orientations in extensional and conjugate strike slip environments and their implication: Geology, **9**, 1116-1120.

Tombale,A.R.,1986, Geological map of the Jwaneng area, QDS 2424D (1:125,000): Geological Survey of Botswana.

Tombale,A.R., in prep, Geological map of the Mmathethe area, QDS 2525A,(1:125,000): Geological Survey of Botswana, (Unpublished).

Turcotte,D.L. and Schubbert,G.,1982, Geodynamics: Applications of continuum physics to geological problems: John Wiley and Sons, Toronto, 450p.

Turner,F.J. and Weiss,L.E.,1963, Structural analysis of metamorphic tectonites: McGraw Hill, New Hill, 545p.

Van Haren,I and Spaans,S.,1988, Aspects of recharge in a small basin in S.E.Botswana: Institute of Earth Sciences, Free University of Amsterdam (Unpublished).

Van Niekerk,C.B.,1968, The suitability of extrusive rocks for U-Pb radiometric dating; Phd thesis, University of Cape Town (Unpublished).

Van Niekerk,C.B. and Burger,A.J.1968, The age of the Ventersdorp System; Annals of the Geological Survey of South Africa,3, 75-86.

Van Niekerk,C.B. and Burger,A.J.,1978, A new age for the Ventersdorp acidic lavas: Transactions of the Geological Society of South Africa,**81**, 155-163.

Vermaak,C.F.,1962, Discussion of "The stratigraphy, structure and igneous rocks of the Transvaal System at Western Areas Gold Mine" by C.A.Cousins: Transactions of the Geological Society of South Africa,**LXV**,32.

Viak AB,1984, Lineament studies in the area between Molepolole and Letlhakeng: Geological Survey of Botswana, Ministry of Mineral Resources and Water Affairs (Unpublished).

Von Hoyer,M.,1982, Report on borehole siting for the Intergrated Farming Pilot Project (IFPP), Pelotshetlha, Diabo, Southern District: Geological Survey of Botswana, MvH/1/82, 12p (Unpublished).

Walsh,J.J. and Watterson,J.,1988, Analysis of the relationship between displacements and dimensions of faults: Journal of Structural Geology, **10**, 239-247.

Wilcox,R.E.,Harding,T.P.and Seeley,D.R.,1973, Basic wrench tectonics:American Association of Petroleum Geologists Bulletin, **57**,74-96.

Wilson,G.,1982, Introduction to Small-scale Geological Structures: George Allen &

Unwin, London, 127p.

Wilson,J.F.,Jones,D.L. and Kramers,J.D.,1987, Mafic dyke swarms in Zimbabwe, in H.C.Hall and W.F.Fahrig, Mafic Dyke Swarms: Geological Association of Canada Special Paper **34**, p.433-444, 503p.

Windley,B.F.,1984, The Evolving Continents: John Wiley,399p.

Woodcock,N.H. and Fischer,M.,1986, Strike-slip duplexes: Journal of Structural Geology,**8**, 725-735.

Zhao,G. and Johnson,A.M.,1992, Sequence of deformations recorded in joints and faults, Arches National Park, Utah: Journal of Structural Geology,**14**,225-236.

Zoback,M.L.,1992, First and second-order patterns of stress in the lithosphere: the world stress map project: Journal Geophysical Research, **97**, 11703-11728.

APPENDIX A:

STEREOGRAPHIC PROJECTION OF BEDDING, JOINTS, SLICKEN STRIAE AND FOLD AXES MEASURED AT STATIONS SHOWN IN FIGURES 7.12 AND 7.13.

Planar data shown as lower hemisphere projection of poles to planes. Where bedding exists, the mean bedding attitude is shown as a girdle. The combination stations 1-40 show "mean lineation azimuth and plunge," which is the mean pole to planes on stereonet.

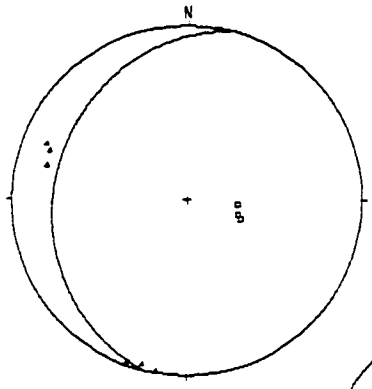

Station 1, Block Reef Quartzite (BRQ)
Projection ..... Schmidt
Number of Sample Points 10

▫ Bedding planes
▵ Joints

A1

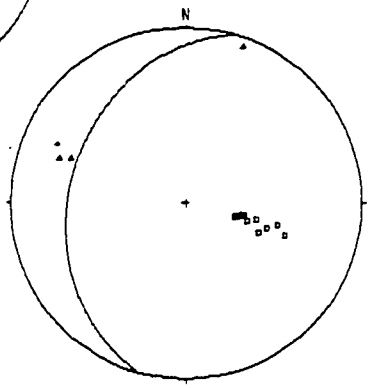

Station 2, BRQ
Projection ..... Schmidt
Number of Sample Points 15

▫ bedding
▵ joints

A2

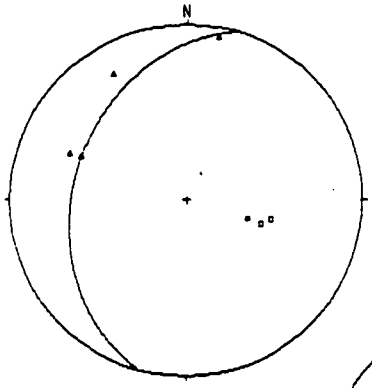

station 3, BRQ
Projection ..... Schmidt
Number of Sample Points 8

▫ bedding
▵ joints

A3

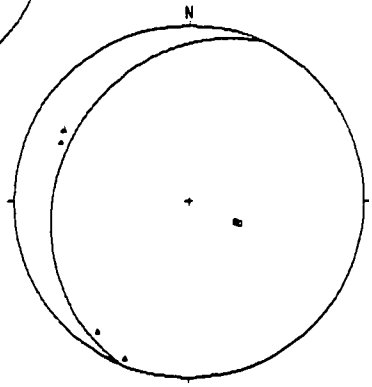

station4, BRQ
Projection ..... Schmidt
Number of Sample Points 7

▫ bedding
▵ joints

A4

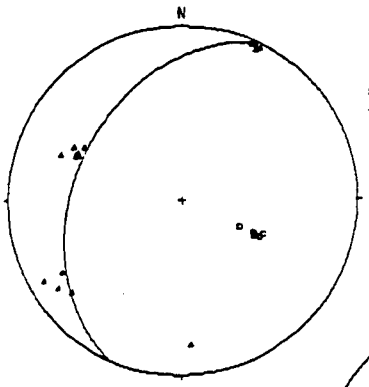

Station 5, BRQ
Projection ..... Schmidt
Number of Sample Points 22

▫ bedding
▪ joints

A5

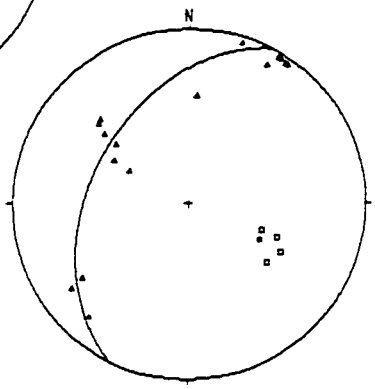

station 6, Black Reef Quartzite
Projection ..... Schmidt
Number of Sample Points 22

▫ Bedding
▪ joints

A6

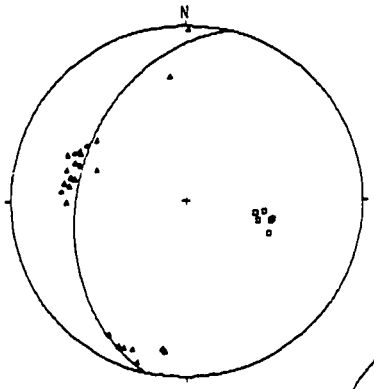

Station7, BRQ
Projection ..... Schmidt
Number of Sample Points 32

▫ Bedding
▪ joints

A7

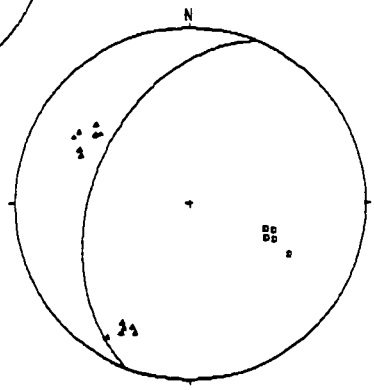

Station 8, BRQ
Projection ..... Schmidt
Number of Sample Points 19

▫ bedding
▪ joints

A8

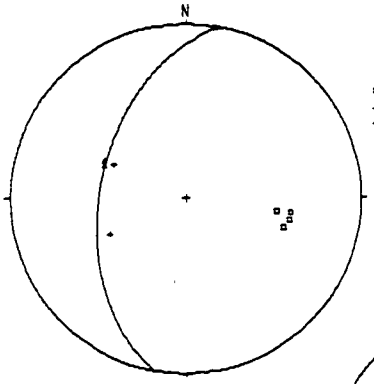

Station 9, BRO
Projection ..... Schmidt
Number of Sample Points ... 9

▫ bedding
▵ joints
+ bedding plane slicken strias

A9

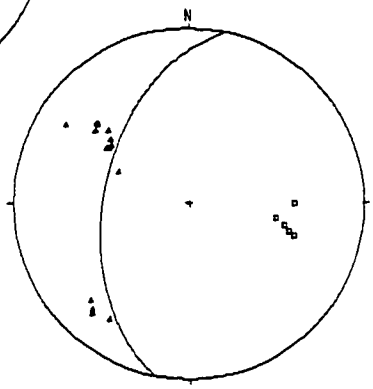

Station 10, BRO
Projection ..... Schmidt
Number of Sample Points ... 21

▫ bedding
▵ joints

A10

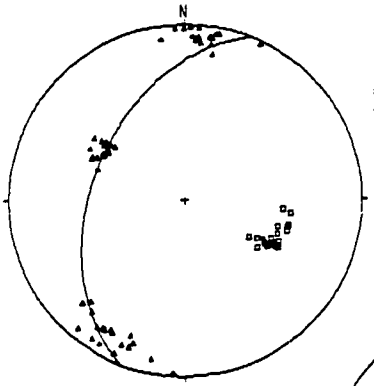

Station 11, BRO
Projection ..... Schmidt
Number of Sample Points ... 78

▫ bedding
▵ joints

A11

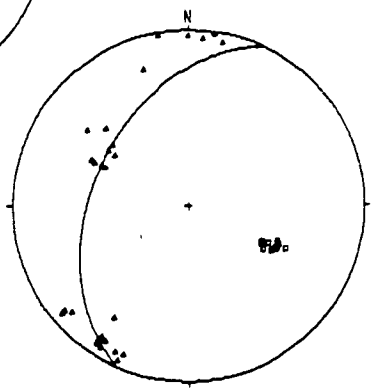

station 12, BRO
Projection ..... Schmidt
Number of Sample Points ... 40

▫ bedding
▵ joints

A12

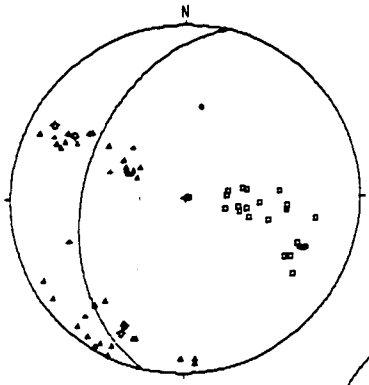

Station 13, BRO
Projection ..... Schmidt
Number of Sample Points 69

▫ bedding
▵ joints
+ Slicken strips on bedding
• Slicken strips on joints
◆ Fold axes

A13

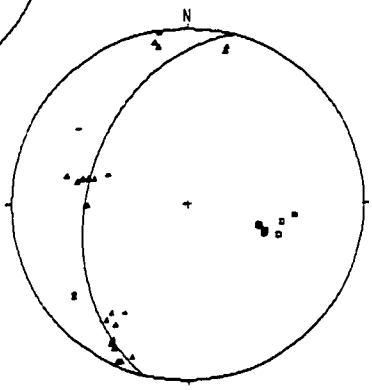

station 14, Block Reef Quartzite
Projection ..... Schmidt
Number of Sample Points 34

▫ Bedding
▵ Joints
+ slicken strips in bedding plane

A14

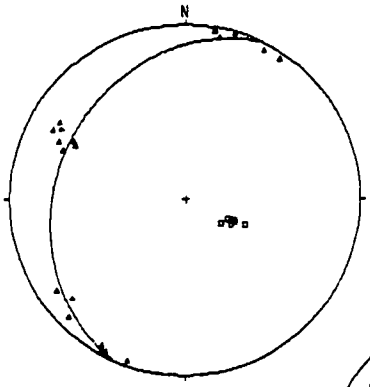

Station 15, BRO
Projection ..... Schmidt
Number of Sample Points 29

▫ bedding
▵ joints

A15

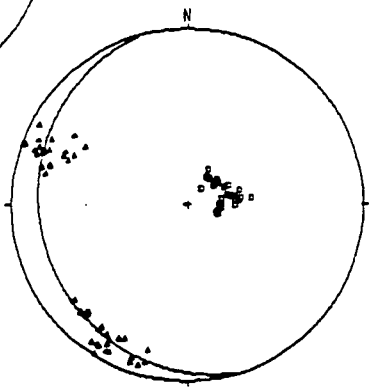

Station 16, BRO
Projection ..... Schmidt
Number of Sample Points 72

▫ bedding
▵ joints

A16

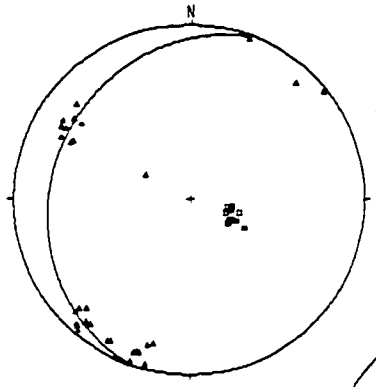

Station 17, BRD
Projection ..... Schmidt
Number of Sample Points ... 44

▫ Bedding
▵ Joints

A17

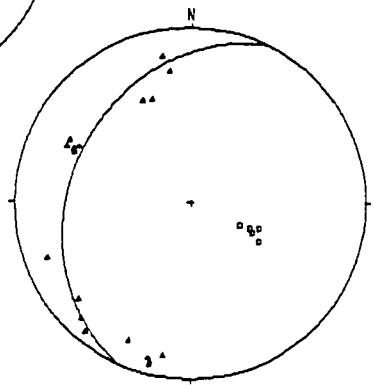

Station 18, BRD
Projection ..... Schmidt
Number of Sample Points ... 24

▫ Bedding
▵ Joints

A18

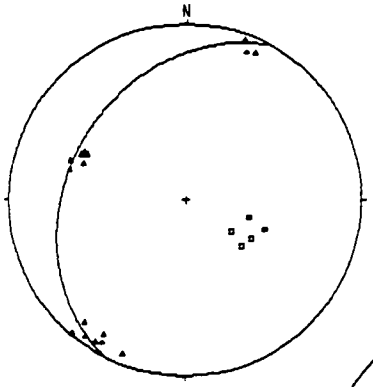

Station 19, BRD
Projection ..... Schmidt
Number of Sample Points ... 22

▫ Bedding
▵ Joints

A19

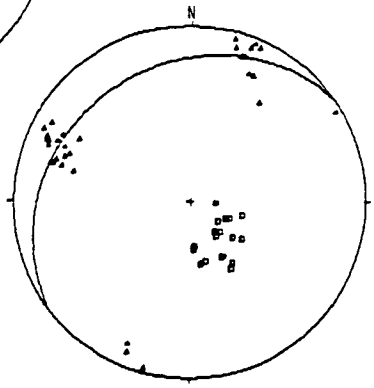

Station 20, BRD
Projection ..... Schmidt
Number of Sample Points ... 50

▫ Bedding
▵ Joints

A20

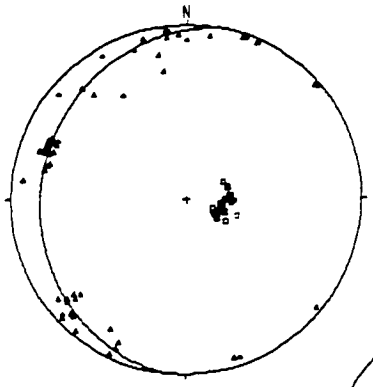

Station 21, BRD
Projection ..... Schmidt
Number of Sample Points 84

▫ Bedding
▵ Joints

A21

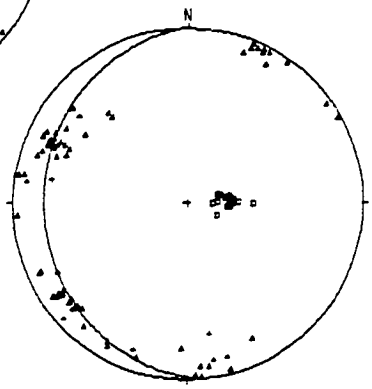

Station 22, BRD
Projection ..... Schmidt
Number of Sample Points 93

▫ Bedding
▵ Joints
▵ slicken stride on bedding surface

A22

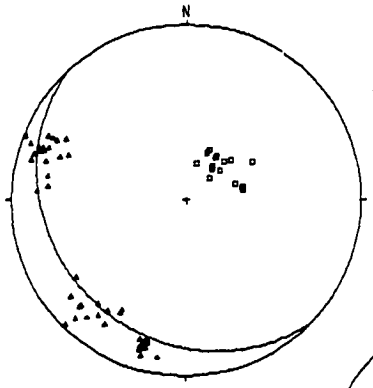

Station 23, BRD
Projection ..... Schmidt
Number of Sample Points 60

▫ Bedding
▵ Joints

A23

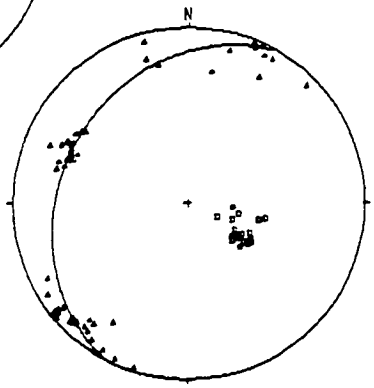

Station 24, BRD
Projection ..... Schmidt
Number of Sample Points 83

▫ Bedding
▵ Joints

A24

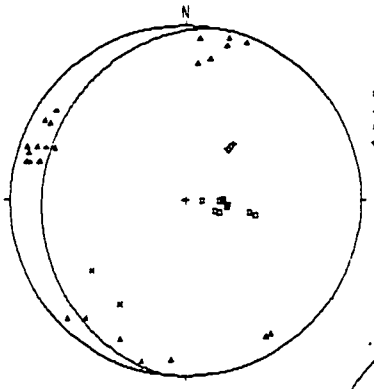

Station 25, BRO
Projection ..... Schmidt
Number of Sample Points 39

▫ Bedding
▵ Joints
× Slicken strios in fault planes
◆ Fault planes

A25

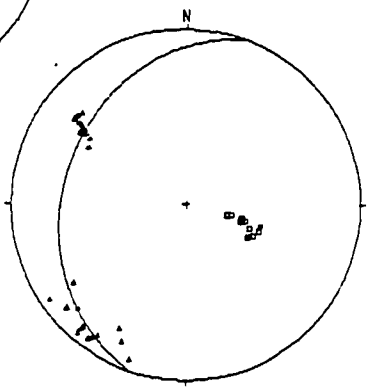

Station 26, BRO
Projection ..... Schmidt
Number of Sample Points 34

▫ Bedding
▵ Joints

A26

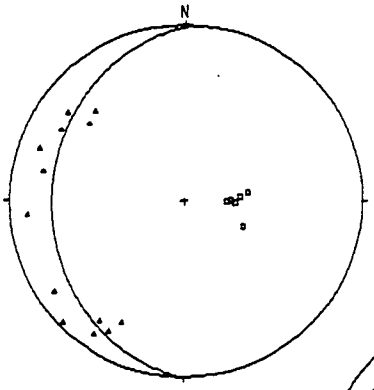

Station 27, BRO
Projection ..... Schmidt
Number of Sample Points 20

▫ Bedding
▵ Joints

A27

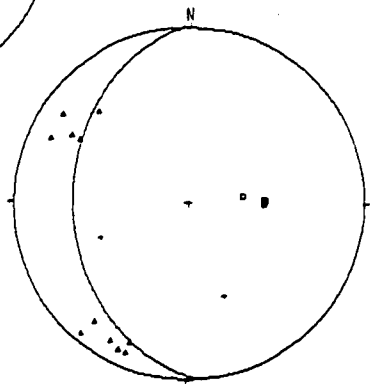

Station 28, BRO
Projection ..... Schmidt
Number of Sample Points 18

▫ Bedding
▵ Joints
+ Slicken strios in bedding plane

A28

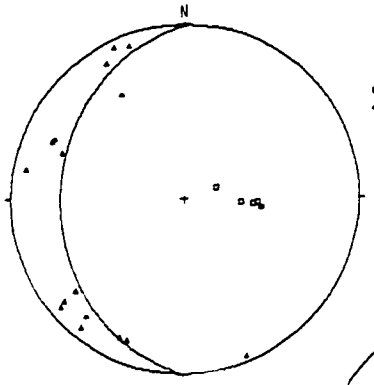

Station 29, BRD
Projection ..... Schmidt
Number of Sample Points 23

▫ Bedding
▵ Joints

A29

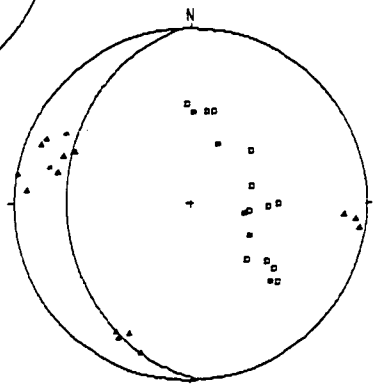

Station 30, BRD
Projection ..... Schmidt
Number of Sample Points 34

▫ Bedding
▵ Joints

A30

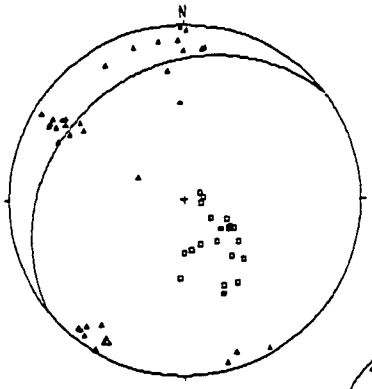

Station 31, BRD
Projection ..... Schmidt
Number of Sample Points 58

▫ Bedding
▵ Joints

A31

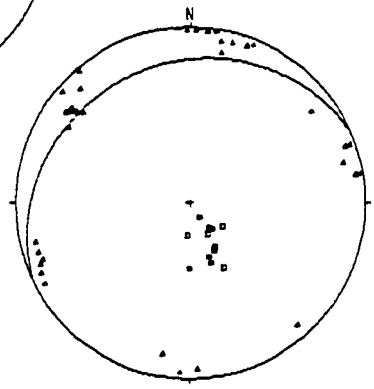

Station 32, BRD
Projection ..... Schmidt
Number of Sample Points 49

▫ Bedding
▵ Joints

A32

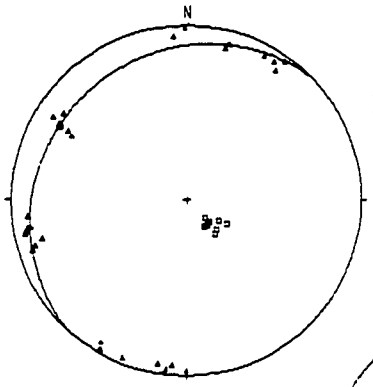

Station 33, BRD
Projection ..... Schmidt
Number of Sample Points 41

▫ Bedding
▵ Joints

A33

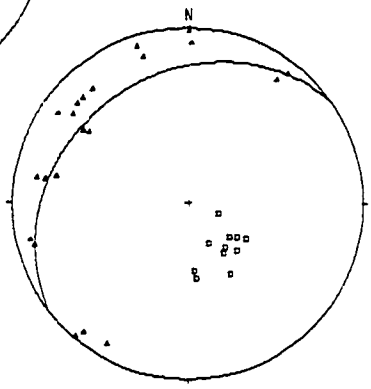

Station 34, BRD
Projection ..... Schmidt
Number of Sample Points 33

▫ Bedding
▵ Joints

A34

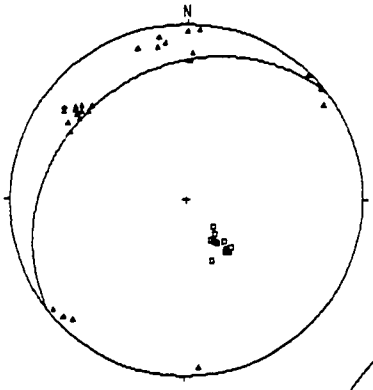

Station 35, BRD
Projection ..... Schmidt
Number of Sample Points 39

▫ Bedding
▵ Joints

A35

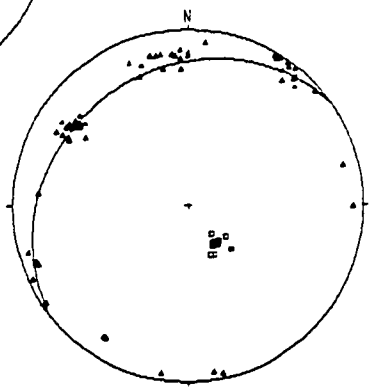

Station 36, BRD
Projection ..... Schmidt
Number of Sample Points 71

▫ Bedding
▵ Joints

A36

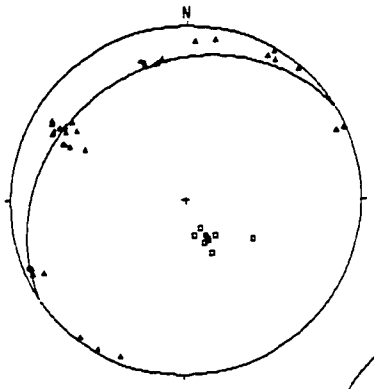

Station 37, BRD
Projection ..... Schmidt
Number of Sample Points 44

▫ Bedding
▵ Joints

A37

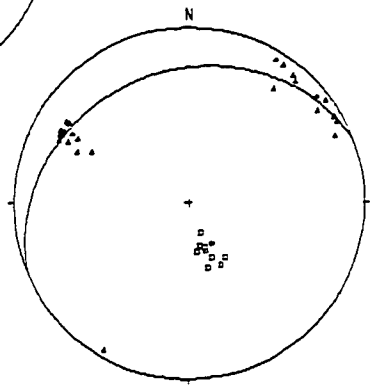

Station 38, BRD
Projection ..... Schmidt
Number of Sample Points 36

▫ Bedding
▵ Joints

A38

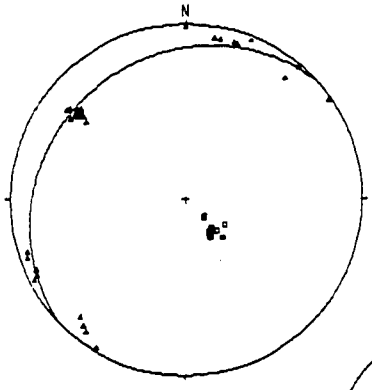

Station 39, BRD
Projection ..... Schmidt
Number of Sample Points 42

▫ Bedding
▵ Joints

A39

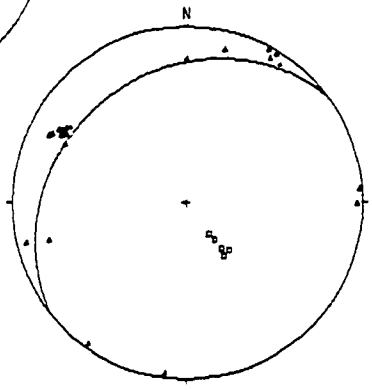

Station 40, BRD
Projection ..... Schmidt
Number of Sample Points 28

▫ Bedding
▵ Joints

A40

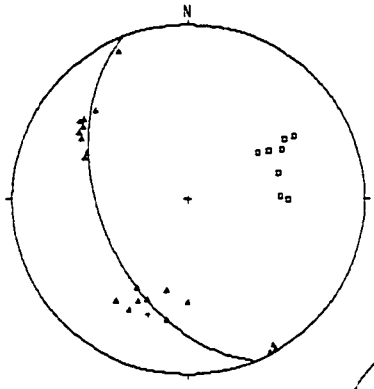

Station 41, Upper Quartzite
Projection ... Schmidt
Number of Sample Points ... 30

▫ Bedding
▵ Joints
• Slicken stripe on bedding plane

A41

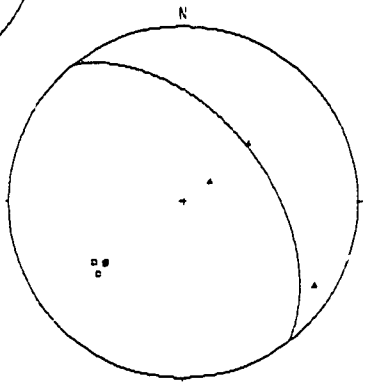

Station 42, BRO (overturned bedd
Projection ... Schmidt
Number of Sample Points ... 8

▫ bedding
▵ joints

A42

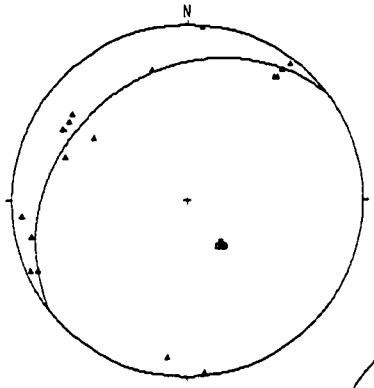

Station 43, Upper Quartzite
Projection ... Schmidt
Number of Sample Points ... 24

▫ Bedding
▵ Joints

A43

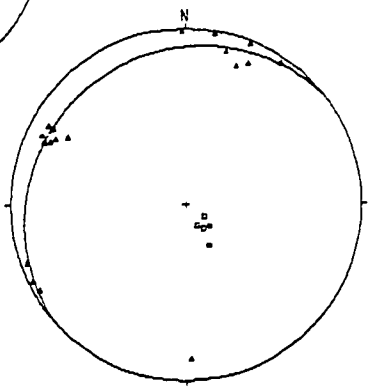

Station 44, Upper Quartzite
Projection ... Schmidt
Number of Sample Points ... 25

▫ Bedding
▵ Joints

A44

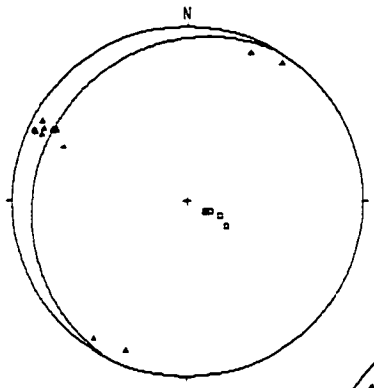

Station 45, Upper Quartzite
Projection ..... Schmidt
Number of Sample Points ... 18

▫ Bedding
▵ Joints

A45

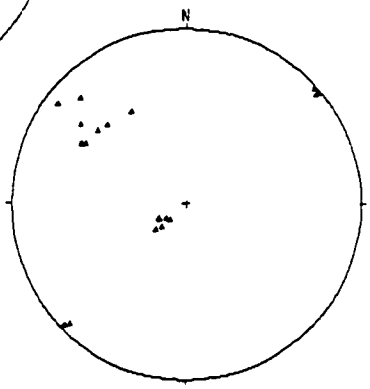

Station 46, Konye Volcanic outlier
Projection ..... Schmidt
Number of Sample Points ... 20

▵ joints

A46

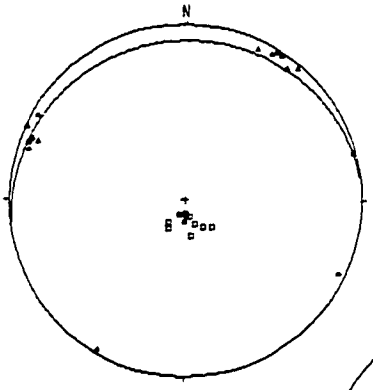

Station 47, Upper Quartzite
Projection ..... Schmidt
Number of Sample Points ... 28

▫ Bedding
▵ Joints

A47

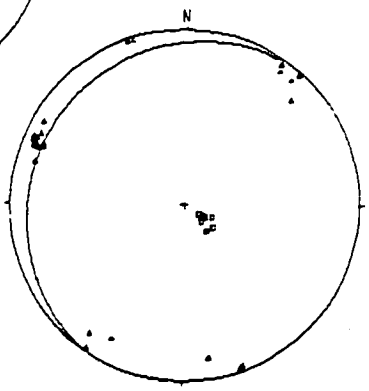

Station 48, Upper Quartzite
Projection ..... Schmidt
Number of Sample Points ... 35

▫ Bedding
▵ Joints

A48

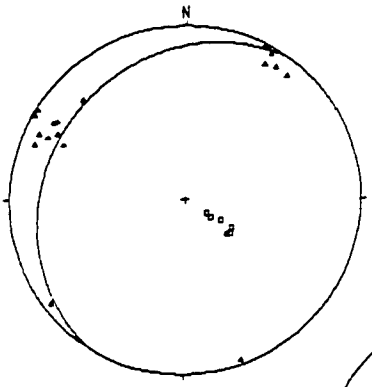

Station 49, Upper Quartzite
Projection ..... Schmidt
Number of Sample Points 25

o Bedding
▲ Joints

A49

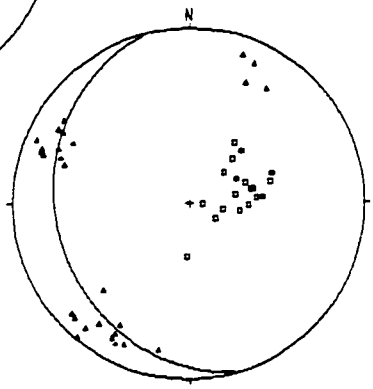

Station 50, Upper Quartzite
Projection ..... Schmidt
Number of Sample Points 47

o Bedding
▲ Joints

A50

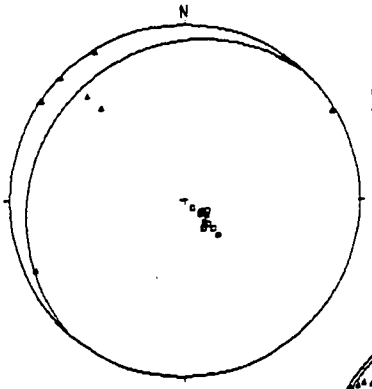

Station 51, Upper Quartzite
Projection ..... Schmidt
Number of Sample Points 19

o Bedding
▲ Joints

A51

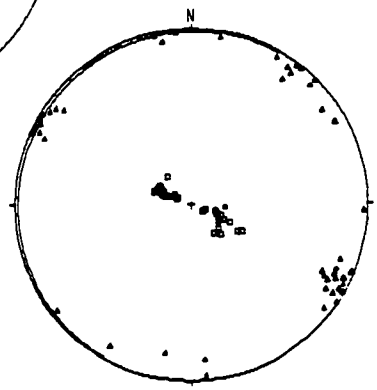

Station 52, Dolomite
Projection ..... Schmidt
Number of Sample Points 89

o Bedding
▲ Joints

A52

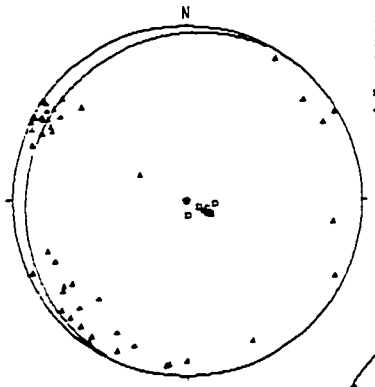

Station 53, Dolomite
Projection ..... Schmidt
Number of Sample Points .. 56

▫ Bedding
▵ Joints

A53

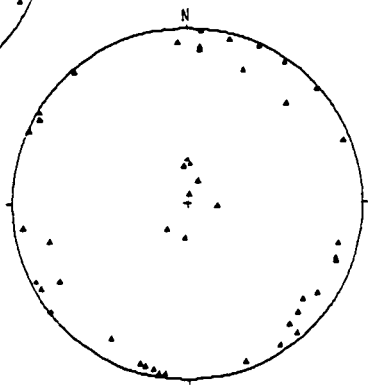

Station 54, Syenite
Projection ..... Schmid
Number of Sample Points . 46

▵ Joints

A54

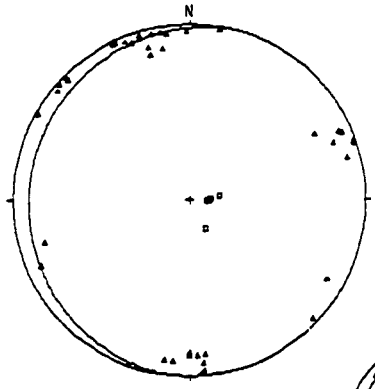

Station 55, Waterberg sandstone
Projection ..... Schmidt
Number of Sample Points 44

▫ Bedding
▵ Joints

A55

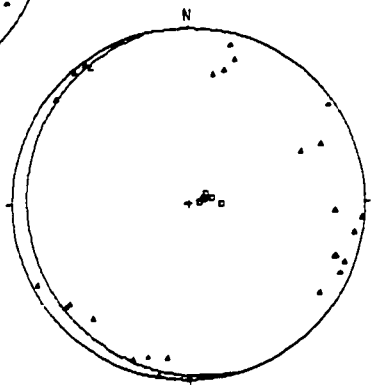

Station 56, Waterberg sandstone
Projection ..... Schmidt
Number of Sample Points ... 35

▫ Bedding
▵ Joints

A56

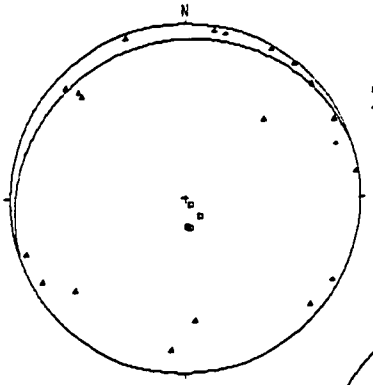

Station 58, Waterberg sandstone
Projection ..... Schmidt
Number of Sample Points 25

▫ Bedding
▵ Joints

A57

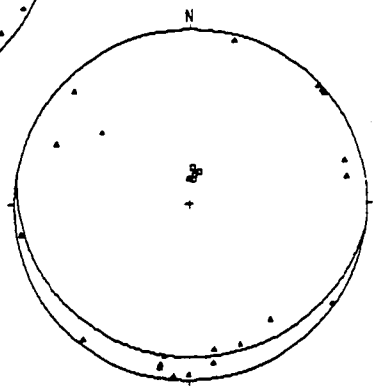

Station 59, BRD
Projection ..... Schmidt
Number of Sample Points 27

▫ Bedding
▵ Joints

A58

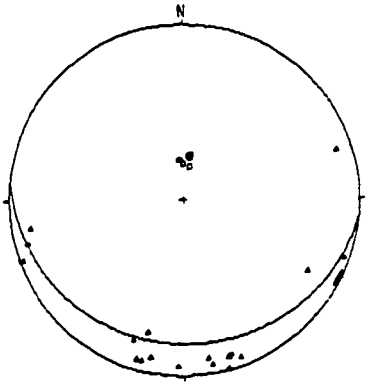

Station 61, BRD
Projection ..... Schmidt
Number of Sample Points 30

▫ Bedding
▵ Joints

A59

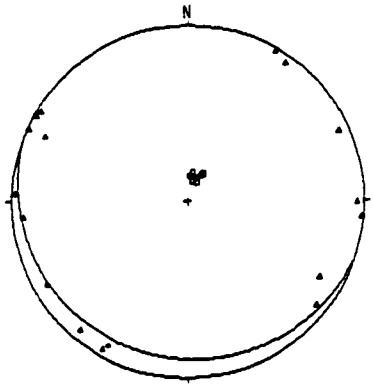

Station 62, BRD
Projection ..... Schmidt
Number of Sample Points 25

▫ Bedding
▵ Joints

A60

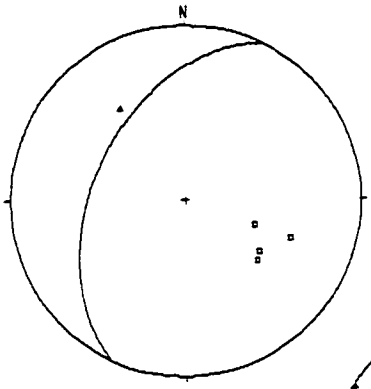

Station 63, Upper Quartzite
Projection ..... Schmidt
Number of Sample Points 7

o bedding
▲ joints

A61

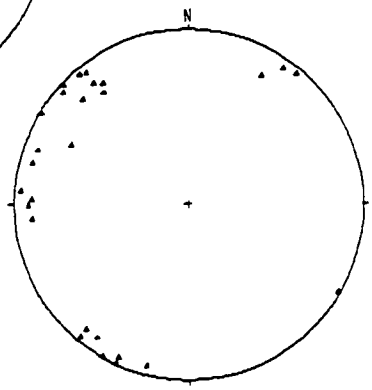

Station 72, Dolerite
Projection ..... Schmidt
Number of Sample Points ... 27

▲ Joints

A62

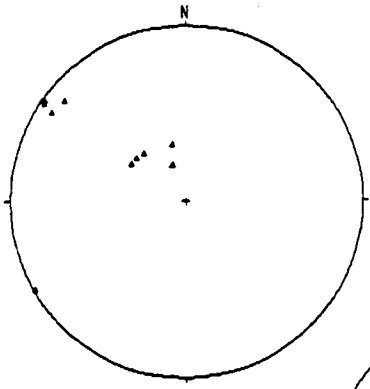

Station 73, Granite
Projection ..... Schmidt
Number of Sample Points ... 10

▲ Joints

A63

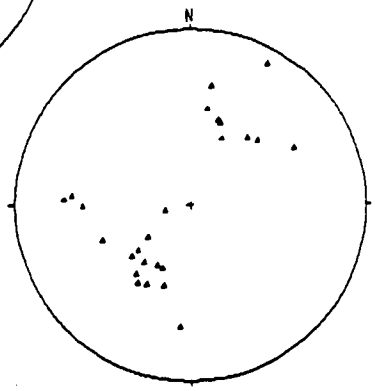

Station 74, Granite
Projection ..... Schmidt
Number of Sample Points ... 26

▲ Joints

A64

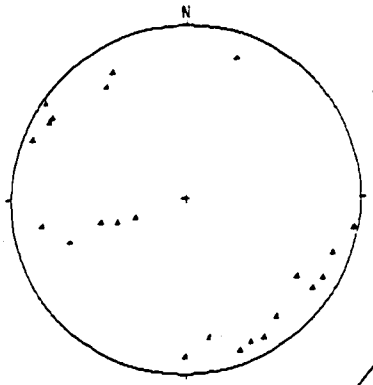

Station 75, Graywacke
Projection ..... Schmidt
Number of Sample Points 24

▲ Joints

A65

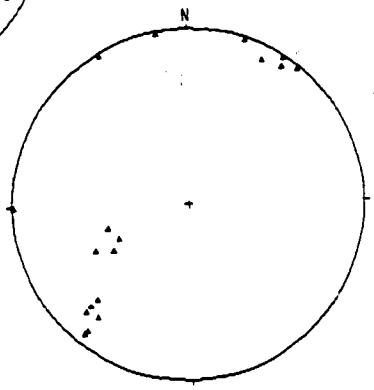

Station 76, Konye Volcanics
Projection ..... Schmidt
Number of Sample Points 19

▲ Joints

A66

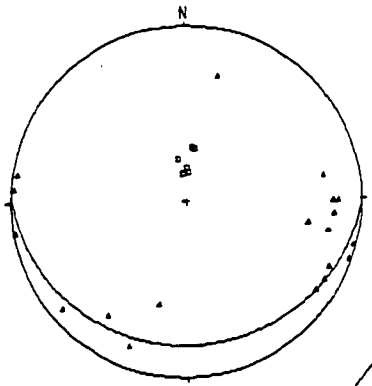

Station 77, BRD
Projection ..... Schmidt
Number of Sample Points 25

□ Bedding
▲ Joints

A67

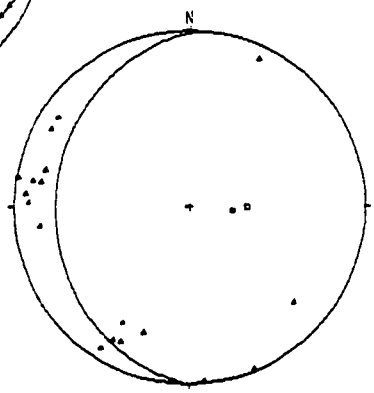

Station 78, BRD
Projection ..... Schmidt
Number of Sample Points 21

□ Bedding
▲ Joints

A68

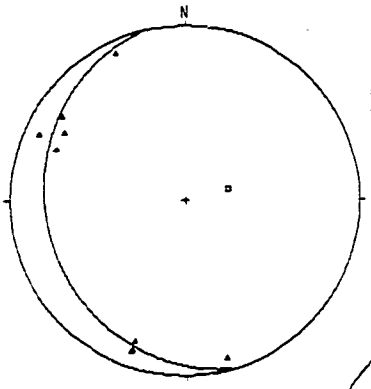

Station 79, Dolomite and chert
Projection ..... Schmidt
Number of Sample Points ... 11

o Bedding
▲ Joints

A69

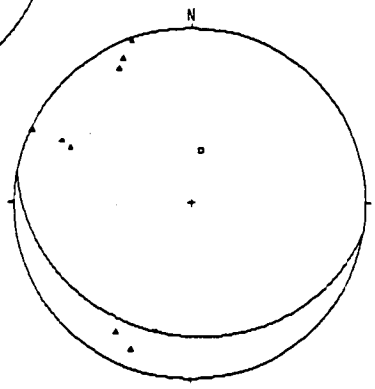

Station 80, Dolomite and chert
Projection ..... Schmidt
Number of Sample Points ... 13

o Bedding
▲ Joints

A70

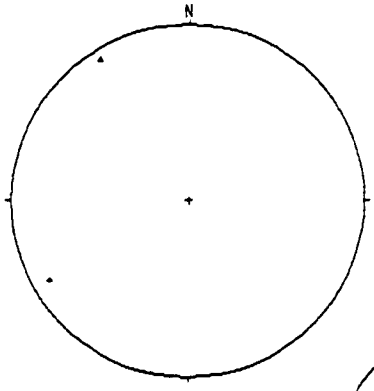

Station 81, dolerite
Projection ..... Schmidt
Number of Sample Points ... 2

▲ joints

A71

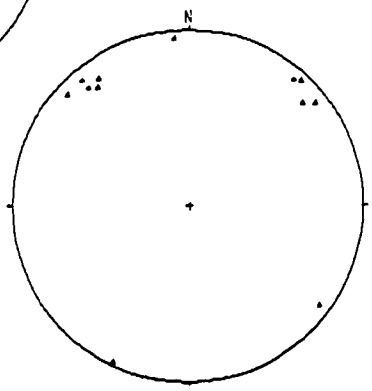

Station 82, Chert breccia
Projection ..... Schmidt
Number of Sample Points ... 12

▲ Joints

A72

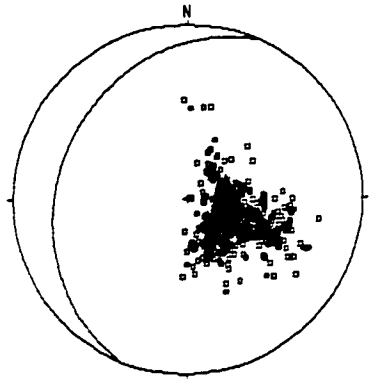

Stations 1-40, Black Reef Quartzite (BRQ)
Projection ..... Schmidt
Number of Sample Points 425
Mean Lineation Azimuth 112.9
Mean Lineation Plunge 64.1

A73

• BEDDING

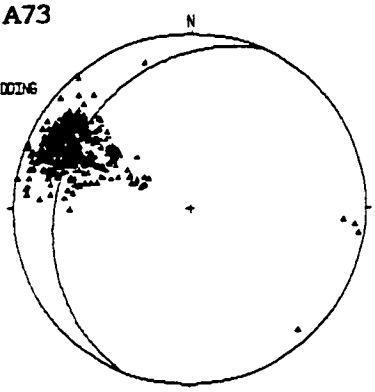

Stations 1-40, BRQ
Projection ..... Schmidt
Number of Sample Points 422
Mean Lineation Azimuth 297.6
Mean Lineation Plunge 23.8

A74

▲ set 1 joints

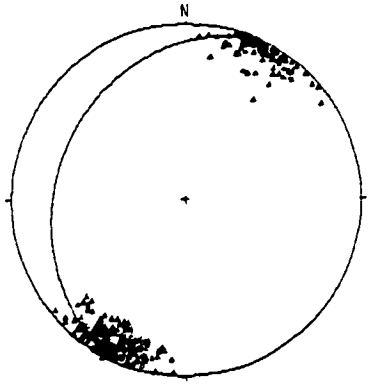

Stations 1-40, BRQ
Projection ..... Schmidt
Number of Sample Points 286
Mean Lineation Azimuth 207.5
Mean Lineation Plunge 4.5

A75

▲ set 2 joints

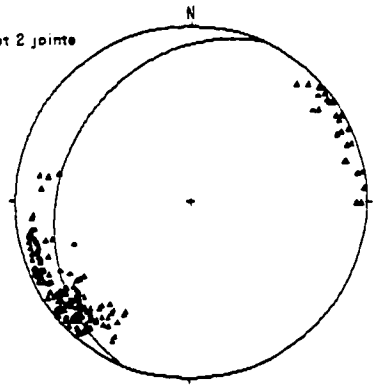

Stations 1-40, BRQ
Projection ..... Schmidt
Number of Sample Points 184
Mean Lineation Azimuth 234.2
Mean Lineation Plunge 9.3

A76

▲ set 3 joints

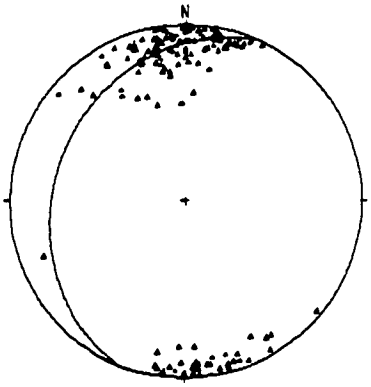

Stations 1-40, BRQ
Projection ..... Schmidt
Number of Sample Points 152
Mean Lineation Azimuth 355.4
Mean Lineation Plunge 6.9

A77

▲ set 4 joints

APPENDIX B:

SAMPLE CALCULATIONS FOR EIGENVECTORS USING SPHERISTAT COMPUTER PROGRAMME.

STATIONS 1 TO 10

BEDDING

EigenVector Results

Data File : BED110
No. of Data: 50

Vector	Trend	Plunge	Eigenvalue
1	197.77	0.10	0.3075 +/- 0.0115
2	287.85	38.86	1.0956 +/- 0.0227
3	107.65	51.14	48.5969 +/- 0.0255

Confidence Cones

Vector	Major	Minor	Average	Angle
1	14.55	1.30	7.93	1.75
2	14.53	3.02	8.77	0.76
3	3.04	1.59	2.31	-0.02

Eigenvalue Ratios (after Woodcock, 1977)

K-ratio [ln(E3/E2)/ln(E2/E1)]: 2.99 +/- 0.11
C-ratio [ln(E3/E1)] : 5.06 +/- 0.04

Pattern: Strongly developed cluster.

SET 1

EigenVector Results

Data File : SET1110
No. of Data: 53

Vector	Trend	Plunge	Eigenvalue
1	180.47	33.77	0.9156 +/- 0.0217
2	57.81	38.91	1.4017 +/- 0.0275
3	296.20	33.00	50.6827 +/- 0.0399

Confidence Cones

Vector	Major	Minor	Average	Angle
1	43.07	2.60	22.84	-0.10
2	43.07	3.23	23.15	-0.24
3	3.26	2.61	2.94	0.79

Eigenvalue Ratios (after Woodcock, 1977)

K-ratio [ln(E3/E2)/ln(E2/E1)]: 8.42 +/- 0.64
C-ratio [ln(E3/E1)] : 4.01 +/- 0.02

Pattern: Strongly developed cluster.

SET 2

EigenVector Results

Data File : SET2110
No. of Data: 33

Vector	Trend	Plunge	Eigenvalue
1	109.87	37.65	0.6150 +/- 0.0238
2	305.82	51.26	1.0898 +/- 0.0373
3	205.96	7.83	31.2951 +/- 0.0389

Confidence Cones

Vector	Major	Minor	Average	Angle
1	31.06	3.43	17.24	0.63
2	31.05	4.70	17.87	0.12
3	4.70	3.51	4.10	-0.71

Eigenvalue Ratios (after Woodcock, 1977)

K-ratio [ln(E3/E2)/ln(E2/E1)]: 5.87 +/- 0.57
C-ratio [ln(E3/E1)] : 3.93 +/- 0.04

Pattern: Moderately developed cluster.

SET 3

EigenVector Results

Data File : SET3110
No. of Data: 7

Vector	Trend	Plunge	Eigenvalue
1	21.04	69.16	0.0583 +/- 0.0095
2	140.04	10.46	0.0692 +/- 0.0143
3	233.44	17.82	6.8725 +/- 0.0175

Confidence Cones

Vector	Major	Minor	Average	Angle
1	80.51	5.14	42.83	-0.10
2	80.51	3.45	41.98	0.38
3	5.73	5.28	5.51	0.31

Eigenvalue Ratios (after Woodcock, 1977)

K-ratio [ln(E3/E2)/ln(E2/E1)]: 26.85 +/- 42.21
C-ratio [ln(E3/E1)] : 4.77 +/- 0.16

Pattern: Strongly developed uniaxial cluster.

SET 4

EigenVector Results

Data File : SET4110
No. of Data: 6

Vector	Trend	Plunge	Eigenvalue
1	92.87	20.49	0.2503 +/- 0.0349
2	236.38	65.07	0.7013 +/- 0.0654
3	357.69	13.58	5.0483 +/- 0.0891

Confidence Cones

Vector	Major	Minor	Average	Angle
1	48.22	13.92	31.07	0.66
2	48.40	24.01	36.20	-3.57
3	24.84	13.99	19.42	0.18

Eigenvalue Ratios (after Woodcock, 1977)

K-ratio [ln(E3/E2)/ln(E2/E1)]: 1.92 +/- 0.37
C-ratio [ln(E3/E1)] : 3.00 +/- 0.14

Pattern: Moderately developed girdle and cluster.

STATIONS 22 TO 24

BEDDING

EigenVector Results

Data File : BED2224
No. of Data: 57

Vector	Trend	Plunge	Eigenvalue
1	249.35	19.52	0.4114 +/- 0.0131
2	341.87	7.07	2.8057 +/- 0.0513
3	90.86	69.14	53.7829 +/- 0.0516

Confidence Cones

Vector	Major	Minor	Average	Angle
1	7.48	1.63	4.55	-0.73
2	7.47	4.39	5.93	0.06
3	4.39	1.64	3.01	0.03

Eigenvalue Ratios (after Woodcock, 1977)

K-ratio [ln(E3/E2)/ln(E2/E1)]: 1.54 +/- 0.04
C-ratio [ln(E3/E1)] : 4.87 +/- 0.03

Pattern: Strongly developed girdle and cluster.

SET 1

EigenVector Results Data File : SET12224
No. of Data: 60

Vector	Trend	Plunge	Eigenvalue
1	194.59	20.10	0.4672 +/- 0.0128
2	62.59	61.33	1.0371 +/- 0.0200
3	292.06	19.56	58.4957 +/- 0.0245

Confidence Cones

Vector	Major	Minor	Average	Angle
1	22.65	1.56	12.11	-0.53
2	22.65	2.44	12.54	0.12
3	2.44	1.63	2.04	-0.29

Eigenvalue Ratios (after Woodcock, 1977)

K-ratio [ln(E3/E2)/ln(E2/E1)]: 5.06 +/- 0.23
C-ratio [ln(E3/E1)] : 4.83 +/- 0.03

Pattern: Strongly developed cluster.

SET 2

EigenVector Results Data File : SET22224
No. of Data: 39

Vector	Trend	Plunge	Eigenvalue
1	294.80	25.13	0.2899 +/- 0.0132
2	105.23	64.56	0.9929 +/- 0.0292
3	203.06	3.71	37.7172 +/- 0.0313

Confidence Cones

Vector	Major	Minor	Average	Angle
1	15.88	1.96	8.92	-0.59
2	15.89	3.68	9.79	-1.04
3	3.73	1.99	2.86	-0.21

Eigenvalue Ratios (after Woodcock, 1977)

K-ratio [ln(E3/E2)/ln(E2/E1)]: 2.95 +/- 0.14
C-ratio [ln(E3/E1)] : 4.87 +/- 0.05

Pattern: Strongly developed cluster.

SET 3

EigenVector Results

Data File : SET32224
No. of Data: 51

Vector	Trend	Plunge	Eigenvalue
1	331.33	51.61	0.5219 +/- 0.0142
2	129.82	36.39	1.2222 +/- 0.0352
3	227.72	10.56	49.2559 +/- 0.0370

Confidence Cones

Vector	Major	Minor	Average	Angle
1	20.05	1.93	10.99	-0.95
2	20.07	2.92	11.49	-1.52
3	3.12	2.05	2.58	-0.13

Eigenvalue Ratios (after Woodcock, 1977)

K-ratio [ln(E3/E2)/ln(E2/E1)]: 4.34 +/- 0.23
C-ratio [ln(E3/E1)] : 4.55 +/- 0.03

Pattern: Strongly developed cluster.

SET 4

EigenVector Results

Data File : SET42224
No. of Data: 14

Vector	Trend	Plunge	Eigenvalue
1	262.41	28.61	0.3348 +/- 0.0280
2	82.27	61.39	0.7248 +/- 0.0692
3	172.38	0.06	12.9404 +/- 0.0763

Confidence Cones

Vector	Major	Minor	Average	Angle
1	41.94	6.10	24.02	0.84
2	41.93	9.19	25.56	0.32
3	9.20	6.27	7.74	0.94

Eigenvalue Ratios (after Woodcock, 1977)

K-ratio [ln(E3/E2)/ln(E2/E1)]: 3.73 +/- 0.71
C-ratio [ln(E3/E1)] : 3.65 +/- 0.08

Pattern: Moderately developed cluster.

STATIONS 52 AND 53

BEDDING

EigenVector Results — Data File : BED5253, No. of Data: 39

Vector	Trend	Plunge	Eigenvalue
1	27.41	0.08	0.0843 +/- 0.0039
2	297.41	3.68	2.1085 +/- 0.0443
3	118.70	86.32	36.8072 +/- 0.0444

Confidence Cones

Vector	Major	Minor	Average	Angle
1	4.61	1.04	2.83	1.98
2	5.68	4.56	5.12	4.92
3	5.65	1.09	3.37	-0.04

Eigenvalue Ratios (after Woodcock, 1977)

K-ratio [ln(E3/E2)/ln(E2/E1)]: 0.89 +/- 0.02
C-ratio [ln(E3/E1)] : 6.08 +/- 0.05

Pattern: Strongly developed girdle and cluster.

SET 1

EigenVector Results — Data File : SET15253, No. of Data: 51

Vector	Trend	Plunge	Eigenvalue
1	209.13	9.32	0.2992 +/- 0.0075
2	33.20	80.66	1.7402 +/- 0.1116
3	299.23	0.65	48.9607 +/- 0.1139

Confidence Cones

Vector	Major	Minor	Average	Angle
1	14.33	1.47	7.90	0.78
2	14.34	2.98	8.66	-1.29
3	3.07	1.49	2.28	3.21

Eigenvalue Ratios (after Woodcock, 1977)

K-ratio [ln(E3/E2)/ln(E2/E1)]: 1.90 +/- 0.11
C-ratio [ln(E3/E1)] : 5.10 +/- 0.03

Pattern: Strongly developed girdle and cluster.

SET 2

EigenVector Results

Data File : SET22525
No. of Data: 25

Vector	Trend	Plunge	Eigenvalue
1	312.21	76.45	0.3233 +/- 0.0163
2	130.67	13.55	1.3999 +/- 0.1175
3	220.75	0.35	23.2767 +/- 0.1203

Confidence Cones

Vector	Major	Minor	Average	Angle
1	19.38	3.36	11.37	-0.06
2	19.62	5.49	12.55	5.04
3	6.43	3.33	4.88	2.24

Eigenvalue Ratios (after Woodcock, 1977)

K-ratio [ln(E3/E2)/ln(E2/E1)]: 1.92 +/- 0.18
C-ratio [ln(E3/E1)] : 4.28 +/- 0.05

Pattern: Strongly developed girdle and cluster.

SET 3

EigenVector Results

Data File : SET353
No. of Data: 10

Vector	Trend	Plunge	Eigenvalue
1	331.41	20.44	0.1424 +/- 0.0175
2	121.68	66.78	0.3393 +/- 0.0432
3	237.43	10.56	9.5183 +/- 0.0425

Confidence Cones

Vector	Major	Minor	Average	Angle
1	36.48	5.65	21.06	0.80
2	36.74	6.63	21.69	-4.14
3	8.87	5.76	7.32	0.19

Eigenvalue Ratios (after Woodcock, 1977)

K-ratio [ln(E3/E2)/ln(E2/E1)]: 3.84 +/- 0.89
C-ratio [ln(E3/E1)] : 4.20 +/- 0.12

Pattern: Strongly developed cluster.

STATIONS 1 TO 40

BEDDING

EigenVector Results

Data File : BED140
No. of Data: 425

Vector	Trend	Plunge	Eigenvalue
1	223.55	9.68	15.6775 +/- 0.0503
2	317.86	23.75	21.6135 +/- 0.0797
3	112.96	64.12	387.7091 +/- 0.1012

Confidence Cones

Vector	Major	Minor	Average	Angle
1	23.32	1.36	12.34	0.06
2	23.33	1.36	12.35	0.90
3	1.58	1.35	1.46	-4.97

Eigenvalue Ratios (after Woodcock, 1977)

K-ratio [ln(E3/E2)/ln(E2/E1)]: 8.99 +/- 0.15
C-ratio [ln(E3/E1)] : 3.21 +/- 0.00

Pattern: Moderately developed cluster.

SET 1

EigenVector Results

Data File : SET1140
No. of Data: 421

Vector	Trend	Plunge	Eigenvalue
1	203.98	8.26	7.9017 +/- 0.0352
2	96.17	64.60	18.5625 +/- 0.0745
3	297.66	23.84	394.5358 +/- 0.0823

Confidence Cones

Vector	Major	Minor	Average	Angle
1	7.72	0.93	4.32	-0.86
2	7.72	1.39	4.56	-1.54
3	1.45	0.95	1.20	0.15

Eigenvalue Ratios (after Woodcock, 1977)

K-ratio [ln(E3/E2)/ln(E2/E1)]: 3.58 +/- 0.03
C-ratio [ln(E3/E1)] : 3.91 +/- 0.00

Pattern: Moderately developed cluster.

SET 2

EigenVector Results — Data File : SET2140; No. of Data: 285

Vector	Trend	Plunge	Eigenvalue	
1	317.62	77.07	6.3809 +/-	0.0346
2	116.67	12.10	7.1770 +/-	0.0484
3	207.64	4.49	271.4421 +/-	0.0589

Confidence Cones

Vector	Major	Minor	Average	Angle
1	50.04	1.27	25.65	-0.02
2	50.04	1.32	25.68	-0.01
3	1.32	1.27	1.30	2.38

Eigenvalue Ratios (after Woodcock, 1977)

K-ratio [ln(E3/E2)/ln(E2/E1)]: 30.90 +/- 2.32
C-ratio [ln(E3/E1)] : 3.75 +/- 0.01

Pattern: Moderately developed uniaxial cluster.

SET 3

EigenVector Results — Data File : SET3140; No. of Data: 183

Vector	Trend	Plunge	Eigenvalue	
1	5.79	76.08	3.3549 +/-	0.0284
2	142.56	10.24	11.3204 +/-	0.0823
3	234.26	9.33	168.3247 +/-	0.0922

Confidence Cones

Vector	Major	Minor	Average	Angle
1	9.45	1.43	5.44	-0.61
2	9.48	2.58	6.03	-2.48
3	2.70	1.44	2.07	0.99

Eigenvalue Ratios (after Woodcock, 1977)

K-ratio [ln(E3/E2)/ln(E2/E1)]: 2.22 +/- 0.02
C-ratio [ln(E3/E1)] : 3.92 +/- 0.01

Pattern: Moderately developed cluster.

SET 4

EigenVector Results

Data File : SET4140
No. of Data: 151

Vector	Trend	Plunge	Eigenvalue	
1	107.55	71.92	5.2087 +/-	0.0536
2	263.46	16.59	10.0020 +/-	0.1083
3	355.55	6.97	135.7893 +/-	0.1204

Confidence Cones

Vector	Major	Minor	Average	Angle
1	16.59	2.01	9.30	1.62
2	16.57	3.01	9.79	-0.19
3	3.01	2.22	2.62	-0.45

Eigenvalue Ratios (after Woodcock, 1977)

K-ratio [ln(E3/E2)/ln(E2/E1)]: 4.00 +/- 0.10
C-ratio [ln(E3/E1)] : 3.26 +/- 0.01

Pattern: Moderately developed cluster.

END

18-11-94

FIN